Applications of Whole Cell Biotransformations for the Production of Chiral Alcohols

A Dissertation submitted to the

Faculty of Mathematics and Natural Sciences

Rheinische Friedrich-Wilhelms University of Bonn

for the degree of

Doctor of Natural Sciences (Dr. rer. nat.)

by

Ai Wei Ivy Tan

Singapore

Bonn 2006

Angefertigt mit Genehmigung der Mathematisch-Naturwissenschaftlichen Fakultät der Rheinischen Friedrich-Wilhelms-Universität Bonn

1. Referent: Prof. Dr. C. Wandrey
2. Referent: Prof. Dr. S. Waldvogel

Tag der Promotion: 26. April 2006

To my family and friends,

Je ne regrette pas.

The work towards this doctoral thesis was carried out between April 2002 to August 2005 at the Chair of Biotechnology of the Rheinische Friedrich-Wilhelms University of Bonn, Germany, under the supervision of Prof. C. Wandrey at the laboratories of the Institute of Biotechnology 2, Forschungszentrum Juelich GmbH, Germany.

Acknowledgements

I am grateful to my Doktorvater (Supervisor), Prof. Christian Wandrey, for the immense scientific opportunities for the successful completion of this work. His stimulating scientific discussions, strong encouragement, fruitful insights and open-door policy for advice, support and ideas have been instrumental in making life comfortable throughout this period.

To my mentor, Prof. Andreas Liese, for his friendly, open-door approach for advice and ideas, and for his tremendous help and listening ear whenever needed. For helping me settle in a new environment, and making me very comfortable within Enzyme Group.

I am also grateful to Mrs. Ursula Mackfeld for her immense and reliable work in the laboratories. Without her wealth of knowledge, ideas, suggestions and help, this work would not have been possible. To Mrs. Heike Offermann, for her friendly help in and out of the laboratories.

To Enzyme Group, for the fun factor, friendliness, laughters, help, listening ear and for always making learning barrier-free.

I am thankful to Dr. Juergen Haberland for his never-ending friendly and helpful nature, for his suggestions, ideas, encouragement and fun. From imparting skills and knowledge at the start of this work, to proof-reading the thesis at the end.

To Dr. Nagaraj Rao, RRR Laboratories, for his scientific help in the laboratories, his insights and encouragement.

To Mrs. Sarah Schaffhausen, Mr. Matthias Pitsch and Mrs. Cornelia Zemlin who have helped me in this work during their practical stay or Diplom work.

I am also thankful to Dr. Hong Li, University of Oxford, for his scientific insights on microbiological work, and for advice.

To Dr. Thomas Daussmann, Mr. Ralf Feldmann, Mr. Thomas Kalthoff and Dr. Hans-Georg Hennemann of Juelich Fine Chemicals GmbH for the friendly collaboration, trust, and for their willingness and openness in the exchange of ideas and information.

I am thankful to Prof. W. Hummel and Mr. Frank Schneider of the Institute of Molecular Enzyme Technology, Heinrich-Heine University of Duesseldorf, as collaboration partners, for their scientific discussions and for sharing insights into *Lactobacillus kefiri*.

I am also thankful to Drs. Stephanie Bringer-Meyer and Bjoern Kaup from the Institute of Biotechnology 1, Forschungszentrum Juelich GmbH, as collaboration partners in the work with the recombinant *Escherichia coli*. For imparting the knowledge and skills, and for discussions of results. To Prof. Hermann Sahm for making the collaboration possible.

To Prof. Rainer Buchholz and Dr. Holger Huebner from the Institute of Bioprocess Engineering at the Friedrich-Alexander University of Erlangen-Nuremberg, for the opportunity to spend a week in the laboratories to learn the immobilisation techniques with sodium cellulose sulphate. Especially to Dr. Holger Huebner and to Dr. Mathias Fischbach (EuroFerm GmbH), for imparting skills and knowledge, and for never hesitating to answer my questions on immobilisation. Also for the trust and the loan of the encapsulation apparatus, for a long period of time.

I am also thankful to Drs. Peter Wittlich and Ulrich Jahnz (GeniaLab GmbH) for their exchange of ideas and scientific help in the immobilisation technology of LentiKats®.

To Dr. Marion Ansorge-Schumacher of Rheinische Westphalia Technical University of Aachen, for the opportunity to learn and perform immobilisation work with polyvinyl alcohol at her laboratories.

I am thankful to Drs. Ralf Takors and Marco Oldiges for the possibility and trust of working in the Technikum Hall. To Mr. Hans-Juergen Brandt, Mrs. Melanie Rueping and Mr. Matthias Moch for friendly support in the work at the Technikum Hall. Also to Mr. Robert Bujnicki, Dr. Michel Brik-Ternbach, Mr. Matthias Kunze and the rest of Fermentation Group, for scientific discussions, ideas, a listening ear and friendliness.

To Prof. Michael Mueller, at the Institute of Pharmaceutical Sciences, University of Freiburg, and Mr. Peer Kling (Central Library, Forschungszentrum Juelich GmbH) for their unassuming help in the literature search for (5*R*)-hydroxyhexane-2-one.

To Dr. Sabine Wilbold at the Department of the Central Analytics, Forschungszentrum Juelich GmbH, for the NMR analysis of (5*R*)-hydroxyhexane-2-one.

Not forgetting also, my roommates Mrs. Rita Mertens and Dr. Stephan Luetz, for tremendous amount of fun, laughter, help and trust. For being excellent translators of German to English, for explaining the German language and for assistance in administrative matters. And to Dr. Stephan Luetz for the proof-reading of my thesis.

To Mrs. Marianne Hess for her friendliness and help.

I am also thankful to Mr. Andreas Franz and Mr. Horst Kiehl for their instant assistance in computers.

To the very hardworking staff at the mechanical, glass and electronic workshops, who helped in my laboratory setups in one way or another.

To the other staff of Institute of Biotechnology, whom in one way or another, have helped me during my stay in Juelich.

Gratitude to Anneliese and Heinrich Emunds, for the comfortable living environment and help. To Dirk for being nice and helpful always whenever needed. To Peggy, Snookie and Farrah for unconditional love and immense fun.

Last but not the least, to my family and friends, for unconditional love, understanding and support during difficult times.

Abstract

Bioreduction of (2,5)-hexanedione to highly enantiopure (5*R*)-hydroxyhexane-2-one (*ee* > 99 %) with *Lactobacillus kefiri* DSM 20587 was investigated. Cell immobilisation with sodium cellulose sulphate (technical grade) was chosen as the most suitable encapsulation matrix, giving an immobilisation yield of 40 %. Despite the lowered biocatalytic activity from cell immobilisation, the bioreduction process was vastly improved with the help of reaction engineering techniques (batch to a plug flow reactor setup). High selectivity (95 %) and space-time yield (87 g L^{-1} d^{-1}), with a biocatalyst consumption of 1.4 g_{wcw} g^{-1} was achieved in the plug flow reactor. The biocatalyst remained active (68 % residual activity) after 6 days of operation. Downstream processing of (5*R*)-hydroxyhexane-2-one was obtained by column chromatography, yielding a product of more than 99 % purity (GC) and enantiomeric excess on a gram-scale.

The same bioreduction was applied on an enzyme-coupled system consisting of alcohol dehydrogenase from *Lactobacillus brevis* (*Lb*ADH) and formate dehydrogenase (FDH) from *Pseudomonas* sp. In a similar enzyme-coupled system, the biotransformation was extended from a batch to a continuous setup to reduce methyl acetoacetate to highly enantiopure (*R*)-methyl 3-hydroxybutanoate (*ee* > 99 %). The highest total turnover numbers (2.4 x 10^6 mol mol_{ADH}^{-1}, 2.5 x 10^4 mol mol_{FDH}^{-1} and 329 mol mol_{NADP}^{-1}) and therefore, lowest biocatalyst consumption (0.015 $g_{ADH+FDH}$ g^{-1}) was achieved in the continuous setup.

From an enzyme-coupled system to whole cell biotransformation of methyl acetoacetate with genetically modified *Escherichia coli* coexpressing genes of *Lb*ADH and FDH from *Mycobacterium vaccae*, high enantiopure (*R*)-methyl 3-hydroxybutanoate (*ee* > 99 %) was also obtained. Through reaction engineering, the lowest biocatalyst consumption (0.9 g_{wcw} g^{-1}) was yielded in a continuous reactor. The biocatalyst deactivated rapidly (k_{des} of about 5 % h^{-1}) under continuous production, possibly due to a leaky cell membrane.

In this study, comparison of the whole cells and enzyme-coupled systems revealed higher activities for enzyme-coupled bioreductions with high production costs. Although whole cells biotransformations yielded lower activities, they are more inexpensive. Through reaction engineering techniques, the biocatalyst consumption of whole cell bioreductions could be reduced. In addition, the biocatalyst consumption of a process can be further reduced with whole cell immobilisation.

Contents

Acknowledgements i

Abstract iv

Contents v

List of Figures x

List of Tables xix

List of Abbreviations and Symbols xx

1. Introduction 1

1.1 Chiral alcohols…….....1

1.1.1 γ-Hydroxyketones……..1

1.1.2 3-Hydroxybutanoates…….....3

1.2 Biocatalysts……5

1.2.1 Isolated enzymes……5

1.2.2 Wild type microorganism *Lactobacillus kefiri*……..7

1.2.3 Genetically modified microorganisms……...8

1.2.4 Whole cell immobilisation……...10

2. Aims 12

3. γ-Hydroxyketone synthesis with wild type biocatalyst *Lactobacillus kefiri* 14

3.1 Biocatalyst production……..14

3.2 General definition of terms used……..15

3.3 Characteristics of biocatalyst…….....17

3.3.1 Batch characterisation……..17

3.3.2 Repetitive batch run…….21

3.4 Whole cell immobilisation……...22

3.4.1 Choice of immobilisation matrix…….22

3.4.2 Reaction conditions……..28

3.4.3 Repetitive batch investigations……29

3.4.4 Plug flow reactor (PFR) run…….30

3.5 Downstream processing……...34

3.6 Conclusions……..36

4. Syntheses of chiral alcohols with an enzyme-coupled system 38

4.1 General definitions of terms used…….39

4.2 γ-Hydroxyketone synthesis……..40

4.3 3-Hydroxybutanoate synthesis…….41

4.3.1 Reaction conditions……..41

4.3.2 Stability of enzymes…….44

4.3.2.1 Temperature……44

4.3.2.2 Incubation chemicals……..46

4.3.3 Stability of cofactors……49

4.3.4 Batch kinetics……...51

4.3.4.1 Kinetics of *Lb*ADH…….51

4.3.4.2 Kinetics of FDH…….54

4.3.4.3 Enzyme-coupled batch run..……...55

4.3.5 Enzyme-coupled repetitive batch studies…….56

4.3.6 Enzyme-coupled continuous run in enzyme membrane reactor……..58

4.4 Conclusions……..62

5. 3-Hydroxybutanoate synthesis with genetically modified biocatalyst *Escherichia coli* BL21 Star (DE3) 64

5.1 Biocatalyst production…….64

5.1.1 Genetic transformation……64

5.1.2 Fermentation……66

5.2 General definitions of terms used……68

5.3 Storage of induced cells……...69

5.4 Selection of biotransformation medium……...70

5.5 Characteristics of biocatalyst……....72

5.5.1 Reaction conditions……..72

5.5.2 Reaction kinetics……..73

5.5.3 Batch characterisation……..76

5.6 Continuously stirred tank reactor (CSTR)……...76

5.7 Stability studies……79

5.7.1. Repetitive batch investigations……79

5.7.2 Methyl acetoacetate:formate ratio……..……..83

5.7.3 Biotransformation medium studies in repetitive batch……84

5.8 Conclusions…….86

6. Discussion and outlook 87

6.1 γ-Hydroxyketone syntheses with whole cells of *Lactobacillus kefiri* versus enzyme-coupled system……87

6.1.1 Process parameters and stability……..87

6.1.2 Economics……90

6.1.3 Problems and outlook……..91

6.2 3-Hydroxybutanoate syntheses with whole cells of recombinant *Escherichia coli* versus enzyme-coupled system……..…..93

6.2.1 Process parameters and stability……..……93

6.2.2 Economics……...……95

6.2.3 Problems and outlook……...……96

6.3 Choice of biocatalyst system……98

7. Conclusions 100

8. References 102

9. Materials and methods 113

9.1 Materials……...……..113

9.1.1 Laboratory equipment……...……113

9.1.2 Chemicals and biological materials……...115

9.2 Analytical methods……116

9.2.1 Gas chromatography……..116

9.2.1.1 System involving γ-hydroxyketone production……...116

9.2.1.2 System involving 3-hydroxybutanoate production……..118

9.2.2 High pressure liquid chromatography……...…120

9.2.3 Nuclear magnetic resonance……...121

9.2.4 Bradford assay……122

9.3 Biotransformations methods……..123

9.3.1 Genetic work……..123

9.3.1.1 Plasmids amplification……123

9.3.1.2 Plasmids purification……124

9.3.1.3 Transformation of two plasmids……..124

9.3.2 Fermentation……..125

9.3.3 Whole cell immobilisation……127

9.3.3.1 Treatment of cells……..…127

9.3.3.2 Immobilisation equipment……127

9.3.3.3 Polyvinyl alcohol matrix……..127

9.3.3.4 Alginate matrices……..127

9.3.3.5 κ-Carrageenan matrices……128

9.3.3.6 Sodium cellulose sulphate matrix (NaCS)……...128

9.3.4 Reaction techniques for *Lactobacillus kefiri*……..129

9.3.4.1 Batch runs……129

9.3.4.2 Repetitive batch runs……...…….129

9.3.4.3 Plug flow reactor (PFR)……...129

9.3.5 Reaction techniques for enzymes……..…….130

9.3.5.1 Activity assay (pH)……...130

9.3.5.2 Activity assay (temperature)……130

9.3.5.3 Stability of isolated enzymes……131

9.3.5.4 Stability of cofactors……..……..132

9.3.5.5 Batch kinetics of isolated enzymes……..133

9.3.5.6 Enzyme-coupled batch run……...133

9.3.5.7 Enzyme-coupled repetitive batch run……...134

9.3.5.8 Enzyme-coupled continuous run……..……135

9.3.6 Reaction techniques for recombinant *Escherichia coli*……..136

9.3.6.1 Batch run……..136

9.3.6.2 Repetitive batch runs……136

9.3.6.3 Continuous run (CSTR)……...136

10. Appendices 138

List of Figures

Figure 1.1. Structures of γ-hydroxyketones and 3-hydroxybutanoates where R1, R2 and R3 refer to alkyl groups……...1

Figure 1.2. Products from (5*R*)-hydroxyhexane-2-one…….2

Figure 1.3. Industrial route to (2*R*,5*R*)-hexanediol by whole cell biotransformation with *Lactobacillus kefiri* DSM 20587……..3

Figure 1.4. Products of 3-hydroxybutanoates……...4

Figure 1.5. Industrial route to (*R*)-methyl-3-hydroxybutanoate by isolated enzymes with cofactor regeneration by means of isopropanol…….….5

Figure 1.6. Cofactor regeneration with substrate-coupled (left) and enzyme-coupled (right) system……...6

Figure 1.7. Alternative routes for the electrochemical regeneration of $NAD(P)^+$ from NADPH…….7

Figure 1.8. Production of (2*R*,5*R*)-hexanediol with whole resting cells of *Lactobacillus kefiri* DSM 20587……8

Figure 1.9. Recombinant whole cells transformed with carbonyl reductase and cofactor regeneration systems with formate dehydrogenase or glucose dehydrogenase……..9

Figure 1.10. Principal methods of immobilisation……...10

Figure 2.1. Enantioselective reduction of (2,5)-hexanedione (**A**) to (5*R*)-hydroxyhexane-2-one (**B**) with resting whole cells of *Lactobacillus kefiri* or enzyme-coupled system……...……...12

Figure 2.2. Enantioselective reduction of methyl acetoacetate (**MAA**) to (*R*)-methyl-3-hydroxybutanoate (**MHB**) with resting whole cells of recombinant *Escherichia coli* or enzyme-coupled system...……...12

Figure 3.1. Enantioselective reduction of (2,5)-hexanedione (**A**) to (5*R*)-hydroxyhexane-2-one (**B**) and subsequently to (2*R*,5*R*)-hexanediol (**C**) with resting whole cells of *Lactobacillus kefiri*……..14

Figure 3.2. Characteristics of batch, continuously stirred tank (CSTR) and plug flow reactor (PFR)……...16

Figure 3.3. Concentration of reactants in a typical batch reactor as a function of time…….....17

Figure 3.4. Fitting of experimental data of (2,5)-hexanedione (**A**) with respect to time for rate constant determination……18

Figure 3.5. Selectivity of (5*R*)-hydroxyhexane-2-one (**B**) as a function of conversion of (2,5)-hexanedione (**A**) in a typical batch reaction at pH 6, 7 and 8……20

Figure 3.6. Concentration of (5*R*)-hydroxyhexane-2-one (**B**) as a function of time in a typical batch reaction at pH 6, 7 and 8……20

Figure 3.7. Concentration of (5*R*)-hydroxyhexane-2-one (**B**) in a repetitive batch as a function of time……...21

Figure 3.8. Activity of *L. kefiri* at pH 6 in a repetitive batch run as a function of time……..21

Figure 3.9. Concentration profiles of (5*R*)-hydroxyhexane-2-one (**B**) in a typical non-immobilised and a polyvinyl alcohol (LentiKats®) immobilised batch as a function of normalised time……...23

Figure 3.10. Concentration profiles of (5*R*)-hydroxyhexane-2-one (**B**) in a typical non-immobilised and different κ-carrageenan immobilised batches as a function of normalised time……24

Figure 3.11. Concentration profiles of (5*R*)-hydroxyhexane-2-one (**B**) in a typical non-immobilised and different alginate immobilised batches as a function of normalised time……...……..24

Figure 3.12. Concentration profiles of (5*R*)-hydroxyhexane-2-one (**B**) in a typical non-immobilised and different NaCS immobilised batches as a function of normalised time……25

Figure 3.13. Immobilisation yield of a typical batch reaction……26

Figure 3.14. Encapsulation method (left) for technical grade NaCS immobilisates (right) made from encapsulation device (centre)…….27

Figure 3.15. Activity of NaCS immobilisates and final concentration of (5*R*)-hydroxyhexane-2-one (**B**) (after 24 h) in a typical batch reaction (immobilised cells) at pH 5, 6 and 7……28

Figure 3.16. Selectivity of (5*R*)-hydroxyhexane-2-one (**B**) as a function of conversion of (2,5)-hexanedione (**A**) in a typical batch reaction (immobilised cells) at pH 5, 6 and 7……...28

Figure 3.17. Concentration of (5*R*)-hydroxyhexane-2-one (**B**) in a repetitive batch run with technical grade NaCS immobilised cells as a function of time……...29

Figure 3.18. Activities of non-immobilised and technical grade NaCS immobilised cells at pH 6 in a repetitive batch run as a function of time……...30

Figure 3.19. Scheme of PFR setup in series…….……31

Figure 3.20. Production of (5*R*)-hydroxyhexane-2-one (**B**) with the PFR setup (left) and a close-up on the thermally insulated PFRs (right)…..…….31

Figure 3.21. Concentration profile of reactants packed with NaCS immobilisates in the first column of PFR (in series) as a function of the number of residence time…….....32

Figure 3.22. Selectivity of (5*R*)-hydroxyhexane-2-one (**B**) and conversion of (2,5)-hexanedione (**A**) as a function of the number of residence time in the first column of PFR (in series) packed with NaCS immobilisates……..…….....32

Figure 3.23. Concentration profile of reactants packed with NaCS immobilisates from the second column of PFR (in series) as a function of the number of residence time…….33

Figure 3.24. Selectivity of (5*R*)-hydroxyhexane-2-one (**B**) and conversion of (2,5)-hexanedione (**A**) as a function of the number of residence time from the second column of PFR (in series) packed with NaCS immobilisates……...33

Figure 3.25. Concentration of reactants as a function of the volume of eluent used in the column……...……35

Figure 3.26. Purity of (5*R*)-hydroxyhexane-2-one (**B**) as a function of the volume of eluent used in the column……...…35

Figure 3.27. Cyclisation of (5*R*)-hydroxyhexane-2-one (**B**) to (2,5*R*)-dimethyl-tetrahydrofuran-2-ol……..…36

Figure 3.28. Final product (5*R*)-hydroxyhexane-2-one (**B**), a yellow oil……....36

Figure 4.1. Enantioselective reduction of (2,5)-hexanedione (**A**) to (5*R*)-hydroxyhexane-2-one (**B**) and subsequently to (2*R*,5*R*)-hexanediol (**C**) with isolated enzyme-coupled system…..…38

Figure 4.2. Enantioselective reduction of methyl acetoacetate (**MAA**) to (*R*)-methyl-3-hydroxybutanoate (**MHB**) with isolated enzyme-coupled system……...39

Figure 4.3. Concentration of reactants in a batch reactor as a function of time……..41

Figure 4.4. Activity of *Lb*ADH and FDH as a function of pH……..41

Figure 4.5. Activity of *Lb*ADH as a function of temperature……43

Figure 4.6. Activity of FDH as a function of temperature……..43

Figure 4.7. Comparison of residual activity of *Lb*ADH incubated at different temperatures and 2 mM $MgSO_4$-containing buffer……..44

Figure 4.8. Deactivation of *Lb*ADH incubated at in buffer at different temperatures…….……45

Figure 4.9. Comparison of residual activity of FDH incubated at different temperatures and 2 mM $MgSO_4$-containing buffer……..45

Figure 4.10. Residual activity of *Lb*ADH incubated with methyl acetoacetate-containing buffer……..46

Figure 4.11. Residual activity of *Lb*ADH incubated with (*R*)-methyl-3-hydroxybutanoate-containing buffer……47

Figure 4.12. Residual activity of *Lb*ADH incubated with 100 mM sodium formate-containing buffer……47

Figure 4.13. Residual activity of FDH incubated with methyl acetoacetate-containing buffer……..48

Figure 4.14. Residual activity of FDH incubated with (*R*)-methyl-3-hydroxybutanoate-containing buffer……48

Figure 4.15. Residual activity of FDH incubated with 100 mM sodium formate-containing buffer……49

Figure 4.16. Residual absorbance of $NADP^+$ incubated at different temperatures over time……49

Figure 4.17. Residual absorbance of NADPH incubated at different temperatures over time……50

Figure 4.18. Deactivation constants of NADPH incubated at different temperatures……50

Figure 4.19. Activity of *Lb*ADH with NAD(P)H as a function of the concentration of reduced cofactors NAD(P)H……51

Figure 4.20. Activity of *Lb*ADH with NAD(P)H as a function of the concentration of cofactors $NAD(P)^+$……52

Figure 4.21. Activity of *Lb*ADH with NAD(P)H as a function of the concentration of methyl acetoacetate (**MAA**)……52

Figure 4.22. Activity of *Lb*ADH with NAD(P)H as a function of the concentration of (*R*)-methyl-3-hydroxybutanoate (**MHB**)……...53

Figure 4.23. Activity of FDH as a function of the concentration of formate……...54

Figure 4.24. Activity of FDH as a function of the concentration of $NADP^+$……...54

Figure 4.25. Activity of FDH as a function of the concentration of NADPH……..55

Figure 4.26. Concentration profile of reactants in an enzyme-coupled batch as a function of time……56

Figure 4.27. Concentration of (*R*)-methyl-3-hydroxybutanoate (**MHB**) in an enzyme-coupled repetitive batch run as a function of time…….57

Figure 4.28. Overall activity of enzyme-coupled repetitive batch run as a function of time……...57

Figure 4.29. Activities of ADH and FDH in enzyme-coupled repetitive batch run as a function of time……...58

Figure 4.30. Scheme of enzyme-coupled continuous run in an enzyme membrane reactor……59

Figure 4.31. Conversion of methyl acetoacetate (**MAA**) as a function of the number of residence time in an enzyme-coupled continuous reactor……...59

Figure 4.32. Concentration profile of reactants as a function of the number of residence time in an enzyme-coupled continuous reactor……...60

Figure 4.33. Activity of *Lb*ADH as a function of the number of residence time in an enzyme-coupled continuous reactor……...60

Figure 4.34. Activity of FDH as a function of the number of residence time in an enzyme-coupled continuous reactor……..…….61

Figure 4.35. Equilibrium of carbon dioxide in solution, with the pH range for the dominant species……...62

Figure 5.1. Enantioselective reduction of methyl acetoacetate (**MAA**) to (*R*)-methyl-3-hydroxybutanoate (**MHB**) with resting whole cells of *Escherichia coli* BL21 Star (DE3)…….....64

Figure 5.2. Concentration of reactants in a batch reactor with different modes of genetically transformed biocatalysts as a function of time……65

Figure 5.3. Enzymatic activity of FDH and ADH of the different modes of genetic transformed rec. *E. coli*……..65

Figure 5.4. Comparison of the effects of different fermentation protocols on the activity of rec. *E. coli*……..…..67

Figure 5.5. Comparison of the effects of baffles (B) in fermentation shakeflasks on the activity of rec. *E. coli*……67

Figure 5.6. Fermentation profile of rec. *E. coli* (with and without induction)…...68

Figure 5.7. Residual activity of induced rec. *E. coli* in various storage conditions…….69

Figure 5.8. Activity of induced rec. *E. coli* stored in phosphate buffer over time……...70

Figure 5.9. Batch activity of rec. *E. coli* in different biotransformation media…..71

Figure 5.10. Activity of rec. *E. coli* as a function of pH……...72

Figure 5.11. Activity of rec. *E. coli* as a function of temperature……73

Figure 5.12. Activity of rec. *E. coli* as a function of the concentration of methyl acetoacetate (**MAA**)……74

Figure 5.13. Activity of rec. *E. coli* as a function of the concentration of (*R*)-methyl-3-hydroxybutanoate (**MHB**)……74

Figure 5.14. Activity of rec. *E. coli* (in terms of formate consumption) as a function of the concentration of formate……75

Figure 5.15. Activity of rec. *E. coli* (in terms of formation of (*R*)-methyl-3-hydroxybutanoate (**MHB**)) as a function of the concentration of formate…….……75

Figure 5.16. Concentration of reactants in a batch reactor as a function of time……...76

Figure 5.17. Scheme of CSTR setup……77

Figure 5.18. Production of (*R*)-methyl-3-hydroxybutanoate (**MHB**) with the CSTR setup (left) and a close-up on the reactor and ultrafiltration membrane (right)……...…..77

Figure 5.19. Concentration profile of reactants in the CSTR as a function of the number of residence time……....78

Figure 5.20. Conversion of methyl acetoacetate (**MAA**) as a function of the number of residence time in the CSTR……...78

Figure 5.21. Concentration of reactants in repetitive batch studies as a function of time……..81

Figure 5.22. Activities of rec. *E. coli* in repetitive batch systems containing different chemicals……..…….82

Figure 5.23. Deactivation constants of rec. *E. coli* in repetitive batch systems containing different chemicals…….82

Figure 5.24. Yield of (*R*)-methyl-3-hydroxybutanoate (**MHB**) in a batch reactor as a function of the ratio of methyl acetoacetate (**MAA**) to formate...83

Figure 5.25. Activity in a batch reactor as a function of the ratio of methyl acetoacetate (**MAA**) to formate……....84

Figure 5.26. Concentration of (*R*)-methyl-3-hydroxybutanoate (**MHB**) in a repetitive batch run containing phosphate buffer as biotransformation medium as a function of time……..…...85

Figure 5.27. Concentration of (*R*)-methyl-3-hydroxybutanoate (**MHB**) in a repetitive batch run containing minimal medium as biotransformation medium as a function of time……...…85

Figure 5.28. Comparison of residual activity in a repetitive batch containing phosphate buffer and minimal medium as biotransformation media……..……...86

Figure 6.1. Enantioselective reduction of (2,5)-hexanedione (**A**) to (5*R*)-hydroxyhexane-2-one (**B**) with resting whole cells of *Lactobacillus kefiri* or enzyme-coupled system……....87

Figure 6.2. Comparison of biocatalyst consumption with respect to whole cell immobilisation, reactor setup and the use of enzymes…….88

Figure 6.3. Comparison of space-time yield (STY) with respect to whole cell immobilisation, reactor setup and the use of enzymes…….89

Figure 6.4. Comparison of deactivation constant with respect to whole cell immobilisation and reactor setup…….89

Figure 6.5. Comparison of production cost with respect to whole cell immobilisation, reactor setup, the use of enzymes and sale price of the process by Juelich Fine Chemicals GmbH (JFC)……...90

Figure 6.6. Comparison of production cost with respect to costs of biocatalyst, immobilisation matrix, substrate and cofactors……91

Figure 6.7. Thermodynamic equilibrium of (5*R*)-hydroxyhexane-2-one (**B**) and (*R*)-(2,5)-dimethyl-tetrahydrofuran-2-ol……....93

Figure 6.8. Enantioselective reduction of methyl acetoacetate (**MAA**) to (*R*)-methyl-3-hydroxybutanoate (**MHB**) with resting whole cells of recombinant *Escherichia coli* or enzyme-coupled system……..….94

Figure 6.9. Comparison of biocatalyst consumption with respect to the use of whole cells or enzymes and reactor setup……..……..94

Figure 6.10. Comparison of deactivation constant with respect to whole cells or enzymes and reactor setup……...95

Figure 6.11. Comparison of production cost with respect to the use of whole cells or enzymes and reactor setup……...96

Figure 6.12. Comparison of production cost with respect to costs of biocatalyst, substrate and cofactors……97

Figure 6.13. Comparison of activity of wild type *L. kefiri*, rec. *E. coli* and isolated enzyme-coupled system in a batch reduction of (2,5)-hexanedione (**A**)……..….99

Figure 6.14. Comparison of activity of wild type *L. kefiri*, rec. *E. coli* and isolated enzyme-coupled system in a batch reduction of methyl acetoacetate (**MAA**)……....99

Figure 9.1. Gas chromatogram of ethanol (2.9 min), (2,5)-hexanedione (**A**) (12.0 min), (5*R*)-hydroxyhexane-2-one (**B**) (13.7 min) and (2*R*,5*R*)-hexanediol **(C)** (18.8 min) with *n*-butanol (7.0 min) as internal standard……117

Figure 9.2. Gas chromatogram of (2,5)-hexanedione (**A**) (11.6 min), (5*R*)-hydroxyhexane-2-one (**B**) (9.9 min), (5*S*)-hydroxyhexane-2-one (10.3 min), (2*R*,5*R*)-hexanediol **(C)** (9.0 min) and (2*S*,5*S*)-hexanediol (7.9 min)……..118

Figure 9.3. Gas chromatogram of methyl acetoacetate (**MAA**) (10.6 min) and (*R*)-methyl-3-hydroxybutanoate (**MHB**) (11.5 min) with *n*-butanol (6.9 min) as internal standard……119

Figure 9.4. Gas chromatogram of methyl acetoacetate (**MAA**) (17.5 min), (*R*)-methyl-3-hydroxybutanoate (**MHB**) (10.8 min) and (*S*)-methyl-3-hydroxybutanoate (8.6 min)……119

Figure 9.5. High pressure liquid chromatogram of glucose (10.8 min) detected with an evaporative light scattering detector……...120

Figure 9.6. High pressure liquid chromatogram of lactate (14.9 min) and acetate (17.4 min) detected with a diode array detector……120

Figure 9.7. High pressure liquid chromatogram of formate (16.1 min) detected with a diode array detector……121

Figure 9.8. Full spectrum of nuclear magnetic resonance analysis of (5*R*)-hydroxyhexane-2-one (**B**)……..122

Figure 9.9. Zoomed spectrum (20 – 70 ppm) of nuclear magnetic resonance analysis of (5*R*)-hydroxyhexane-2-one (**B**)……122

Figure 9.10. Summary of genetic work on *Escherichia coli* (www.accessexcellence.org)……...…123

Figure 9.11. Amplification of plasmids……..124

Figure 9.12. Summary of fermentation and induction protocol for rec. *E. coli*….125

List of Tables

Table 1.1. Examples of recombinant *Escherichia coli* transformant cells coexpressing carbonyl reductase and cofactor regeneration systems....9

Table 3.1. De Man-Rogosa-Sharpe (MRS) medium composition for fermentation of *Lactobacillus kefiri* DSM 20587……15

Table 3.2. Cell lysis attempts on *L. kefiri* and the detection of residual (2*R*,5*R*)-hexanediol (**C**)……19

Table 3.3. Summary of comparison of the different immobilisation matrices…..27

Table 3.4. Summary of results from NaCS-immobilised PFR……..34

Table 4.1. Kinetics constants of NAD(P)H-bounded *Lb*ADH……..53

Table 4.2. Kinetics constants of $NADP^+$-dependent FDH……55

Table 4.3. Summary of results from enzyme-coupled batch run.……56

Table 4.4. Summary of results from enzyme-coupled repetitive batch run..……58

Table 4.5. Summary of results from continuous run of enzyme-coupled system……..62

Table 5.1. Luria-Bertani (LB) medium composition for fermentation of *Escherichia coli* BL21 Star (DE3)……..66

Table 5.2. Highly enriched minimal medium composition for fermentation of a weak strain of *Escherichia coli* LJ110…….71

Table 5.3. Repetitive batch investigations for rec. *E. coli* system.……80

Table 6.1. Summary of the different means to produce (5*R*)-hydroxyhexane-2-one (**B**)……..92

Table 6.2. Summary of the different means to produce (*R*)-methyl-3-hydroxybutanoate (**MHB**)……96

Table 6.3. Comparison of kinetics constants of NAD(P)H-bounded *Lb*ADH and rec. *E. coli*……98

Table 9.1. MRS medium composition for fermentation of *Lactobacillus kefiri* DSM 20587……...125

Table 9.2. Luria-Bertani (LB) medium composition for fermentation of *Escherichia coli* BL21 Star (DE3)……126

List of Abbreviations and Symbols

List of Abbreviations

A	(2,5)-Hexanedione
ADH	Alcohol dehydrogenase
AR	Aldehyde reductase
B	Baffles
B	(5*R*)-Hydroxyhexane-2-one
Biocat	Biocatalyst
C	(2*R*,5*R*)-Hexanediol
Conc.	Concentration (mM)
*CP*CR	*Candida parapsilosis* carbonyl reductase
CR	Carbonyl reductase
CS	Cellulose sulphate
CSTR	Continuously stirred tank reactor
e^-	Electron
EMR	Enzyme membrane reactor
FDH	Formate dehydrogenase
FG	Functional group
GC	Gas chromatohraphy
GDH	Glucose dehydrogenase
HPLC	High pressure liquid chromatography
ID	Inner diameter (mm)
IPTG	Isopropyl-β-D-thiogalactopyranoside
Immob	Immobilised
ind	Induced
JFC	Juelich Fine Chemicals GmbH
KP_i	Potassium phosphate buffer
LB	Luria-Bertani medium
*Lb*ADH	*Lactobacillus brevis* alcohol dehydrogenase
MAA	Methyl acetoacetate
MHB	(*R*)-Methyl-3-hydroxybutanoate
MRS	De Man-Rogosa-Sharpe
Min. med.	Minimal medium
NaCS	Sodium cellulose sulphate
$NAD(P)^+$	Nicotinamide cofactor (phosphorylated), oxidised
NAD(P)H	Nicotinamide cofactor (phosphorylated), reduced
NMR	Nuclear magnetic resonance
O.D.	Optical density
o.d.	Outer diameter (mm)
ox	Oxidised
PDADMAC	Poly(diallyldimethylammonium chloride)

PFR	Plug flow reactor
PMMA	Poly(methyl methacrylate)
Prod	Production
PVA	Polyvinyl alcohol
R	*R*-isomer
rec.	Recombinant
red	Reduced
Rep. batch	Repetitive batch
S	*S*-isomer
Std	Standard
TFAA	Trifluoroacetic acid anhydride
Vit.	Vitamin
wcw	Wet cell weight
w/o	Without
ZCH	Department of Central Analytics

List of Symbols

ε	Fraction of porosity (-)
λ	Wavelength (nm)
θ	Number of residence time of one column or reactor (-)
θ_{PFRs}	Total number of residence time for PFR setup (-)
τ	Residence time of one column or reactor (h)
τ_{PFRs}	Total residence time for PFR setup (h)
A	Activity (U mg^{-1})
A_0	Initial activity (U mg^{-1})
C_A	Concentration of (2,5)-hexanedione (mM)
C_{A0}	Initial concentration of (2,5)-hexanedione (mM)
C_B	Concentration of (5*R*)-hydroxyhexane-2-one (mM)
C_C	Concentration of (2*R*,5*R*)-hexanediol (mM)
$C_{Acetate}$	Concentration of acetate (mM)
$C_{Ethanol}$	Concentration of ethanol (mM)
$C_{Formate}$	Concentration of formate (mM)
$C_{Glucose}$	Concentration of glucose (mM)
$C_{Lactate}$	Concentration of lactate (mM)
C_{MAA}	Concentration of methyl acetoacetate (mM)
C_{MAA0}	Initial concentration of methyl acetoacetate (mM)
C_{MHB}	Concentration of (*R*)-3-methyl-hydroxybutanoate (mM)
C_R	Concentration of (*R*)-isomer (mM)
C_S	Concentration of (*S*)-isomer (mM)
de	Diastereomeric excess (%)
E	Extinction (-)
E_a	Activation energy (kJ mol^{-1})
E_d	Deactivation energy (kJ mol^{-1})
E_0	Initial extinction (-)
ee	Enantiomeric excess (%)
K_i, K_m	Michealis-Menten constants (mM)
k, k_1, k_2, k_{MAA}	Reaction rate constant (min^{-1})

k_d	Rate of denaturation (min^{-1})
k_{des}	Deactivation constant (h^{-1}, % h^{-1})
M	Molecular weight (-)
m	Mass (g)
n	Molar amount (mol)
R	Rate constant (8.314 J mol^{-1} K^{-1})
r_A	Rate of reaction with respect to (2,5)-hexanedione (mM min^{-1})
r_B	Rate of reaction with respect to (5*R*)-hydroxyhexane-2-one (mM min^{-1})
r_C	Rate of reaction with respect to (2*R*,5*R*)-hexanediol (mM min^{-1})
r_{MAA}	Rate of reaction with respect to methyl acetoacetate (mM min^{-1})
r_{MHB}	Rate of reaction with respect to (*R*)-methyl-3-hydroxybutanoate (mM min^{-1})
STY	Space-time yield (g L^{-1} h^{-1}, g L^{-1} d^{-1})
T	Temperature (K)
t	Time (min, h)
ttn	Total turnover number (g g^{-1}, mol mol^{-1})
U	Rate of change of chemical (µmol min^{-1})
V	Volume of reactor (mL, L)
V_{biocat}	Volume occupied by NaCS immobilised cells (mL)
V_{PFR}	Volume of PFR column (mL)
v	Activity (U mg^{-1}, U g^{-1})

1 Introduction

1.1 Chiral alcohols

Chiral alcohols are versatile building blocks for fine chemicals, for example, in pharmaceuticals and agrochemicals (Ager, 1999; Liese et al., 2000a). In general, organic chemical syntheses yield alcohols of various isomers. In order to produce enantiopure chiral alcohols through organic synthesis, among others optical resolution of racemic alcohols is employed. Several asymmetric catalysts, such as BINAP, were developed and used for the asymmetric synthesis of chiral alcohols (Mikami et al. 2000; Noyori and Ohkuma 2001).

On the other hand, biocatalysts can rival conventional chemical catalysts in terms of its chemo-, regio- and stereo-selectivity (Yamada and Shimizu, 1988; Koeller and Wong, 2001). In addition, the mild working conditions needed for biocatalysis are becoming more attractive for industrial production (Liese et al., 2000a; Ogawa and Shimizu, 2002; Schmid et al., 2001; Straathof et al., 2002). In 2003, Frost and Sullivan reported that the use of biocatalysis in chiral technologies would increase from 10 % in 2002 to 22 % in 2009. Therefore, biocatalysts may increasingly also be used as promising catalysts for the asymmetric production of chiral alcohols.

In this work, the syntheses of two classes of chiral alcohols are of interest: γ-Hydroxyketones and 3-hydroxybutanoates (Figure 1.1).

Figure 1.1. Structures of γ-hydroxyketones and 3-hydroxybutanoates where R1, R2 and R3 refer to alkyl groups.

1.1.1 γ-Hydroxyketones

γ-Hydroxyketones can be used as intermediates in the preparation of optically active tetrahydrofurans used in biodegradable polymers, perfumes and in medicines (Watanabe et al., 1998). Additionally, follow-up chemistry on the keto and hydroxy groups of the γ-hydroxyketones would yield a broad range of other possible interesting intermediates. In particular, (5*R*)-hydroxyhexane-2-one can be reduced to its corresponding (2*R*,5*R*)-hexanediol, which is an intermediate of the DuPHOS catalyst (Figure 1.2).

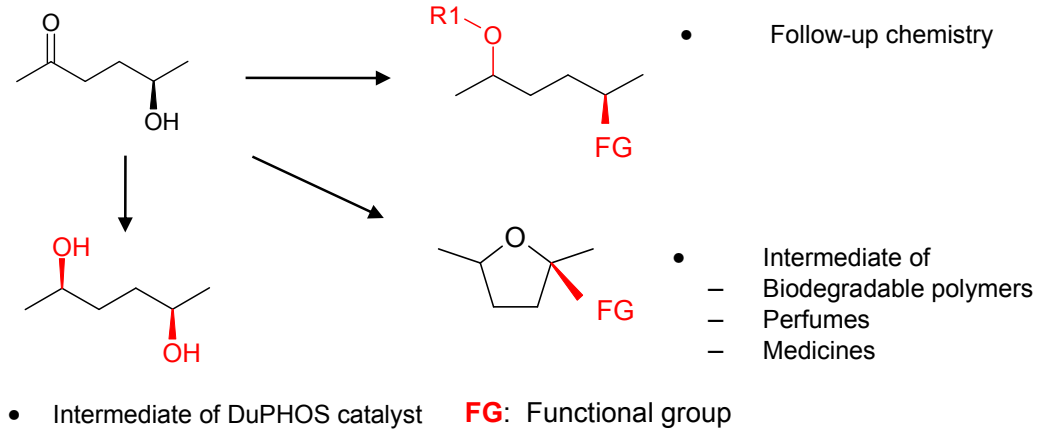

Figure 1.2. Products from (5*R*)-hydroxyhexane-2-one.

To date, only 3 known chemical methods exist to obtain (5*R*)-hydroxyhexane-2-one. Firstly, the oxidation of (2*R*,5*R*)-hexanediol with silver carbonate-Celite yielded 46 % of (5*R*)-hydroxyhexane-2-one with a low enantiomeric excess (*ee*) of 71 % (Davis et al., 1977). Secondly, the asymmetric hydrogenation of 2,5-hexanedione with chemically modified nickel catalysts gave a broad range of yields (7 - 83 %) with very low enantiopurity (0.3 - 7.3 % *ee*) of (5*R*)-hydroxyhexane-2-one (Brunner et al., 1991). Both processes gave very low optical purity and low yield of (5*R*)-hydroxyhexane-2-one, and therefore, the product cannot be used industrially. The last chemical method involved the asymmetric hydrogenation of 2,5-hexanedione with a range of optically active ruthenium phosphine complexes, where high optically pure (5*R*)-hydroxyhexane-2-one (82.7 - above 99 % *ee*) with moderate to high yields (38 – 86 %) was obtained (Watanabe et al., 1998). However, the main drawback of this process besides its long reaction time was the high operating pressure of 50 bar.

(5*R*)-hydroxyhexane-2-one can also be made by biotechnological means. It was produced as an intermediate in two whole cell biotransformation processes using resting cells of *Lactobacillus kefiri* DSM 20587 (Hummel et al., 2000; Haberland et al., 2002a, 2002b) and *Pichia farinosa* IAM 4682 (Ikeda et al., 1996). In both processes that were optimised in view of the respective diol synthesis, (5*R*)-hydroxyhexane-2-one was not the target product and as such, no specific data on it was given. Studies by other researchers have shown that the isolated enzyme alcohol dehydrogenase (ADH) from *Lactobacillus kefiri* or *Lactobacillus brevis* (Bradshaw et al., 1992; Hummel, 1997; Wolberg et al., 2000) was a suitable biocatalyst for the reduction of keto-groups to form (*R*)-alcohols of high yields and enantioselectivities. Therefore, it would also be possible to form (5*R*)-hydroxyhexane-2-one starting from (2,5)-hexanedione as starting material with the use of ADH as biocatalyst. However, as in the cases with the whole cell biotransformations, no data on the enzymatic production of (5*R*)-hydroxyhexane-2-one were known.

Before the start of this work, enantiopure hydroxyketone (5*R*)-hydroxyhexane-2-one could not be purchased from ordinary suppliers/companies as there was no efficient and simple process available for its production. However, an industrial biocatalytic process by Juelich Fine Chemicals GmbH producing (2*R*,5*R*)-hexanediol on a 50-kg

scale yielded (5*R*)-hydroxyhexane-2-one as an intermediate (Figure 1.3). With an inexpensive starting material of (2,5)-hexanedione, a high-value product (2*R*,5*R*)-hexanediol was obtained. Recently, an initial sample of (5*R*)-hydroxyhexane-2-one was commercialised at a high price under Fluka.

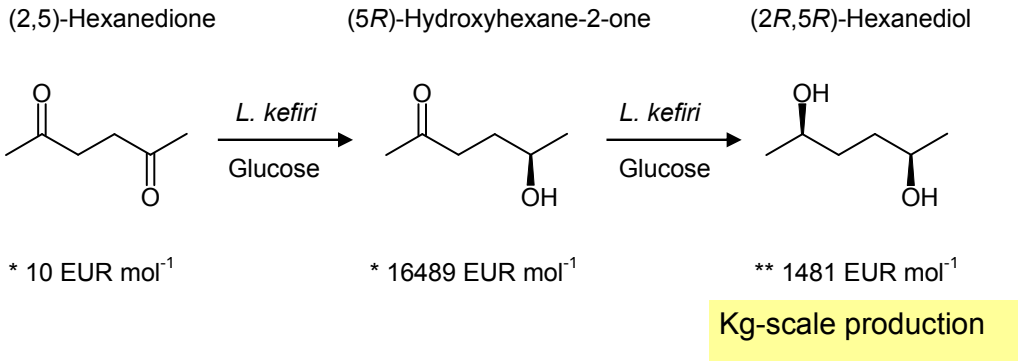

Figure 1.3. Industrial route to (2*R*,5*R*)-hexanediol by whole cell biotransformation with *Lactobacillus kefiri* DSM 20587. Prices quoted are from *Fluka (2005/2006) and **Juelich Fine Chemicals GmbH (2004) catalogues.

1.1.2 3-Hydroxybutanoates

3-Hydroxybutanoates have been widely employed as synthetic intermediates (Carnell et al., 2004). The chiral alcohols are used in the syntheses of β–lactam antibiotics and β–lactamase inhibitors (Nakai and Chiba, 1986), and as building blocks for a wide range of other useful intermediates (Seebach and Zueger, 1982; Seebach et al., 1993) like (*R*)-hydroxybutyrolactone (Fraeter, 1979; Seebach and Zueger, 1985; Kramer and Pfanler, 1982) and (*R*)-1,3-butanediol. 3-Hydroxybutanoates are also employed in the syntheses of phosphorous ligands by Kolbe electrochemical coupling for (*R*,*R*) and (*S*,*S*)-2,5-hexanediols, which are subsequently used in the production of DuPHOS catalysts (Burk et al., 1991, 1992). In particular, (*R*)-methyl-3-hydroxybutanoate is used in the manufacture of the anti-glaucoma drug, Trusopt (Blacker and Holt, 1997). A summary of some important intermediates of 3-hydroxybutanoates is illustrated in Figure 1.4.

To date, there exist 5 known chemical and biotransformations routes to obtain (*R*)-3-hydroxybutanoates. Firstly, homogeneous catalysis with BINAP or BIFAPS catalysts gave excellent enantiopurity and yield of (*R*)-methyl-3-hydroxybutanoate of above 99 % (Gelpke AES et al., 1999). However, the processes are expensive and require a high operating pressure (4 bar) and temperature (60 °C) (Wolfson et al., 2003; Kitamura et al., 1993). The second means to obtain (*R*)-methyl-3-hydroxybutanoate was by heterogeneous catalysis with modified Raney nickel catalyst. Kukula and Červený (2002) demonstrated that at best, only 80 % *ee* and 95 % yield of (*R*)-methyl-3-hydroxybutanoate was obtained, in addition to the high pressure (10 bar) applied at 60 °C.

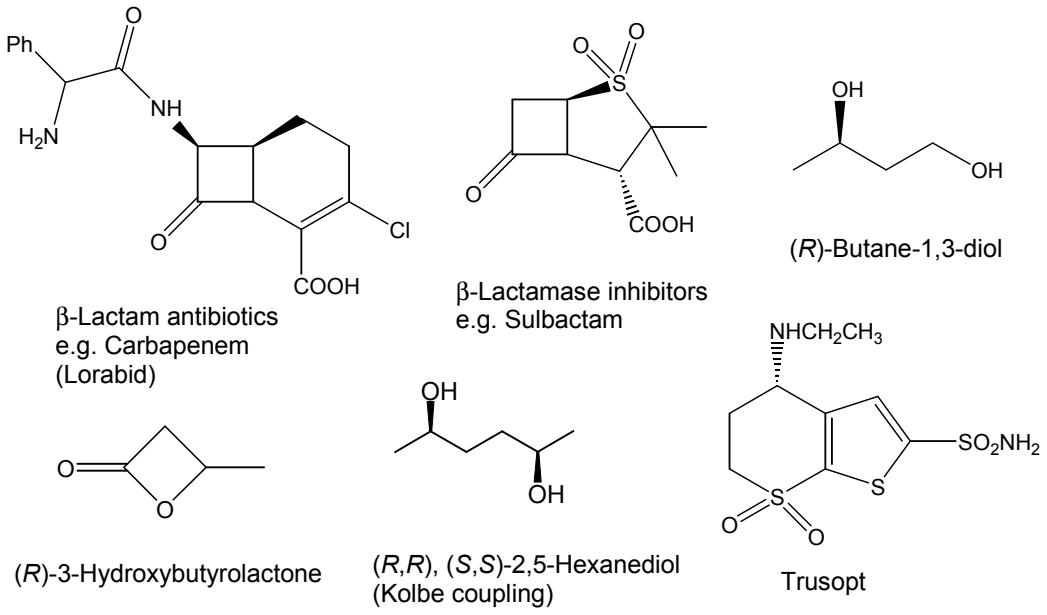

Figure 1.4. Products of 3-hydroxybutanoates.

When whole cell biotransformations were explored, the processes gave varied enantiopurity and productivity of (*R*)-3-hydroxybutanoates. As most wild type microorganisms usually possess (*S*)- rather than (*R*)-specific carbonyl reductases for the bioreduction of β-ketoesters, not much data are available for the production of (*R*)-3-hydroxybutanoates with wild type microorganisms. Ribeiro et al. (2003) reported that *Aspergillus niger* and *Kluyveromyces marxianus* yielded low enantiomeric excess of the (*R*)-isomer at 30 and 18 % respectively. Wild type *Saccharomyces cerevisiae* was found to produce the (*S*)-isomer predominantly, but there appeared to be a shift in enantioselectivity of the biocatalyst in the long term (Chin-Joe et al., 2002a, b). Low productivity was also observed by Seebach et al. (1990) with the use of baker's yeast.

On the other hand, with recombinant *Escherichia coli* coexpressing carbonyl reductases from *Lactobacillus brevis*, *Sporobolomyces salmonicolor* or *Candida magnoliae* as biocatalyst in place of wild type microorganisms, high enantioselectivity (above 95 % *ee*) and yield (above 92 %) of the processes were obtained (Ernst et al., 2003, 2005; Kataoka et al., 1997, 1999, 2003; Shimizu et al., 1998; Yamamoto et al., 2002). However, no data were given on the long term stability of the processes.

The fourth method to produce (*R*)-3-hydroxybutanoates was by enzymatic biotransformations through the use of lipases or dehydrogenases (Carnell et al., 2004). The main drawback of using the lipase resolution method to yield the (*R*)-isomer was the lack of efficient means to recycle the (*S*)-isomer. On the other hand, the use of dehydrogenases with efficient cofactor recycling could yield a kilogram-scale production of high space-time yield (Daussmann, 2005).

Lastly, (*R*)-methyl-3-hydroxybutanoate could be produced from alcoholysis of the biopolymer 3-hydroxybutanoate. In this process, high enantiomeric excess of above 98 % and relatively high yield of 78 % of (*R*)-methyl-3-hydroxybutanoate was obtained (Seebach et al., 1993).

An example of a cost-effective production of (*R*)-methyl-3-hydroxybutanoate was developed with the use of isolated enzymes (alcohol dehydrogenase from *Lactobacillus brevis Lb*ADH). The process is now commercialised on a ton scale by Juelich Fine Chemicals GmbH and Wacker Chemie (Figure 1.5).

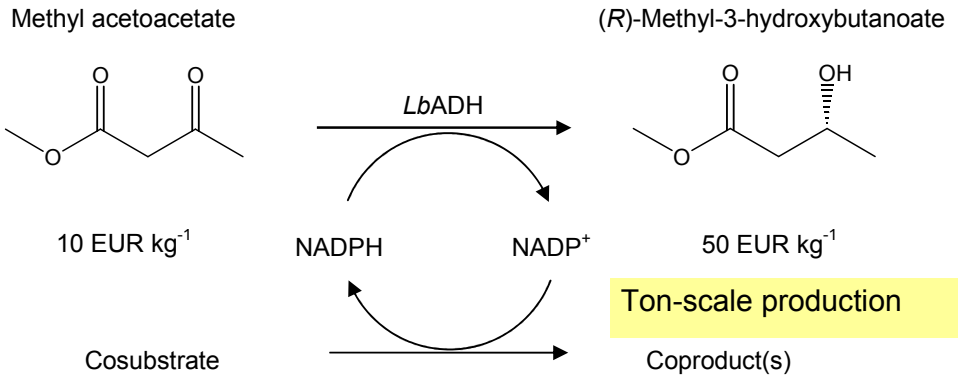

Figure 1.5. Industrial route to (*R*)-methyl-3-hydroxybutanoate by isolated enzymes (*Lactobacillus brevis* alcohol dehydrogenase *Lb*ADH) with cofactor regeneration by means of isopropanol. Prices quoted are from Juelich Fine Chemicals GmbH (2004) catalogue.

1.2 Biocatalysts

Production of chiral alcohols by bioreduction of prochiral carbonyl compounds with microbial cells and commercially available oxidoreductases have been widely investigated (Csuk and Glaenzer, 2000; D'Arrigo et al., 2000; Grunwald et al., 1986; Hummel, 1999; Kula and Kragl, 2000; Liese et al., 2000a; Mori, 2000; Mueller et al., 2005; Patel et al., 1992; Wong et al., 1985). The use of isolated enzymes and microorganisms (wild type and genetically modified) as biocatalysts for the reduction of prochiral ketones to chiral alcohols is briefly discussed here.

1.2.1 Isolated enzymes

The bioreduction of carbonyl compounds with oxidoreductases require cofactors. To ensure a sufficient amount of cofactors for the bioreduction, regeneration of the cofactors in the system is employed. There are a variety of ways to regenerate cofactors enzymatically (Chenault et al., 1988). Two enzymatic systems (substrate-coupled and enzyme-coupled) incorporating cofactor regeneration during the reduction of ketones to alcohols are illustrated in Figure 1.6 (Kroutil et al., 2004).

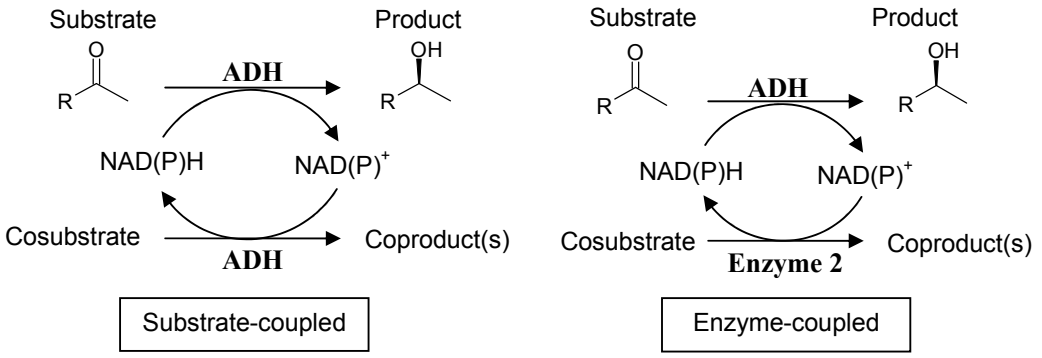

Figure 1.6. Cofactor regeneration with substrate-coupled (left) and enzyme-coupled (right) system.

In the substrate-coupled system, the use of one enzyme, an alcohol dehydrogenase (ADH), is used for the reduction of a substrate (ketone) to its product (alcohol) with the use of the reduced cofactors NAD(P)H. The recycling of the cofactors was achieved through the oxidation of a cosubstrate (alcohol) to its coproduct (aldehyde or ketone) with the same ADH, but utilising the oxidised cofactors $NAD(P)^+$. Examples of this system were given by Schubert et al. (2001), Wolberg et al. (2001) and Villela (2003) where isopropanol was used as a cosubstrate to regenerate the cofactors. In order to obtain high conversion of the substrate (ketone), a large amount of cosubstrate (isopropanol) was required to drive the thermodynamic equilibrium in the desired direction. However, the high concentration of coproduct could be toxic or inhibitory to the enzyme (Kula and Kragl, 2000). To reduce the amount of undesired coproducts in the system, additional techniques like stripping with air and pervaporation could be employed (Stillger et al., 2002, 2004).

On the other hand, the enzyme-coupled system involves the use of two separate enzymes. The alcohol dehydrogenase (ADH) reduces the substrate to its product with the use of reduced cofactors NAD(P)H while the second enzyme, for instance, formate dehydrogenase (FDH) oxidises the cosubstrate formate to its product carbon dioxide with the use of the oxidised cofactors $NAD(P)^+$, and thereby simultaneously recycles the cofactors in the system. Examples of this system have been widely explored by Eckstein et al. (2004), Groeger et al. (2003), Rissom (1999) and Tishkov et al. (1999).

A variety of ways other than enzymatic means to regenerate cofactors has also been developed (Vuorilehto et al., 2004; Wichmann and Vasic-Racki, 2005). Figure 1.7 summarises the use of electrochemical reactions (direct cathodic reduction, indirect-electrochemical regeneration and indirect electroenzymatic regeneration) as one feasible route to regenerate cofactors (Hollmann and Schmid, 2004). Cofactors could additionally be regenerated by photochemical means. A review of the electro- and photo-chemical routes by Hollmann and Schmid (2004) is referred to for in depth information.

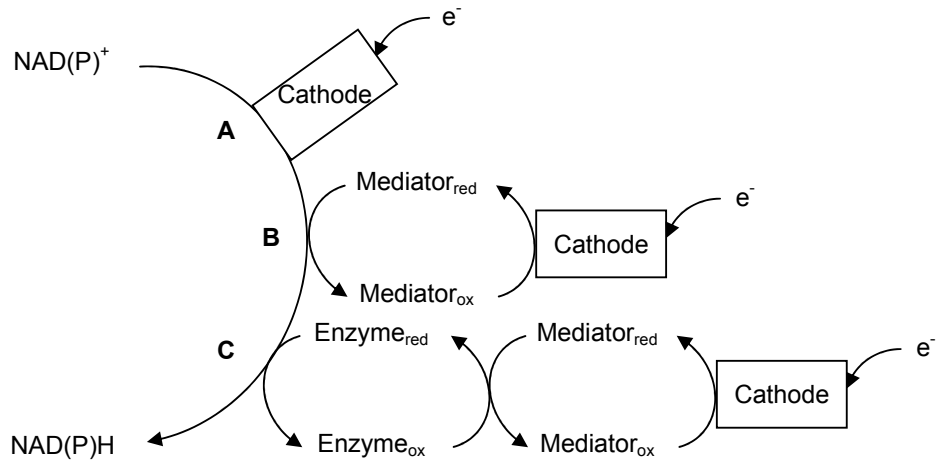

Figure 1.7. Alternative routes for the electrochemical regeneration of NAD(P)$^+$ from NADPH. A: Direct cathodic reduction, B: Indirect-electrochemical regeneration, C: Indirect electroenzymatic regeneration (Hollmann and Schmid, 2004).

1.2.2 Wild type microorganism *Lactobacillus kefiri*

Lactobacillus kefiri DSM 20587 (previously known as *Lactobacillus kefir*, Trueper and De' Clare, 1997) was discovered by Kandler and Kunath (1983) from kefir grains. This lactic acid bacterium is heterofermentative and cultivated on De Man-Rogosa-Sharpe (MRS) medium (Sharpe, 1981). It consists of gram-positive, non motile and non spore-forming rods with rounded ends, and is typically 0.7 by 3 - 15 μm long, with a tendency to form chains of short rods or long filaments. Being aerotolerant, it grows better in reduced oxygen concentration, with an optimal growth temperature of 30 °C (Kandler and Kunath, 1983). To date, the metabolism of *L. kefiri* is yet to be fully mapped out (Hummel, 2005). However, it has already been found to be an interesting candidate as a biocatalyst.

Hummel et al. (1989a, b, 1990) have first discovered a new, NAD$^+$-dependent alcohol dehydrogenase from *L. kefiri* capable of enantioselective reduction of prochiral ketones to chiral alcohols. Wong and Bradshaw (1994) have further extended the range of prochiral ketones catalysed by a NADP$^+$-dependent alcohol dehydrogenase from *L. kefiri*. In 1996, Hummel and Riebel have found and characterised a (*R*)-specific and NADP$^+$-dependent alcohol dehydrogenase from *L. kefiri*. The substrate range of this non metal-containing, short-chain, NADP$^+$-dependent alcohol dehydrogenase is broad and it encompasses aromatic, cyclic, polycyclic and aliphatic ketones. Currently, the commercially available alcohol dehydrogenases from *Lactobacillus kefiri* are the NAD$^+$-dependent diacetyl reductase (Hummel, 1997) and a NADP$^+$-dependent reductase (Sigma-Aldrich catalogue, 2004/2005). There exist more than one alcohol dehydrogenases in *L. kefiri* and not all have been fully isolated (Hummel, 2005). Therefore, if whole cells are used as biocatalysts in place of the isolated enzyme, other interesting substrates could be yielded.

Haberland et al. (2002a, b, 2003) have demonstrated that *Lactobacillus kefiri* was a useful biocatalyst for the industrial production of (2*R*,5*R*)-hexanediol (Figure 1.8). One of the advantages of this system over the use of isolated enzymes is the intracellular cofactor regeneration. No additional coupled system is required to recycle the spent cofactors, since it is done by the metabolism of the cell. In addition, the process was much cheaper than the isolated enzyme technology used by Dow Pharma, Cambridge, United Kingdom. However, one of the drawbacks of the whole cell system was the instability of the cells. After 5 days of continuous production of (2*R*,5*R*)-hexanediol, there was an unexplained sudden cell death. One way to enhance the stability of the cells is cell immobilisation, which is discussed in Chapter 1.2.4.

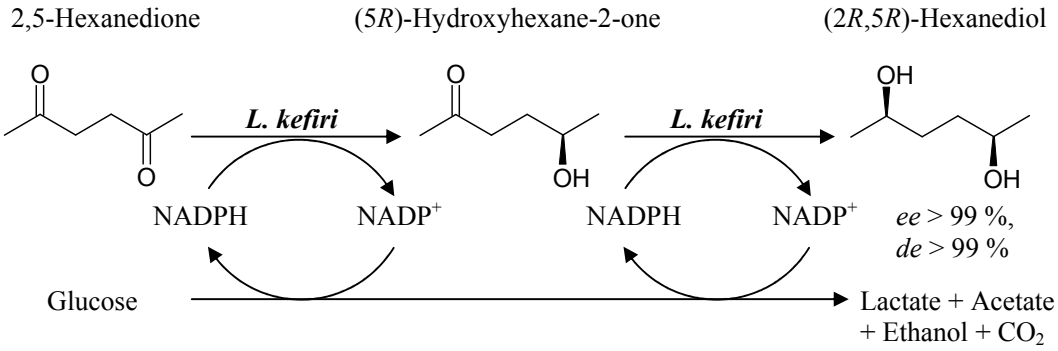

Figure 1.8. Production of (2*R*,5*R*)-hexanediol with whole resting cells of *Lactobacillus kefiri* DSM 20587.

1.2.3 Genetically modified microorganisms

Although some wild type microorganisms are relatively inexpensive, commercially available and their enzymes are rather well-characterised, most of these microbes are not practical for use in industrial production (Kataoka et al., 2003). Baker's yeast or related strains were widely studied as biocatalysts for a broad range of prochiral ketones (Chin-Joe et al., 2002a, b; Csuk and Glaenzer, 1991; D'Arrigo et al., 1997; Komentani et al., 1993; Nakamura et al., 1991; Shieh et al., 1985; Ward and Young, 1990). However, it was found that baker's yeast contains at least 7 NADPH-dependent out of 49 possible carbonyl reductases with different properties (Stewart, 2000). Some of these carbonyl reductases are (*R*)- and others (*S*)-specific. As a result, the enantiomeric excess of the chiral alcohol produced was low when whole cells of baker's yeast containing a bag of enzymes were used (Kataoka et al., 2003; Stewart, 2000).

In order to achieve high enantiopurity of the chiral alcohol when whole cells are used, an effective bioreduction system could be designed in a host cell. The host could contain one or two enzyme systems. In the former, the carbonyl reductase reduces the prochiral ketone and oxidises the cofactor NAD(P)H. Simultaneously, it oxidises the cosubstrate (alcohol) present, producing NAD(P)H in the process, and thereby regenerating the cofactor in the system. This system is similar to the substrate-coupled enzyme system in Chapter 1.2.1. In the two-enzyme system, the carbonyl

reductase is employed for the asymmetric reduction of prochiral ketones to chiral alcohols, while the other enzyme regenerates the cofactor, supplying NAD(P)H which is needed by the carbonyl reductase as a cofactor. This system is similar to the enzyme-coupled system in Chapter 1.2.1. To ensure high productivity of the carbonyl reductase system, there should be sufficient supply of cofactors in the same host cell. However, only a few wild type microorganisms contain high activities of both their carbonyl reductase and cofactor regeneration systems. Various methods like drying by air or acetone have been used to treat the wild type microorganisms, but it was still difficult to construct an efficient bioreduction system with them (Kataoka et al., 2003).

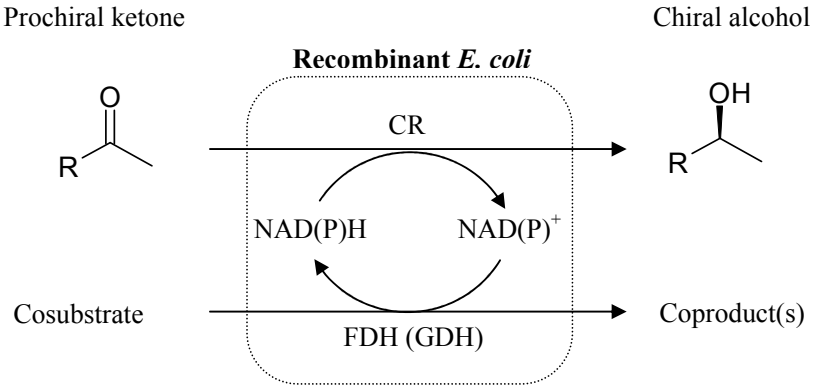

Figure 1.9. Recombinant whole cells transformed with carbonyl reductase (CR) and cofactor regeneration systems with formate dehydrogenase (FDH) or glucose dehydrogenase (GDH).

Table 1.1. Examples of recombinant *Escherichia coli* transformant cells coexpressing carbonyl reductase and cofactor regeneration systems. ADH: Alcohol dehydrogenase, AR: Aldehyde reductase, CR: Carbonyl reductase, FDH: Formate dehydrogenase, GDH: Glucose dehydrogenase.

References	Carbonyl reductase system	Cofactor regeneration system
Ernst et al. (2003, 2005)	NAD(P)H-dependent ADH (*Lactobacillus brevis*)	NAD^+-dependent FDH (*Mycobacterium vaccae*)
Kaluzna et al. (2005), Walton and Stewart (2004), Yang et al. (2005)	NADPH-dependent ADH (*Saccharomyces cerevisiae*)	Glucose metabolism (*Escherichia coli*)
Kataoka et al. (1999, 2003), Shimizu et al. (1999)	NADPH-dependent AR (*Sporobolomyces salmonicolor*)	$NADP^+$-dependent GDH (*Bacillus megaterium*)
Kizaki et al. (2001)	NADPH-dependent CR (*Candida magnoliae*)	$NADP^+$-dependent GDH (*Bacillus megaterium*)

Recently, there have been many approaches of recombinant DNA technology applied to whole cell bioconversion (Endo and Koizumi, 2001; Kataoka et al., 2003). *Escherichia coli* cells transformed with carbonyl reductases and their genes, and cofactor regeneration enzymes and their genes (formate dehydrogenase, FDH, or

glucose dehydrogenase, GDH) have been shown to be promising biocatalysts (Ernst et al., 2003, 2005; Kaluzna et al., 2005; Kataoka et al., 1999, 2003; Kizaki et al., 2001; Shimizu et al., 1998; Stewart, 2000; Walton and Stewart, 2004; Yang et al., 2005). Table 1.1 and Figure 1.9 summarise the two-enzyme system coexpressed in these works, capable of highly enantioselective β-ketoesters reduction. For NADP(H) regeneration, $NADP^+$-dependent glucose dehydrogenase (GDH) or glucose-6-phosphate dehydrogenase could be used in parallel to the NADPH-dependent carbonyl reductase system. However, glucose as a substrate is much cheaper than glucose-6-phosphate and is therefore preferred. On the other hand, formate dehydrogenase (FDH) in recombinant cells preferentially utilises NAD^+ to $NADP^+$, and may lead to an imbalance in cofactor pools in the cells. Lately, there have been many attempts to change the cofactor requirement of NAD^+-dependent formate dehydrogenases (Gul-Karaguler et al., 2001, Serov et al., 2002, Tishkov et al., 1999). However, more work is also needed to further screen for $NAD(P)^+$- or strictly $NADP^+$-dependent formate dehydrogenase if formate dehydrogenase (FDH) is to be efficiently coupled to NADPH-dependent carbonyl reductases in recombinant cells.

1.2.4 Whole cell immobilisation

Whole cell immobilisation can be defined as the physical confinement or localisation of intact cells to a certain defined region of space with the preservation of some desired activity (Karel et al., 1985). The principal methods for whole cell immobilisation are adsorption, covalent binding, encapsulation, entrapment and cross-linking (Figure 1.10, Bickerstaff, 1997). There exist many advantages such as increased chemical and mechanical stability with whole cell immobilisation (Wilaert and Baron, 1996). To date, many industrial applications have been developed using microbial, plant and animal cells. For instance, the production of L-aspartic acid was found to yield higher activities when immobilised cells were used (Sato and Tosa, 1993). In addition, the stability and operational productivity of the immobilised cells were much higher.

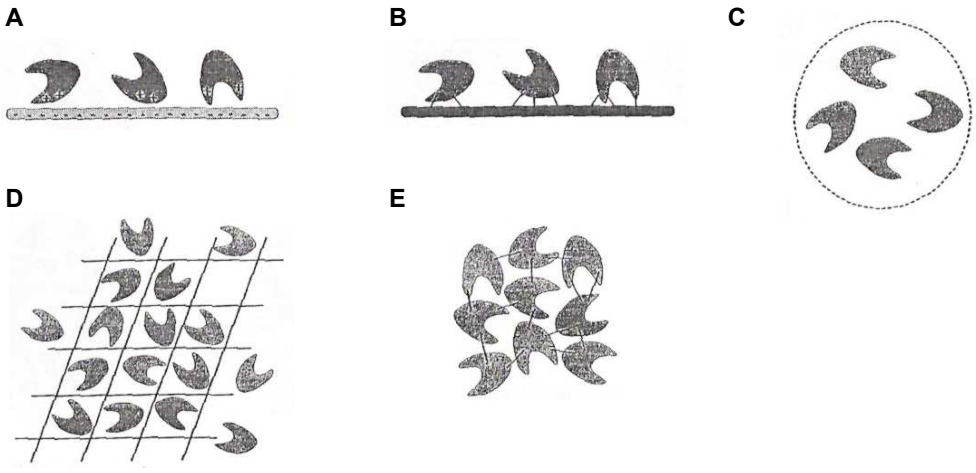

Figure 1.10. Principal methods of immobilisation. A: Adsorption, B: Covalent binding, C: Encapsulation, D: Entrapment, E: Cross-linking (Bickerstaff, 1997).

There are various methods and classifications of cell immobilisation where natural and synthetic materials as suitable immobilisation matrices have been studied (Huebner and Buchholz, 1999; Nedović and Wilaert, 2004; Wilaert and Baron, 1996). One method of cell immobilisation is microencapsulation, where spherical beads of immobilised cells are formed. These spherical immobilisates are best suited for use in bioreactors due to their hydrodynamic characteristics and abrasion resistance properties. This method of cell immobilisation is already widely employed in various fields, ranging from food industry (Groboillot et al., 1994; Sun et al., 1995) to wastewater treatment (Santos et al., 1993) to production of high-value drugs like taxol (Seki and Furusaki, 1996), and even as a controlled drug delivery system in medical treatment (Brown et al., 1995; Chickering et al., 1996; Embleton and Tighe, 1993).

Immobilisation matrices from natural sources like alginate and κ-carrageenan have been intensely investigated due to their mild immobilisation procedures which enable cells to survive the immobilisation procedures (Leenen, 2001; Murano, 1998). In particular, the many applications of immobilised cells of lactic acid bacteria stem from these matrices (Doleyres et al., 2004; Kondo et al., 2004; Scannell et al., 2000). However, one of the main disadvantages of alginate and κ-carrageenan matrices is the dissolution of the material in the presence of chelating chemicals like phosphate, lactate and citrate. To circumvent this, special coating of chitosan to the alginate matrix (Gåserød O, 1999; Klinkenberg et al., 2001; Le-Tien et al., 2004), or addition of locus bean gum to the carrageenan matrix (Arnaud et al., 1989; Audet et al., 1988, 1990; Lacroix et al., 1990) have been shown to strengthen the original matrices. On the other hand, non-toxic and inexpensive synthetic gels like polyvinyl alcohol (Chen and Lin, 1994, Durieux et al., 2000; Jekel et al., 1998; Wittlich and Vorlop, 1998) possessing strong mechanical and chemical stability properties have been used as alternative matrices.

Whole cell immobilisation with polyelectrolytes complexes has also been demonstrated to have strong mechanical and chemical stability (Huebner and Buchholz, 1999). Besides coating of alginates, the combination of cellulose sulphate (CS) and poly(diallyldimethylammonium chloride) (PDADMAC) as materials for microcapsules has been investigated. The CS-PDADMAC microcapsules have been widely applied in fields of gene therapy (Tai and Sun, 1993), monoclonal antibodies production (Mansfeld and Dautzenberg, 1997) and insect cell culture (Huebner and Buchholz, 1997). Although the CS-PDADMAC matrix is gentle enough for insect cells, not much information on microbial cell immobilisation with it are known. To date, only Foerster et al. (1994) and Mansfeld et al. (1995) have used this matrix for immobilisation of microbial cells in the production of citric acid.

2 Aims

The main aim of this work is to investigate the production of chiral alcohols from prochiral ketones with different biocatalysts: Wild type microorganism (*Lactobacillus kefiri*), isolated enzymes (alcohol dehydrogenase from *Lactobacillus brevis* coupled with formate dehydrogenase from *Pseudomonas* sp.) and genetically modified microorganism (*Escherichia coli* BL21 Star (DE3)).

Two classes of chiral alcohols (γ-hydroxyketones and 3-hydroxybutanoates) are of interest:

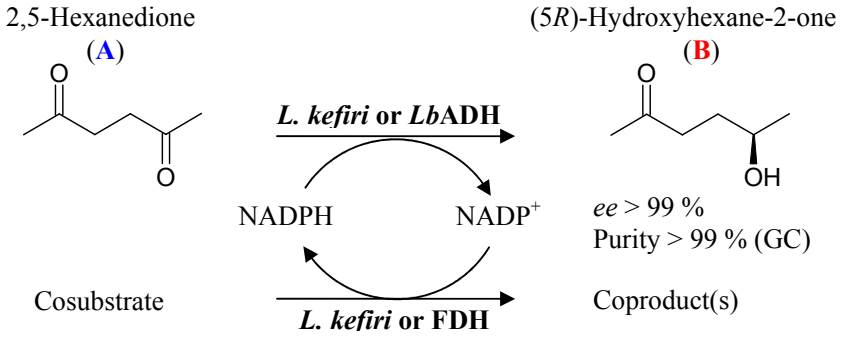

Figure 2.1. Enantioselective reduction of (2,5)-hexanedione (A) to (5*R*)-hydroxyhexane-2-one (B) with resting whole cells of *Lactobacillus kefiri* or enzyme-coupled system (*Lb*ADH: Alcohol dehydrogenase from *Lactobacillus brevis*, FDH: Formate dehydrogenase from *Pseudomonas* sp.).

and

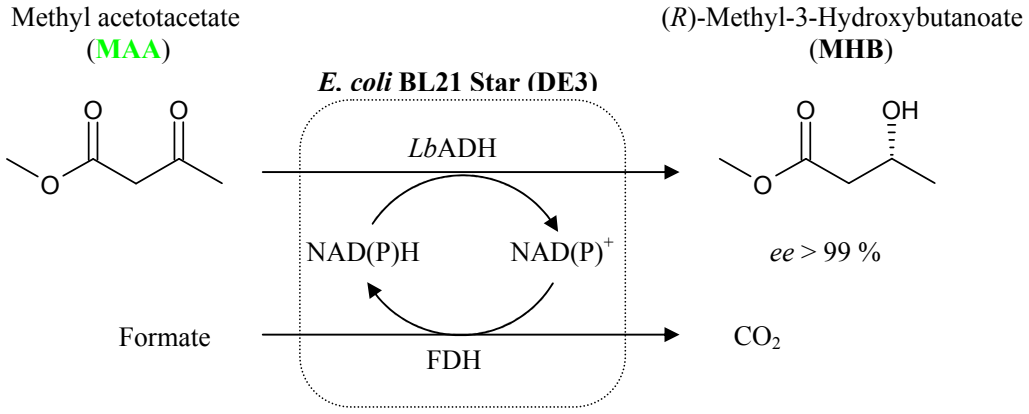

Figure 2.2. Enantioselective reduction of methyl acetoacetate (MAA) to (*R*)-methyl-3-hydroxybutanoate (MHB) with resting whole cells of recombinant *Escherichia coli* or enzyme-coupled system (*Lb*ADH: Alcohol dehydrogenase from *Lactobacillus brevis*, FDH: Formate dehydrogenase from *Pseudomonas* sp.).

In whole cell biotransformation with *Lactobacillus kefiri*, the objectives are:

- Characterisation of non-immobilised cells,
- Characterisation of immobilised cells,
- Determination of the most suitable reactor,
- Downstream processing of (5*R*)-hydroxyhexane-2-one (**B**).

In whole cell biotransformation with rec. *Escherichia coli*, the objectives are:

- Characterisation of transformed cells,
- Development of reactor setups for the synthesis of (*R*)-methyl-3-hydroxybutanoate (**MHB**).

In the isolated enzyme-coupled system (*Lb*ADH and FDH), the objectives are:

- Feasibility of syntheses of (5*R*)-hydroxyhexane-2-one (**B**) and (*R*)-methyl-3-hydroxybutanoate (**MHB**),
- Characterisation of enzymes,
- Kinetics studies and modelling of system producing (*R*)-methyl-3-hydroxybutanoate (**MHB**),
- Development of reactor setups for the synthesis of (*R*)-methyl-3-hydroxybutanoate (**MHB**),
- As comparison studies with whole cell biotransformations.

3 γ-Hydroxyketone Synthesis with Wild Type Biocatalyst *Lactobacillus kefiri*

A process for the whole cell reduction of (2,5)-hexanedione (**A**) to (2*R*,5*R*)-hexanediol (**C**) with wild type biocatalyst *Lactobacillus kefiri* DSM 20587 was established by Haberland *et al.* (2002a, b) (Figure 3.1). Glucose, a cheap cosubstrate, was used to regenerate the cofactors in the cells. In this chapter, the focus is on the synthesis and isolation of the intermediate (5*R*)-hydroxyhexane-2-one (**B**) with resting whole cells of *L. kefiri* by a combination of biotechnological and chemical engineering methods.

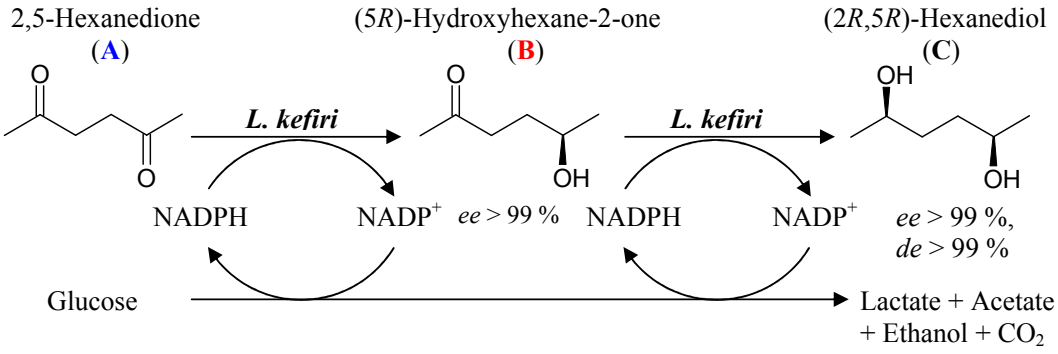

Figure 3.1. Enantioselective reduction of (2,5)-hexanedione (A) to (5*R*)-hydroxyhexane-2-one (B) and subsequently to (2*R*,5*R*)-hexanediol (C) with resting whole cells of *Lactobacillus kefiri*.

3.1 Biocatalyst production

A single pool of biocatalyst of uniform activity was desired for the biosynthesis of (5*R*)-hydroxyhexane-2-one (**B**). Therefore, a large-scale fermentation of *L. kefiri* on a 2800 L-scale was performed by bitop AG. The fermentation protocol with MRS medium (Table 3.1) was similar to that used by De Man *et al.* (1960) and Haberland (2003) where the active biomass was harvested at the stationary growth phase. The harvested cells (10 kg wet biomass) were packed in multiple smaller portions and stored at –20 °C before use.

Table 3.1. De Man-Rogosa-Sharpe (MRS) medium composition for fermentation of *Lactobacillus kefiri* DSM 20587.

Medium composition	Concentration (g L^{-1})
Glucose·H_2O	22
Casein peptone	10
Meat extract	10
Yeast extract	5
Sodium acetate	5
K_2HPO_4	2
Ammonium citrate	2
Tween 80	1
$MgSO_4 \cdot 7H_2O$	0.2
$MnSO_4 \cdot H_2O$	0.05

3.2 General definitions of terms used

In this chapter, a number of general terms would be used with regards to the chemicals and the processes.

The enantiopurity of the desired product (5*R*)-hydroxyhexane-2-one (**B**) is determined by the enantiomeric excess (*ee*), and is defined as:

$$ee = \frac{C_R - C_S}{C_R + C_S} \qquad \text{(eq. 3.1)}$$

The conversion of the process is defined as the amount of (2,5)-hexanedione (**A**) reacted per initial concentration.

$$Conversion = \frac{C_{A0} - C_A}{C_{A0}} \qquad \text{(eq. 3.2)}$$

Due to the consecutive bioreduction, the selectivity of the process, in terms of the desired product (5*R*)-hydroxyhexane-2-one (**B**), is given as the proportion of (5*R*)-hydroxyhexane-2-one (**B**) over the sum of (5*R*)-hydroxyhexane-2-one (**B**) and (2*R*,5*R*)-hexanediol (**C**).

$$Selectivity = \frac{C_B}{C_B + C_C} \qquad \text{(eq. 3.3)}$$

The yields of (5*R*)-hydroxyhexane-2-one (**B**) and (2*R*,5*R*)-hexanediol (**C**) are defined as the fraction of (5*R*)-hydroxyhexane-2-one (**B**) and (2*R*,5*R*)-hexanediol (**C**) obtained respectively per initial amount of (2,5)-hexanedione (**A**).

$$Yield = \frac{C_B}{C_{A0}} \; or \; \frac{C_C}{C_{A0}} \qquad \text{(eq. 3.4)}$$

The biocatalyst consumption of a process is given as the ratio of the amount of wet biomass used per unit mass of (5*R*)-hydroxyhexane-2-one (**B**) obtained.

$$Biocat\ consumption = \frac{m_{wet\ cells}}{m_B} \qquad \text{(eq. 3.5)}$$

This term is similar to the total turnover number (refer to Chapter 4.1 for the definition) used for enzymes. For example, a biocatalyst consumption of 1 g of product (with a molecular weight of 100) per g of cells (wet weight) containing 0.1 % wt of enzymes (with a molecular weight of 100 kD) corresponds to a total turnover number of 10^6.

In determining the most suitable reactor setup for the bioreduction, the characteristics of some reactor setup are considered (Figure 3.2, Liese et al., 2000b).

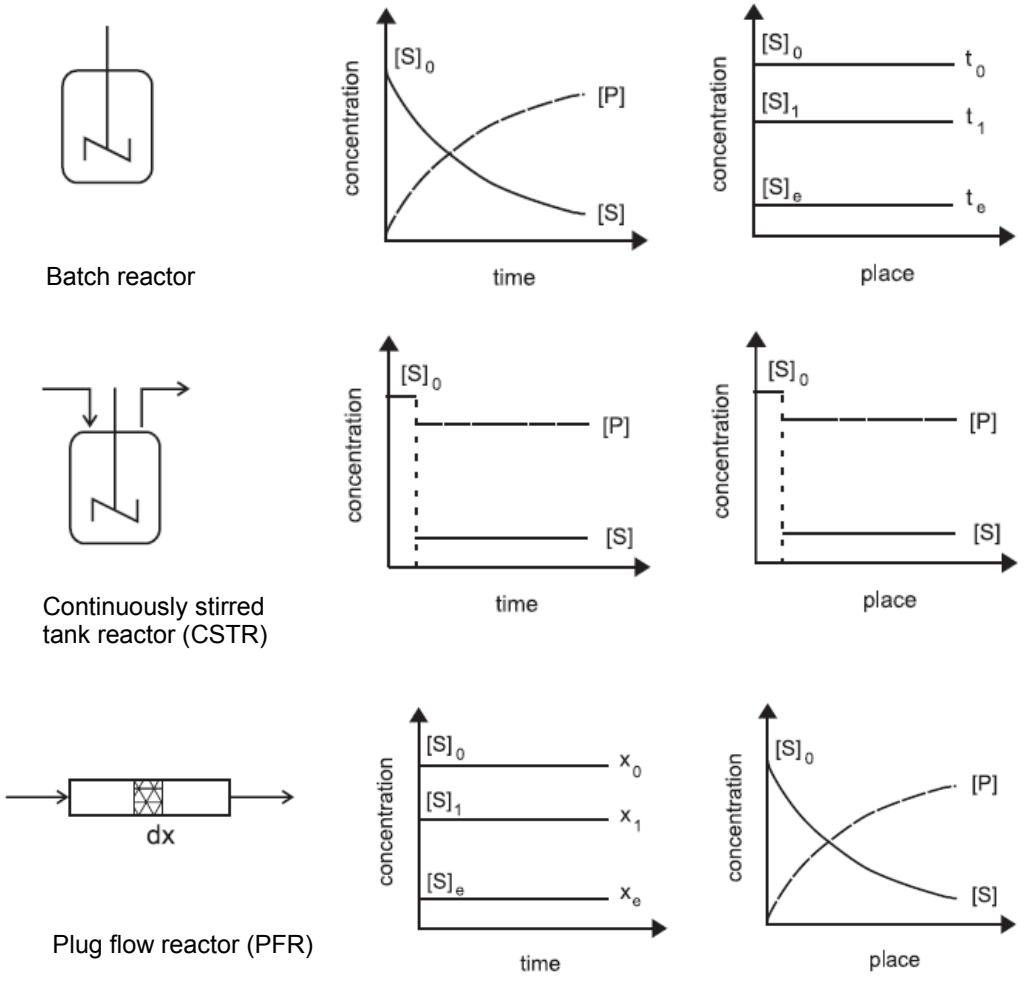

Figure 3.2. Characteristics of batch, continuously stirred tank (CSTR) and plug flow reactor (PFR). P: Product, S: Substrate, t: Time, x: Length of reactor. Conditions: 0 (Initial conditions), 1 (at a certain time) and e (at the end) (Liese et al., 2000b).

3.3 Characteristics of biocatalyst

3.3.1 Batch characterisation

Lactobacillus kefiri was tested with (2,5)-hexanedione (**A**) in a typical batch reactor (Figure 3.3). (2,5)-Hexanedione (**A**) was reduced, (5*R*)-hydroxyhexane-2-one (**B**) was produced to a maximum before being consecutively reduced to (2*R*,5*R*)-hexanediol (**C**). The concentration profiles obtained were typical for a consecutive reaction. The conversion of (2,5)-hexanedione (**A**) was greater than 99 % and the maximum yield of (5*R*)-hydroxyhexane-2-one (**B**) was 53 %. The biocatalyst consumption in the batch was 33.3 g_{wcw} g_B^{-1} and the *ee* of (5*R*)-hydroxyhexane-2-one (**B**) was more than 99 %.

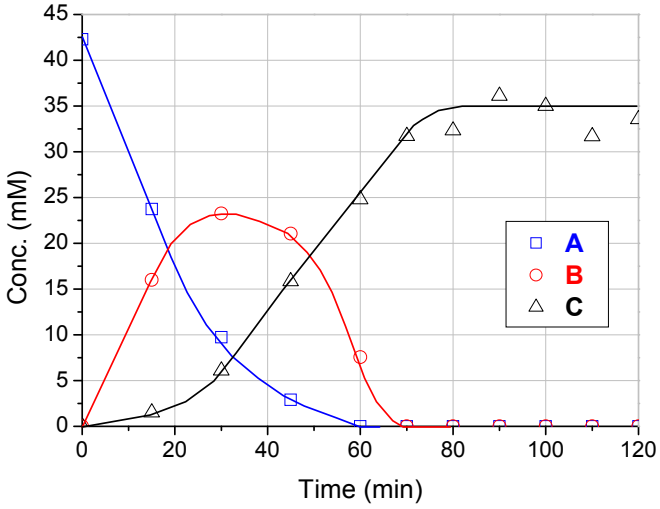

Figure 3.3. Concentration of reactants in a typical batch reactor as a function of time. Conditions: V = 0.1 L, 30 °C, pH 6 (titrated with 4 M NaOH), 50 mM potassium phosphate buffer, 400 mM glucose, 50 mM (2,5)-hexanedione (A), 2 mM $MgSO_4$, 0.7 mM $MnSO_4$, 10 g-wet cell weight *L. kefiri*.

Assuming first order reaction rates for the consecutive reactions, and that the overall bioreduction proceeded irreversibly to form (2*R*,5*R*)-hexanediol (**C**),

the rate equations for the components are

$$r_A = \frac{dC_A}{dt} = -k_1 C_A \qquad \text{(eq. 3.6)}$$

$$r_B = \frac{dC_B}{dt} = k_1 C_A - k_2 C_B \qquad \text{(eq. 3.7)}$$

$$r_C = \frac{dC_C}{dt} = k_2 C_B \qquad \text{(eq. 3.8)}$$

Integrating the above rate equations gave the equations of the individual components with respect to time (Eqs. 3.9 – 3.11). The rate constants k_1 and k_2 were then determined graphically.

$$C_A = C_{A0} e^{-k_1 t} \qquad \text{(eq. 3.9)}$$

$$C_B = C_{A0} k_1 \left(\frac{e^{-k_1 t}}{k_2 - k_1} + \frac{e^{-k_2 t}}{k_1 - k_2} \right) \qquad \text{(eq. 3.10)}$$

$$C_C = C_{A0} \left(1 + \frac{k_2 e^{-k_1 t}}{k_1 - k_2} + \frac{k_1 e^{-k_2 t}}{k_2 - k_1} \right) \qquad \text{(eq. 3.11)}$$

As an example, the determination of rate constant k_1 is illustrated (Figure 3.4).

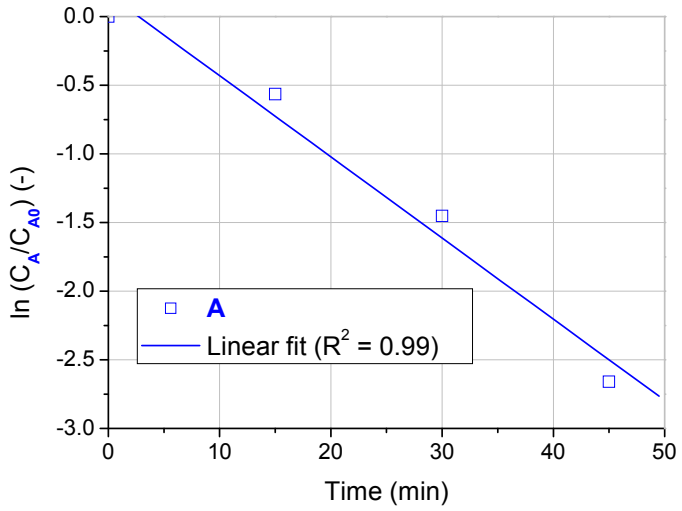

Figure 3.4. Fitting of experimental data of (2,5)-hexanedione (A) with respect to time for rate constant determination.

The rate constants obtained for the overall reaction were k_1 = 0.0489 ± 0.003 min^{-1} and k_2 = 0.0431 ± 0.004 min^{-1}. The empirical maximum concentration of (5*R*)-hydroxyhexane-2-one (**B**) and its corresponding time in a batch reactor are given by Eqs. 3.12 and 3.13.

$$\frac{C_{B,\max}}{C_{A0}} = \left(\frac{k_1}{k_2}\right)^{k_2/(k_2-k_1)} \qquad \text{(eq. 3.12)}$$

$$t_{B,\max} = \frac{\ln(k_2/k_1)}{k_2 - k_1} \qquad \text{(eq. 3.13)}$$

From the determined rate constants, the maximum concentration of (5*R*)-hydroxyhexane-2-one (**B**) of 19.6 mM was expected at t = 22 min, rather similar to the experimental value of 23 mM at t = 30 min.

Unlike the rate constant values obtained by Haberland (2003), the first reduction step was only slightly faster than the second reduction step, implying that the cells used in the synthesis of (5*R*)-hydroxyhexane-2-one (**B**) possessed different behaviour as compared to that used by Haberland in the production of (2*R*,5*R*)-hexanediol (**C**). In addition, the yield of (2*R*,5*R*)-hexanediol (**C**) at the end of the reaction was not 100 %.

It was suspected that the residual (2*R*,5*R*)-hexanediol (**C**) was either trapped intracellularly, or in the cell membrane. However, attempts to detect the chemical intracellularly proved unsuccessful (Table 3.2). The main problem faced was the mechanical resistance of the cell wall to various conventional methods of cell lysis. The exception was with glass milling where there was some degree of cell lysis. However, (2*R*,5*R*)-hexanediol (**C**) was not detected in the cell lysate. Treatment of the cells with ethyl acetate as organic solvent was then performed to extract any residual (2*R*,5*R*)-hexanediol (**C**) trapped in the cell membrane. Likewise, no traces of (2*R*,5*R*)-hexanediol (**C**) were detected. Hence, the fate of the residual (2*R*,5*R*)-hexanediol (**C**) remained unknown, and it could be metabolised by the cells.

Table 3.2. Cell lysis attempts on *L. kefiri* and the detection of residual (2*R*,5*R*)-hexanediol (C).

Cell lysis methods	Success of cell lysis	Presence of **C**
Sonification	-	N
French press	-	N
Glass milling	+/-	N
Freezing	-	N
Addition of detergent	-	N

From Haberland *et al.* (2002a), it seemed that a more alkaline pH favoured the production of (5*R*)-hydroxyhexane-2-one (**B**). In this present batch of cells, the phenomenon was not observed. There was no change in selectivity of the reaction in the pH range of 6 to 8 (Figure 3.5). However, there was a faster rate of production of (5*R*)-hydroxyhexane-2-one (**B**) with an acidic pH (Figure 3.6).

Due to the above differences in behaviour of the current biocatalyst, it must be noted that direct comparisons of the *L. kefiri* used in this work and in Haberland's would not be accurate. The different behaviour observed could be attributed to the different fermentation and harvesting conditions of the biocatalyst.

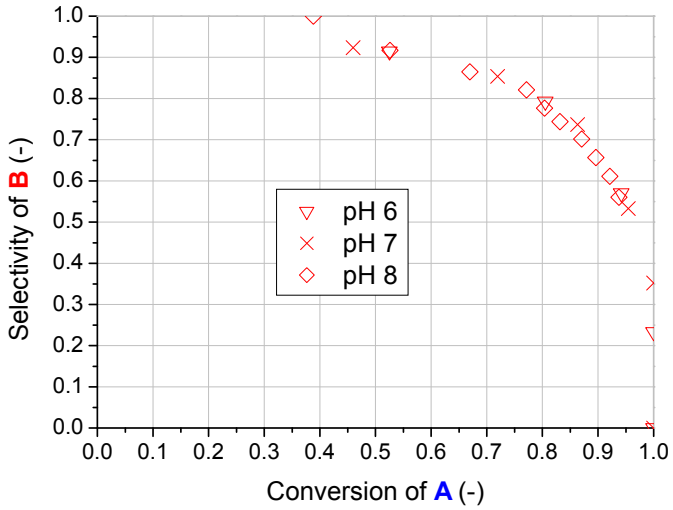

Figure 3.5. Selectivity of (5*R*)-hydroxyhexane-2-one (B) as a function of conversion of (2,5)-hexanedione (A) in a typical batch reaction at pH 6, 7 and 8. Conditions: V = 0.1 L, 30 °C, 50 mM potassium phosphate buffer, 400 mM glucose, 50 mM (2,5)-hexanedione (A), 2 mM $MgSO_4$, 0.7 mM $MnSO_4$, 10 g-wet cell weight *L. kefiri.* The pH was controlled by titration with 4 M NaOH.

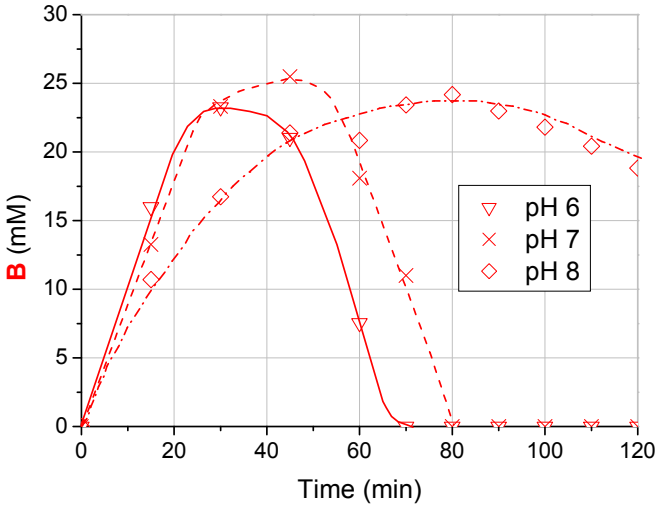

Figure 3.6. Concentration of (5*R*)-hydroxyhexane-2-one (B) as a function of time in a typical batch reaction at pH 6, 7 and 8. Conditions: V = 0.1 L, 30 °C, 50 mM potassium phosphate buffer, 400 mM glucose, 50 mM (2,5)-hexanedione (A), 2 mM $MgSO_4$, 0.7 mM $MnSO_4$, 10 g-wet cell weight *L. kefiri.* The pH was controlled by titration with 4 M NaOH.

3.3.2 Repetitive batch run

A repetitive batch run with *L. kefiri* was performed to study the stability of the cells. At the end of each batch run, the biocatalyst was separated by centrifugation (5000 rpm, 4 °C, 10 min) and the supernatant was discarded. The cell pellet was suspended with 50 mM potassium phosphate buffer (pH 6) and centrifuged at the above conditions. The cleaned biomass was then resuspended in 50 mM potassium phosphate buffer (pH 6) for use in the next batch.

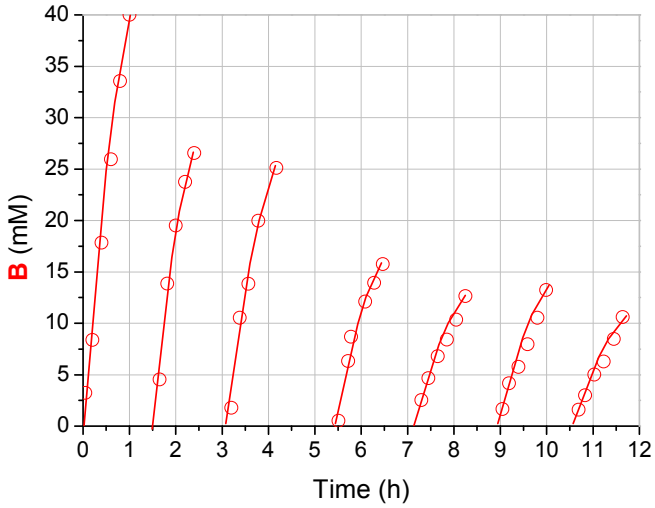

Figure 3.7. Concentration of (5*R*)-hydroxyhexane-2-one (B) in a repetitive batch as a function of time. Conditions: V = 0.1 L, 30 °C, pH 6 (titrated with 4 M NaOH), 50 mM potassium phosphate buffer, 400 mM glucose, 50 mM (2,5)-hexanedione (A), 2 mM $MgSO_4$, 0.7 mM $MnSO_4$, 10 g-wet cell weight *L. kefiri.*

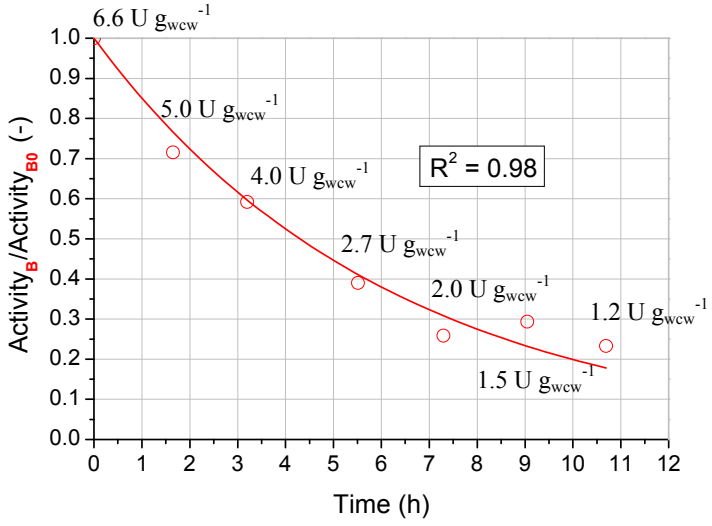

Figure 3.8. Activity of *L. kefiri* at pH 6 in a repetitive batch run as a function of time.

Over 7 repetitive batches (around 12 h), there was a drop in production of (5*R*)-hydroxyhexane-2-one (**B**) (Figure 3.7). With this set-up, the biocatalyst consumption (5.9 g_{wcw} $g_{\mathbf{B}}^{-1}$) was slightly lower than that obtained in a single batch (Refer to Section 3.3.1). However, at the end of 12 h, only 15 % of the initial activity (in terms of **B**) of the biocatalyst remained (Eq. 3.14). From Figure 3.8, the activity of *L. kefiri* decayed exponentially at the rate of 16.1 % h^{-1}.

$$Activity_B = \frac{(dC_B/dt)_{initial}}{m_{wet\ cell}} \qquad \text{(eq. 3.14)}$$

3.4 Whole cell immobilisation

Due to the consecutive bioreduction reactions, a better reactor system was needed to simplify the production of (5*R*)-hydroxyhexane-2-one (**B**) on a continuous scale.

From the reaction profile in a batch reactor (Figures 3.2 and 3.3), a plug flow reactor (PFR) packed with biocatalyst could be designed to obtain a high concentration of (5*R*)-hydroxyhexane-2-one (**B**) with minimal concentration of (2*R*,5*R*)-hexanediol (**C**). Alternatively, a continuously stirred tank reactor (CSTR) design could be used. From Haberland (2003), it was found that the biocatalyst was unstable after 5 days of operation in a CSTR. Therefore, it would not be advantageous to run a similar CSTR setup where the biocatalyst may not remain active over a period of time.

On the other hand, running a PFR would require whole cell immobilisation of *L. kefiri* as a fixed bed biocatalyst. It is known that one of the main advantages of cell immobilisation is the improvement in cell stability (Sato and Tosa, 1993), and this would be very advantageous in a continuous operation over a period of time. The drastic loss in activity of the cells seen in the repetitive batch run for non-immobilised *L. kefiri* (Section 3.3.2) could be circumvented with cell immobilisation. Hence, the PFR setup was chosen for the synthesis of (5*R*)-hydroxyhexane-2-one (**B**).

3.4.1 Choice of immobilisation matrix

Various immobilisation matrices were employed in the encapsulation of *L. kefiri*: Polyvinyl alcohol (LentiKats®) (Durieux et al., 2000), κ-carrageenan (mixed with Mg^{2+}/Mn^{2+} salts in phosphate buffer, or with NaCl) (Lacroix et al., 1990), alginate (with and without chitosan coating) (Le-Tien et al., 2004) and sodium cellulose sulphate (medical and technical grade NaCS) (Huebner and Buchholz, 1999). The immobilisates were tested in a typical batch reactor. The criteria for selecting the best immobilisation matrix were: High rate of production of (5*R*)-hydroxyhexane-2-one (**B**) in a batch reactor, fast conversion of (2,5)-hexanedione (**A**) in a batch reactor, high chemical and mechanical stability of the matrix and thereby easy handling of the immobilisates, and reasonable cost of matrix.

In all immobilised cells, the initial rates of production of (5*R*)-hydroxyhexane-2-one (**B**) from (2,5)-hexanedione (**A**) were drastically reduced. In particular, the immobilisates entrapped with polyvinyl alcohol (LentiKats®) yielded the lowest initial rate of production of (5*R*)-hydroxyhexane-2-one (**B**) (Figure 3.9). Although the thin and lens-shaped immobilisates had high surface area to volume ratio for minimal diffusion limitations in biotransformations, it did not improve the rate of (5*R*)-hydroxyhexane-2-one (**B**) production. However, a higher concentration of (5*R*)-hydroxyhexane-2-one (**B**) could be yielded in the immobilised than the non-immobilised batch.

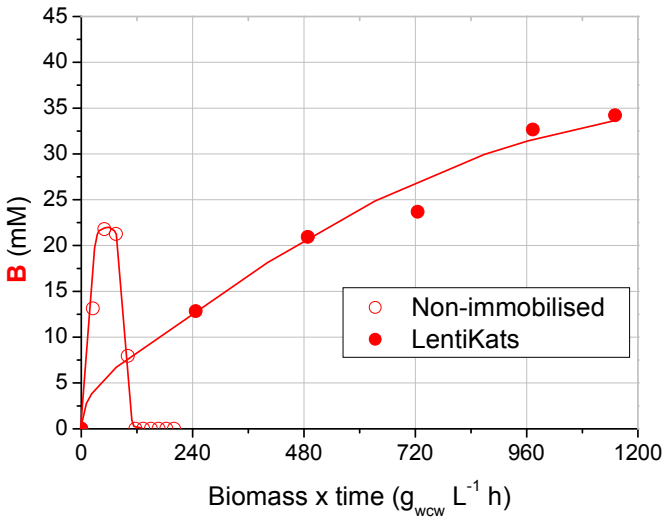

Figure 3.9. Concentration profiles of (5*R*)-hydroxyhexane-2-one (B) in a typical non-immobilised (○) and a polyvinyl alcohol (LentiKats®) immobilised (●)batch as a function of normalised time. Conditions: V = 0.05 L, 30 °C, pH 6 (titrated with 4 M NaOH), 50 mM potassium phosphate buffer, 400 mM glucose, 50 mM (2,5)-hexanedione (A), 2 mM $MgSO_4$, 0.7 mM $MnSO_4$, 5 g polyvinyl alcohol immobilisates (LentiKats®) containing 0.5 g-wet cell weight *L. kefiri.*

The addition of Mg^{2+} and Mn^{2+} salts (which may be required by the cells for the bioreduction) to the κ-carrageenan matrix did not improve the initial rate of production of (5*R*)-hydroxyhexane-2-one (**B**) (Figure 3.10). In addition, there was a reaction time lag in both carrageenan systems, implying that there could be diffusion limitations of the substrate (2,5)-hexanedione (**A**), and/or cosubstrate glucose, and/or product (5*R*)-hydroxyhexane-2-one (**B**), and/or glucose metabolites through the immobilisation matrix.

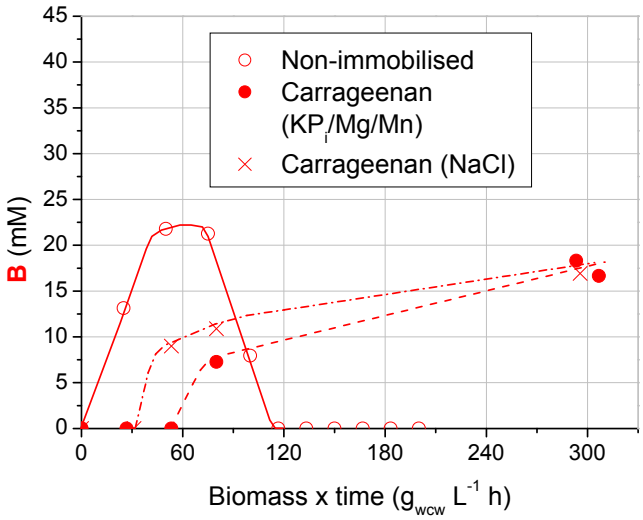

Figure 3.10. Concentration profiles of (5*R*)-hydroxyhexane-2-one (B) in a typical non-immobilised (○) and different κ-carrageenan immobilised batches as a function of normalised time. κ-Carrageenan immobilisates: consisting of Mg^{2+}/Mn^{2+}-containing phosphate buffer (2 mM Mg^{2+}, 0.7 mM Mn^{2+}, 50 mM phosphate buffer, pH 6) (●), and containing 0.9 % w/v NaCl (0.15 M) (×). Conditions: V = 0.05 L, 30 °C, pH 6 (titrated with 4 M NaOH), 50 mM potassium phosphate buffer, 400 mM glucose, 50 mM (2,5)-hexanedione (A), 2 mM $MgSO_4$, 0.7 mM $MnSO_4$, 5 g κ-carrageenan immobilisates containing 0.5 g-wet cell weight *L. kefiri.*

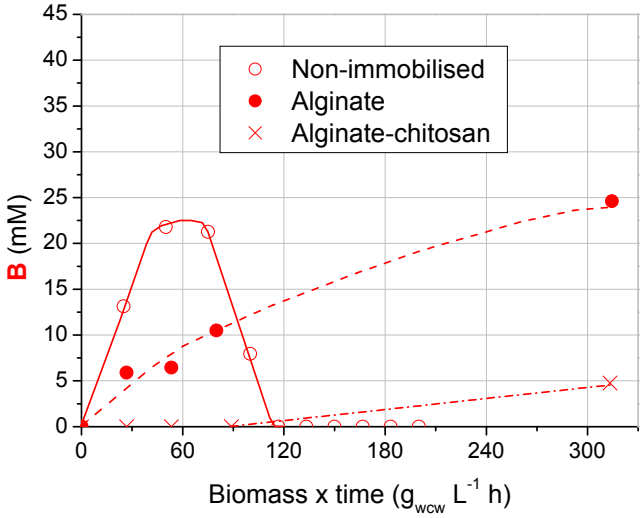

Figure 3.11. Concentration profiles of (5*R*)-hydroxyhexane-2-one (B) in a typical non-immobilised (○) and different alginate immobilised batches as a function of normalised time. Alginate immobilisates: alginate (●) and alginate-chitosan (×), made with Mg^{2+}/Mn^{2+}-containing phosphate buffer (2 mM Mg^{2+}, 0.7 mM Mn^{2+}, 50 mM phosphate buffer, pH 6). Conditions: V = 0.05 L, 30 °C, pH 6 (titrated with 4 M NaOH), 50 mM potassium phosphate buffer, 400 mM glucose, 50 mM (2,5)-hexanedione (A), 2 mM $MgSO_4$, 0.7 mM $MnSO_4$, 5 g alginate or alginate-chitosan immobilisates, each containing 0.5 g-wet cell weight *L. kefiri.*

The alginate-chitosan immobilisates, with improved mechanical strength, however, gave a much lower initial rate of production of (5*R*)-hydroxyhexane-2-one (**B**) as compared to the alginate immobilisates (Figure 3.11). It is not known why there was a stark difference in behaviour of the alginate and alginate-chitosan immobilisates. It could be due to the chemicals used in the additional steps for the chitosan coating. In the case of the alginate immobilisates, a higher concentration of (5*R*)-hydroxyhexane-2-one (**B**) was obtained in the batch as opposed to the freely suspended cells, and this was not seen for the alginate-chitosan immobilisates. The presence of a reaction time lag for the alginate-chitosan immobilisates could imply a diffusion limitation of the reactants and/or products and metabolites through the chitosan coating, since this was not observed for the alginate immobilisates.

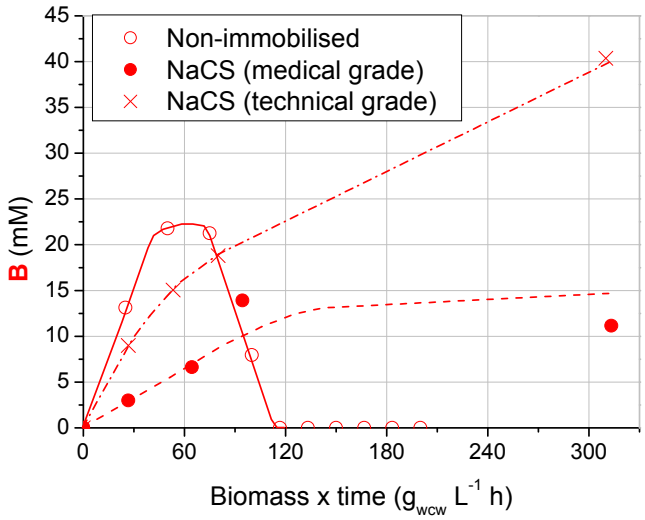

Figure 3.12. Concentration profiles of (5*R*)-hydroxyhexane-2-one (B) in a typical non-immobilised (○) and different NaCS immobilised batches as a function of normalised time. NaCS immobilisates: a medical grade (●) and a technical grade (×) made with Mg^{2+}/Mn^{2+}-containing phosphate buffer (2 mM Mg^{2+}, 0.7 mM Mn^{2+}, 50 mM phosphate buffer, pH 6). Conditions: V = 0.05 L, 30 °C, pH 6 (titrated with 4 M NaOH), 50 mM potassium phosphate buffer, 400 mM glucose, 50 mM (2,5)-hexanedione (A), 2 mM $MgSO_4$, 0.7 mM $MnSO_4$, 5 g NaCS immobilisates, each containing 0.5 g-wet cell weight *L. kefiri*.

In general, the sodium cellulose sulphate (NaCS) immobilisates gave a slower initial rate of production of (5*R*)-hydroxyhexane-2-one (**B**) as opposed to the non-immobilised cells (Figure 3.12). However, the rate was faster with the technical grade rather than the medical grade NaCS. In addition, a higher concentration of (5*R*)-hydroxyhexane-2-one (**B**) was yielded in the batch with immobilisates made from technical grade NaCS. In spite of the trace amounts of iron in the technical grade NaCS matrix, it did not have an adverse effect on the initial rate of production of (5*R*)-hydroxyhexane-2-one (**B**).

In determining the rates of conversion of (2,5)-hexanedione (**A**) in each batch, the immobilisation yield was used. The immobilisation yield of each matrix is defined as the ratio of activity of the immobilised cells over the non-immobilised cells, where the activity is the initial rate of conversion of 2,5-hexanedione (**A**) per unit of effective

(prior to immobilisation) wet biomass (Eqs. 3.15 and 3.16). The case of the non-immobilised cells is set to 100 %.

$$Activity_A = \frac{(dC_A/dt)_{initial}}{m_{wet\ cell}} \qquad \text{(eq. 3.15)}$$

$$Immobilisation\ yield = \frac{Activity_{immobilised}}{Activity_{non-immobilised}} \qquad \text{(eq. 3.16)}$$

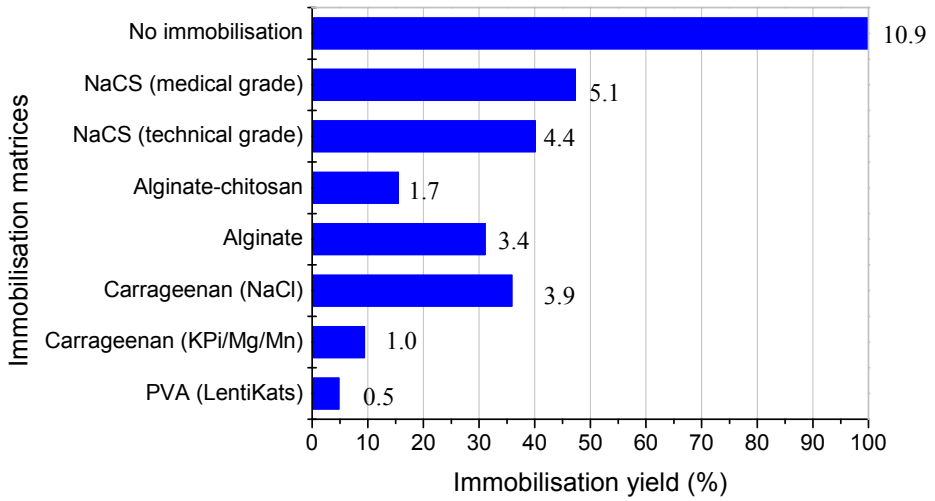

Figure 3.13. Immobilisation yield of a typical batch reaction. Conditions: V = 0.05 L, 30 °C, pH 6 (titrated with 4 M NaOH), 50 mM potassium phosphate buffer, 400 mM glucose, 50 mM (2,5)-hexanedione (A), 2 mM $MgSO_4$, 0.7 mM $MnSO_4$, 5 g immobilisates (containing 0.5 g-wet cell weight *L. kefiri*). The values of activities in terms of U_A g_{wcw}^{-1} (based on Eq. 3.15) are given on the right.

Among the immobilised batches, the sodium cellulose sulphate (NaCS) immobilisates gave the highest immobilisation yields (Figure 3.13). The κ-carrageenan (containing NaCl) and the alginate immobilisates had comparably high immobilisation yields. On the other hand, the polyvinyl alcohol (LentiKats®) immobilisates had the lowest immobilisation yield.

The comparison between the different immobilisation matrices is summarised in Table 3.3. Although the polyvinyl alcohol (LentiKats®) immobilisates were very stable mechanically and chemically and had the cheapest matrix, they were the least active in the bioreduction. Therefore, the polyvinyl alcohol matrix was not preferred. The alginate and the κ-carrageenan immobilisates were also not chosen as the matrices were chemically unstable in the biotransformation medium. It is known that the presence of chelating agents (e.g. phosphate, lactate, acetate) can extract the divalent cations (in the case of alginates) and potassium ions (in the case of κ-carrageenan) from the immobilisation matrices, thereby weakening the overall structure of the matrices (Leenen, 2001).

Table 3.3. Summary of comparison of the different immobilisation matrices. A rating of 1 denotes the least, while 7 denotes the most. For example, a 7 in all categories refers to the highest activity (in terms of immobilisation yield), the best chemical/mechanical stability and the highest matrix cost.

Matrices	Activity	Chemical/mechanical stability	Cost
Polyvinyl alcohol (LentiKats®)	1	7	1
κ-Carrageenan (KP_i/Mg/Mn)	2	1	3
κ-Carrageenan (NaCl)	5	2	3
Alginate	4	4	1
Alginate-chitosan	3	3	5
NaCS (medical grade)	7	5	7
NaCS (technical grade)	6	5	6

Therefore, the most suitable choice was the sodium cellulose sulphate (NaCS) immobilisates (Figure 3.14), with the highest immobilisation yield among the immobilisates. Despite the high cost of the matrix, it was mechanically and chemically strong, and would be suitable for use in the continuous operation of a PFR. In particular, the technical grade NaCS with 40 % immobilisation yield was chosen as it was much less expensive than the medical grade. All immobilisation results shown in the following sections were obtained from the technical grade NaCS immobilisates.

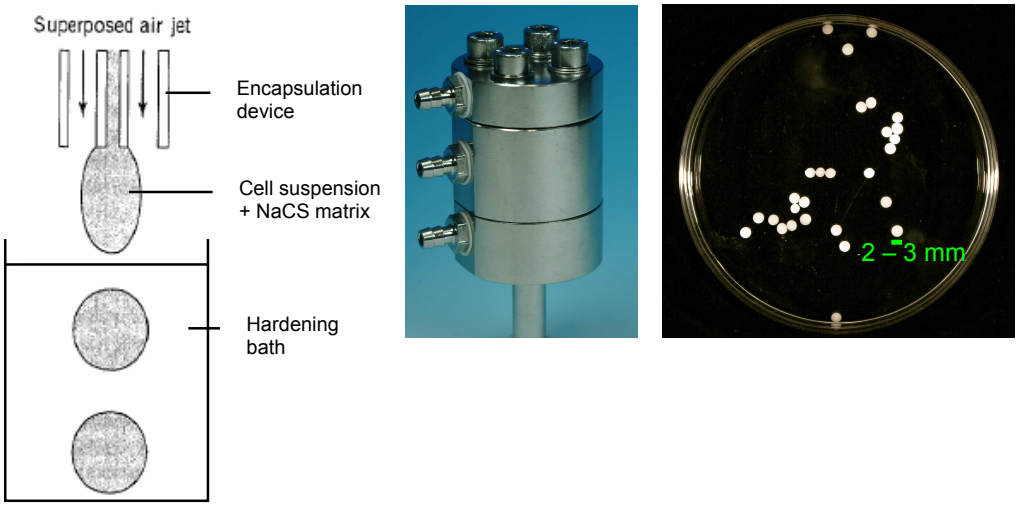

Figure 3.14. Encapsulation method (left) for technical grade NaCS immobilisates (right) made from encapsulation device (centre).

3.4.2 Reaction conditions

In a plug flow reactor (PFR), a pH gradient exists due to the production of acids from glucose metabolism. To simplify the design and operation of the PFR without pH titration, the effects of the activity of the NaCS immobilised cells (Eq. 3.14, Figure 3.15) and selectivity (Figure 3.16) of (5*R*)-hydroxyhexane-2-one (**B**) over a pH range were studied in a typical batch reactor containing technical grade NaCS immobilised cells.

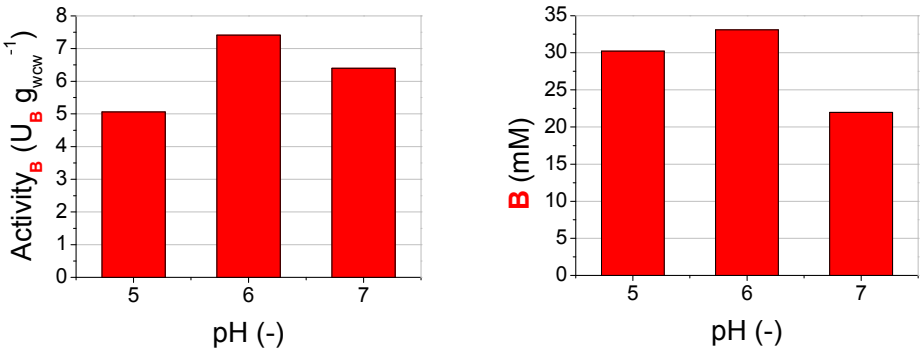

Figure 3.15. Activity of NaCS immobilisates and final concentration of (5*R*)-hydroxyhexane-2-one (B) (after 24 h) in a typical batch reaction (immobilised cells) at pH 5, 6 and 7. Conditions: V = 0.05 L, 30 °C, 50 mM potassium phosphate buffer, 400 mM glucose, 50 mM (2,5)-hexanedione (A), 2 mM $MgSO_4$, 0.7 mM $MnSO_4$, 5 g NaCS immobilisates of technical grade (containing 0.5 g-wet cell weight *L. kefiri*). The pH was controlled by titration with 4 M NaOH.

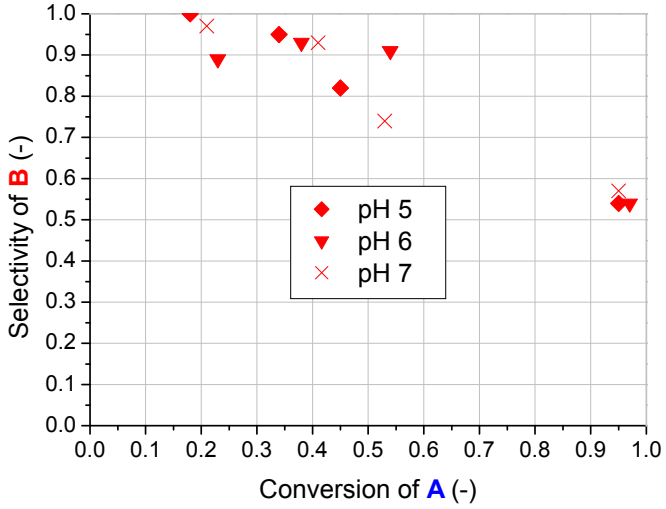

Figure 3.16. Selectivity of (5*R*)-hydroxyhexane-2-one (B) as a function of conversion of (2,5)-hexanedione (A) in a typical batch reaction (immobilised cells) at pH 5, 6 and 7. Conditions: V = 0.05 L, 30 °C, 50 mM potassium phosphate buffer, 400 mM glucose, 50 mM (2,5)-hexanedione (A), 2 mM $MgSO_4$, 0.7 mM $MnSO_4$, 5 g NaCS immobilisates of technical grade (containing 0.5 g-wet cell weight *L. kefiri*). The pH was controlled by titration with 4 M NaOH.

It was found that over the pH range of 5 to 7, there were no significant differences in the activity of the NaCS immobilised cells and selectivity of (5*R*)-hydroxyhexane-2-one (**B**). In addition, the biocatalyst consumption in the batch was 2.4 g_{wcw} $g_{\mathbf{B}}^{-1}$ (at pH 6) and the *ee* of (5*R*)-hydroxyhexane-2-one (**B**) produced with NaCS immobilised cells was more than 99 %. Therefore, the allowable working pH range of the PFR was set at 5 to 7.

3.4.3 Repetitive batch investigations

The test of stability of the NaCS immobilised cells (technical grade) was performed in a repetitive batch mode. Over a period of 165 h (around 7 days), the NaCS immobilised cells were capable of producing (5*R*)-hydroxyhexane-2-one (**B**) (Figure 3.17). However, only 13.3 % of the initial activity (in terms of **B**) remained after 165 h (Eq. 3.14). The activity of the NaCS immobilisates decayed exponentially at the rate of 1.3 % h^{-1} (Figure 3.18). Despite the decrease in activity, the overall biocatalyst consumption of the repetitive batch (0.5 g_{wcw} $g_{\mathbf{B}}^{-1}$) was slightly lower than that in a batch (at pH 6). With this knowledge of activity of the NaCS immobilisates, it would be possible to run the PFR for at least 7 days.

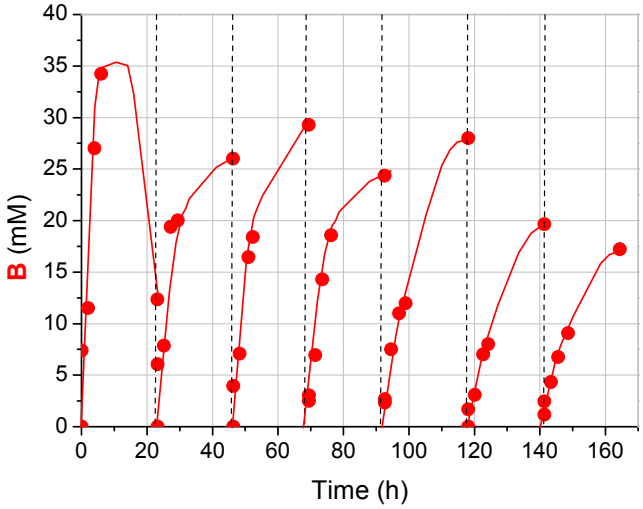

Figure 3.17. Concentration of (5*R*)-hydroxyhexane-2-one (B) in a repetitive batch run with technical grade NaCS immobilised cells as a function of time. NaCS immobilisates: a technical grade made with Mg^{2+}/Mn^{2+}-containing phosphate buffer (2 mM Mg^{2+}, 0.7 mM Mn^{2+}, 50 mM phosphate buffer, pH 6). Conditions: V = 0.1 L, 30 °C, pH 6 (titrated with 4 M NaOH), 50 mM potassium phosphate buffer, 400 mM glucose, 50 mM (2,5)-hexanedione (A), 2 mM $MgSO_4$, 0.7 mM $MnSO_4$, 10 g NaCS immobilisates, each containing 1 g-wet cell weight *L. kefiri.*

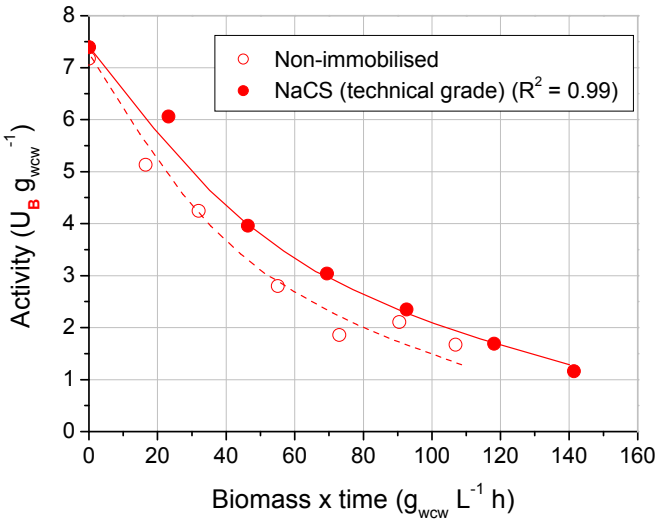

Figure 3.18. Activities of non-immobilised and technical grade NaCS immobilised cells at pH 6 in a repetitive batch run as a function of time.

3.4.4 Plug flow reactor (PFR) run

In order to maximise the production of (5*R*)-hydroxyhexane-2-one (**B**) in a packed bed reactor, two similar PFRs (Fraction of porosity ε = 0.3, refer to Eq. 3.17) were set up in series (Figures 3.19 and 3.20). Different residence times for a single column τ and for the entire setup τ_{PFRs} (Eq. 3.18) and the corresponding number of residence time θ and θ_{PFRs} (Eq. 3.19) were used in the continuous run to establish the most suitable operating conditions. The inlet of the second column was titrated with 4 M NaOH to pH 7, similar to the initial pH of the first column. This ensured that the remaining unreacted (2,5)-hexanedione (**A**) could be further reduced to (5*R*)-hydroxyhexane-2-one (**B**). However, the existing (5*R*)-hydroxyhexane-2-one (**B**) could be further reduced to (2*R*,5*R*)-hexanediol (**C**) in the second column. Therefore, besides the product outlet at the fraction collector, samples from the outlet of the first column were also collected and the two columns were examined separately over the operation period of 6 days.

$$\varepsilon = \frac{V_{PFR} - V_{biocat}}{V_{PFR}} \qquad \text{(eq. 3.17)}$$

$$\tau = \frac{V_{PFR}}{F_v} \qquad \text{(eq. 3.18)}$$

$$\theta = \frac{\varepsilon \times V_{PFR}}{F_v} \qquad \text{(eq. 3.19)}$$

$$Space\text{-}time\ yield\ (STY) = \frac{C_B \times M_B}{\tau} \qquad \text{(eq. 3.20)}$$

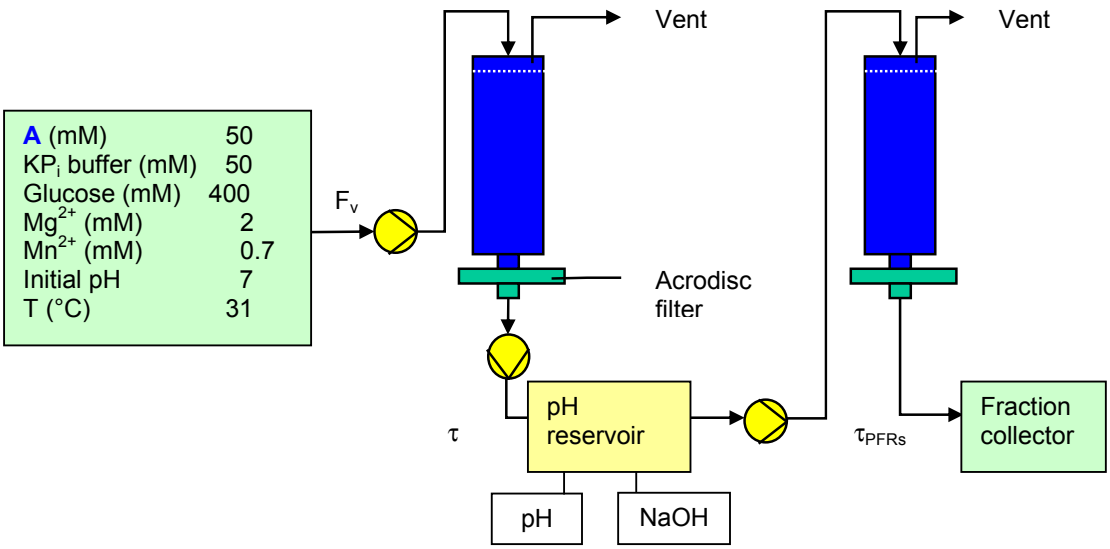

Figure 3.19. Scheme of PFR setup in series.

Figure 3.20. Production of (5*R*)-hydroxyhexane-2-one (B) with the PFR setup (left) and a close-up on the thermally insulated PFRs (right).

In the first column, most of the (2,5)-hexanedione (**A**) present in the first section (τ = 3.3 h) were reduced to a mixture of (5*R*)-hydroxyhexane-2-one (**B**) and (2*R*,5*R*)-hexanediol (**C**) (Figure 3.21). However, a steady state of production of (5*R*)-hydroxyhexane-2-one (**B**) was not achieved. This was most probably due to the loss in activity of the NaCS immobilisates. A 50 % reduction in the residence time (τ = 1.6 h) in the second section resulted in less (2,5)-hexanedione (**A**) being converted, and more (5*R*)-hydroxyhexane-2-one (**B**) than (2*R*,5*R*)-hexanediol (**C**) was produced. In order to maximise the production of (5*R*)-hydroxyhexane-2-one (**B**), the residence time of the column was further reduced to 25 % of the initial residence time (τ = 0.8 h). Much more (5*R*)-hydroxyhexane-2-one (**B**) than (2*R*,5*R*)-hexanediol (**C**) were produced in comparison to the first two sections. In addition, a relatively high

amount of (2,5)-hexanedione (A) remained unreacted. When the flow rate of the feed solution was reverted back to its original value (τ = 3.3 h), the concentration profiles of the reactants were dissimilar to that in the first section (θ = 0 – 18.5).

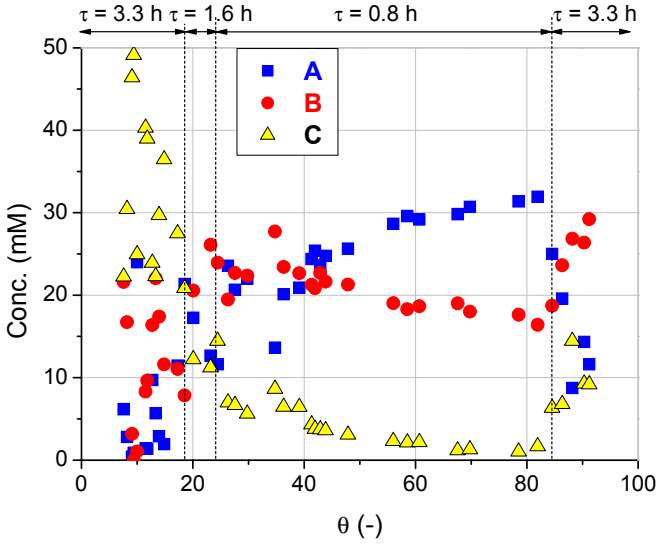

Figure 3.21. Concentration profile of reactants packed with NaCS immobilisates in the first column of PFR (in series) as a function of the number of residence time. Conditions: V = 0.06 L, ε = 0.3, 31 °C, initial pH 7, 50 mM potassium phosphate buffer, 400 mM glucose, 50 mM (2,5)-hexanedione (A), 2 mM $MgSO_4$, 0.7 mM $MnSO_4$, 60 g technical grade NaCS immobilisates (containing 6 g-wet cell weight *L. kefiri*).

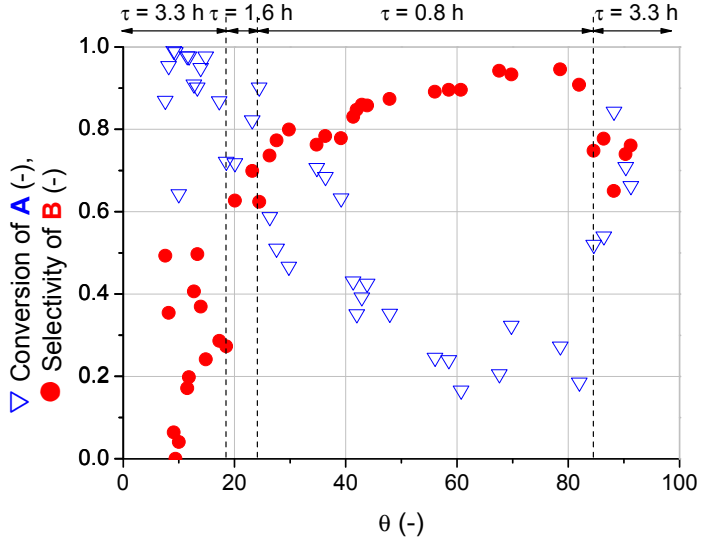

Figure 3.22. Selectivity of (5*R*)-hydroxyhexane-2-one (B) and conversion of (2,5)-hexanedione (A) as a function of the number of residence time in the first column of PFR (in series) packed with NaCS immobilisates. Conditions: V = 0.06 L, ε = 0.3, 31 °C, initial pH 7, 50 mM potassium phosphate buffer, 400 mM glucose, 50 mM (2,5)-hexanedione (A), 2 mM $MgSO_4$, 0.7 mM $MnSO_4$, 60 g technical grade NaCS immobilisates (containing 6 g-wet cell weight *L. kefiri*).

Further examination into the first column revealed the highest selectivity of (5*R*)-hydroxyhexane-2-one (**B**) and the lowest conversion of (2,5)-hexanedione (**A**) in the third section (θ = 24.5 – 84.5) (Figure 3.22). The corresponding activity of the NaCS immobilisates with respect to (2,5)-hexanedione (**A**) decayed exponentially during the third phase (τ = 0.8 h) at a rate of 2.8 % h^{-1} (R^2 = 0.65).

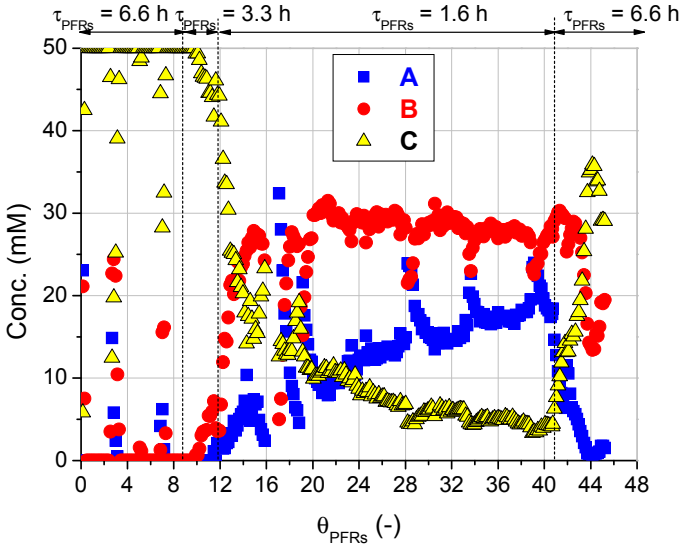

Figure 3.23. Concentration profile of reactants packed with NaCS immobilisates from the second column of PFR (in series) as a function of the number of residence time. Conditions: V = 0.06 L, ε = 0.3, 31 °C, initial pH 7, 50 mM potassium phosphate buffer, 400 mM glucose, 50 mM (2,5)-hexanedione (A), 2 mM $MgSO_4$, 0.7 mM $MnSO_4$, 60 g technical grade NaCS immobilisates (containing 6 g-wet cell weight *L. kefiri*).

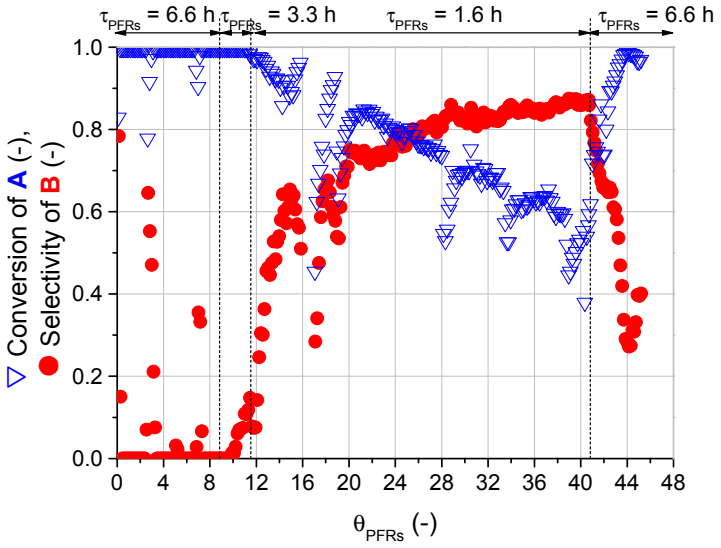

Figure 3.24. Selectivity of (5*R*)-hydroxyhexane-2-one (B) and conversion of (2,5)-hexanedione (A) as a function of the number of residence time from the second column of PFR (in series) packed with NaCS immobilisates. Conditions: V = 0.06 L, ε = 0.3, 31 °C, initial pH 7, 50 mM potassium phosphate buffer, 400 mM glucose, 50 mM (2,5)-hexanedione (A), 2 mM $MgSO_4$, 0.7 mM $MnSO_4$, 60 g technical grade NaCS immobilisates (containing 6 g-wet cell weight *L. kefiri*).

The concentration of the reactants in the second column with respect to the changing residence time followed a similar trend as seen in the first column (Figure 3.23). Likewise, the highest selectivity of (5*R*)-hydroxyhexane-2-one (**B**) occurred at the third phase (τ_{PFRs} = 1.6 h) (Figure 3.24). The activity of the NaCS immobilisates (in terms of (2,5)-hexanedione (**A**)) during this phase decayed exponentially by 2.3 % h^{-1} (R^2 = 0.76), similar to the deactivation constant observed in the first column.

Comparing the efficiencies of both columns, the first column of the PFR in series was sufficient in producing a high selectivity (95 %) of (5*R*)-hydroxyhexane-2-one (**B**) at a high space-time yield of 87 g_B L^{-1} d^{-1} (Eq. 3.20) and a corresponding biocatalyst consumption of 1.41 g_{wcw} g_B^{-1} (Table 3.4). After 6 days of operation, the residual activity of the NaCS immobilisates (in terms of conversion of (2,5)-hexanedione (**A**)) in the first column was 68 %. In the second column, there was a drop in selectivity to 85 % as more (2*R*,5*R*)-hexanediol (**C**) was formed. The space-time yield (52 g_B L^{-1} d^{-1}) of (5*R*)-hydroxyhexane-2-one (**B**) decreased due to the total residence time in the entire setup. However, the biocatalyst consumption of (5*R*)-hydroxyhexane-2-one (**B**) in the second column remained rather similar (1.45 g_{wcw} g_B^{-1}) to the first. It seemed that the higher concentration of (2,5)-hexanedione (**A**) rather than (5*R*)-hydroxyhexane-2-one (**B**) or (2*R*,5*R*)-hexanediol (**C**) as seen in the first column could be toxic to the biocatalyst. Therefore, in the second column, the residual activity of the NaCS immobilisates was higher (close to 100 %).

Table 3.4. Summary of results from NaCS-immobilised PFR. STY: space-time yield, θ, θ_{PFRs} : number of residence time.

Parameters	First column	Second column
Maximum conversion of **A** (%)	100	100
Selectivity of **B** (%)	95	85
STY (g_B L^{-1} d^{-1})	87	52
Biocatalyst consumption (g_{wcw} g_B^{-1})	1.41	1.45
θ (-)	91	46
Production time (d)	6	6

3.5 Downstream processing

Separation of (5*R*)-hydroxyhexane-2-one (**B**) from the reactants mixture largely composed of (2,5)-hexanedione (**A**) and (5*R*)-hydroxyhexane-2-one (**B**) was performed by column chromatography on a lab-scale. Distillation of the mixture was unfavourable since the boiling points of the reactants are rather similar, and would require a long distillation column with many theoretical plates for efficient separation of (5*R*)-hydroxyhexane-2-one (**B**).

The aqueous mixture containing (5*R*)-hydroxyhexane-2-one (**B**) was extracted with chloroform. To obtain a concentrated sample of (5*R*)-hydroxyhexane-2-one (**B**), most of the chloroform was rotary evaporated. The concentrated sample was then fed into a column (40 cm long × 24 mm o.d.) packed with silica gel (0.040 – 0.063 mm

diameter, 35 cm packed height). The eluent used was ethyl acetate with a flow rate of 0.8 mL min^{-1}. Upon column chromatography, (5*R*)-hydroxyhexane-2-one (**B**) was separated rather well from the other reactants (Figure 3.25). The resulting yield of (5*R*)-hydroxyhexane-2-one (**B**) was 0.56 g_B (70 %), and the purity of (5*R*)-hydroxyhexane-2-one (**B**) was above 99 % in some fractions (Figure 3.26). A drop in purity of (5*R*)-hydroxyhexane-2-one (**B**) thereafter was due to an increasing concentration of (2*R*,5*R*)-hexanediol (**C**) eluting together with a decreasing concentration of (5*R*)-hydroxyhexane-2-one (**B**).

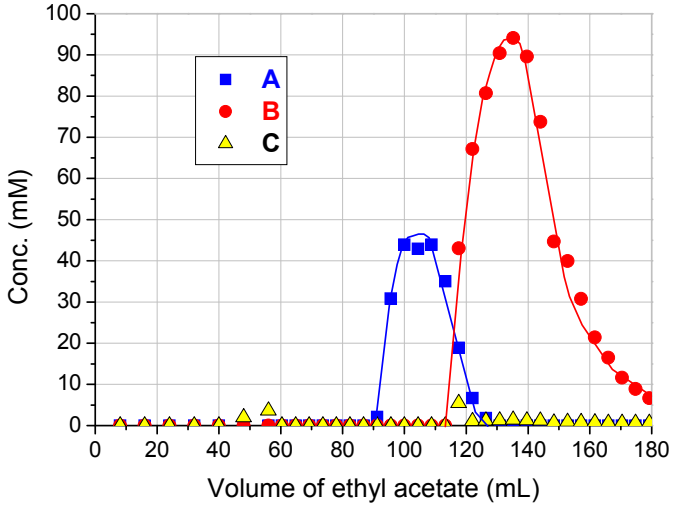

Figure 3.25. Concentration of reactants as a function of the volume of eluent used in the column. Conditions: Flow rate = 0.8 mL min^{-1}, column (40 cm long × 24 mm o.d.) packed with silica gel (0.040 – 0.063 mm diameter, 35 cm packed height).

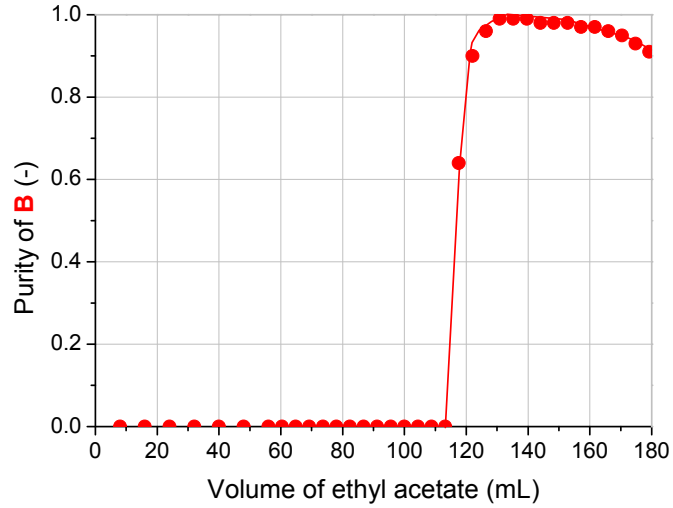

Figure 3.26. Purity of (5*R*)-hydroxyhexane-2-one (B) as a function of the volume of eluent used in the column.

To obtain pure (5*R*)-hydroxyhexane-2-one (**B**) on a gram-scale, scale-up of the column chromatography process (silica gel, ethyl acetate) was performed. With a larger column (47 cm long × 65 mm o.d.), 1.2 g_B of (*5R*)-hydroxyhexane-2-one (**B**) was yielded from a mixture of (2,5)-hexanedione (**A**) and (*5R*)-hydroxyhexane-2-one (**B**). Rotary evaporation of the eluent was performed to yield an end product of (5*R*)-hydroxyhexane-2-one (**B**). The enantiomeric excess and GC purity of (*5R*)-hydroxyhexane-2-one (**B**) obtained were greater than 99 %. NMR analysis confirmed the presence of (5*R*)-hydroxyhexane-2-one (**B**) together with some impurities, which could possibly be the cyclic structure, (2,*5R*)-dimethyl-tetrahydrofuran-2-ol (Figures 3.27, 9.8 and 9.9). The end product is a yellow oil (Figure 3.28).

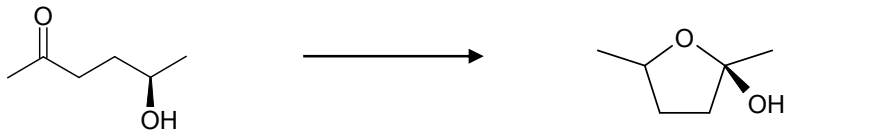

(5*R*)-Hydroxyhexane-2-one (**B**) (2,5*R*)-Dimethyl-tetrahydrofuran-2-ol

Figure 3.27. Cyclisation of (5*R*)-hydroxyhexane-2-one (B) to (2,5*R*)-dimethyl-tetrahydrofuran-2-ol.

Figure 3.28. Final product (5*R*)-hydroxyhexane-2-one (B), a yellow oil.

3.6 Conclusions

In the synthesis of (5*R*)-hydroxyhexane-2-one (**B**) with wild type biocatalyst *Lactobacillus kefiri*, the following findings were obtained:

- Whole cell immobilisation reduced cell activity but increased cell stability and lowered the biocatalyst consumption,
- Best encapsulation matrix was sodium cellulose sulphate (technical grade),
- Lowest biocatalyst consumption (0.5 g_{wcw} g_B^{-1}) was obtained in the repetitive batch setup with NaCS immobilisates,
- High selectivity (95 %) and space-time yield (87 g_B L^{-1} d^{-1}) were obtained in the plug flow reactor setup,

- From the plug flow reactor setup, (2,5)-hexanedione (**A**) seemed to be more toxic to the cells than its biotransformation products,
- Downstream processing by column chromatography yielded (5*R*)-hydroxyhexane-2-one (**B**) on a gram-scale (1.2 g_B), with *ee* and purity of more than 99 %.

4 Syntheses of Chiral Alcohols with an Enzyme-coupled System

Instead of whole cell biocatalysis, the syntheses of chiral alcohols from prochiral ketones with isolated enzymes incorporating cofactor regeneration were widely investigated (Rissom, 1995, 1999; Seelbach, 1994). Bioreduction of (2,5)-hexanedione (**A**) to (5*S*)-hydroxyhexane-2-one to (2*S*,5*S*)-hexanediol with carbonyl reductase from *Candida parapsilosis* (*CP*CR) was successfully coupled to the oxidation of formate to carbon dioxide with formate dehydrogenase from *Candida boidinii* for the regeneration of NAD(H) (Rissom, 1999). The synthesis of the (*R*)-alcohols, (5*R*)-hydroxyhexane-2-one (**B**) and (2*R*,5*R*)-hexanediol (**C**), could therefore in principle be proceeded with a rather similar setup. Hence, the reduction of (2,5)-hexanedione (**A**) by alcohol dehydrogenase from *Lactobacillus brevis* (*Lb*ADH) was tested. In this setup (Figure 4.1), the cofactor NADPH was regenerated by the oxidation of formate, a cheap cosubstrate, with $NADP^+$-specific formate dehydrogenase from *Pseudomonas* sp. (Tishkov et al., 1999).

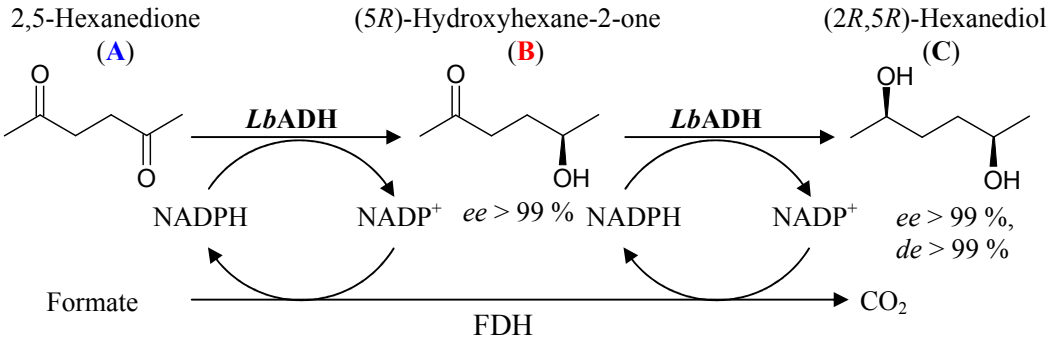

Figure 4.1. Enantioselective reduction of (2,5)-hexanedione (A) to (5*R*)-hydroxyhexane-2-one (B) and subsequently to (2*R*,5*R*)-hexanediol (C) with isolated enzyme-coupled system.

Using the same principle, the isolated enzyme coupled system was also investigated to produce another (*R*)-alcohol, (*R*)-methyl-3-hydroxybutanoate (**MHB**). The bioreduction of methyl acetoacetate (**MAA**) to (*R*)-methyl-3-hydroxybutanoate (**MHB**) was performed by *Lb*ADH, with NADPH regeneration by means of FDH (Figure 4.2). As *Lb*ADH is also known to accept the non-phosphorylated cofactor NADH (Hummel, 1997) and that both cofactors are present in whole cells, the relationship between the cofactors NAD(P)H and the bioreduction of methyl acetoacetate (**MAA**) was also studied.

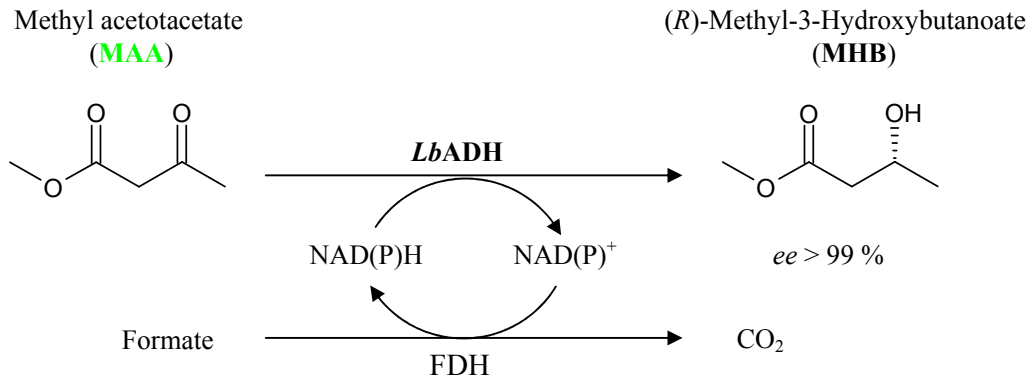

Figure 4.2. Enantioselective reduction of methyl acetoacetate (MAA) to (*R*)-methyl-3-hydroxybutanoate (MHB) with isolated enzyme-coupled system.

4.1 General definitions of terms used

For the system with methyl acetoacetate (**MAA**), the conversion of the process is defined as the amount of methyl acetoacetate (**MAA**) reacted per initial concentration.

$$Conversion = \frac{C_{MAA0} - C_{MAA}}{C_{MAA0}} \qquad \text{(eq. 4.1)}$$

The corresponding yield of (*R*)-methyl-3-hydroxybutanoate (**MHB**) is given as the fraction of (*R*)-methyl-3-hydroxybutanoate (**MHB**) obtained per initial amount of methyl acetoacetate (**MAA**).

$$Yield = \frac{C_{MHB}}{C_{MAA0}} \qquad \text{(eq. 4.2)}$$

The total turnover number (*ttn*) of a process, in terms of the biocatalyst, is given as the molar ratio of (5*R*)-hydroxyhexane-2-one (**B**), or (*R*)-methyl-3-hydroxybutanoate (**MHB**) obtained per mole of enzyme (ADH and FDH). The molecular weight of ADH and FDH are 105 and 44 kD respectively.

$$ttn_{ADH} = \frac{n_B}{n_{ADH}} \; or \; \frac{n_{MHB}}{n_{ADH}} \qquad \text{(eq. 4.3)}$$

$$ttn_{FDH} = \frac{n_B}{n_{FDH}} \; or \; \frac{n_{MHB}}{n_{FDH}} \qquad \text{(eq. 4.4)}$$

In terms of the cofactors, the total turnover number (*ttn*) is defined as the molar ratio of (5*R*)-hydroxyhexane-2-one (**B**), or (*R*)-methyl-3-hydroxybutanoate (**MHB**) formed per unit mole of oxidised cofactor ($NADP^+$).

$$ttn_{NADP^+} = \frac{n_B}{n_{NADP^+}} \; or \; \frac{n_{MHB}}{n_{NADP^+}} \qquad \text{(eq. 4.5)}$$

The biocatalyst consumption of the process is given as the ratio of the total mass of enzymes (ADH and FDH) per unit mass of (5*R*)-hydroxyhexane-2-one (**B**), or (*R*)-methyl-3-hydroxybutanoate (**MHB**) formed.

$$Biocat\ consumption = \frac{m_{ADH+FDH}}{m_B} \; or \; \frac{m_{ADH+FDH}}{m_{MHB}} \qquad \text{(eq. 4.6)}$$

In batch reactions, the space-time yield (STY) is defined by the initial gradient of the concentration profile of (5*R*)-hydroxyhexane-2-one (**B**), or (*R*)-methyl-3-hydroxybutanoate (**MHB**) over time, multiplied by the corresponding molecular weight of the alcohol. Due to the rapid reactions obtained with the use of enzymes as compared to whole cells, the unit of time used to calculate STY in this chapter is expressed in terms of hours rather than days.

$$STY_B = \left(\frac{dC_B}{dt}\right)_{initial} \times M_B \qquad \text{(eq. 4.7)}$$

$$STY_{MHB} = \left(\frac{dC_{MHB}}{dt}\right)_{initial} \times M_{MHB} \qquad \text{(eq. 4.8)}$$

4.2 γ-Hydroxyketone synthesis

The reduction of (2,5)-hexanedione (**A**) to (5*R*)-hydroxyhexane-2-one (**B**) and (2*R*,5*R*)-hexanediol (**C**) was achieved in a batch run with the enzyme-coupled system comprising of *Lb*ADH and FDH (Figure 4.3). Similar to the case for whole cells (refer to Chapter 3.3.1), more than 99 % of (2,5)-hexanedione (**A**) was converted. The maximum yield of (5*R*)-hydroxyhexane-2-one (**B**) was 82 %, and the *ee* was above 99 %. The space-time yield of (5*R*)-hydroxyhexane-2-one (**B**) was 5.2 $g_{\mathbf{B}}$ L^{-1} h^{-1} with total turnover numbers (*ttn*) of 47069 $mol_{\mathbf{B}}$ mol_{ADH}^{-1}, 569 $mol_{\mathbf{B}}$ mol_{FDH}^{-1} and 225 $mol_{\mathbf{B}}$ mol_{NADP}^{-1}. The activity with respect to (5*R*)-hydroxyhexane-2-one (**B**) was 0.34 $U_{\mathbf{B}}$ $mg_{ADH+FDH}$. In the enzyme-coupled batch, the bioreduction proceeded to yield more than 99 % (2*R*,5*R*)-hexanediol (**C**). With the above batch results, it was concluded that the reduction of a prochiral ketone to its corresponding alcohol was possible with the use of the enzyme-coupled system (*Lb*ADH and FDH). Therefore, in the following sections of this chapter, the enzyme-coupled system was extended to investigate the reduction of methyl acetoacetate (**MAA**).

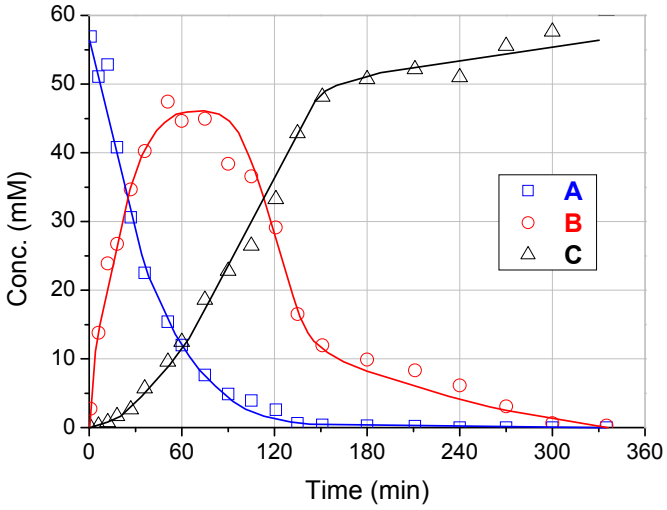

Figure 4.3. Concentration of reactants in a batch reactor as a function of time. Conditions: V = 1.5 mL, 20 °C, initial pH 6, 50 mM potassium phosphate buffer, 300 mM sodium formate, 50 mM (2,5)-hexanedione (A), 2 mM $MgSO_4$, 0.2 mM $NADP^+$, 0.1 g L^{-1} *Lb*ADH (61.8 U_A mg_{ADH}^{-1}), 3.6 g L^{-1} FDH (0.44 $U_{formate}$ mg_{FDH}^{-1}).

4.3 3-Hydroxybutanoate synthesis

4.3.1 Reaction conditions

The pH and temperature of the biotransformation with the enzyme-coupled system was studied separately for each enzyme (*Lb*ADH and FDH). Thereafter, the best conditions were selected for the enzyme-coupled batch.

From Figure 4.4, the maximal activities of *Lb*ADH and FDH occurred at pHs 7.0 and 6.2 respectively. Since there would not be pH control in batch reactors, and that the pH of the enzyme-coupled batch would increase due to the production of dissolved CO_2 in the form of alkaline bicarbonates, a lower starting pH value was desired. The compromised starting pH value for future batches was therefore chosen at a lower value of 6, where the activities of *Lb*ADH and FDH were more than 50 % of the attainable maximum activities.

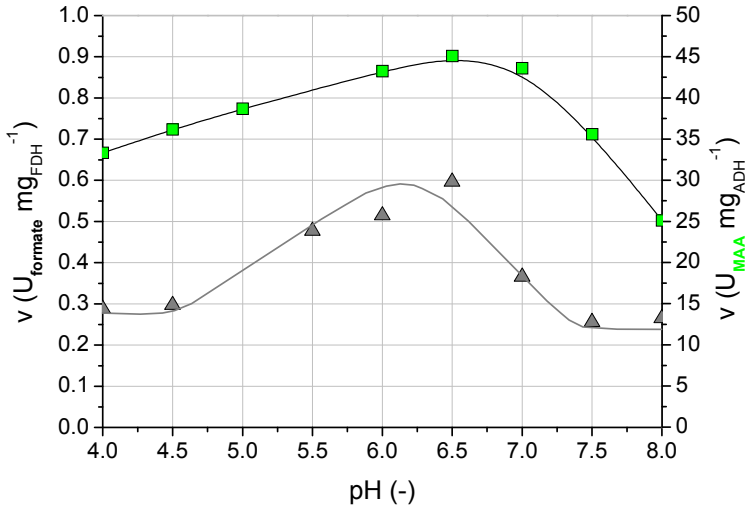

Figure 4.4. Activity of *Lb*ADH and FDH as a function of pH. Conditions (*Lb*ADH): V = 1.0 mL, 20 °C, 50 mM potassium phosphate buffer, 40 mM methyl acetoacetate (MAA), 2 mM $MgSO_4$, 0.2 mM NADPH, 12.6 mg L^{-1} *Lb*ADH (89.0 U_{MAA} mg_{ADH}^{-1}). Conditions (FDH): V = 1.0 mL, 25 °C, 50 mM potassium phosphate buffer, 240 mM sodium formate, 0.2 mM $NADP^+$, 5.6 mg L^{-1} FDH (0.44 $U_{formate}$ mg_{FDH}^{-1}).

The activities of *Lb*ADH and FDH behaved according to Arrhenius' equation (see Eq. 4.9) in the range of 290 to 308 K (FDH) and up to 333 K (*Lb*ADH) (Figures 4.5 and 4.6). The corresponding activation energies were 36.8 ± 0.8 kJ mol^{-1} (R^2 = 0.99) (*Lb*ADH) and 27.9 ± 0.2 kJ mol^{-1} (R^2 = 0.99) (FDH). The values for thermal activation obtained were consistent to the usual range of values found in enzyme-catalysed reactions (Schuler and Kargi, 1992). Although an increase in temperature increased the activities of both enzymes exponentially, the stability of the enzymes (see Chapter 4.3.2.1) and cofactors (refer to Chapter 4.3.3) with temperature had to be taken in account before choosing a suitable operating temperature for the enzyme-coupled system.

$$k = Ae^{-E_a/RT} \qquad \text{(eq. 4.9)}$$

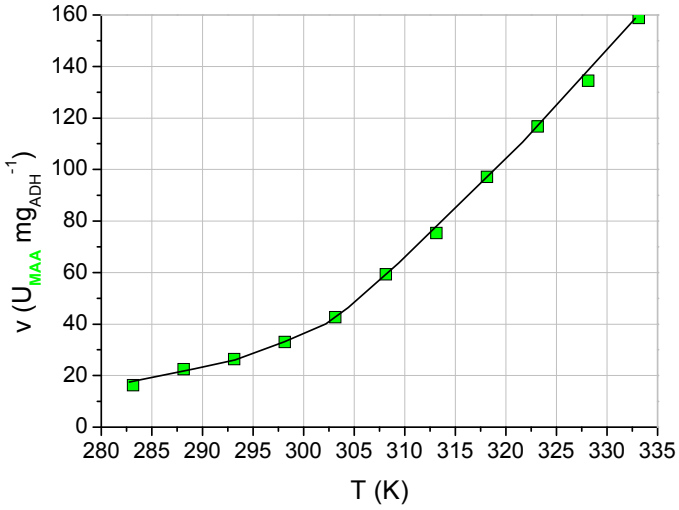

Figure 4.5. Activity of *Lb*ADH as a function of temperature. Conditions: V = 1.0 mL, initial pH 6, 50 mM potassium phosphate buffer, 40 mM methyl acetoacetate (MAA), 2 mM $MgSO_4$, 0.2 mM NADPH, 12.6 mg L^{-1} *Lb*ADH (89.0 U_{MAA} mg_{ADH}^{-1}).

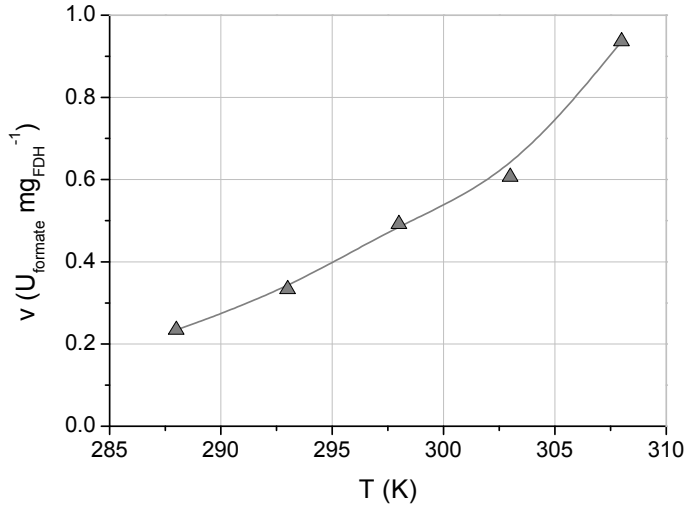

Figure 4.6. Activity of FDH as a function of temperature. Conditions: V = 1.0 mL, initial pH 6, 50 mM potassium phosphate buffer, 240 mM sodium formate, 0.2 mM $NADP^+$, 5.6 mg L^{-1} FDH (0.44 $U_{formate}$ mg_{FDH}^{-1}).

4.3.2 Stability of enzymes

The stability of *Lb*ADH and FDH with respect to incubation temperatures and chemicals was explored. From the results, the operating temperature for the enzyme-coupled system was determined. The effects of chemical toxicity on the activity of the enzymes were also obtained.

4.3.2.1 Temperature

From Figure 4.7, it was found that there was an overall exponential decay in activity of *Lb*ADH in 50 mM potassium phosphate buffer from 20 to 30 °C over a period of 5 days. The rate of deactivation of *Lb*ADH was lowest at 20 °C (3.3 % h^{-1}) and it increased with increasing temperature (Figure 4.8). However, the activity of *Lb*ADH remained constant when the enzyme was incubated with potassium phosphate buffer containing 2 mM $MgSO_4$ (Figure 4.7). Therefore, a lower temperature (20 °C) and the addition of $MgSO_4$ were essential in maintaining the activity of *Lb*ADH over time.

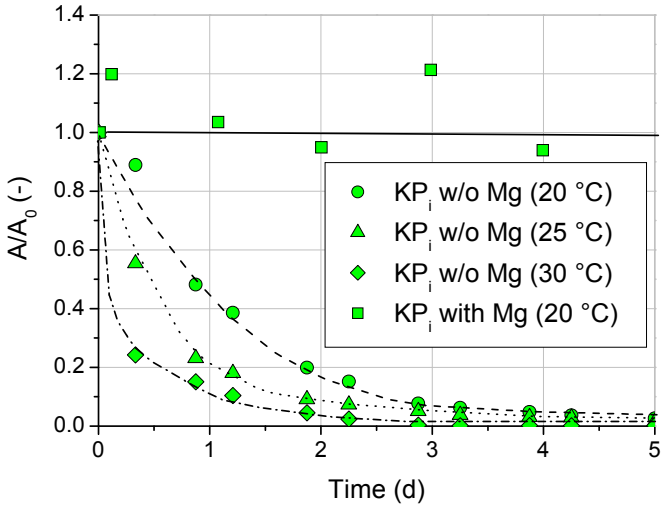

Figure 4.7. Comparison of residual activity of *Lb*ADH incubated at different temperatures and 2 mM $MgSO_4$-containing buffer. Conditions (temperature): V = 1.0 mL, initial pH 6, 50 mM potassium phosphate buffer, 11 mM methyl acetoacetate (MAA), 0.2 mM NADPH, 6.7 mg L^{-1} *Lb*ADH (89.0 U_{MAA} mg_{ADH}^{-1}). Conditions (Mg-containing buffer): V = 1.0 mL, 20 °C, initial pH 6, 50 mM potassium phosphate buffer, 40 mM methyl acetoacetate (MAA), 2 mM $MgSO_4$, 0.2 mM NADPH, 3.3 mg L^{-1} *Lb*ADH (89.0 U_{MAA} mL_{ADH}^{-1}).

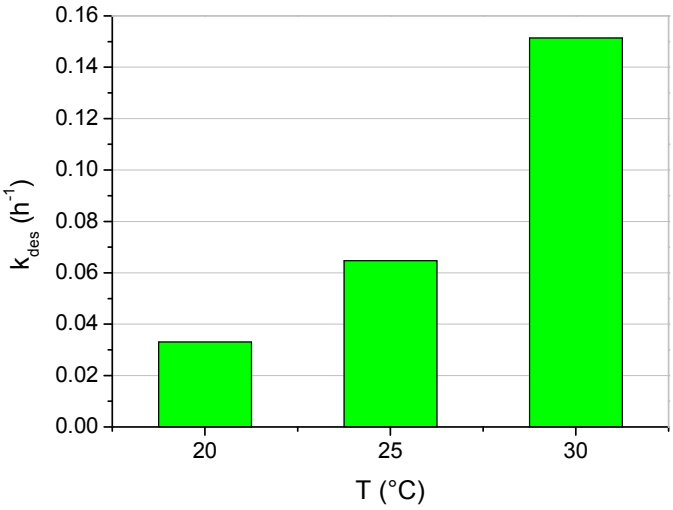

Figure 4.8. Deactivation of *Lb*ADH incubated in buffer at different temperatures. Conditions (temperature): V = 1.0 mL, initial pH 6, 50 mM potassium phosphate buffer, 11 mM methyl acetoacetate (MAA), 0.2 mM NADPH, 6.7 mg L^{-1} *Lb*ADH (89.0 U_{MAA} mL_{ADH}^{-1}).

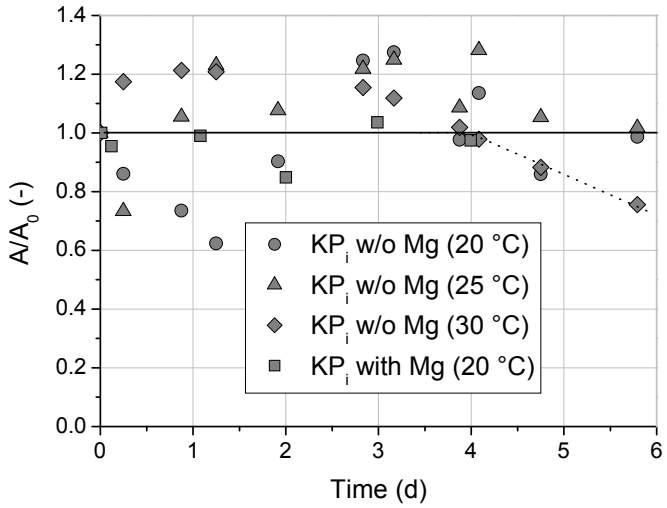

Figure 4.9. Comparison of residual activity of FDH incubated at different temperatures and 2 mM $MgSO_4$-containing buffer. Conditions (temperature): V = 1.0 mL, initial pH 6, 50 mM potassium phosphate buffer, 240 mM sodium formate, 0.2 mM $NADP^+$, 5.6 mg L^{-1} FDH (0.44 $U_{formate}$ mg_{FDH}^{-1}). Conditions (Mg-containing buffer): V = 1.0 mL, 20 °C, initial pH 6, 50 mM potassium phosphate buffer, 200 mM sodium formate, 2 mM $MgSO_4$, 0.2 mM $NADP^+$, 5.6 mg L^{-1} FDH (0.44 $U_{formate}$ mg_{FDH}^{-1}).

In the case of FDH, it was stable over a period of 6 days regardless of the presence of $MgSO_4$ (Figure 4.9). However, there was deactivation of FDH at higher temperature of 30 °C after 4 days of incubation. In view of the enzyme-coupled system, a compromise between the findings of *Lb*ADH and FDH led to the choice of 20 °C as operating temperature.

4.3.2.2 Incubation chemicals

In a typical enzyme-coupled setup, the enzymes are exposed to the biotransformation substrate, methyl acetoacetate (**MAA**), its product, (*R*)-methyl-3-hydroxybutanoate (**MHB**) and the cosubstrate, sodium formate.

The incubation of *Lb*ADH with methyl acetoacetate (**MAA**) over a period of 10 days showed that up to a concentration of 40 mM **MAA**, the activity of *Lb*ADH remained fairly unchanged (Figure 4.10). There was however, significant loss in activity of the *Lb*ADH incubated with 100 mM **MAA**.

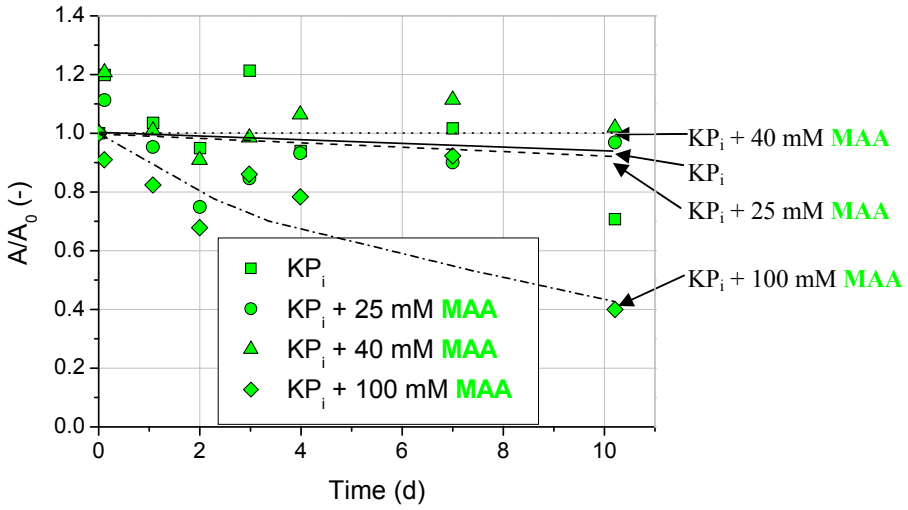

Figure 4.10. Residual activity of *Lb*ADH incubated with methyl acetoacetate-containing buffer. Reaction conditions: V = 1.0 mL, 20 °C, initial pH 6, 50 mM potassium phosphate buffer, 40 mM methyl acetoacetate (MAA), 2 mM $MgSO_4$, 0.2 mM NADPH, 3.3 mg L^{-1} *Lb*ADH (89.0 U_{MAA} mg_{ADH}^{-1}).

On the other hand, the activity of *Lb*ADH was not significantly affected by the presence of (*R*)-methyl-3-hydroxybutanoate (**MHB**) (up to 100 mM) (Figure 4.11). More than 85 % of the activity of *Lb*ADH remained after 10 days of incubation.

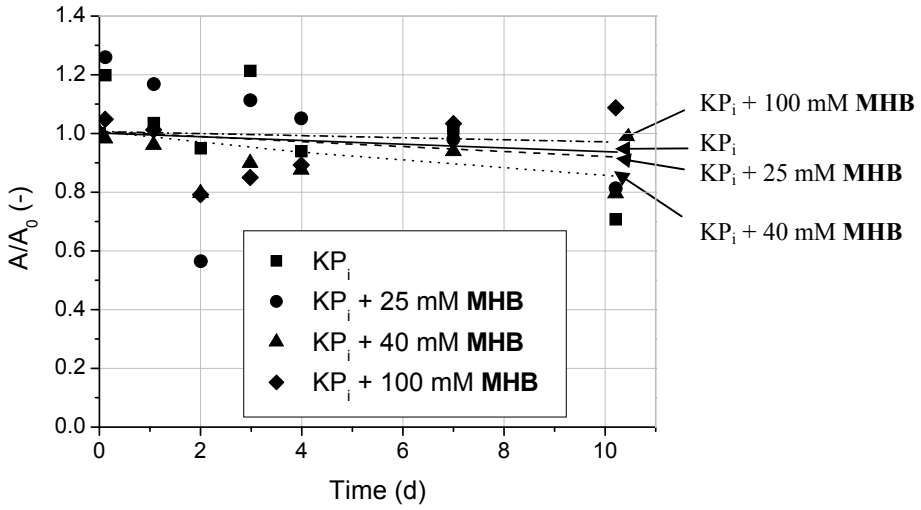

Figure 4.11. Residual activity of *Lb*ADH incubated with (*R*)-methyl-3-hydroxybutanoate-containing buffer. Reaction conditions: V = 1.0 mL, 20 °C, initial pH 6, 50 mM potassium phosphate buffer, 40 mM methyl acetoacetate (MAA), 2 mM $MgSO_4$, 0.2 mM NADPH, 3.3 mg L^{-1} *Lb*ADH (89.0 U_{MAA} mg_{ADH}^{-1}).

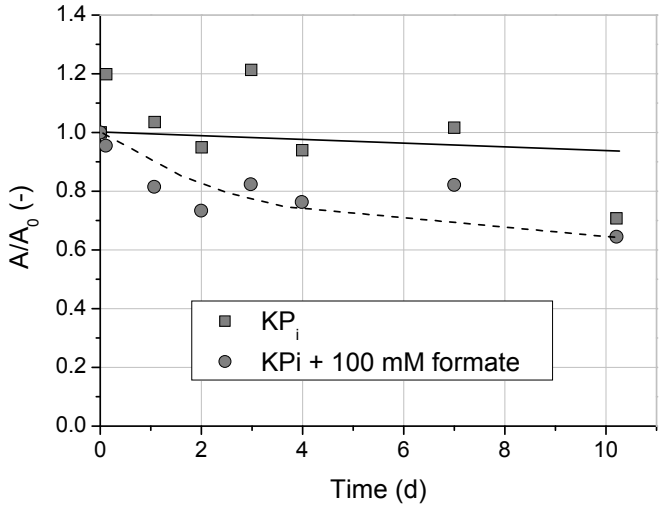

Figure 4.12. Residual activity of *Lb*ADH incubated with 100 mM sodium formate-containing buffer. Reaction conditions: V = 1.0 mL, 20 °C, initial pH 6, 50 mM potassium phosphate buffer, 40 mM methyl acetoacetate (MAA), 2 mM $MgSO_4$, 0.2 mM NADPH, 3.3 mg L^{-1} *Lb*ADH (89.0 U_{MAA} mg_{ADH}^{-1}).

From Figure 4.12, the activity of *Lb*ADH decayed over 10 days in the presence of 100 mM sodium formate, giving a residual activity of 70 %. Therefore, it appeared that methyl acetoacetate (**MAA**) of above 40 mM, and 100 mM sodium formate were toxic to *Lb*ADH over time. The product, (*R*)-methyl-3-hydroxybutanoate (**MHB**) (up to 100 mM), did not exhibit significant toxicity on *Lb*ADH over 10 days.

In contrary, the presence of methyl acetoacetate (**MAA**) of up to 100 mM did not exhibit major toxic effects on FDH (Figure 4.13). Similar to that observed for

*Lb*ADH, (*R*)-methyl-3-hydroxybutanoate (**MHB**) (up to 100 mM) did not have much toxic effects on FDH (Figure 4.14). Likewise, incubation of FDH with 100 mM sodium formate resulted in an activity drop of 30 % over 10 days (Figure 4.15).

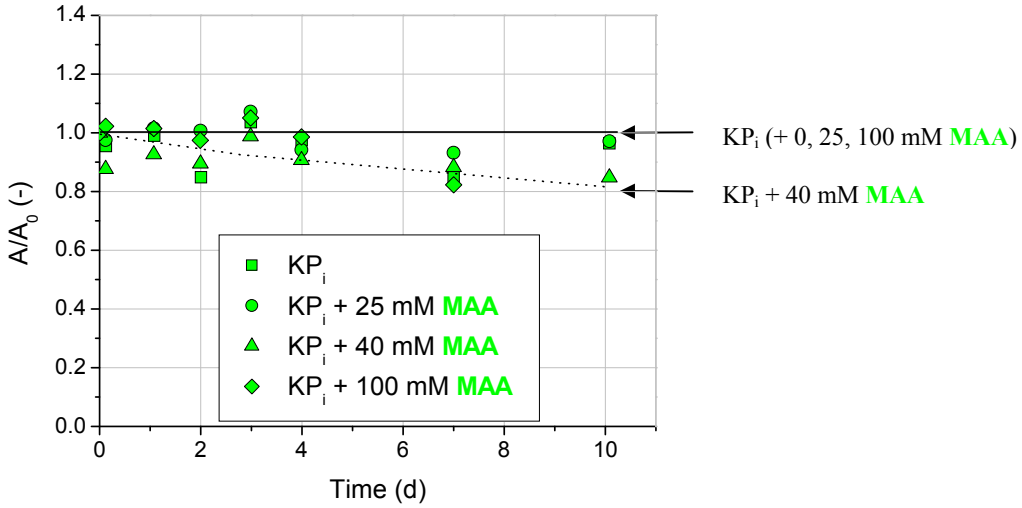

Figure 4.13. Residual activity of FDH incubated with methyl acetoacetate-containing buffer. Reaction conditions: V = 1.0 mL, 20 °C, initial pH 6, 50 mM potassium phosphate buffer, 200 mM sodium formate, 2 mM $MgSO_4$, 0.2 mM $NADP^+$, 5.6 mg L^{-1} FDH (0.44 $U_{formate}$ mg_{FDH}^{-1}).

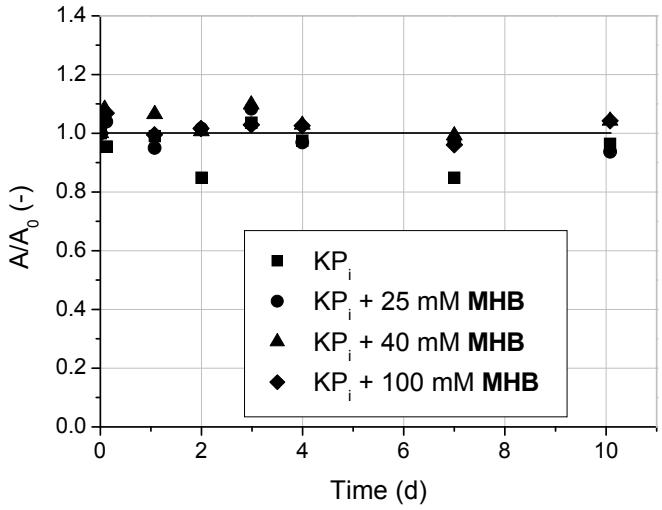

Figure 4.14. Residual activity of FDH incubated with (*R*)-methyl-3-hydroxybutanoate-containing buffer. Reaction conditions: V = 1.0 mL, 20 °C, initial pH 6, 50 mM potassium phosphate buffer, 200 mM sodium formate, 2 mM $MgSO_4$, 0.2 mM $NADP^+$, 5.6 mg L^{-1} FDH (0.44 $U_{formate}$ mg_{FDH}^{-1}).

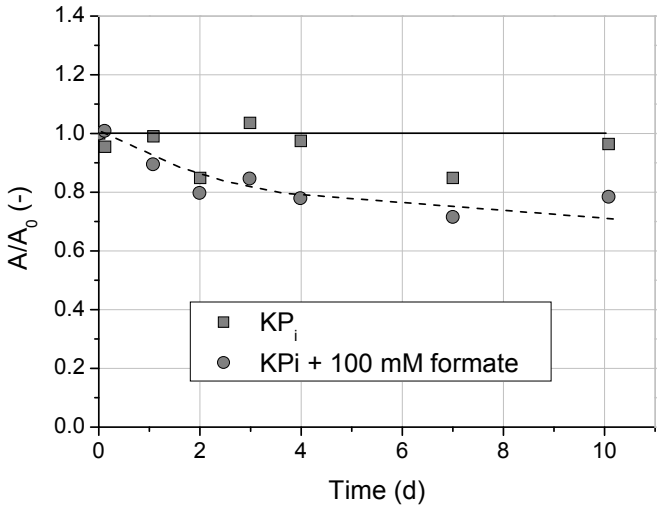

Figure 4.15. Residual activity of FDH incubated with 100 mM sodium formate-containing buffer. Reaction conditions: V = 1.0 mL, 20 °C, initial pH 6, 50 mM potassium phosphate buffer, 200 mM sodium formate, 2 mM $MgSO_4$, 0.2 mM $NADP^+$, 5.6 mg L^{-1} FDH (0.44 $U_{formate}$ mg_{FDH}^{-1}).

4.3.3 Stability of cofactors

With the above knowledge of temperature stability of the enzymes (refer to Chapter 4.3.2.1), the thermal stability of the cofactors over time is also essential in operating the enzyme-coupled system.

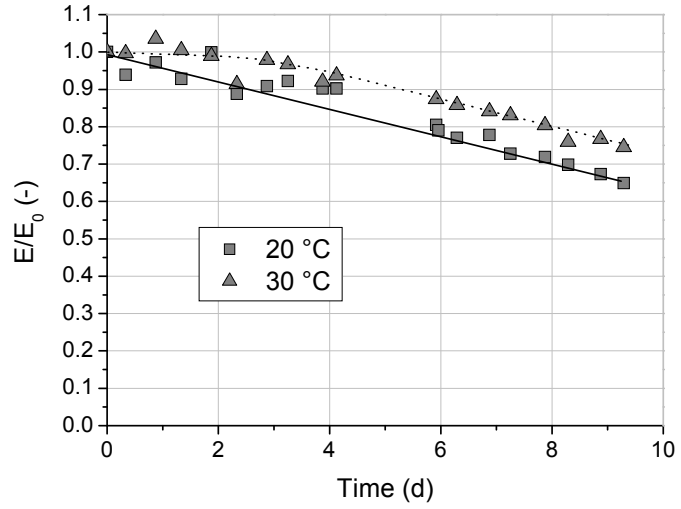

Figure 4.16. Residual absorbance of $NADP^+$ incubated at different temperatures over time. Conditions: V = 1.0 mL, initial pH 6, 50 mM potassium phosphate buffer, 240 mM sodium formate, 0.2 mM $NADP^+$, 5.6 mg L^{-1} FDH (0.44 $U_{formate}$ mg_{FDH}^{-1}).

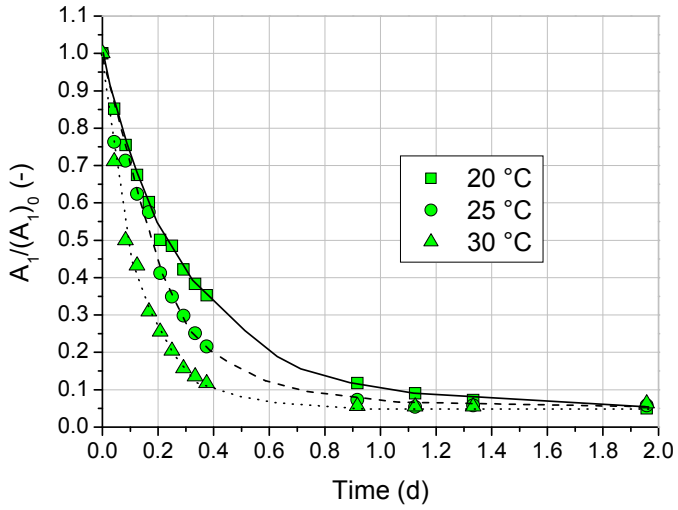

Figure 4.17. Residual absorbance of NADPH incubated at different temperatures over time. Conditions: V = 1.0 mL, initial pH 6, 50 mM potassium phosphate buffer, 11 mM methyl acetoacetate (MAA), 0.2 mM NADPH, 6.7 mg L^{-1} *Lb*ADH (89.0 U_{MAA} mg_{ADH}^{-1}).

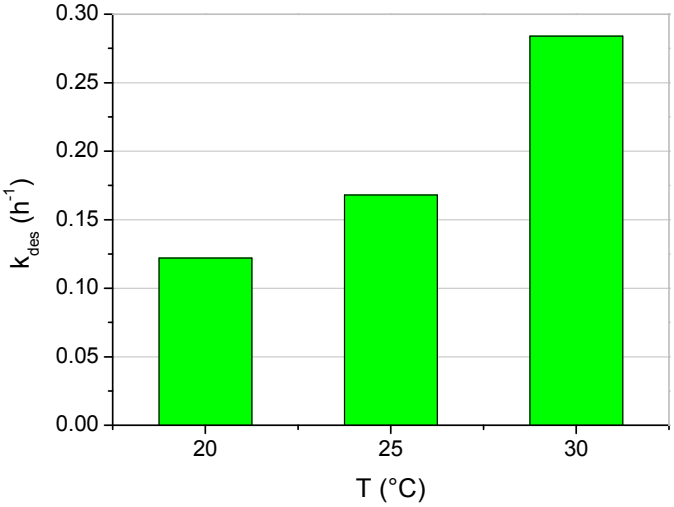

Figure 4.18. Deactivation constants of NADPH incubated at different temperatures. Conditions: V = 1.0 mL, initial pH 6, 50 mM potassium phosphate buffer, 11 mM methyl acetoacetate (MAA), 0.2 mM NADPH, 6.7 mg L^{-1} *Lb*ADH (89.0 U_{MAA} mg_{ADH}^{-1}).

It was observed in Figure 4.16 that $NADP^+$ deactivated at the rates of 0.16 % h^{-1} (20 °C) and 0.13 % h^{-1} (30 °C) over a period of over 9 days. In contrast, NADPH deactivated rapidly with increasing temperature (Figures 4.17 and 4.18). Since the rate of deactivation for NADPH was almost 100-fold more than that of $NADP^+$, it was necessary to choose a lower operating temperature of 20 °C to prevent excess deactivation of the reduced cofactor. Simultaneously, there was negligible deactivation of the oxidised cofactor. In fact, the stability of the enzymes, in

particular *Lb*ADH, was also best at 20 °C (refer to Chapter 4.3.2.1). Therefore, in view of the stability of *Lb*ADH and NADPH, it was determined that the best temperature to operate the enzyme-coupled system was 20 °C.

4.3.4 Batch kinetics

The batch kinetics of *Lb*ADH and FDH were firstly investigated and separately modelled with the program MicroMath® Scientist® for Windows™. Due to the instability of NADPH, a slight excess of *Lb*ADH was used in the studies to reduce the concentration of NADPH to a minimal. The obtained data were then combined and the enzymes were coupled in a batch.

4.3.4.1 Kinetics of *Lb*ADH

The reduced and oxidised cofactors NAD(P)(H) were not inhibitory to NADPH- and NADH-bounded *Lb*ADH (Figures 4.19 and 4.20). When NADPH was employed as cofactor, methyl acetoacetate (**MAA**) was found to be inhibitory to *Lb*ADH (Figure 4.21). On the other hand, if NADH was used, there was no inhibition of methyl acetoacetate (**MAA**), up to 250 mM, observed. In contrast, the product, (*R*)-methyl-3-hydroxybutanoate (**MHB**), showed no significant inhibition effects on the NADPH-bounded *Lb*ADH. Up to a concentration of 250 mM (*R*)-methyl-3-hydroxybutanoate (**MHB**), there was also no inhibition effect seen on the NADH-bounded *Lb*ADH (Figure 4.22).

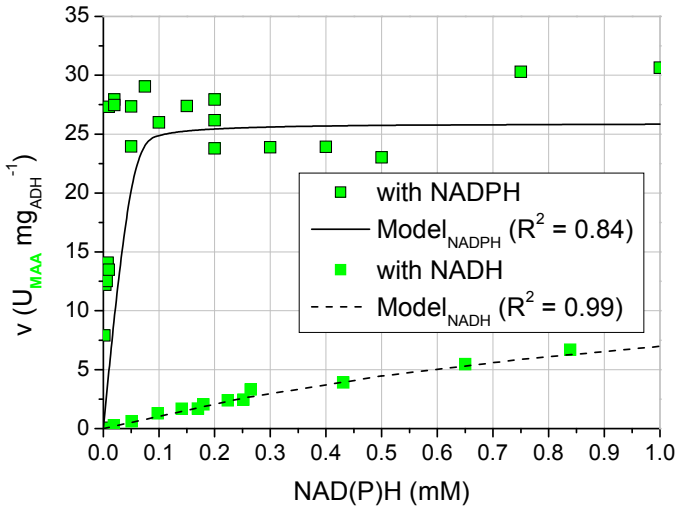

Figure 4.19. Activity of *Lb*ADH with NAD(P)H as a function of the concentration of reduced cofactors NAD(P)H. Conditions: V = 1.0 mL, 20 °C, initial pH 6, 50 mM potassium phosphate buffer, 40 mM methyl acetoacetate (MAA) (or 200 mM MAA when NADH is used), 2 mM $MgSO_4$, 0.126 mg L^{-1} *Lb*ADH (89.0 U_{MAA} mg_{ADH}^{-1}).

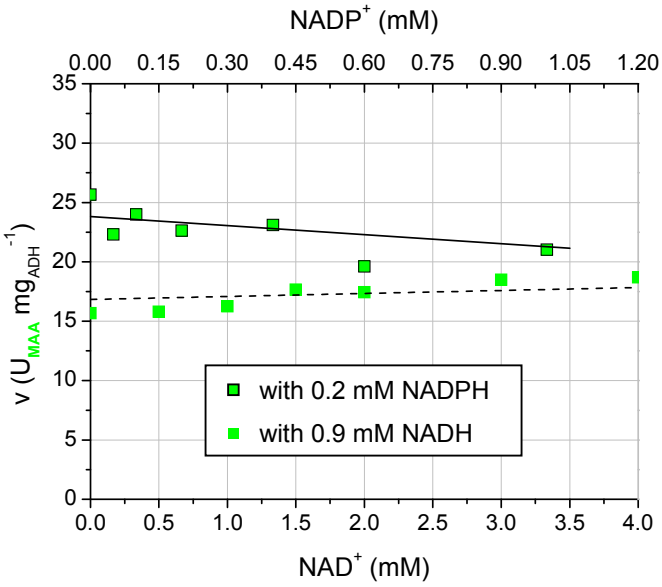

Figure 4.20. Activity of *Lb*ADH with NAD(P)H as a function of the concentration of oxidised cofactors NAD(P)$^+$. Conditions: V = 1.0 mL, 20 °C, initial pH 6, 50 mM potassium phosphate buffer, 40 mM methyl acetoacetate (MAA) (or 200 mM MAA when NADH is used), 2 mM $MgSO_4$, 0.2 mM NADPH (or 0.9 mM NADH), 0.126 mg L^{-1} *Lb*ADH (89.0 U_{MAA} mg_{ADH}^{-1}).

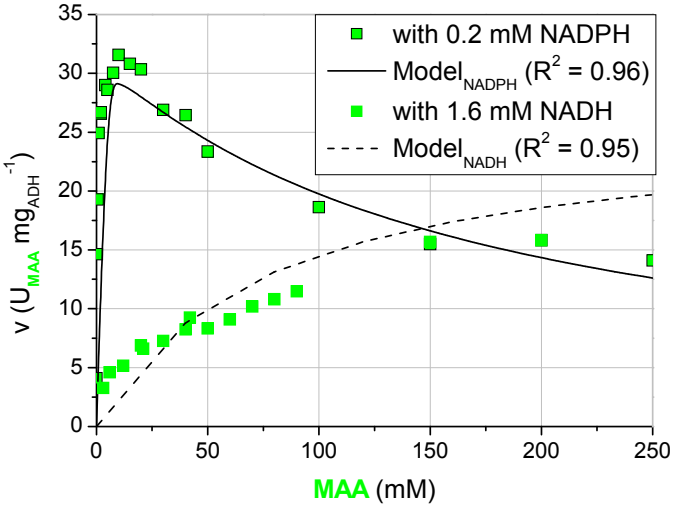

Figure 4.21. Activity of *Lb*ADH with NAD(P)H as a function of the concentration of methyl acetoacetate (MAA). Conditions: V = 1.0 mL, 20 °C, initial pH 6, 50 mM potassium phosphate buffer, 2 mM $MgSO_4$, 0.2 mM NADPH (or 1.6 mM NADH), 0.126 mg L^{-1} *Lb*ADH (89.0 U_{MAA} mg_{ADH}^{-1}).

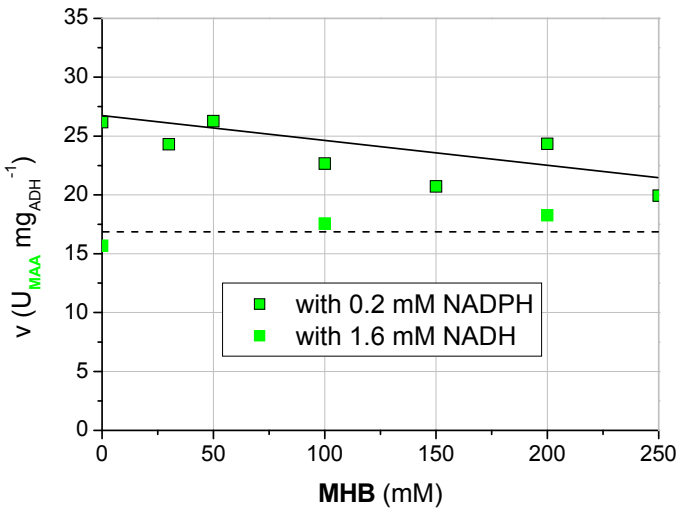

Figure 4.22. Activity of *Lb*ADH with NAD(P)H as a function of the concentration of (*R*)-methyl-3-hydroxybutanoate (MHB). Conditions: V = 1.0 mL, 20 °C, initial pH 6, 50 mM potassium phosphate buffer, 40 mM methyl acetoacetate (MAA) (or 200 mM MAA when NADH is used), 2 mM $MgSO_4$, 0.2 mM NADPH (or 1.6 mM NADH), 0.126 mg L^{-1} *Lb*ADH (89.0 U_{MAA} mg_{ADH}^{-1}).

The results suggested that *Lb*ADH behaved differently, depending on which cofactor it used in the bioreduction of methyl acetoacetate (**MAA**). Using a 2-substrate Michealis-Menten equation for methyl acetoacetate (**MAA**) and NAD(P)H, two equations described the batch kinetics of NAD(P)H-bounded *Lb*ADH. In the case of NADPH-bounded *Lb*ADH, there existed substrate inhibition of methyl acetoacetate (**MAA**) with no product inhibition of (*R*)-methyl-3-hydroxybutanoate (**MHB**) and NADPH (Eq. 4.10). For NADH-bounded *Lb*ADH, there existed no substrate and product inhibition (Eq. 4.11). The kinetics constants are summarised in Table 4.1.

Model for *Lb*ADH/NADPH reaction:

$$v = \frac{v_{max,MAA} \times C_{MAA}}{K_{m,MAA} + C_{MAA} + \frac{C_{MAA}^{\ 2}}{K_{i,MAA}}} \times \frac{C_{NADPH}}{K_{m,NADPH} + C_{NADPH}} \qquad \text{(eq. 4.10)}$$

Model for *Lb*ADH/NADH reaction:

$$v = \frac{v_{max,MAA} \times C_{MAA}}{K_{m,MAA} + C_{MAA}} \times \frac{C_{NADH}}{K_{m,NADH} + C_{NADH}} \qquad \text{(eq. 4.11)}$$

Table 4.1. Kinetics constants of NAD(P)H-dependent *Lb*ADH.

Kinetics constants	NADPH-dependency	NADH-dependency*
$v_{max,MAA}$ (U_{MAA} mg_{ADH}^{-1})	32.47 ± 0.05	30.41
$K_{m,MAA}$ (mM)	0.31 ± 0.001	84.27 ± 0.94
$K_{m,NAD(P)H}$ (mM)	0.0038 ± 6×10^{-5}	1.6
$K_{i,MAA}$ (mM)	163.98 ± 0.53	-

*Due to the convergence of small values in the iterations in the program, the $v_{max,MAA}$ and $K_{m,NAD(P)H}$ values were firstly obtained through trial and error, set and then re-iterated with the program to yield sensible results.

4.3.4.2 Kinetics of FDH

The $NADP^+$-dependent FDH showed no inhibition to its substrate, formate, of up to 200 mM (Figure 4.23). $NADP^+$ (up to 1 mM) was also found to exhibit no inhibition towards FDH (Figure 4.24). However, the reduced cofactor NADPH (up to 0.2 mM) inhibited the FDH rather significantly despite the low concentration present (Figure 4.25).

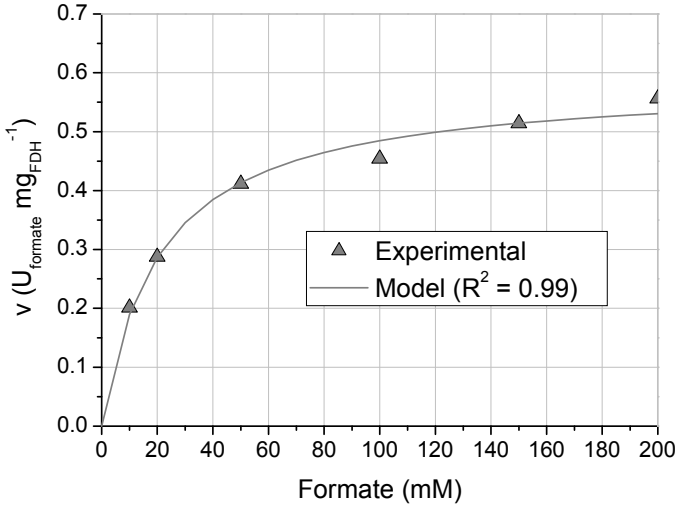

Figure 4.23. Activity of FDH as a function of the concentration of formate. Conditions: V = 1.0 mL, 20 °C, initial pH 6, 50 mM potassium phosphate buffer, 2 mM $MgSO_4$, 0.2 mM $NADP^+$, 8.7 mg L^{-1} FDH (0.44 $U_{formate}$ mg_{FDH}^{-1}).

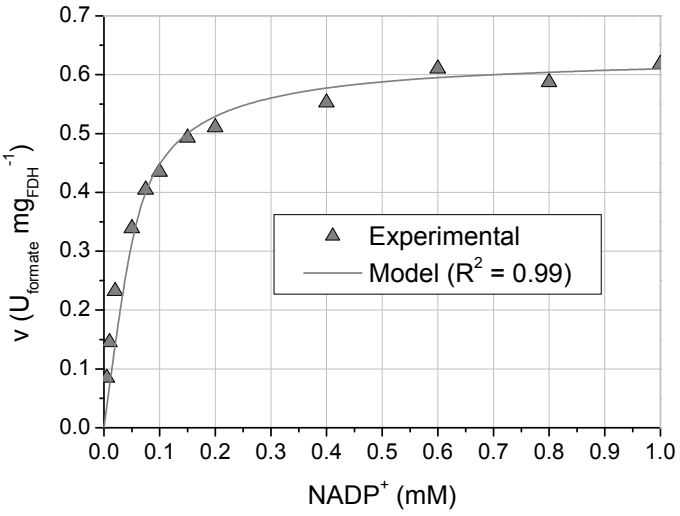

Figure 4.24. Activity of FDH as a function of the concentration of $NADP^+$. Conditions: V = 1.0 mL, 20 °C, initial pH 6, 50 mM potassium phosphate buffer, 200 mM sodium formate, 2 mM $MgSO_4$, 8.7 mg L^{-1} FDH (0.44 $U_{formate}$ mg_{FDH}^{-1}).

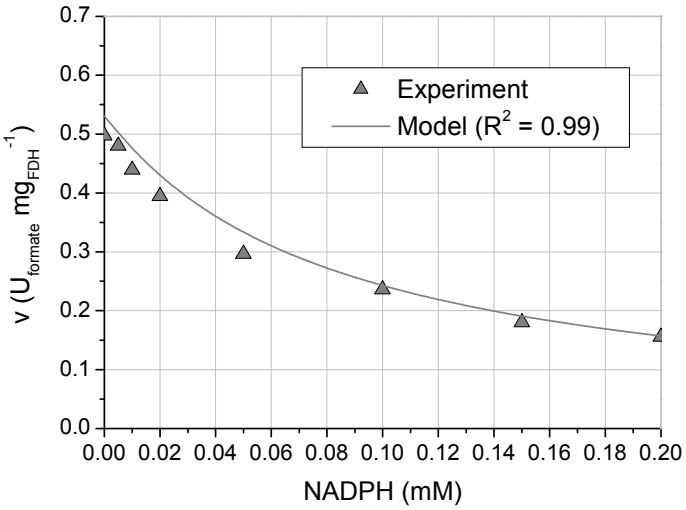

Figure 4.25. Activity of FDH as a function of the concentration of NADPH. Conditions: V = 1.0 mL, 20 °C, initial pH 6, 50 mM potassium phosphate buffer, 200 mM sodium formate, 2 mM $MgSO_4$, 0.2 mM $NADP^+$, 8.7 mg L^{-1} FDH (0.44 $U_{formate}$ mg_{FDH}^{-1}).

Using a 2-substrate Michealis-Menten equation for formate and $NADP^+$, the behaviour of FDH was expressed (Eq. 4.12). The kinetics constants are summarised in Table 4.2.

$$v = \frac{v_{\max,formate} \times C_{formate}}{K_{m,formate} + C_{formate}} \times \frac{C_{NADP^+}}{K_{m,NADP^+} \times \left(1 + \frac{C_{NADPH}}{K_{i,NADPH}}\right) + C_{NADP^+}} \qquad \text{(eq. 4.12)}$$

Table 4.2. Kinetics constants of $NADP^+$-dependent FDH.

Kinetics constants	$NADP^+$-dependency
$v_{max,formate}$ ($U_{formate}$ mg_{FDH}^{-1})	$0.70 \pm 9\times10^{-3}$
$K_{m,formate}$ (mM)	20.90 ± 0.14
$K_{m,NADP}$ (mM)	$0.039 \pm 2\times10^{-5}$
$K_{i,NADPH}$ (mM)	$0.014 \pm 3\times10^{-4}$

4.3.4.3 Enzyme-coupled batch run

*Lb*ADH and FDH were combined in a batch for the bioreduction of methyl acetoacetate (**MAA**), and the regeneration of NADP(H) through the oxidation of formate. The profile of a typical enzyme-coupled batch system is illustrated in Figure 4.26, where a conversion of more than 99 % of methyl acetoacetate (**MAA**) and yield of (*R*)-methyl-3-hydroxybutanoate (**MHB**) (ee > 99 %) were achieved experimentally. For this batch reaction, the amount of reactant in the reactor is equal to the sum of the amount of reactant lost due to the chemical reaction and the residual amount of

unreacted reactant. With this mass balance, modelling of the enzyme-coupled batch with MicroMath® Scientist® using the above Michealis-Menten equations (Eqs. 4.10 and 4.12) gave good fit of R^2 = 0.99 (**MAA**), and 0.98 (**MHB**). The total turnover numbers, initial rate of production of (*R*)-methyl-3-hydroxybutanoate (**MHB**) and the biocatalyst consumption of a typical enzyme-coupled batch are summarised in Table 4.3.

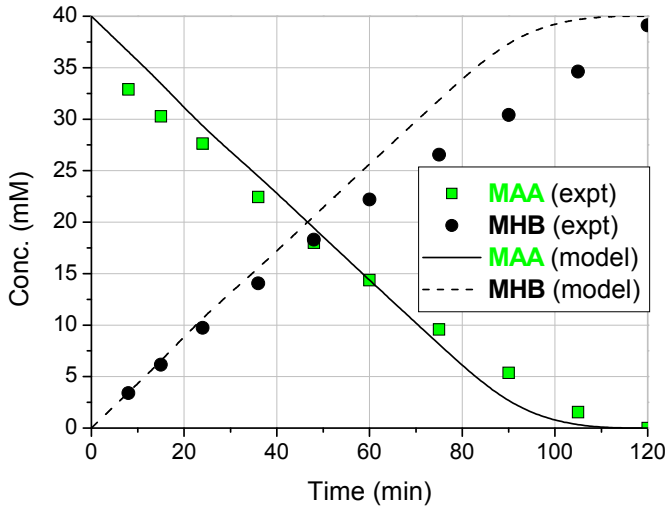

Figure 4.26. Concentration profile of reactants in an enzyme-coupled batch as a function of time. Conditions: V = 1.5 mL, 20 °C, initial pH 6, 50 mM potassium phosphate buffer, 100 mM sodium formate, 40 mM methyl acetoacetate (MAA), 2 mM $MgSO_4$, 0.2 mM $NADP^+$, 0.025 g L^{-1} *Lb*ADH (89.0 U_{MAA} mg_{ADH}^{-1}), 1.0 g L^{-1} FDH (0.44 $U_{formate}$ mg_{FDH}^{-1}).

Table 4.3. Summary of results from enzyme-coupled batch run.

Parameters	Values
ttn_{ADH} (mol_{MHB} mol_{ADH}^{-1})	168178
ttn_{FDH} (mol_{MHB} mol_{FDH}^{-1})	1753
ttn_{NADP} (mol_{MHB} mol_{NADP}^{-1})	200
STY (g_{MHB} L^{-1} h^{-1})	2.36
Initial rate of production (U mL^{-1})	0.33
Biocat consumption ($g_{ADH+FDH}$ g_{MHB}^{-1})	0.22

4.3.5 Enzyme-coupled repetitive batch studies

In order to improve the enzyme-coupled process, repetitive batch mode was performed to obtain higher total turnover numbers. After 4 repetitive batches, there was an increase in total turnover numbers (with respect to ADH and FDH) and a drop in the biocatalyst consumption (Table 4.4). In addition, the enzymes appeared to produce (*R*)-methyl-3-hydroxybutanoate (**MHB**) at about the same rates (Figure 4.27). However, the activity of the batches revealed an exponential deactivation rate

of 4.6 % h^{-1} (R^2 = 0.95) (Figure 4.28). The decrease in activity of the repetitive batches was due to the loss in activity of *Lb*ADH and FDH (Figure 4.29). *Lb*ADH decayed exponentially at 4.0 % h^{-1} while the residual activity of FDH was 79 % after about 9 h.

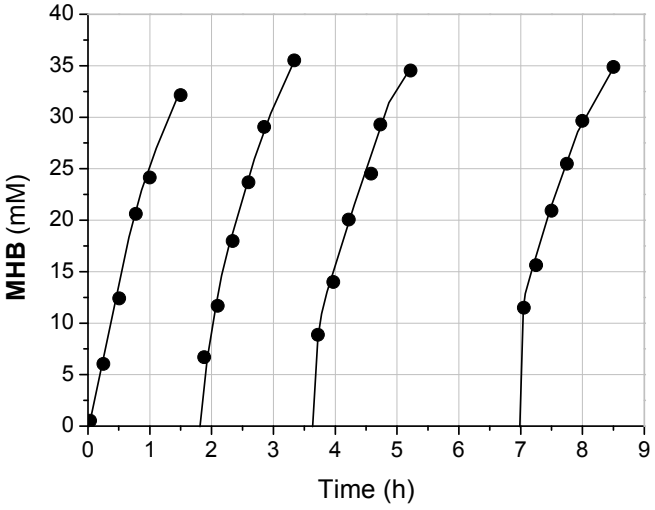

Figure 4.27. Concentration of (*R*)-methyl-3-hydroxybutanoate (MHB) in an enzyme-coupled repetitive batch run as a function of time. Conditions: V = 10 mL, 20 °C, initial pH 6, 50 mM potassium phosphate buffer, 100 mM sodium formate, 40 mM methyl acetoacetate (MAA), 2 mM $MgSO_4$, 0.2 mM $NADP^+$, 0.03 g L^{-1} *Lb*ADH (89.0 U_{MAA} mg_{ADH}^{-1}), 1.2 g L^{-1} FDH (0.44 $U_{formate}$ mg_{FDH}^{-1}).

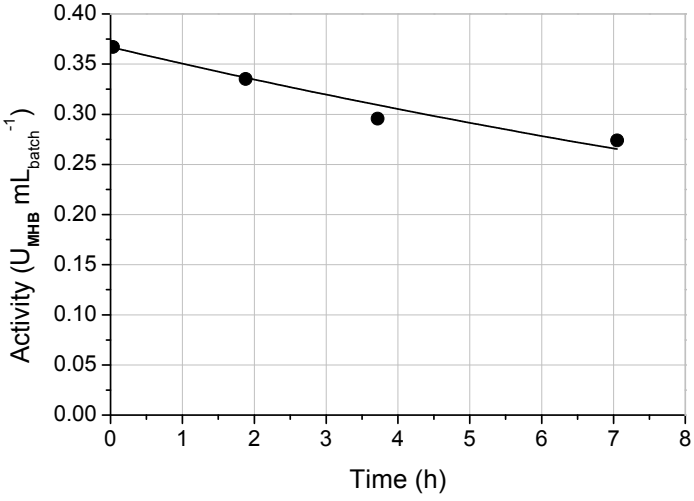

Figure 4.28. Overall activity of enzyme-coupled repetitive batch run as a function of time. Conditions: V = 10 mL, 20 °C, initial pH 6, 50 mM potassium phosphate buffer, 100 mM sodium formate, 40 mM methyl acetoacetate (MAA), 2 mM $MgSO_4$, 0.2 mM $NADP^+$, 0.03 g L^{-1} *Lb*ADH (89.0 U_{MAA} mg_{ADH}^{-1}), 1.2 g L^{-1} FDH (0.44 $U_{formate}$ mg_{FDH}^{-1}).

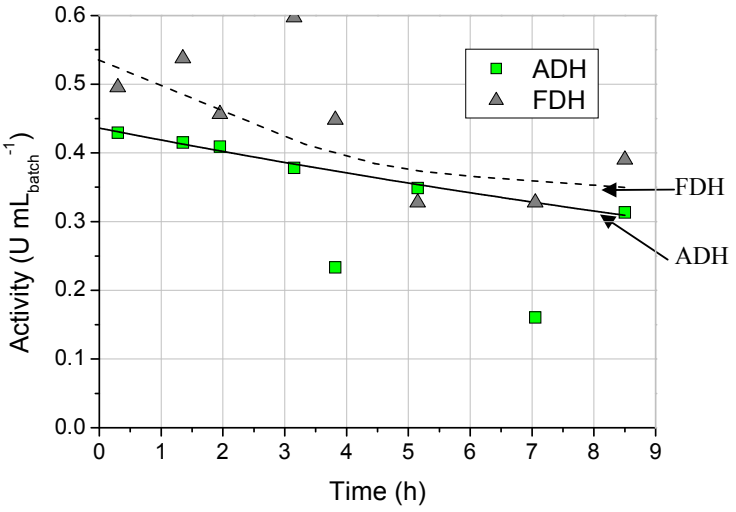

Figure 4.29. Activities of ADH and FDH in enzyme-coupled repetitive batch run as a function of time. Conditions: V = 10 mL, 20 °C, initial pH 6, 50 mM potassium phosphate buffer, 100 mM sodium formate, 40 mM methyl acetoacetate (MAA), 2 mM $MgSO_4$, 0.2 mM $NADP^+$, 0.03 g L^{-1} *Lb*ADH (89.0 U_{MAA} mg_{ADH}^{-1}), 1.2 g L^{-1} FDH (0.44 $U_{formate}$ mg_{FDH}^{-1}).

Table 4.4. Summary of results from enzyme-coupled repetitive batch run.

Parameters	Values
ttn_{ADH} (mol_{MHB} mol_{ADH}^{-1})	559703
ttn_{FDH} (mol_{MHB} mol_{FDH}^{-1})	5854
ttn_{NADP} (mol_{MHB} mol_{NADP}^{-1})	200
Biocat consumption ($g_{ADH+FDH}$ g_{MHB}^{-1})	0.07

4.3.6 Enzyme-coupled continuous run in enzyme membrane reactor

Continuous reduction of methyl acetoacetate (**MAA**) with the enzyme-coupled system for regeneration of cofactors was performed in an enzyme membrane reactor (EMR) at a residence time of 1 h (Figure 4.30).

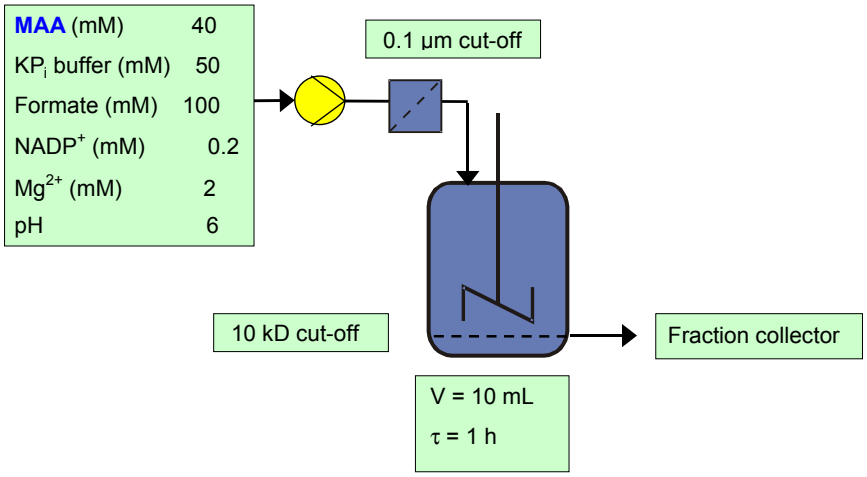

Figure 4.30. Scheme of enzyme-coupled continuous run in an enzyme membrane reactor.

In the first 16 h of operation, more than 99 % of methyl acetoacetate (**MAA**) was converted and more than 99 % of (*R*)-methyl-3-hydroxybutanoate (**MHB**) was yielded (Figures 4.31 and 4.32). Following which, there was a rapid drop in conversion and yield of the process. Analyses of the enzymes in the EMR showed rapid and mild deactivation of *Lb*ADH and FDH respectively (Figures 4.33 and 4.34).

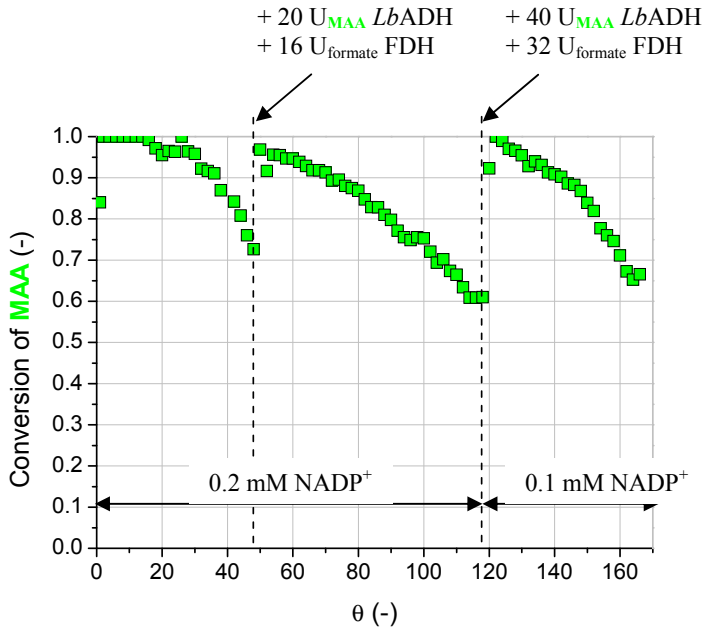

Figure 4.31. Conversion of methyl acetoacetate (MAA) as a function of the number of residence time in an enzyme-coupled continuous reactor. Conditions: V = 10 mL, 20 °C, initial pH 6, 50 mM potassium phosphate buffer, 100 mM sodium formate, 40 mM methyl acetoacetate (MAA), 2 mM $MgSO_4$, 0.2 mM $NADP^+$, initial 0.075 g L^{-1} *Lb*ADH (20.4 U_{MAA} mg_{ADH}^{-1}, 20 U_{MAA}), initial 3 g L^{-1} FDH (0.44 $U_{formate}$ mg_{FDH}^{-1}, 48 $U_{formate}$).

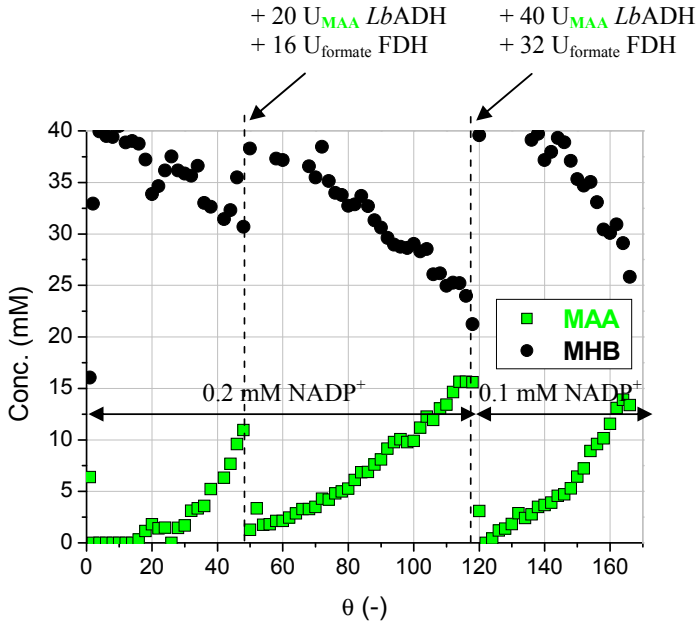

Figure 4.32. Concentration profile of reactants as a function of the number of residence time in an enzyme-coupled continuous reactor. Conditions: V = 10 mL, 20 °C, initial pH 6, 50 mM potassium phosphate buffer, 100 mM sodium formate, 40 mM methyl acetoacetate (MAA), 2 mM $MgSO_4$, 0.2 mM $NADP^+$, initial 0.075 g L^{-1} *Lb*ADH (20.4 U_{MAA} mg_{ADH}^{-1}, 20 U_{MAA}), initial 3 g L^{-1} FDH (0.44 $U_{formate}$ mg_{FDH}^{-1}, 48 $U_{formate}$).

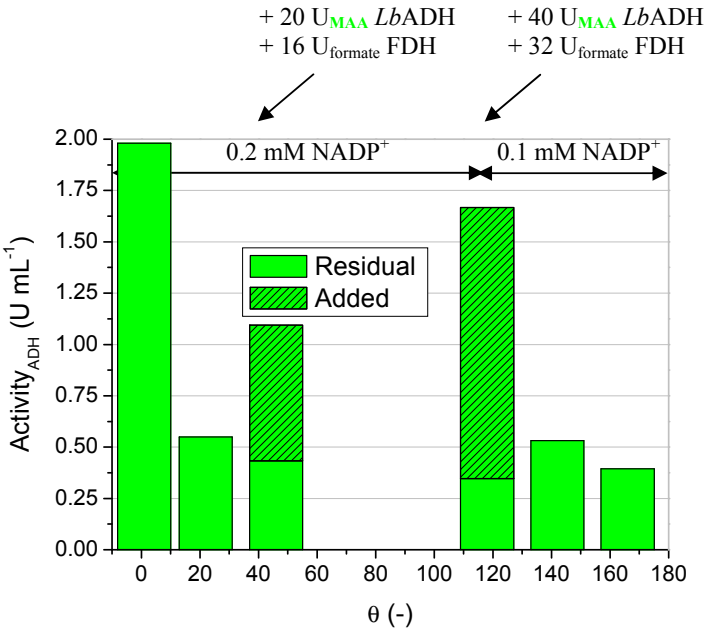

Figure 4.33. Activity of *Lb*ADH as a function of the number of residence time in an enzyme-coupled continuous reactor. Conditions: V = 10 mL, 20 °C, initial pH 6, 50 mM potassium phosphate buffer, 100 mM sodium formate, 40 mM methyl acetoacetate (MAA), 2 mM $MgSO_4$, 0.2 mM $NADP^+$, initial 0.075 g L^{-1} *Lb*ADH (20.4 U_{MAA} mg_{ADH}^{-1}, 20 U_{MAA}), 3 g L^{-1} FDH (0.44 $U_{formate}$ mg_{FDH}^{-1}, 48 $U_{formate}$).

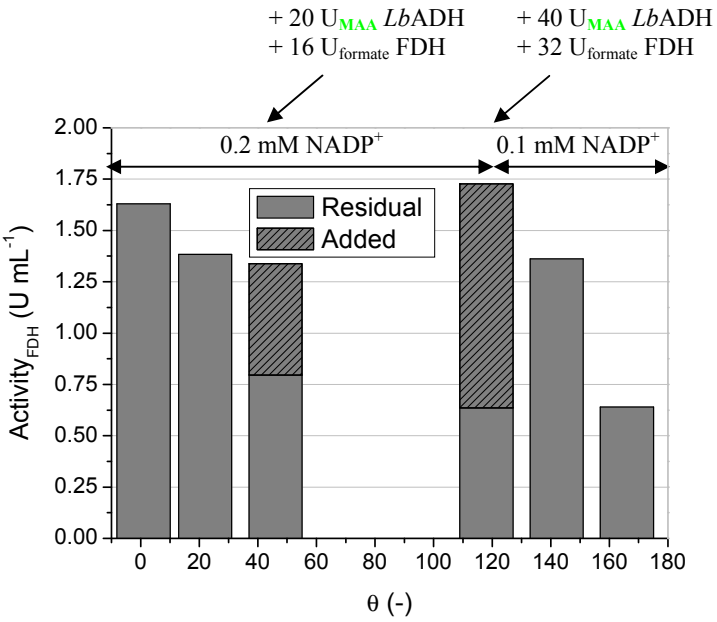

Figure 4.34. Activity of FDH as a function of the number of residence time in an enzyme-coupled continuous reactor. Conditions: V = 10 mL, 20 °C, initial pH 6, 50 mM potassium phosphate buffer, 100 mM sodium formate, 40 mM methyl acetoacetate (MAA), 2 mM $MgSO_4$, 0.2 mM $NADP^+$, initial 0.075 g L^{-1} *Lb*ADH (20.4 U_{MAA} mg_{ADH}^{-1}, 20 U_{MAA}), initial 3 g L^{-1} FDH (0.44 $U_{formate}$ mg_{FDH}^{-1}, 48 $U_{formate}$).

Additional amount of enzymes (33 % of the initial amount) fed into the EMR at θ = 46 gave almost full recovery of the conversion of methyl acetoacetate (**MAA**) and yield of (*R*)-methyl-3-hydroxybutanoate (**MHB**). Although the total amount of *Lb*ADH in the reactor had a lower activity than at the beginning of the run, its activity was sufficient in the reduction of methyl acetoacetate (**MAA**). However, there continued a slide in the amount of (*R*)-methyl-3-hydroxybutanoate (**MHB**) formed after that due to the rapid drop in activity of *Lb*ADH.

At θ = 120, only 39 % of the existing FDH in the reactor was active. Since FDH was found to be stable in the chemicals in the reaction system (See Chapter 4.3.2.2), the rapid loss in activity could be due to the inhibition of FDH by traces of NADPH that were not regenerated to $NADP^+$ (Refer to Chapter 4.3.4.2). Therefore, a lower concentration of $NADP^+$ (0.1 mM) was fed into the reactor to minimise the amount of residual NADPH. In addition, more FDH and *Lb*ADH were added to the reactor to recover the initial activities.

Immediately after θ = 120, more than 99 % of methyl acetoacetate (**MAA**) was converted and more than 99 % of (*R*)-methyl-3-hydroxybutanoate (**MHB**) was yielded, similar to the first 16 h of operation. Therefore, it suggested that the starting concentration of $NADP^+$ was more than sufficient for the biotransformation and that it was not limiting.

In the last section of the continuous run (θ = 120 – 166), there continued to be a rapid decrease in formation of (*R*)-methyl-3-hydroxybutanoate (**MHB**). This was due once again to the rapid loss of activities of *Lb*ADH and FDH. It seemed that the loss in

activity of FDH was not solely due to the presence of trace amount of NADPH. It is not known which other factors caused the deactivation of FDH.

The overall performance of the continuous run is summarised in Table 4.5.

Table 4.5. Summary of results from continuous run of enzyme-coupled system.

Parameters	Values		
θ	0 - 46	46 – 120	120 - 166
$NADP^+$ (mM)	0.2	0.2	0.1
*Lb*ADH (U_{MAA})	20	40	80
FDH ($U_{formate}$)	48	64	96
ttn_{ADH} ($mol_{\mathbf{MHB}}\ mol_{ADH}^{-1}$)	2.2×10^6	2.4×10^6	1.1×10^6
ttn_{FDH} ($mol_{\mathbf{MHB}}\ mol_{FDH}^{-1}$)	2.4×10^4	2.5×10^4	1.1×10^4
ttn_{NADP} ($mol_{\mathbf{MHB}}\ mol_{NADP}^{-1}$)	177	160	329
Biocat consumption ($g_{ADH+FDH}\ g_{\mathbf{MHB}}^{-1}$)	0.016	0.015	0.033

Moreover, as the biotransformation proceeded over time, a white cloudy suspension was observed from the outlet of the reactor. It was non-proteinous in nature, and microscopic analysis for microorganisms in the reactor and outlet stream proved negative.

The suspension was suspected to be magnesium carbonate, formed from the presence of magnesium ions in the buffer and the oxidation of formate to carbon dioxide (Weast, 1986). However, the equilibrium of dissolved carbon dioxide, bicarbonate, carbonate and carbonic acid showed negligible carbonate present at acidic and neutral pHs, similar to the range of 6 to 7 measured from the reactor outlet (see Figure 4.35, Bailey and Ollis, 1986; Schmelzer et al., 2000). Due to the pH-sensitivity of dissolved carbon dioxide and the complex composition of the buffer, the actual equilibrium of dissolved carbon dioxide in solution and hence the identity of the cloudy suspension could not be easily established.

$$CO_2\,(g) + H_2O \leftrightarrow CO_2\,(\text{dissolved}) + H_2O \leftrightarrow H_2CO_3 \leftrightarrow HCO_3^- + H^+ \leftrightarrow CO_3^{2-} + 2\,H^+$$

pH < 5 | 7 < pH < 9 | pH > 11

Figure 4.35. Equilibrium of carbon dioxide in solution, with the pH range for the dominant species.

4.4 Conclusions

Enzyme-coupled system with alcohol dehydrogenase from *Lactobacillus brevis* (*Lb*ADH) and formate dehydrogenase from *Pseudomonas* sp. was able to reduce prochiral ketones to chiral alcohols.

In the synthesis of (*R*)-methyl-3-hydroxybutanoate (**MHB**), the following findings were obtained:

- $MgSO_4$ improved the storage stability of *Lb*ADH,
- Substrate **MAA** (beyond 40 mM) was toxic to *Lb*ADH while formate (100 mM) was slightly toxic to both *Lb*ADH and FDH,
- Product **MHB** (up to 100 mM) was non-toxic to *Lb*ADH and FDH,
- NADPH (k_{des} = 0.12 h^{-1} at 20 °C) was more unstable than $NADP^+$ at reaction conditions,
- For NADP(H)-dependent reactions, **MAA** inhibition was present for *Lb*ADH, while NADPH was inhibitory for FDH,
- No substrate (**MAA**) and product (**MHB**) inhibition were present for NADH-bounded *Lb*ADH reduction,
- Highest total turnover numbers (2.4 x 10^6 $mol_{\mathbf{MHB}}$ mol_{ADH}^{-1}, 2.5 x 10^4 $mol_{\mathbf{MHB}}$ mol_{FDH}^{-1} and 329 $mol_{\mathbf{MHB}}$ mol_{NADP}^{-1}) and lowest biocatalyst consumption (0.015 $g_{ADH+FDH}$ $g_{\mathbf{MHB}}^{-1}$) were obtained in the continuous setup,
- Rapid drop in activities of *Lb*ADH and FDH in continuous setup,
- Unknown white cloudy suspension formed in outlet of continuous reactor, probably due to the interplay of dissolved carbon dioxide and ions in buffer.

5 3-Hydroxybutanoate Synthesis with Genetically Modified Biocatalyst *Escherichia coli* BL21 Star (DE3)

A designer bug system was developed by Ernst et al., (2003, 2005) to catalyse the reduction of methyl acetoacetate (**MAA**) to (*R*)-methyl-3-hydroxybutanoate (**MHB**) (Figure 5.1). For the bioreduction step, *Escherichia coli* BL21 Star (DE3) was genetically coded with an alcohol dehydrogenase gene from *Lactobacillus brevis* (*Lb*ADH). To recycle the internal cofactors of the cells, a NAD^+-specific formate dehydrogenase (FDH) gene from *Mycobacterium vaccae* was incorporated into the biocatalyst. Compared to the $NADP^+$-dependent FDH from *Pseudomonas* sp. used in Chapter 4, this NAD^+-specific FDH was known to have high specific activity and stability (Bringer-Meyer, 2005). Moreover, Ernst et al. (2005) demonstrated that the bioreduction was able to proceed with NAD^+ as cofactor, thereby no $NADP^+$-specific FDH was needed. Formate, a cosubstrate, was oxidised to CO_2 as a result of the cofactor regeneration. This chapter explores the characterisation and synthesis of (*R*)-methyl-3-hydroxybutanoate (**MHB**) with recombinant *E. coli* in different reactor setups.

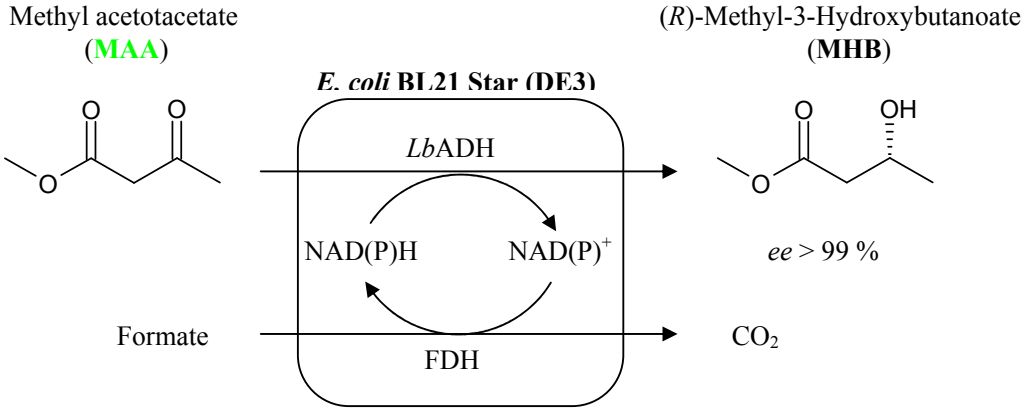

Figure 5.1. Enantioselective reduction of methyl acetoacetate (MAA) to (*R*)-methyl-3-hydroxybutanoate (MHB) with resting whole cells of *Escherichia coli* BL21 Star (DE3).

5.1 Biocatalyst production

5.1.1 Genetic transformation

Recombinant *Escherichia coli* BL21 Star (DE3) was cloned with ADH and FDH plasmids separately into the cells by transformation. The low copy plasmids, pBtacLB-ADH (800 bp, 26.7 kDa, carbenicillin resistance) and pBBR1MCS2*fdh* (1200 bp, 44 kDa, kanamycin resistance) were amplified separately in *Escherichia coli* DH5α before transformation into *Escherichia coli* BL21 Star (DE3). According

to the protocol established by Ernst et al. (2003, 2005) and Kaup (2005), there was no significant difference to the activity of the biocatalyst with regards to whichever plasmid was transformed first in the cells. However, in this genetic transformation work to produce the biocatalyst, only the rec. *E. coli* transformed with the ADH, then FDH plasmids yielded active cells for the bioreduction of methyl acetoacetate (**MAA**) (Figure 5.2).

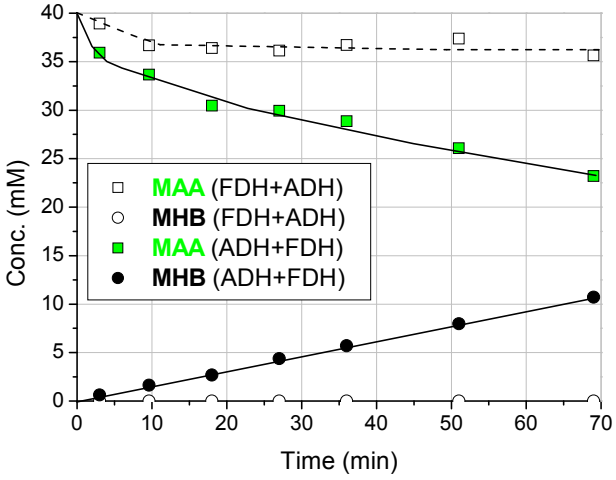

Figure 5.2. Concentration of reactants in a batch reactor with different modes of genetically transformed biocatalysts as a function of time. Conditions: V = 0.04 L, 30 °C, pH 6.5 (titrated with 3 M HCOOH), 500 mM potassium phosphate buffer, 200 mM sodium formate, 40 mM methyl acetoacetate (MAA), 0.8 g-wet cell weight rec. *E. coli*. The filled symbols refer to the biocatalyst transformed with the ADH, then FDH plasmids and the unfilled symbols refer to the biocatalyst transformed with the FDH, then ADH plasmids.

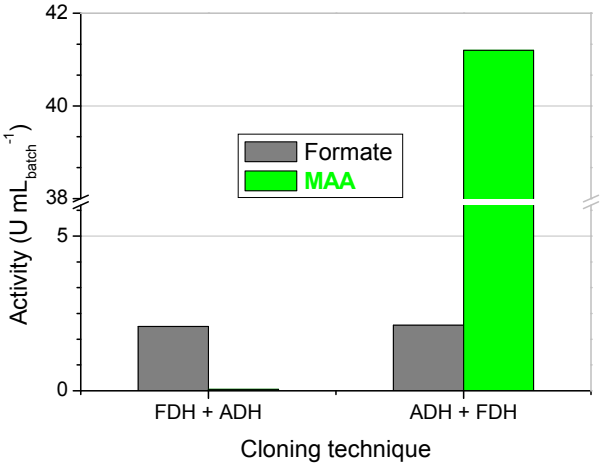

Figure 5.3. Enzymatic activity of FDH and ADH of the different modes of genetic transformed rec. *E. coli*. Grey columns: oxidation of formate by FDH, green columns: reduction of MAA by ADH. Conditions (ADH): V = 1.0 mL, 30 °C, initial pH 7, 50 mM postassium phosphate buffer, 11 mM methyl acetoacetate (MAA), 0.2 mM NADPH, 1 mM $MgSO_4$, 1 µL sonified cell suspension. Conditions (FDH): V = 1.0 mL, 30 °C, initial pH 6.5, 50 mM postassium phosphate buffer, 200 mM sodium formate, 0.2 mM NAD^+, 1 mM $MgSO_4$, 10 µL sonified cell suspension.

The inability of the rec. *E. coli* (transformed with the FDH plasmid first) to reduce methyl acetoactate (**MAA**) was attributed to the unsuccessful subsequent transformation of the ADH plasmid (Figure 5.3). On the other hand, the activity of the FDH in both types of rec. *E. coli* was similar. It is not known why it was not possible to transform the ADH plasmid into the biocatalyst containing the FDH plasmid. Nevertheless, the genetic transformation of the biocatalyst in this work was performed firstly with the ADH then FDH plasmids.

5.1.2 Fermentation

Fermentation of rec. *E. coli* was carried out with standard Luria-Bertani (LB) medium, with carbenicillin and kanamycin added to select cells containing the ADH and FDH plasmids respectively (Table 5.1). Cell colonies from an agar plate were selected and a large pool of feedstock containing cells with similar activities were stored in 50 % v/v glycerol at –80 °C. This feedstock was used for fermentation to yield biomass of uniform activities for the biosynthesis of (*R*)-methyl-3-hydroxybutanoate (**MHB**).

Table 5.1. Luria-Bertani (LB) medium composition for fermentation of *Escherichia coli* BL21 Star (DE3).

Medium composition	Concentration (g L^{-1})
Glucose·H_2O	4
Casein peptone	10
Yeast extract	5
NaCl	10
Carbenicillin	0.05
Kanamycin	0.05

Based on the fermentation protocol of Ernst et al. (2003, 2005) and Kaup (2005) for a 250 mL shakeflask, induction of the rec. *E. coli* with isopropyl-β-D-thiogalactopyranoside (IPTG) to a final concentration of 0.7 mM was initiated in the early exponential phase of growth, for a period of 5 h. The final biomass obtained was 2.5 g_{wcw} L^{-1}. A scale-up in fermentation on a 1 L-scale was performed to obtain more biomass. The biocatalyst was assessed by its activity, defined as the initial rate of production of (*R*)-methyl-3-hydroxybutanoate (**MHB**) per unit wet biomass (Eq. 5.1).

$$Activity_{MHB} = \frac{\left(dC_{MHB}/dt\right)_{initial}}{m_{wet\ cell}} \qquad \text{(eq. 5.1)}$$

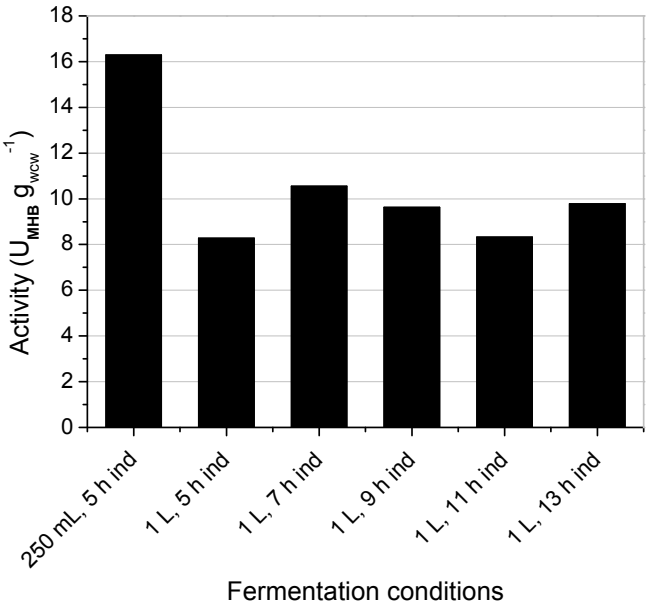

Figure 5.4. Comparison of the effects of different fermentation protocols on the activity of rec. *E. coli*.

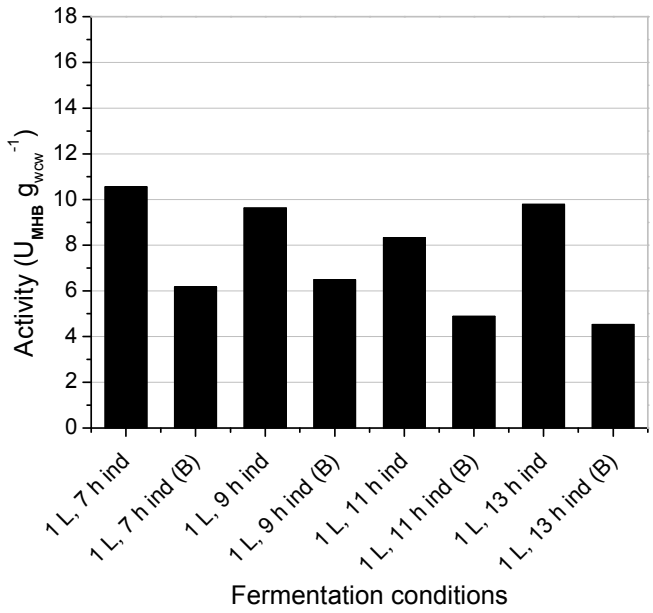

Figure 5.5. Comparison of the effects of baffles (B) in fermentation shakeflasks on the activity of rec. *E. coli*.

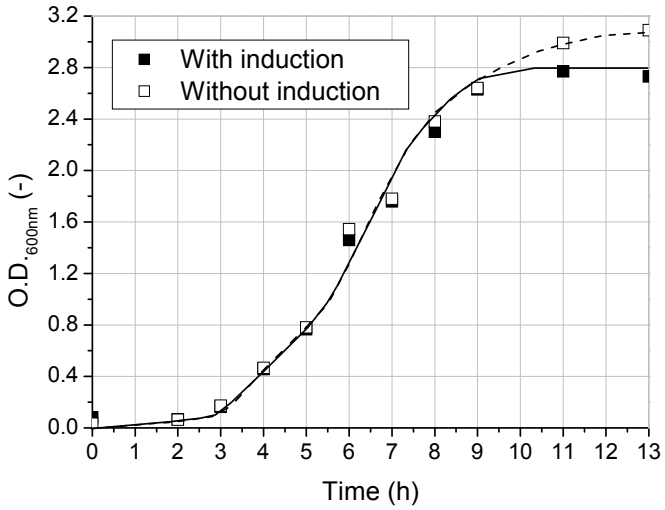

Figure 5.6. Fermentation profile of rec. *E. coli* (with and without induction).

Using a similar fermentation protocol to that on a 250 mL-scale, the biocatalyst obtained in the 1 L shakeflask had a 50 % reduction in activity (Figure 5.4). In order to increase the activity of the cells, the induction time of the fermentation was increased from 5 to 13 h. There was only a slight improvement in activity, and an increase in induction time beyond 7 h did not yield more active cells. When 1 L baffled shakeflasks were used to improve the aeration to the cells, there was a further reduction of up to 55 % in activity of the cells (Figure 5.5). The fermentation on a 1 L-scale (in the absence of baffles) with an induction time of 7 h produced the most active cells (3.0 g_{wcw} L^{-1}). A comparison of the effects of IPTG on the growth of rec. *E. coli* is illustrated in Figure 5.6. A lower biomass concentration was obtained with induced cells, as the cells employed energy to express the genes for FDH and ADH rather than to strictly multiply.

5.2 General definitions of terms used

In addition to the terms defined in Chapter 4, the biocatalyst consumption of the bioreduction process with methyl acetoacetate (**MAA**) is given as the ratio of the wet biomass of the biocatalyst used per unit mass of (*R*)-methyl-3-hydroxybutanoate (**MHB**) obtained.

$$Biocat\ consumption = \frac{m_{wet\ cells}}{m_{MHB}} \qquad \text{(eq. 5.2)}$$

5.3 Storage of induced cells

After fermentation, the induced rec. *E. coli* cells were stored prior to biotransformation. To date, there exist no published methods of storage of induced rec. *E. coli*. Therefore, a variety of storage media and conditions were tested.

The induced cells were stored in potassium phosphate buffer (in the presence of anti-freezing agent, glycerol) and 0.9 % w/v saline solution over a period of about a week. From Figure 5.7, there was a drastic drop in activity of the cells observed. In particular, no activity was observed with the induced cells stored in phosphate buffer containing 50 % v/v glycerol at -80 °C. This storage medium was the same as that used for the feedstock containing non-induced cells. However, the feedstock yielded active cells upon fermentation and induction. It is not known why the induced cells were no longer active in this storage condition. At 4 and –20 °C, the high concentration of glycerol present could have caused the cells to lose water by osmosis, thereby destroying the cells. On the other hand, 0.9 % w/v NaCl solution, a typical medium for storing immobilised cells, did not retain much of the initial activity of the induced cells.

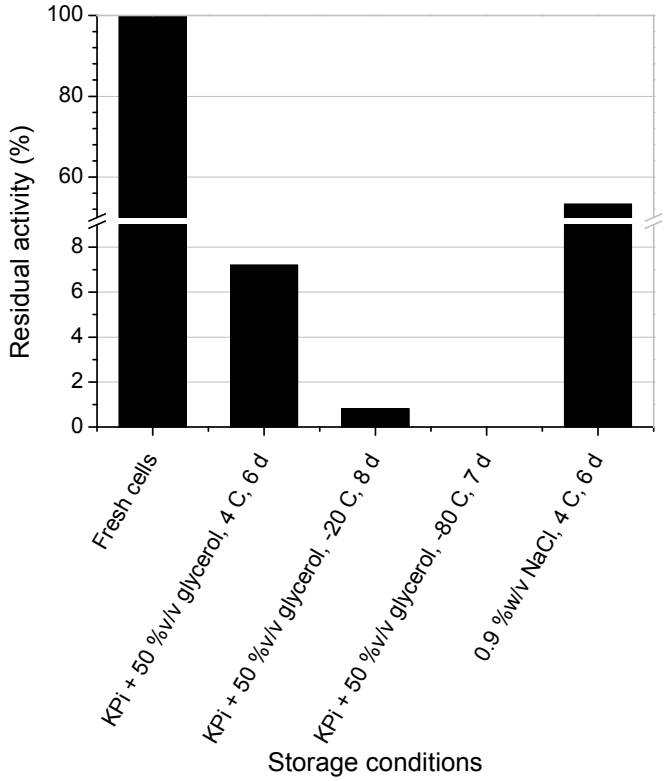

Figure 5.7. Residual activity of induced rec. *E. coli* in various storage conditions. Fresh cells: cells straight out of fermentation, KP_i: 50 mM potassium phosphate buffer (pH 6.5).

An alternative storage medium with 50 mM potassium phosphate buffer (pH 6.5) yielded active induced cells, up to 3 weeks after fermentation (Figure 5.8). With this storage method, there was no loss in activity of the induced rec. *E. coli* for up to 3 weeks.

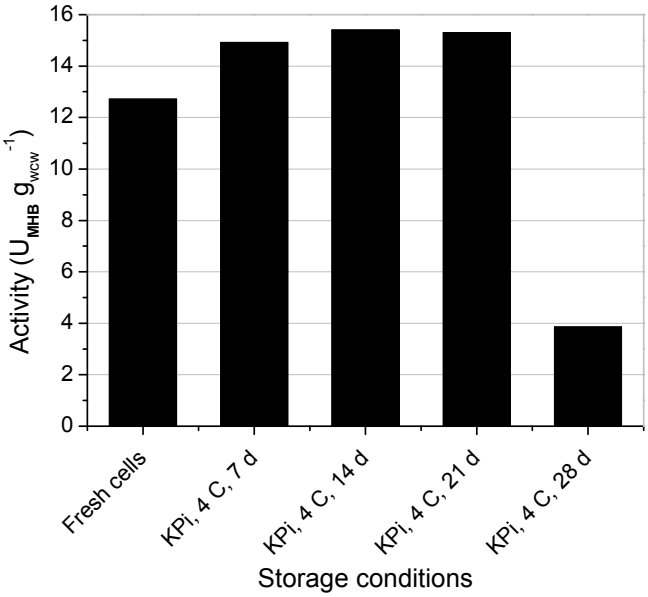

Figure 5.8. Activity of induced rec. *E. coli* stored in phosphate buffer over time. Fresh cells: cells straight out of fermentation, KP_i: 50 mM potassium phosphate buffer (pH 6.5).

5.4 Selection of biotransformation medium

A variety of biotransformation media, in place of potassium phosphate buffer, was investigated. The media contained minerals that could be essential for the regeneration of cofactors in rec. *E. coli* during the bioreduction of methyl acetoacetate (**MAA**). A 10 % dilution of LB medium (as used for the fermentation, refer to Table 5.1), with and without the addition of 500 mM potassium phosphate (pH 6.5), and a highly enriched minimal medium (as used by Bujnicki (2004) for the fermentation of a weak strain of rec. *E. coli* LJ110, refer to Table 5.2) were compared to 500 mM potassium phosphate buffer (pH 6.5) during biotransformation.

Table 5.2. Highly enriched minimal medium composition for fermentation of a weak strain of *Escherichia coli* LJ110 (Bujnicki, 2004).

Medium composition	Concentration (g L^{-1})
Glucose·H_2O	11
$MgSO_4 \cdot 7H_2O$	3
$CaCl_2 \cdot 2H_2O$	0.015
NaCl	1
$(NH_4)_2SO_4$	5
KH_2PO_4	3
$FeSO_4 \cdot 7H_2O$	0.1125
Sodium citrate	1.5
Vitamin B1	0.075
Carbenicillin	0.05
Kanamycin	0.05

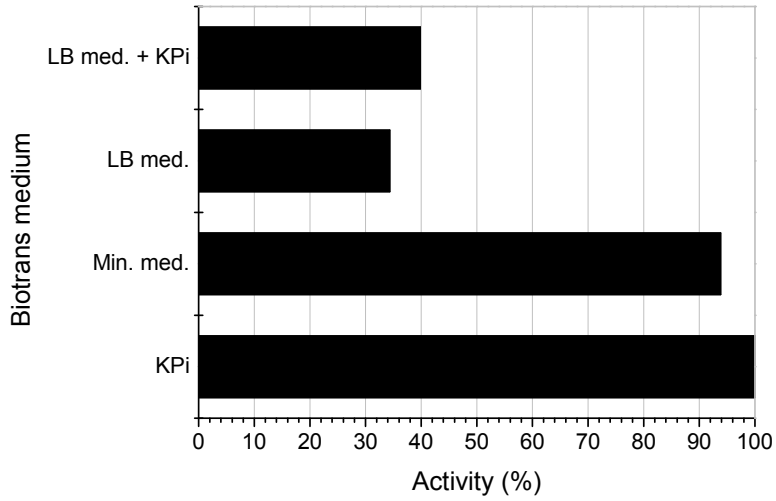

Figure 5.9. Batch activity of rec. *E. coli* in different biotransformation media. KP_i: 500 mM potassium phosphate buffer (pH 6.5), Min. med.: minimal medium, LB med.: LB medium.

The use of diluted LB media (with and without the addition of phosphate) resulted in low activities in a batch (Figure 5.9). It could possibly be due to the consumption of the minerals in the LB media by rec. *E. coli* for metabolism rather than biotransformation. On the other hand, the batch activity of the cells in minimal medium was comparable to that for potassium phosphate buffer, and was also a suitable medium for biotransformation in a batch.

In order to simplify the medium for kinetic studies and determination of reaction conditions, potassium phosphate buffer was chosen as the biotransformation medium. A reduction in the concentration of phosphate buffer to 50 mM gave no significant effects on the activity of the cells. The efficiency of minimal medium and phosphate

buffer in maintaining the activity of rec. *E. coli* were further studied in a repetitive batch mode (refer to Chapter 5.7.3).

5.5 Characteristics of biocatalyst

5.5.1 Reaction conditions

The pH and temperature of the biotransformation were studied in the presence of $MgSO_4$ where the Mg^{2+} salts were found to be essential for the activation of *Lactobacillus brevis* alcohol dehydrogenase (Niefind et al., 2003). The pH value for the highest activity was found to be 6.0 (Figure 5.10) while the activity profile followed an Arrhenius' behaviour up to T = 310 K (Figure 5.11). The corresponding activation energy of the reaction was calculated to be 77.2 ± 16.6 kJ mol^{-1} (R^2 = 0.94) (Eq. 4.9), and the deactivation energy was 3.3-fold higher, at 255.79 kJ mol^{-1} (Eq. 5.3). Assuming that methyl acetoacetate (**MAA**) was reduced only by the induced *Lb*ADH gene in rec. *E. coli*, the values for thermal activation and denaturation are consistent to the values found in enzyme-catalysed reactions (Schuler and Kargi, 1992).

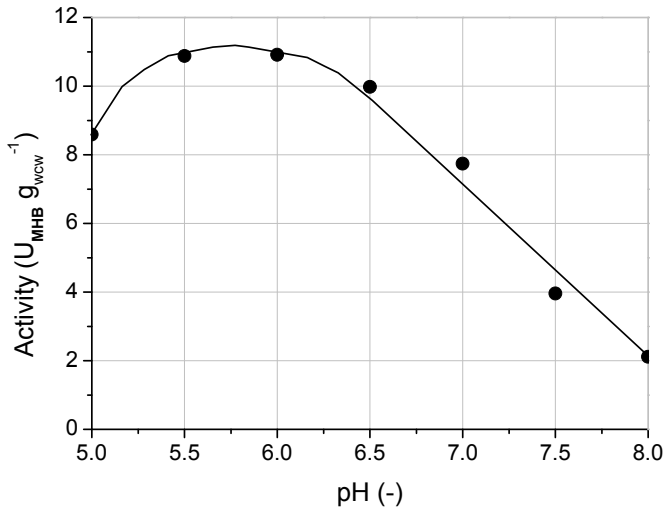

Figure 5.10. Activity of rec. *E. coli* as a function of pH. Conditions: V = 0.35 L, 30 °C, 50 mM potassium phosphate buffer, 50 mM sodium formate, 40 mM methyl acetoacetate (MAA), 2 mM $MgSO_4$, 0.7 g-wet cell weight rec. *E. coli*. The pH was controlled by titration with 5 M HCl.

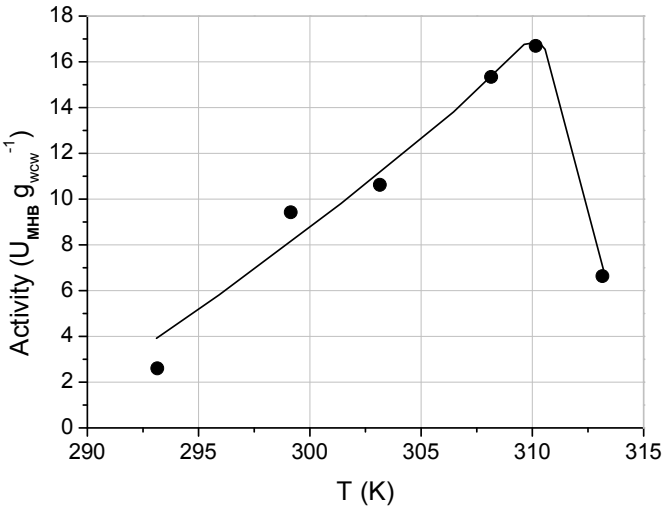

Figure 5.11. Activity of rec. *E. coli* as a function of temperature. Conditions: V = 0.35 L, pH 6 (titrated with 5 M HCl), 50 mM potassium phosphate buffer, 50 mM sodium formate, 40 mM methyl acetoacetate (MAA), 2 mM $MgSO_4$, 0.7 g-wet cell weight rec. *E. coli*.

$$k_d = A_d e^{-E_a/RT} \qquad \text{(eq. 5.3)}$$

Although higher operating temperatures (up to 310 K) yielded higher activities, it was not known if the genetic stability of the rec. *E. coli* would be compromised, since the maximal allowable temperature for the stability of the cells during induction was 303 K (Kaup, 2005). Therefore, the temperature chosen for subsequent studies was fixed at 303 K.

5.5.2 Reaction kinetics

The study of possible substrate(s) and product inhibition was performed with batch experiments. Up to a concentration of 250 mM, the substrate methyl acetoacetate (**MAA**) exhibited no inhibition to the rate of biotransformation (Figure 5.12). The reaction rate with respect to methyl acetoacetate (**MAA**) is described by the Michealis-Menten equation (Eq. 5.4). Although there were difficulties in precise integration of the peak corresponding to (*R*)-methyl-3-hydroxybutanoate (**MHB**) in the GC chromatograms at high concentrations of **MHB**, nevertheless, it can be concluded that there was also no significant product inhibition observed (Figure 5.13).

$$v = \frac{v_{\max,MAA}\, C_{MAA}}{K_{m,MAA} + C_{MAA}} \qquad \text{(eq. 5.4)}$$

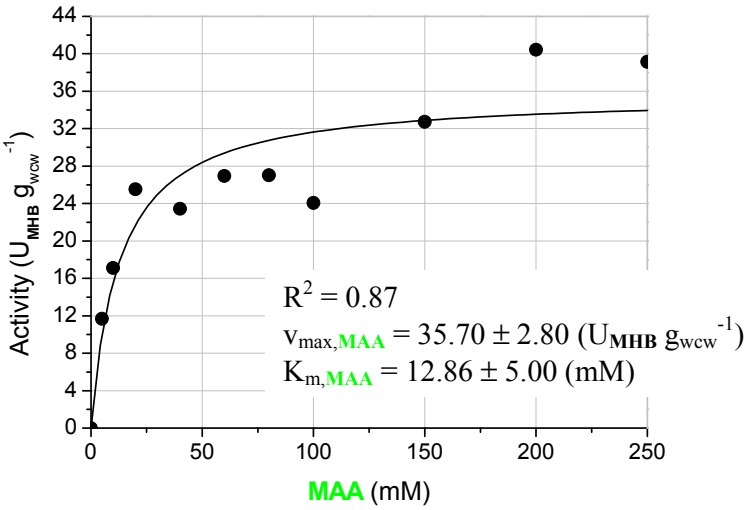

Figure 5.12. Activity of rec. *E. coli* as a function of the concentration of methyl acetoacetate (MAA). Conditions: V = 0.35 L, 30 °C, pH 6 (titrated with 5 M HCl), 50 mM potassium phosphate buffer, 50 mM sodium formate, 2 mM $MgSO_4$, 0.7 g-wet cell weight rec. *E. coli*.

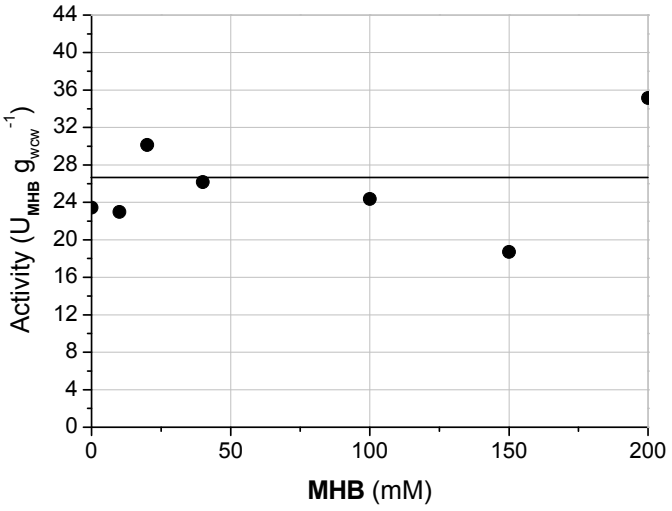

Figure 5.13. Activity of rec. *E. coli* as a function of the concentration of (*R*)-methyl-3-hydroxybutanoate (MHB). Conditions: V = 0.35 L, 30 °C, pH 6 (titrated with 5 M HCl), 50 mM potassium phosphate buffer, 50 mM sodium formate, 40 mM methyl acetoacetate (MAA), 2 mM $MgSO_4$, 0.7 g-wet cell weight rec. *E. coli*.

The reaction rates with regards to formate consumption and the formation of (*R*)-methyl-3-hydroxybutanoate (**MHB**) are illustrated in Figures 5.14 and 5.15 respectively. In both cases, there was no formate inhibition seen (up to 200 mM). The effects of different formate concentration in a batch were expressed by the Michealis-Menten equation (Eq. 5.5). Therefore, it can be concluded that the (co)substrates and the product (up to 200 mM) did not inhibit the bioreduction of methyl acetoacetate (**MAA**).

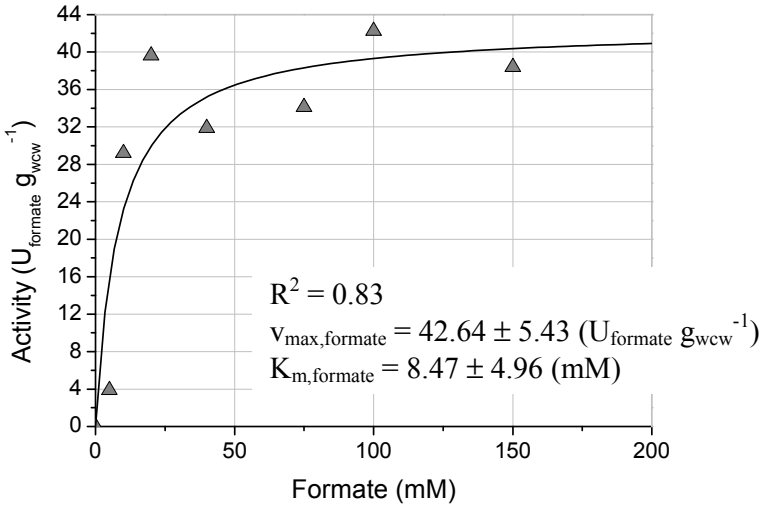

Figure 5.14. Activity of rec. *E. coli* (in terms of formate consumption) as a function of the concentration of formate. Conditions: V = 0.35 L, 30 °C, pH 6 (titrated with 5 M HCl), 50 mM potassium phosphate buffer, 40 mM methyl acetoacetate (MAA), 2 mM $MgSO_4$, 0.7 g-wet cell weight rec. *E. coli*.

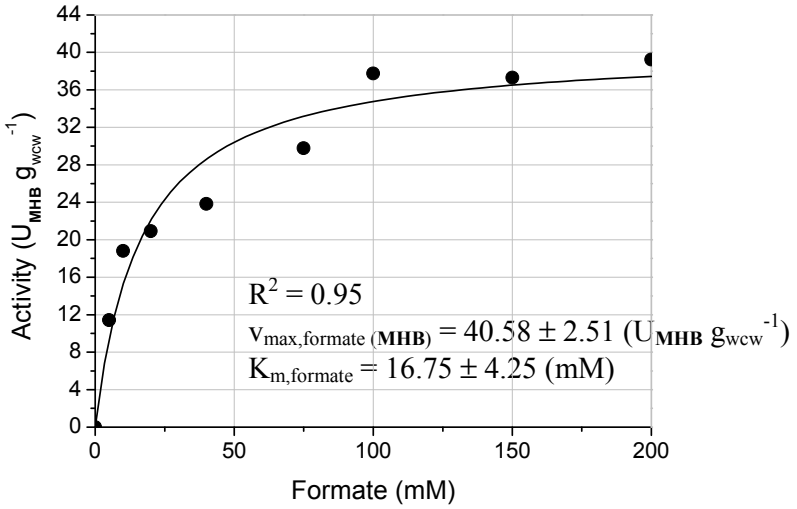

Figure 5.15. Activity of rec. *E. coli* (in terms of formation of (*R*)-methyl-3-hydroxybutanoate (MHB)) as a function of the concentration of formate. Conditions: V = 0.35 L, 30 °C, pH 6 (titrated with 5 M HCl), 50 mM potassium phosphate buffer, 40 mM methyl acetoacetate (MAA), 2 mM $MgSO_4$, 0.7 g-wet cell weight rec. *E. coli*.

$$v = \frac{v_{max,formate}\, C_{formate}}{K_{m,formate} + C_{formate}} \qquad \text{(eq. 5.5)}$$

5.5.3 Batch characterisation

Methyl acetoacetate (**MAA**) was more than 99 % converted to yield more than 99 % (*R*)-methyl-3-hydroxybutanoate (**MHB**) in a batch reactor (Figure 5.16). The *ee* of (*R*)-methyl-3-hydroxybutanoate (**MHB**) was above 99 % and the biocatalyst consumption of the batch was 1.7 g_{wcw} $g_{\mathbf{MHB}}^{-1}$.

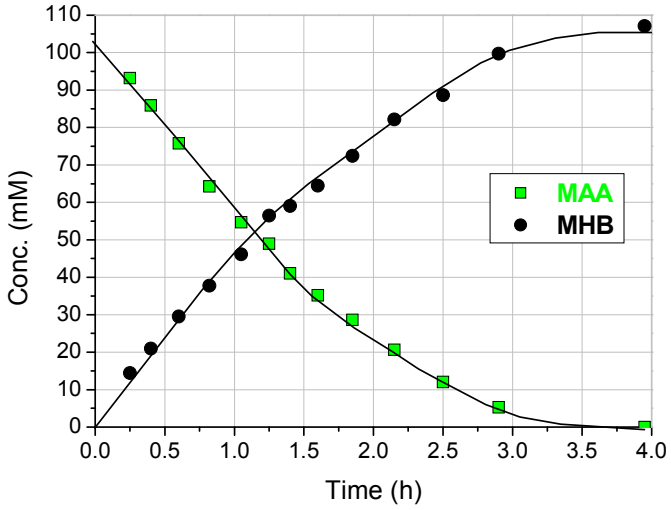

Figure 5.16. Concentration of reactants in a batch reactor as a function of time. Conditions: V = 0.365 L, 30 °C, pH 6 (titrated with 5 M HCl), 50 mM potassium phosphate buffer, 120 mM sodium formate, 100 mM methyl acetoacetate (MAA), 2 mM $MgSO_4$, 0.73 g-wet cell weight rec. *E. coli*.

5.6 Continuously stirred tank reactor (CSTR)

The continuous production of (*R*)-methyl-3-hydroxybutanoate (**MHB**) was set up in a continuously stirred tank reactor (CSTR) (Figures 5.17 and 5.18). The outlet of the reactor passed through an ultrafiltration membrane (of molecular weight cut-off of 300 kD), thereby recycling the biomass back into the reactor while retrieving the product (*R*)-methyl-3-hydroxybutanoate (**MHB**) in the filtrate going into the fraction collector. The pH of the system was kept constant by the addition of 5 M HCl, and was thermostated at 30 °C by a jacket of water around the reactor. An excess of formate was used to ensure that the bioreduction was not limited by cofactor regeneration.

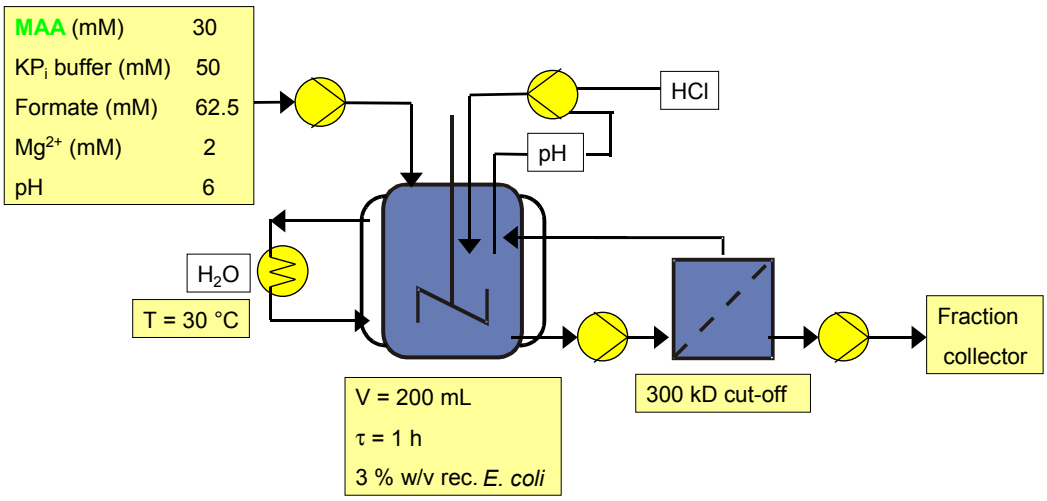

Figure 5.17. Scheme of CSTR setup. τ: residence time.

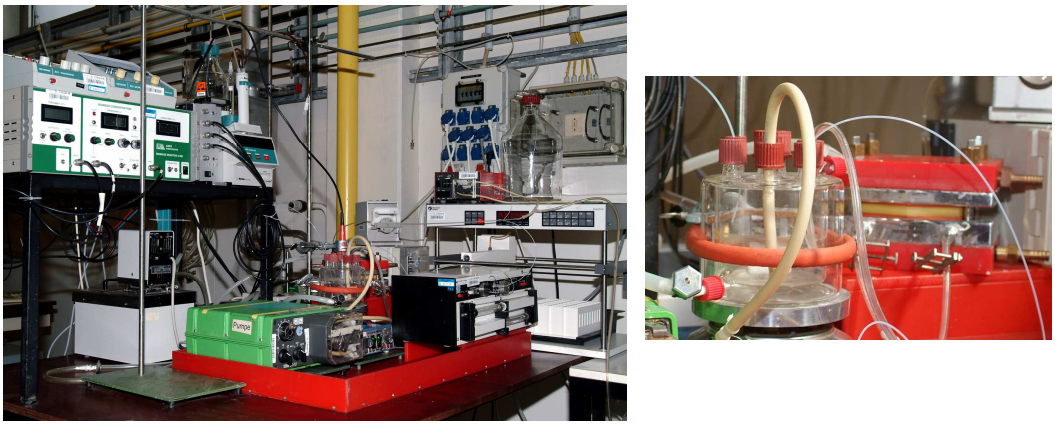

Figure 5.18. Production of (*R*)-methyl-3-hydroxybutanoate (MHB) with the CSTR setup (left) and a close-up on the reactor and ultrafiltration membrane (right).

The highest concentration of (*R*)-methyl-3-hydroxybutanoate (**MHB**) was observed in the initial phase of the continuous run (θ = 0 – 4) (Figure 5.19). After which, no steady state was observed and the conversion of methyl acetoacetate (**MAA**) decreased drastically (Figure 5.20). An additional 1 % w/v of fresh rec. *E. coli* fed into the CSTR after 24 residence time boosted the conversion of methyl acetoacetate (**MAA**) shortly before decreasing.

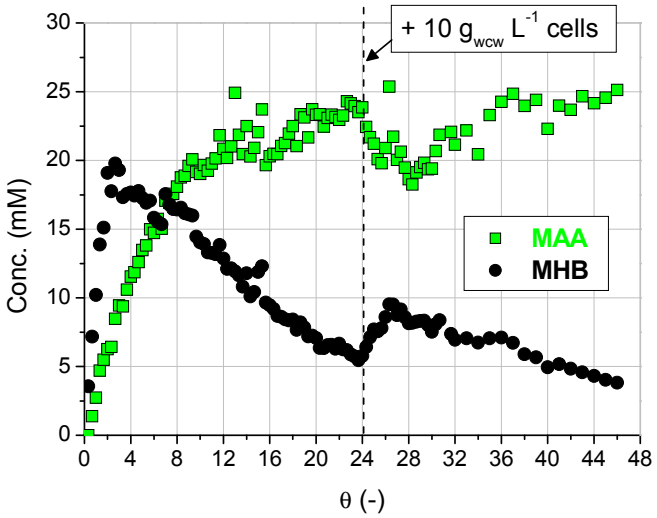

Figure 5.19. Concentration profile of reactants in the CSTR as a function of the number of residence time. Conditions: V = 0.2 L, 30 °C, pH 6 (titrated with 5 M HCl), 50 mM potassium phosphate buffer, 62.5 mM sodium formate, 30 mM methyl acetoacetate (MAA), 2 mM $MgSO_4$, 6.0 g-wet cell weight rec. *E. coli*.

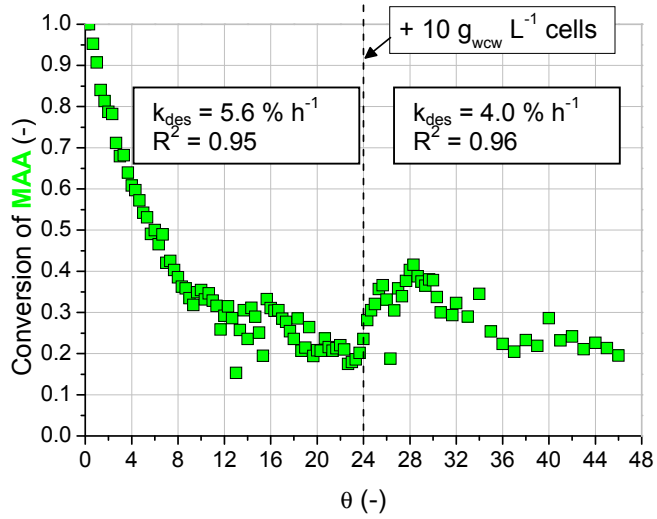

Figure 5.20. Conversion of methyl acetoacetate (MAA) as a function of the number of residence time in the CSTR. Conditions: V = 0.2 L, 30 °C, pH 6 (titrated with 5 M HCl), 50 mM potassium phosphate buffer, 62.5 mM sodium formate, 30 mM methyl acetoacetate (MAA), 2 mM $MgSO_4$, 6.0 g-wet cell weight rec. *E. coli*.

The initial activity of 3 % w/v rec. *E. coli* in the first 24 residence time was 5.00 U_{MHB} g_{wcw}^{-1}. Upon addition of 1 % w/v rec. *E. coli* after 24 residence time, the initial activity was 2.32 U_{MHB} g_{wcw}^{-1}. In both cases, the activities were very much lower to that obtained in a batch reactor (refer to Chapter 5.5). The cells deactivated exponentially at a rate of 5.6 % h^{-1} in the first 24 h, and 4.0 % h^{-1} subsequently

(Figure 5.20). Overall, the biocatalyst consumption in the CSTR obtained was 0.9 g_{wcw} $g_{\mathbf{MHB}}^{-1}$.

It was not known why there was a rapid drop in conversion of methyl acetoacetate (**MAA**). There could be 4 reasons: lysed cells, toxicity of formate, lack of intracellular cofactors, or porous cell membrane. A sample from the CSTR was taken and viewed under the microscope. There was no contamination in the reactor as the cells were solely *rec. E. coli*. Moreover, no lysed cells were observed. This was further substantiated by the lack of ADH and FDH activities detected in the filtrate.

The prolonged exposure to formate in the CSTR could have a toxic effect on the rec. *E. coli*, since formate is known to be an anti-microbial agent. This phenomena was not observed in a batch, where the concentration of formate was always decreasing with time and that the operation time in a batch was short. Therefore, rec. *E. coli* was incubated with formate overnight (11 h) and studied in a repetitive batch mode to observe the toxic effects of formate (refer to Chapter 5.7.1).

It could also be possible that there were insufficient cofactors intracellularly at the start of the CSTR operation. The addition of glucose to the rec. *E. coli* would serve to increase the pool of NADPH (by glycolysis) and the addition of vitamin B6 (a building block of nicotinamide cofactors) would serve to increase the pool of nicotinamide cofactors intracellularly. The studies were also performed in a repetitive batch mode (see Chapter 5.7.1).

The last possible explanation of a rapid drop in activity of the rec. *E. coli* could be a leaky cell membrane. If this was the reason, then the internal cofactors of the cells would be washed out of the reactor and into the product line, making them unavailable after some time for the bioreduction of methyl acetoacetate (**MAA**) and the oxidation of formate. Therefore, the addition of cofactors to the rec. *E. coli* was tested in a repetitive batch system to observe the effects (refer to Chapter 5.7.1).

5.7 Stability studies

5.7.1 Repetitive batch investigations

Six different repetitive batch systems were investigated to understand the rapid drop in activity of rec. *E. coli* in the CSTR. They were the standard repetitive batch system, formate incubated system, and the separate addition of glucose, vitamin B6, NAD^+ and NAD(P)H (Table 5.3). Each repetitive batch system consisted of 4 repetitive batches.

Table 5.3. Repetitive batch investigations for rec. *E. coli* system.

Graph	Repetitive batch test	Conditions	Target	Studies
A	Standard (Std)	Standard	-	-
B	Formate incubated	50 mM formate (11 h incubation)	Whole cell	Toxicity effect
C	Glucose	22 mM	Glycolysis	NADPH generation
D	Vitamin B6 (Vit. B6)	1 mM	Building block of cofactors	NAD(P)(H) generation
E	NAD^+	1 mM	FDH	Oxidation of formate
F	NAD(P)H	1 mM each	*Lb*ADH	Reduction of **MAA**

The concentration profiles of (*R*)-methyl-3-hydroxybutanoate (**MHB**) and formate appeared rather similar for the different repetitive batches, except in the case of the addition of cofactors (Figures 5.21). When NAD^+ was added to the repetitive batch, there was a rapid conversion of formate even before the start of the repetitive batch (Figure 5.21). In contrast, this was not observed in the standard repetitive batch (Figure 5.21). This suggested a leaky cell membrane which allowed easier diffusion of formate and NAD^+ into and out of the cells. In addition, it suggested the oxidation of formate in the cells was rate-limited by the intracellular concentration of NAD^+ needed to drive the reaction. On the other hand, the addition of the reduced cofactors did not yield a similar effect on the conversion of **MAA** (Figure 5.21). In spite of the possibility of the cofactors leaking out of the cell, it seemed that the overall concentration of reduced cofactors needed for the reduction of **MAA** was sufficient to drive the reaction. In the case of the standard repetitive batch, the biocatalyst consumption of the system was 1.1 $g_{wcw}\ g_{\mathbf{MHB}}^{-1}$.

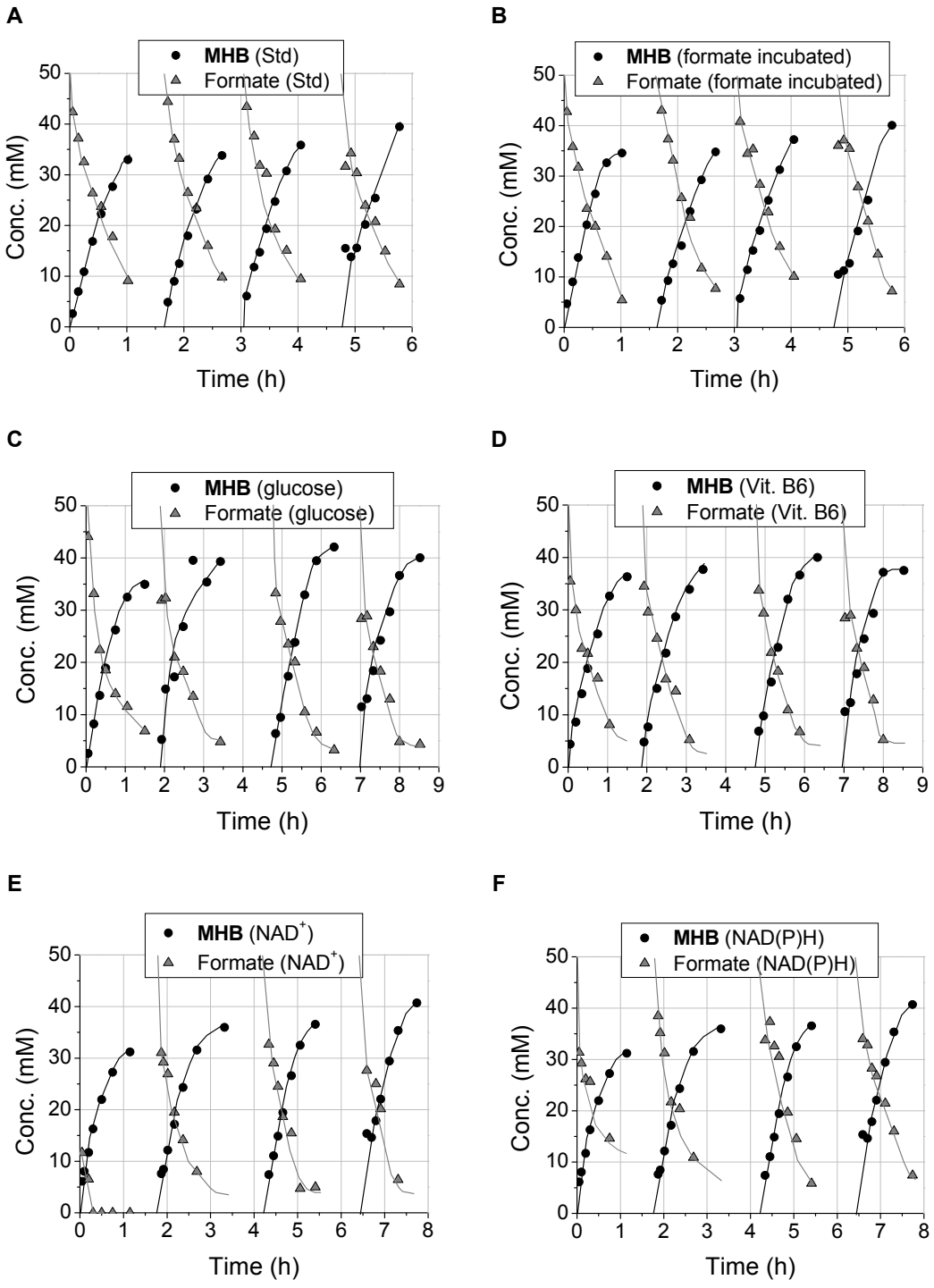

Figure 5.21. Concentration of reactants in repetitive batch studies as a function of time. A: Standard (Std), B: With formate incubated cells, C: With the addition of glucose, D: With the addition of Vitamin B6 (Vit. B6), E: With the addition of NAD^+, F: With the addition of NAD(P)H. Conditions: V = 0.325 L, 30 °C, pH 6 (titrated with 5 M HCl), 50 mM potassium phosphate buffer, 50 mM sodium formate, 40 mM methyl acetoacetate (MAA), 2 mM $MgSO_4$, 0.65 g-wet cell weight rec. *E. coli*.

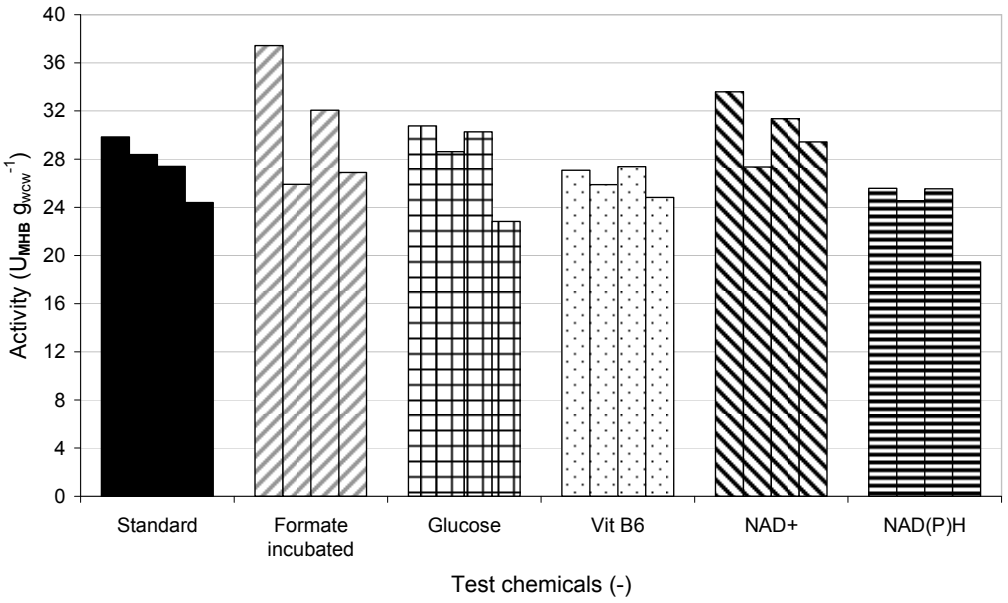

Figure 5.22. Activities of rec. *E. coli* in repetitive batch systems containing different chemicals.

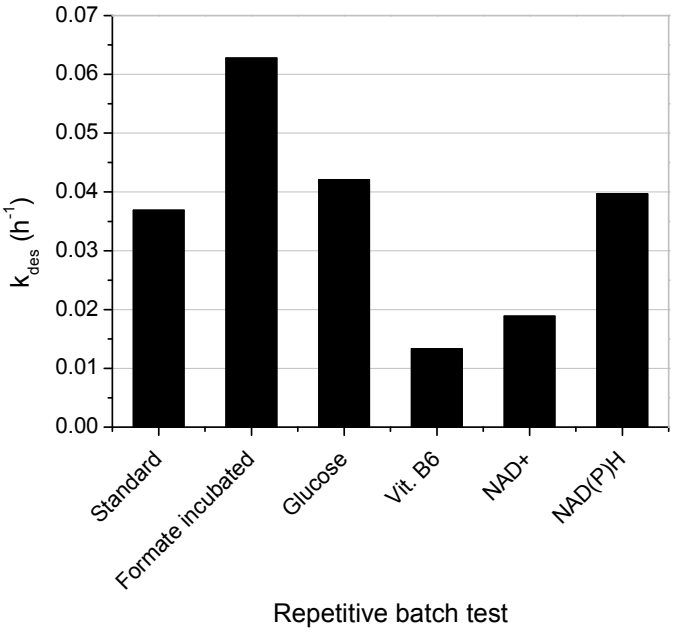

Figure 5.23. Deactivation constants of rec. *E. coli* in repetitive batch systems containing different chemicals.

The activities of rec. *E. coli* in the repetitive batches are summarised in Figure 5.22. In general, there was an overall decrease in activity of the cells with each repetitive batch. The repetitive batches with formate incubated cells and with the addition of NAD^+ seemed to give slightly higher activities as compared to the standard repetitive batch. On the other hand, the addition of reduced cofactors seemed to yield lower

activities. These results implied that formate and the nicotinamide cofactors affect the activities of the cells, although the exact reasons could not be concisely concluded. When the exponential deactivation of the cells were compared, the system containing formate incubated cells gave the highest deactivation constant (Figure 5.23). This showed that formate was toxic to the cells. This was expected, since formate is known to be an anti-microbial agent.

5.7.2 MAA:formate ratio

Since formate was found to be toxic for the cells (see Chapter 5.7.1), the amount of formate required in a batch was investigated. This was done to determine the optimal amount of formate for complete conversion of methyl acetoacetate (**MAA**). By varying the ratio of methyl acetoacetate (**MAA**) to formate, it was observed that an equimolar ratio of methyl acetoacetate (**MAA**) to formate did not give 100 % yield of (*R*)-methyl-3-hydroxybutanoate (**MHB**) (Figure 5.24). On the other hand, the different ratio of methyl acetoacetate (**MAA**) to formate did not have a significant effect on the activity of the rec. *E. coli* (Figure 5.25). For complete yield of (*R*)-methyl-3-hydroxybutanoate (**MHB**), and minimal toxicity to the cells, only a slight excess of formate must be added, and the ratio of methyl acetoacetate (**MAA**) to formate should be at least 1:1.2.

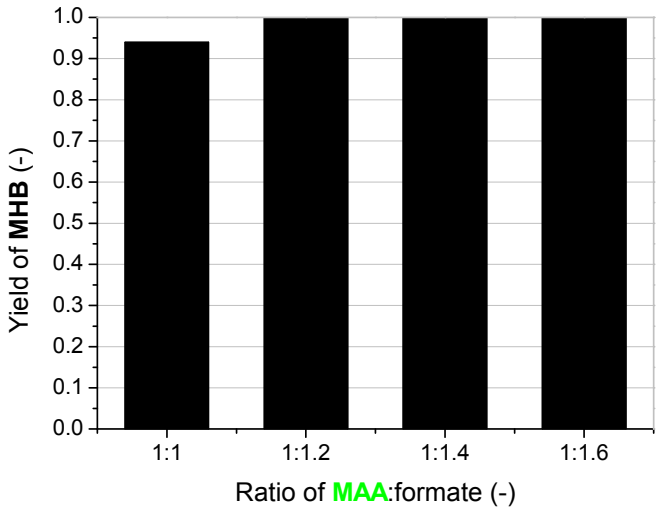

Figure 5.24. Yield of (*R*)-methyl-3-hydroxybutanoate (MHB) in a batch reactor as a function of the ratio of methyl acetoacetate (MAA) to formate. Conditions: V = 0.365 L, 30 °C, pH 6 (titrated with 5 M HCl), 50 mM potassium phosphate buffer, 100 mM methyl acetoacetate (MAA), 2 mM $MgSO_4$, 0.73 g-wet cell weight rec. *E. coli*.

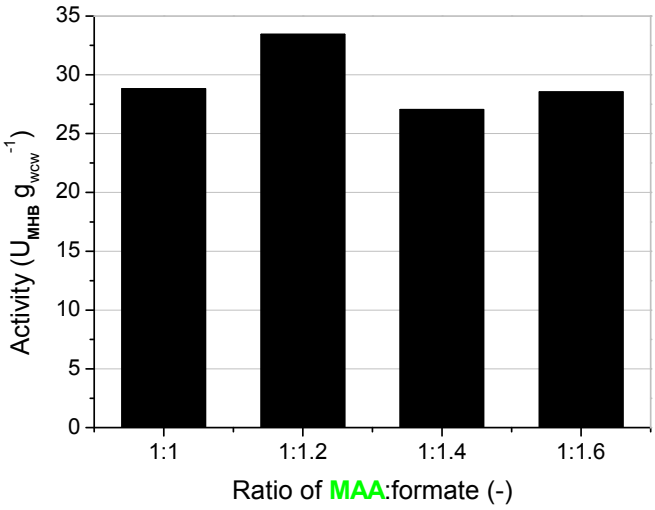

Figure 5.25. Activity in a batch reactor as a function of the ratio of methyl acetoacetate (MAA) to formate. Conditions: V = 0.365 L, 30 °C, pH 6 (titrated with 5 M HCl), 50 mM potassium phosphate buffer, 100 mM methyl acetoacetate (MAA), 2 mM $MgSO_4$, 0.73 g-wet cell weight rec. *E. coli*.

5.7.3 Biotransformation medium studies in repetitive batch

From Chapter 5.4, it was found that minimal medium and potassium phosphate buffer were suitable biotransformation media in a batch. In this section, repetitive batch studies with both biotransformation media were performed to observe the long-term stability effects of both media and obtain a possible method to improve the activity of the biocatalyst in a CSTR. Thus, the batch runs were capped at around an hour each and performed repetitively.

After 10 repetitive batches, the rate of formation of (*R*)-methyl-3-hydroxybutanoate (**MHB**) had decreased over time for both biotransformation media (Figures 5.26 and 5.27). Comparing the activities of rec. *E. coli* in both biotransformation media, the decay in activities were exponential (Figure 5.28). The rates of exponential decay were 5.0 % h^{-1} (phosphate buffer) and 7.1 % h^{-1} (minimal medium). Although both media gave almost similar deactivation constant, the overall biocatalyst consumption obtained with the minimal medium was lower (see Eq. 5.2). Therefore, it seemed that the use of minimal medium may have a beneficial effect to rec. *E. coli*.

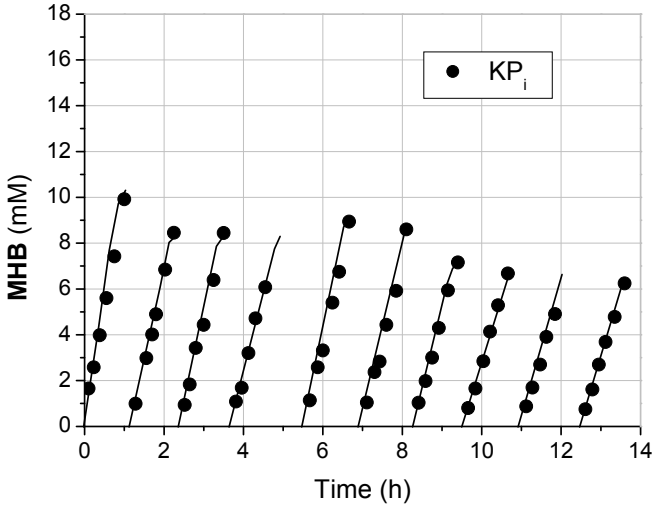

Figure 5.26. Concentration of (*R*)-methyl-3-hydroxybutanoate (MHB) in a repetitive batch run containing phosphate buffer as biotransformation medium as a function of time. Conditions: V = 0.35 L, 30 °C, pH 6 (titrated with 5 M HCl), 50 mM potassium phosphate buffer, 50 mM sodium formate, 40 mM methyl acetoacetate (MAA), 2 mM $MgSO_4$, 0.35 g-wet cell weight rec. *E. coli*.

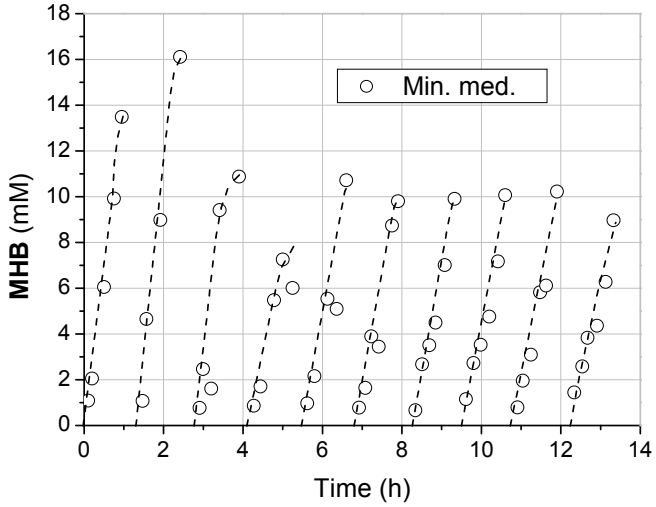

Figure 5.27. Concentration of (*R*)-methyl-3-hydroxybutanoate (MHB) in a repetitive batch run containing minimal medium as biotransformation medium as a function of time. Conditions: V = 0.35 L, 30 °C, pH 6 (titrated with 5 M HCl), 50 mM sodium formate, 40 mM methyl acetoacetate (MAA), 0.35 g-wet cell weight rec. *E. coli*.

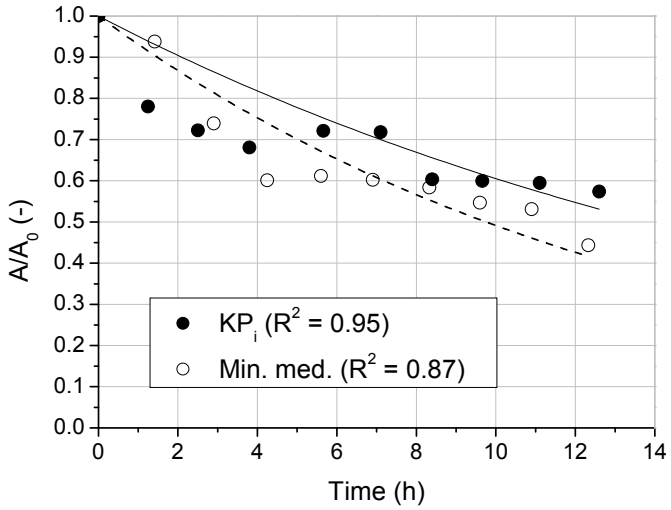

Figure 5.28. Comparison of residual activity in a repetitive batch containing phosphate buffer and minimal medium as biotransformation media.

5.8 Conclusions

In the synthesis of (*R*)-methyl-3-hydroxybutanoate (**MHB**) with genetically modified biocatalyst *Escherichia coli*, the following findings were obtained:

- First known storage of active induced cells in phosphate buffer of up to 3 weeks,
- No substrates (**MAA**, formate) and product (**MHB**) inhibition,
- For complete yield of **MHB**, **MAA**:formate = 1:≥1.2,
- Lowest biocatalyst consumption (0.9 g_{wcw} $g_{\mathbf{MHB}}^{-1}$) was obtained in the continuous setup,
- Rapid drop in conversion of **MAA** in continuous setup could be due to formate toxicity and leaky cell membrane.

6 Discussion and Outlook

The use of isolated enzymes and resting whole cells as biocatalysts are compared in this chapter. In each system, the process parameters (depending on reactor setups) and economics (cost of production and sale) are evaluated. In addition, the stability of the biocatalysts is considered. Other problems and suggestions relating to the bioprocesses are also discussed. Finally, the most viable bioprocess setup for the production of (5*R*)-hydroxyhexane-2-one (**B**) and (*R*)-methyl-3-hydroxybutanoate (**MHB**) is presented.

6.1 γ-Hydroxyketone syntheses with whole cells of *Lactobacillus kefiri* versus enzyme-coupled system

6.1.1 Process parameters and stability

Three essential criteria for feasible synthesis of (5*R*)-hydroxyhexane-2-one (**B**) were evaluated (Figure 6.1). The biocatalyst consumption of the processes with whole cells (refer to Eq. 3.5) and enzymes (see Eq. 4.6) is illustrated (Figure 6.2). In addition, the space-time yield (STY) of the plug flow run with whole cells (refer to Eq. 3.20) and for the batch runs with enzymes (Eq. 4.7) are given in Figure 6.3. With respect to the stability of the biocatalyst, only the processes with exponential deactivation over time are compared (Figure 6.4).

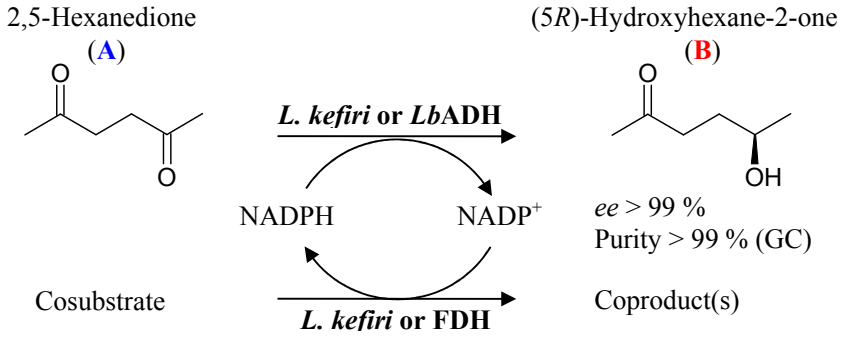

Figure 6.1. Enantioselective reduction of (2,5)-hexanedione (A) to (5*R*)-hydroxyhexane-2-one (B) with resting whole cells of *Lactobacillus kefiri* or enzyme-coupled system (*Lb*ADH: Alcohol dehydrogenase from *Lactobacillus brevis*, FDH: Formate dehydrogenase from *Pseudomonas* sp.).

In the whole cell system, there was a decrease in biocatalyst consumption with whole cell immobilisation (Figure 6.2). A repetitive batch setup with immobilised *Lactobacillus kefiri* yielded the lowest biocatalyst consumption, with a 73-fold decrease as compared to a non-immobilised batch. Besides whole cell immobilisation, the type of reactor setup also affected the biocatalyst consumption of the process. Using a repetitive batch or a plug flow reactor as opposed to a batch

reduced the biocatalyst consumption regardless of immobilisation. A 5.4 and 1.7-fold reduction in biocatalyst consumption were observed when a repetitive batch and plug flow reactor setup were used respectively in place of a batch. When enzymes were used as biocatalyst, the biocatalyst consumption in a batch run was 47 and 3.4-fold lower than that of non-immobilised and immobilised cells respectively.

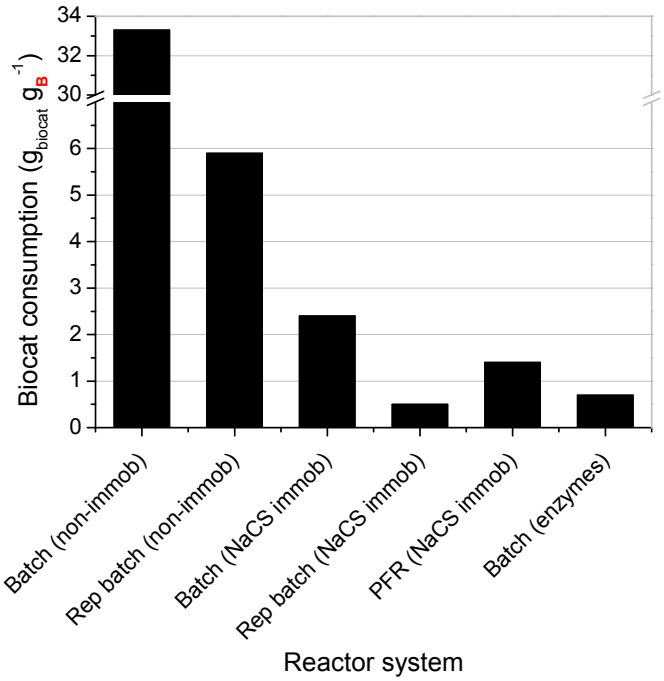

Figure 6.2. Comparison of biocatalyst consumption with respect to whole cell immobilisation, reactor setup and the use of enzymes. The amount of biocatalyst (in the case of whole cells) refers to the wet biomass.

In the whole cell system, there was a decrease in space-time yield (STY) with whole cell immobilisation (Figure 6.3). However, the space-time yield recovered rather well with a continuous setup for immobilised cells. With a continuous operation, there was a 6.7-fold increase in space-time yield for the immobilised cells as compared to a batch. When enzymes were used as biocatalyst, the space-time yield obtained was higher than that of whole cells.

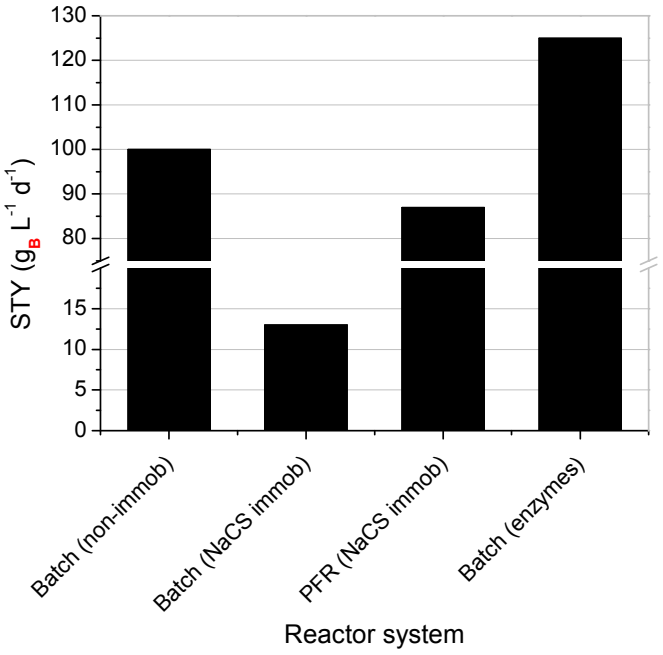

Figure 6.3. Comparison of space-time yield (STY) with respect to whole cell immobilisation, reactor setup and the use of enzymes.

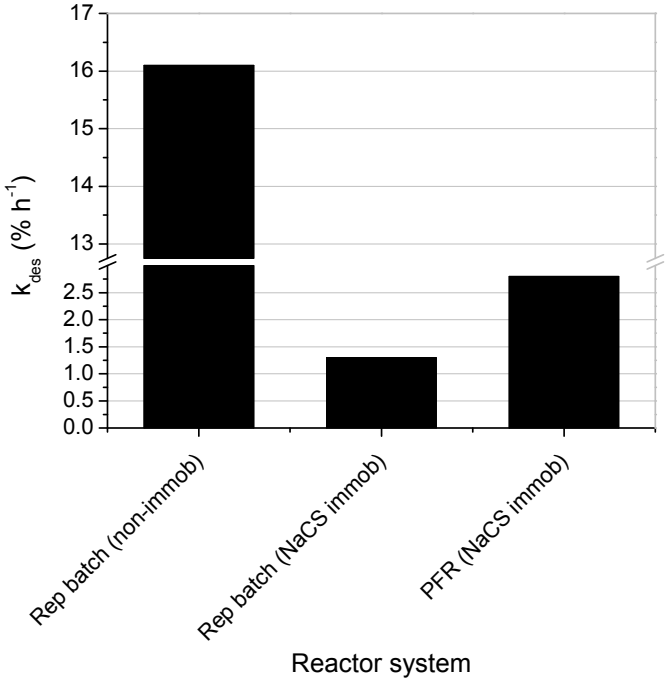

Figure 6.4. Comparison of deactivation constant with respect to whole cell immobilisation and reactor setup.

One of the main advantages of whole cell immobilisation is the increased stability of the biocatalyst. This is substantiated in Figure 6.4. It was observed that the deactivation constant was 12 times lower with cell immobilisation. Even with a continuous operation in a plug flow reactor setup over a period of time, the deactivation constant remained low.

6.1.2 Economics

The economic viability of the processes is summarised in Figure 6.5 based on the production cost (Eq. 6.1). In general, the cost of producing (5*R*)-hydroxyhexane-2-one (**B**) with whole cells is more than 7.3-fold lower than with enzymes. When whole cells were used as biocatalyst, the cost of production decreased by at least 5-fold with more efficient use of the biocatalyst in repetitive batches and plug flow reactor, regardless of cell immobilisation. Comparing to the sale price of (5*R*)-hydroxyhexane-2-one (**B**) by Juelich Fine Chemicals GmbH, the use of whole cells rather than enzymes would be more favourable.

Production cost = Costs of (Biocat + Cofactors + Immobilisation matrix + Substrate) (eq. 6.1)

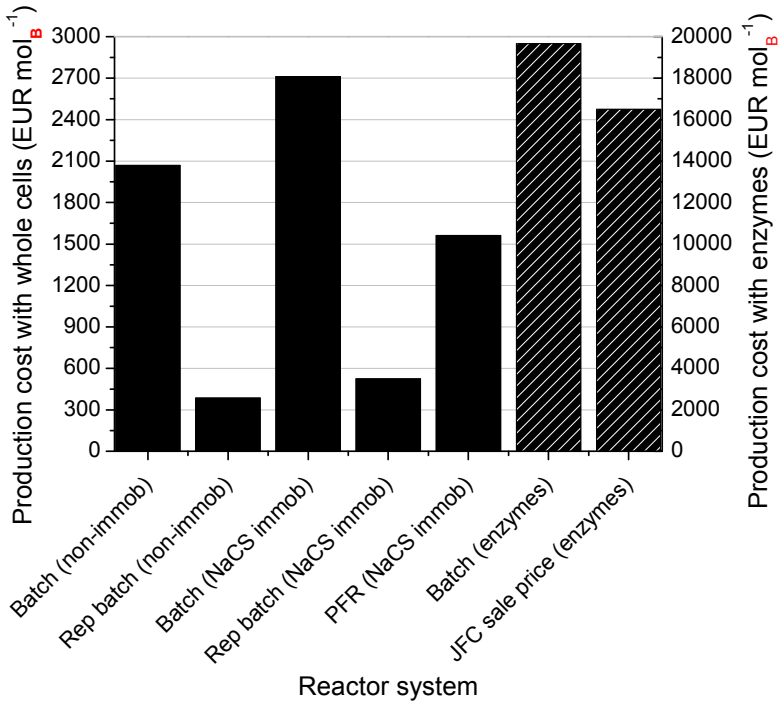

Figure 6.5. Comparison of production cost with respect to whole cell immobilisation, reactor setup, the use of enzymes and sale price of the process by Juelich Fine Chemicals GmbH (JFC). Other prices are obtained from Fluka (2005/2006), bitop (2004) and EuroFerm (2004) catalogues.

A breakdown of the production cost is shown in Figure 6.6. The major contribution of the production cost could be attributed to the price of the immobilisation matrix sodium cellulose sulphate (NaCS) and/or biocatalyst (enzymes or cells). The price of the substrate (2,5)-hexanedione (**A**) and/or cofactor $NADP^+$ remained negligible in all cases.

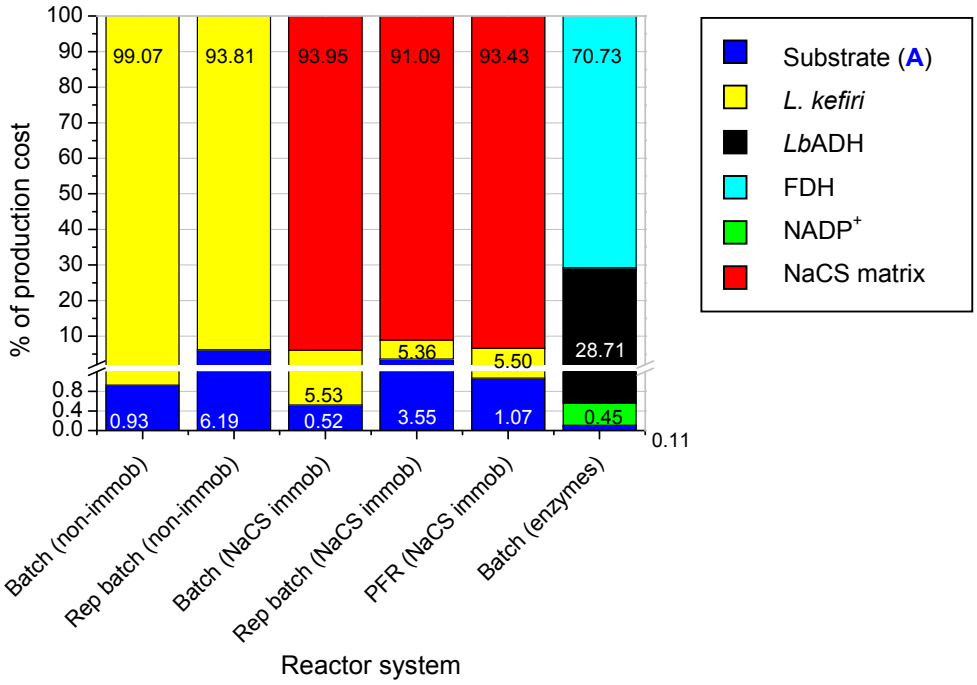

Figure 6.6. Comparison of production cost with respect to costs of biocatalyst, immobilisation matrix, substrate and cofactors. Prices are obtained from Fluka (2005/2006), bitop (2004) and EuroFerm (2004) catalogues.

6.1.3 Problems and outlook

In the whole cell system, the mass balance was incomplete and attempts to investigate the causes gave negative results (refer to Chapter 3.3.1). Therefore, the fate of the residual chemicals remained unknown, and is postulated to be metabolised by the cells.

Through the investigation of different encapsulation matrices, the most suitable matrix was found to be sodium cellulose sulphate (NaCS) (refer to Chapter 3.4). As this matrix was successfully used for the immobilisation of hybridomas and insect cell cultures (Huebner and Buchholz, 1999), it was expected to be gentle enough for the immobilisation of bacteria without substantial loss of activity, yet mechanically strong. Hence, it was expected to give a rather high immobilisation yield (40 %) as compared to the other matrices. To date, this is the first application of lactic acid bacteria immobilised with sodium cellulose sulphate (NaCS). Contrary to the numerous applications of alginate and carrageenan immobilisation for lactic acid bacteria, the NaCS immobilisates did not face some of the general difficulties (e.g.

weakening of the matrix structure in the presence of chelating agents) associated with the other matrices. Therefore, the NaCS matrix may also be useful for a wider range of applications.

From the results of the batch runs with the NaCS-immobilised cells, it was found that the behaviour of the NaCS immobilisates was slightly different from the non-immobilised *L. kefiri* (Haberland et al., 2002a) in view of the selectivity and pH range of the bioreduction process. These results substantiate the common known fact that immobilisation may affect the behaviour of the native cells (Hahn-Haegerdal, 1990). Despite the lower activity of the NaCS immobilisates as compared to the non-immobilised *L. kefiri*, the biocatalyst consumption of the batch process with NaCS immobilisates was 14 times lower (see Chapter 6.2.1).

In the continuous synthesis of (5*R*)-hydroxyhexane-2-one (**B**), the use of one plug flow column without pH control was sufficient to prevent further reduction of (5*R*)-hydroxyhexane-2-one (**B**) to (2*R*,5*R*)-hexanediol (**C**) (refer to Chapter 3.4.4).

In order to reduce the biocatalyst consumption and selectivity of the process, the following could be performed:

- Lower residence time (less than 0.8 h),
- Longer operating time (beyond 6 days) to fully utilise the residual activity of the immobilised cells (68 %).

Since the results suggest a plausible toxicity of the substrate (2,5)-hexanedione (**A**) on the cells, future runs could also be done at lower concentrations, with a reduced packed column or a faster flow rate through the column.

From Table 6.1, it seemed that both the continuous production of (5*R*)-hydroxyhexane-2-one (**B**) with a plug flow reactor or repetitive batch runs with immobilised cells were the better options (based on process parameters and economics). These would be the reactor choices for future production.

Table 6.1. Summary of the different means to produce (5*R*)-hydroxyhexane-2-one (B). STY for batch and repetitive batch setups refer to the initial rate of production of (5*R*)-hydroxyhexane-2-one (B). N.d.: Not determined.

System	Reactor setup	Biocat consumption (g_{biocat} g_B^{-1})	k_{des} (% h^{-1})	STY (g_B L^{-1} d^{-1})	Prod cost (EUR mol_B^{-1})
Whole cells (non-immobilised)	Batch	33.3	n.d.	100	2068.67
	Rep. batch	5.9	16.1	23 - 100	385.53
Whole cells (immobilised)	Batch	2.4	n.d.	13	2710.44
	Rep. batch	0.5	1.3	2 - 13	523.32
	PFR	1.4	2.8	87	1562.03
Enzymes	Batch	0.7	n.d.	125	19665.19

In the downstream processing of pure (5*R*)-hydroxyhexane-2-one (**B**), it was previously suspected that cyclisation of (5*R*)-hydroxyhexane-2-one (**B**) to (2,5*R*)-dimethyl-tetrahydrofuran-2-ol was thermodynamically favourable. However, attempts to accurately analyse the structure of the chemicals could be distorted by physical or chemical treatments prior to analysis. In addition, attempts to minimise the rate of the cyclisation and/or possible photooxidation processes by storage in the dark at a low temperature of 4 °C (of up to 1 year) did not stop the change of (5*R*)-hydroxyhexane-2-one (**B**). The original yellow colour of (5*R*)-hydroxyhexane-2-one (**B**) had turned a darker shade, and the identity of the new compound(s) is/are unknown.

6.2 3-Hydroxybutanoate syntheses with whole cells of recombinant *Escherichia coli* versus enzyme-coupled system

6.2.1 Process parameters and stability

Similar to the production of γ-hydroxyketone, the processes yielding (*R*)-methyl-3-hydroxybutanoate (**MHB**) were evaluated (Figure 6.7).

The biocatalyst consumption of the processes with isolated enzymes was much lower (up to 58.5 times) than that with the use of whole cells (Figure 6.8). With the use of continuous reactors, the biocatalyst consumption of batch processes reduced by 1.9- and 14.7-fold for the case with whole cells and enzymes respectively. On the other hand, the initial rate of production of (*R*)-methyl-3-hydroxybutanoate (**MHB**) in batch reactors (Eq. 4.8) were 2.3-fold faster when whole cells were employed (Table 6.2).

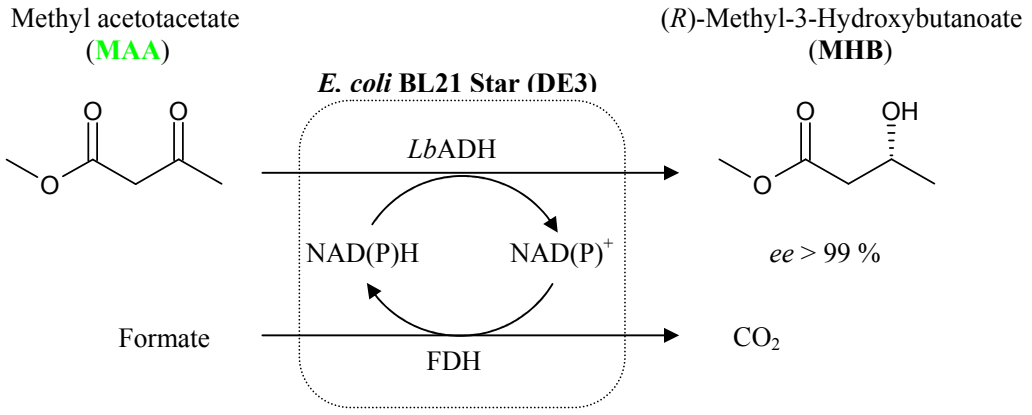

Figure 6.7. Enantioselective reduction of methyl acetoacetate (MAA) to (*R*)-methyl-3-hydroxybutanoate (MHB) with resting whole cells of recombinant *Escherichia coli* or enzyme-coupled system (*Lb*ADH: Alcohol dehydrogenase from *Lactobacillus brevis*, FDH: Formate dehydrogenase from *Pseudomonas* sp.).

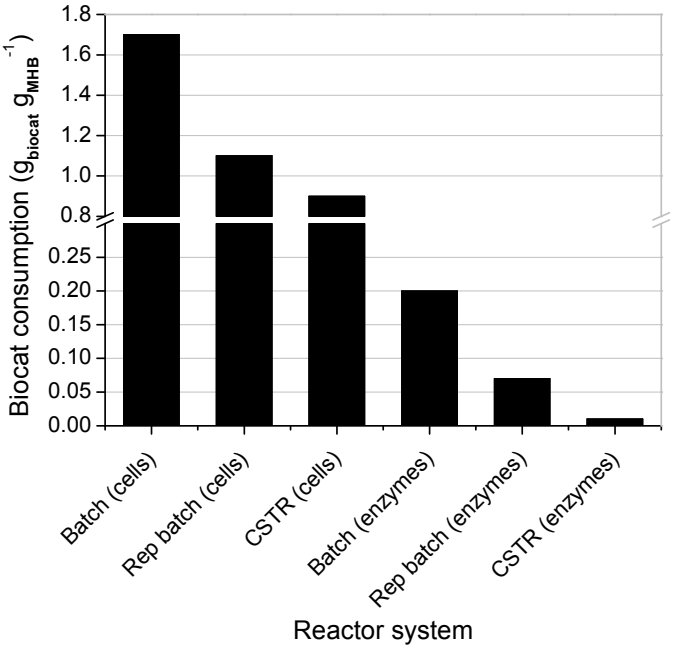

Figure 6.8. Comparison of biocatalyst consumption with respect to the use of whole cells or enzymes and reactor setup. The amount of biocatalyst (in the case of whole cells) refers to the wet biomass.

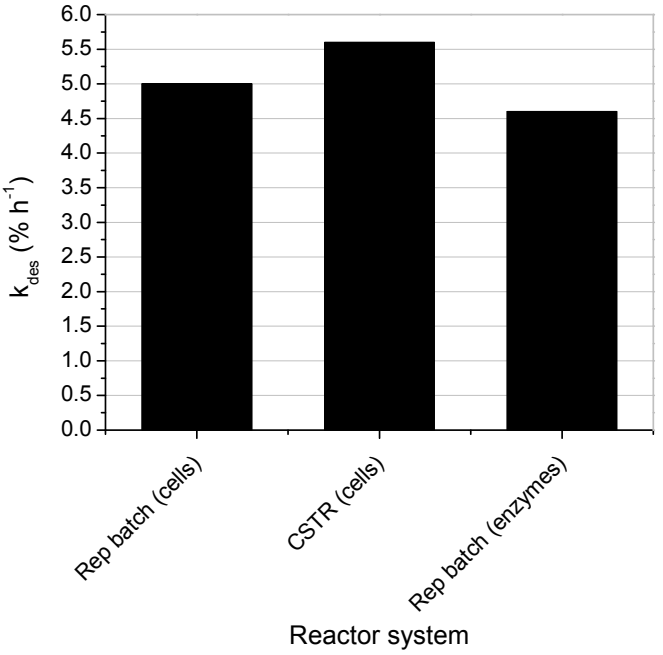

Figure 6.9. Comparison of deactivation constant with respect to whole cells or enzymes and reactor setup.

From Figure 6.9, the rates of deactivation of both whole cells and enzymes were rather similar. Even a change in reactor setup in the case of whole cells did not yield any significant differences in the deactivation constant of the biocatalyst.

6.2.2 Economics

The economic viability of the processes is summarised in Figure 6.10 based on the production cost (Eq. 6.1). In general, the cost of producing (*R*)-methyl-3-hydroxybutanoate (**MHB**) with whole cells was up to 13.9-fold lower than with enzymes. When continuous production was used in place of batch, the production cost decreased by 1.9 to 9.2 times in the case of whole cells and enzymes respectively.

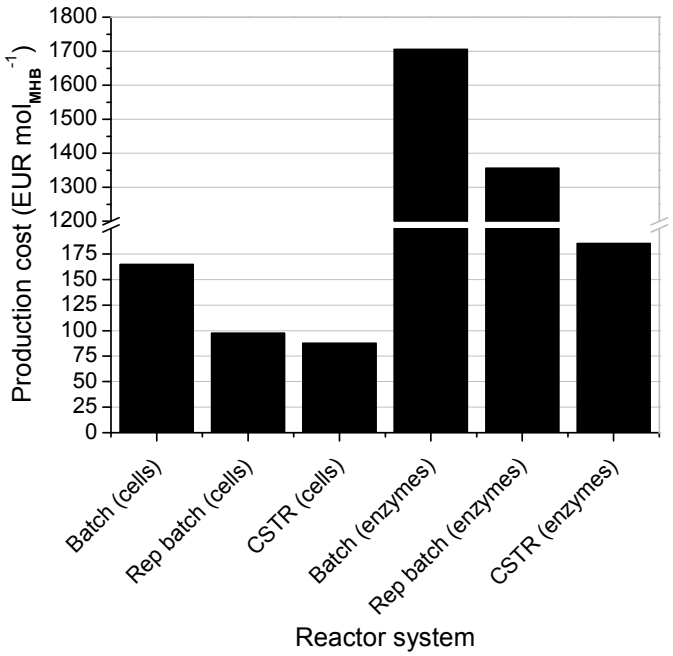

Figure 6.10. Comparison of production cost with respect to the use of whole cells or enzymes and reactor setup. Prices are obtained from Fluka (2005/2006), Roth (2005), Merck (2005/2007) and Juelich Fine Chemicals (2004) catalogues.

A large proportion of the production cost in whole cells and enzymes processes was due to the high cost of biocatalyst (Figure 6.11). The costs of the substrate methyl acetoacetate (**MAA**) and cofactor $NADP^+$ (except in the continuous operation) remained low.

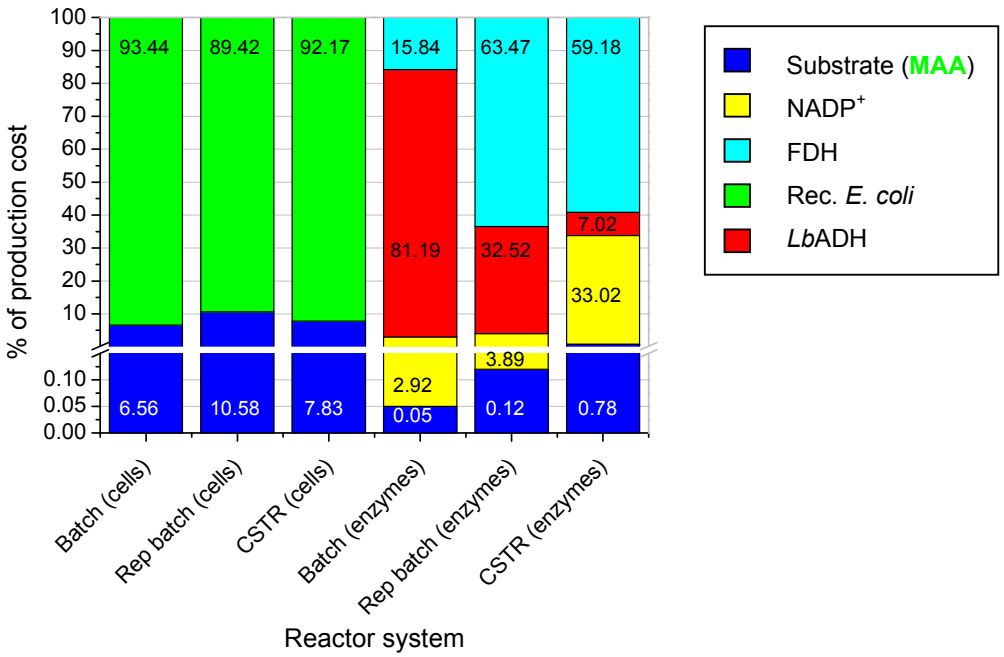

Figure 6.11. Comparison of production cost with respect to costs of biocatalyst, substrate and cofactors. Prices are obtained from Fluka (2005/2006), Roth (2005), Merck (2005/2007) and Juelich Fine Chemicals (2004) catalogues.

Table 6.2. Summary of the different means to produce (*R*)-methyl-3-hydroxybutanoate (MHB). STY for batch and repetitive batch setups refer to the initial rate of production of (*R*)-methyl-3-hydroxybutanoate (MHB). N.d.: Not determined.

System	Reactor setup	Biocat consumption (g_{biocat} g_{MHB}^{-1})	k_{des} (% h^{-1})	STY (g_{MHB} L^{-1} d^{-1})	Prod cost (EUR mol_{MHB}^{-1})
Whole cells	Batch	1.7	n.d.	127	164.81
	Rep. batch	1.1	5.0	75 - 91	97.59
	CSTR	0.9	5.6	16 - 57	87.64
Enzymes	Batch	0.2	n.d.	57	1705.34
	Rep. batch	0.07	4.6	57 - 72	1355.70
	CSTR	0.01	n.d.	57 - 113	185.39

6.2.3 Problems and outlook

In the whole cell system, it seemed that additional amount of oxygen during fermentation through better stirring gave lower biocatalytic activity (Refer to Chapter 5.1.2). This may be due to the cells devoting more energy for biosynthesis by oxidative phosphorylation rather than expressing the plasmids ADH and FDH during induction. Therefore, future fermentation, even on a larger scale, should have reduced stirring and possibly dissolved oxygen content to minimise the channelling of energy from gene expression to biosynthesis. A more detailed study of the fermentation and

induction process is needed to obtain biocatalyst of high activity. Moreover, prior to fermentation, each transformation done to rec. *E. coli* gave different expression level. As a result, every colony from the agar plate gave different activities, and the colony with high activity had to be chosen before fermentation to yield more biomass of high activity.

The storage of active induced cells was possible up to 3 weeks (see Chapter 5.3). It is known that ectoine aided the stability of extracellular proteins in microorganisms living under unfavourable conditions (Knapp et al., 1999). Therefore, the introduction of ectoine in the storage medium could extend the shelf-life of the induced biocatalyst beyond 3 weeks.

In continuous production, the major problem was the instability of rec. *E. coli* (Refer to Chapter 5.6). From repetitive batch studies (see Chapter 5.7.1), it seemed that formate, the cosubstrate, was toxic to the cells. In order to regenerate the intracellular cofactors efficiently, another designer bug system could be considered in place of oxidation of formate by FDH. For example, the cells could be transformed with glucose dehydrogenase (GDH) where glucose is the cosubstrate (Kataoka et al., 2003). Alternatively, the cells could simply be transformed with a single plasmid *Lb*ADH, where isopropanol is used as the cosubstrate. Having to express the genes for a single plasmid instead of two could result in higher *Lb*ADH activity during fermentation and induction, as well as increased stability of the cells. However, isopropanol and its corresponding product acetone are known to be toxic or inhibitory to the enzymes (Kula and Kragl, 2000). In addition, it was sometimes not possible to obtain 100 % bioreduction of the main substrate due to thermodynamic limitations of the isopropanol and acetone system. However, this could be overcome through means of pervaporation or stripping of acetone with air (Stillger et al., 2002, 2004).

One other way to improve the stability of the rec. *E. coli* could be the use of highly enriched minimal medium rather than phosphate buffer as biotransformation medium (Refer to Chapter 5.7.3). Although the deactivation constants for both biotransformation media were quite similar, lower biocatalyst consumption was obtained for the cells in minimal medium. The highly enriched minimal medium could have affected the metabolism of the cells, thereby enhanced the activity as observed in the repetitive batch studies.

In the isolated enzyme-coupled system, the behaviour of *Lb*ADH differed depending on cofactors (Table 6.3). Using this information for application in the whole cell system, it could not be determined if the bioreduction employed NADPH or NADH exclusively. If NADPH was solely used, the larger $K_{m,MAA}$ value for rec. *E. coli* as compared to that for the *Lb*ADH/NADPH system could be explained by the diffusion limitation of methyl acetoacetate (**MAA**) across the cell membrane of rec. *E. coli*. However, there was no inhibition of methyl acetoacetate (**MAA**) observed in the whole cell system, as opposed to the *Lb*ADH/NADPH system. On the other hand, there was no substrate inhibition if NADH was solely used. However, the larger $K_{m,MAA}$ value for *Lb*ADH/NADH system rather than that for rec. *E. coli* would suggest a faster bioreduction of methyl acetoacetate (**MAA**) in whole cells rather than in the isolated enzyme-coupled system, which did not seem plausible. Therefore, the whole cell bioreduction of methyl acetoacetate (**MAA**) appeared to involve a combination of NADPH and NADH as cofactors.

Table 6.3. Comparison of kinetics constants of NAD(P)H-bounded *Lb*ADH and rec. *E. coli*. Note: Temperatures of *Lb*ADH reactions are performed at 20 °C, and 30 °C for rec. *E. coli*.

Kinetics constants	NADPH-bounded *Lb*ADH	NADH-bounded *Lb*ADH	Rec. *E. coli*
$v_{max,MAA}$ (U_{MAA} mg_{ADH}^{-1}, U_{MHB} g_{wcw}^{-1})	32.47 ± 0.05	30.41	35.70 ± 2.80
$K_{m,MAA}$ (mM)	0.31 ± 0.001	84.27 ± 0.94	12.86 ± 5.00
$K_{m,NAD(P)H}$ (mM)	0.0038 ± 6×10^{-5}	1.6	-
$K_{i,MAA}$ (mM)	163.98 ± 0.53	-	-

A direct comparison between the $v_{max,MAA}$ values for the whole cell and enzyme systems would not be accurate. The whole cell system consisted not only of *Lb*ADH, but also of FDH, whereas the kinetics constants for the bioreduction of methyl acetoacetate (**MAA**) in the enzyme systems were obtained solely from *Lb*ADH.

When the enzyme-coupled system was employed in a continuous reactor, the *Lb*ADH and FDH were much less stable as opposed to results obtained in batch studies (Refer to Chapters 4.3.2 and 4.3.6). In addition, the formation of an unknown white, cloudy suspension in the continuous production could not be explained. It is also not known if the suspension had any effects on the enzymes. Therefore, it seemed that conditions in the continuous reactor were very much complex and different due to the on-going biotransformation.

6.3 Choice of biocatalyst system

The activity of wild type *L. kefiri* and genetically modified *E. coli* were compared with isolated enzymes. In a batch reactor, with (2,5)-hexanedione (**A**) as substrate, the activity of isolated enzymes was more than 22.0-fold higher than that seen for whole cells (Figure 6.12). The activity of rec. *E. coli* was 1.6 times higher than that seen in the wild type *L. kefiri*. Similarly, when methyl acetoacetate (**MAA**) was used as substrate, the activity of isolated enzymes was up to 48.8 times higher than that observed for whole cells (Figure 6.13). Higher activity (4.7-fold) was obtained with the use of rec. *E. coli* as biocatalyst rather than wild type *L. kefiri*.

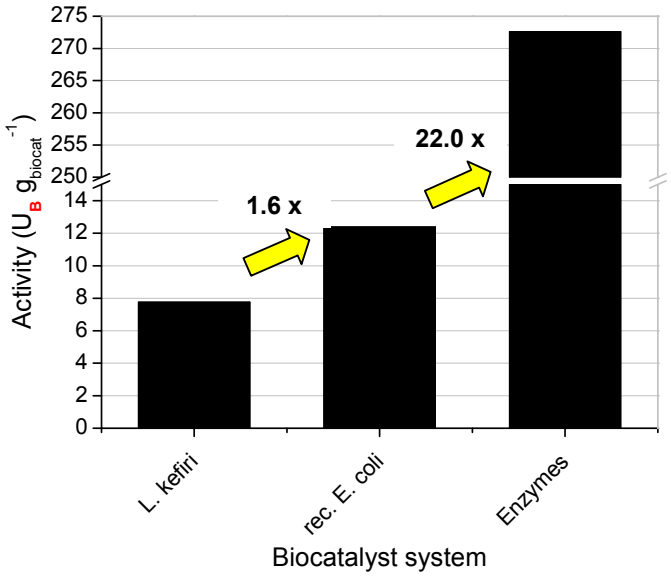

Figure 6.12. Comparison of activity of wild type *L. kefiri*, rec. *E. coli* and isolated enzyme-coupled system in a batch reduction of (2,5)-hexanedione (A).

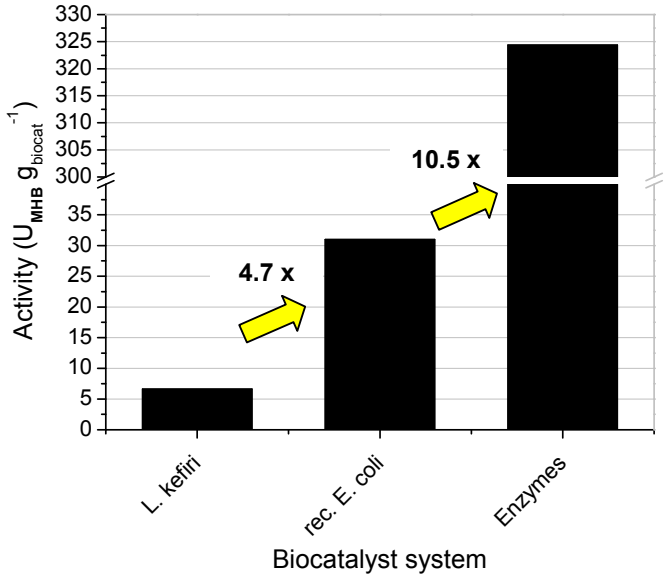

Figure 6.13. Comparison of activity of wild type *L. kefiri*, rec. *E. coli* and isolated enzyme-coupled system in a batch reduction of methyl acetoacetate (MAA).

Although higher activities were obtained with enzymes, the higher production cost was a main disadvantage for industrial production as compared to processes using active whole cells. Despite lower activities seen in whole cell biotransformations, higher activities could be obtained with the genetically modified microorganism rather than the wild type strain. Therefore, a designer bug with high activity using a high copy plasmid could be tailored for an industrial process with minimal production cost.

7 Conclusions

Biotransformations with isolated enzyme-coupled system and resting whole cells (wild type and genetically modified organisms) were investigated and compared.

In the enzyme-coupled system with alcohol dehydrogenase from *Lactobacillus brevis* (*Lb*ADH) and formate dehydrogenase (FDH) from *Pseudomonas* sp.,

- Batch reduction of (2,5)-hexanedione (**A**) to (5*R*)-hydroxyhexane-2-one (**B**) yielded high initial rate of production of 125 g_B L^{-1} d^{-1}, with biocatalyst consumption of 0.7 g_{biocat} g_B^{-1} and total turnover number (*ttn*) of 225 mol_B mol_{NADP}^{-1}.

- Reduction of methyl acetoacetate (**MAA**) to (*R*)-methyl-3-hydroxybutanoate (**MHB**) was performed in batch, repetitive batch and continuous setup.

- Batch kinetics were investigated and modelled. *Lb*ADH behaved differently depending on the cofactor used.

- The lowest biocatalyst consumption of 0.01 g_{biocat} g_{MHB}^{-1} and total turnover number (*ttn*) of 329 mol_{MHB} $mol_{NADP}^{-1}$was obtained in a continuous setup.

- Rapid deactivation of *Lb*ADH and FDH in continuous setup was observed.

In the whole cell biotransformation of (2,5)-hexanedione (**A**) to (5*R*)-hydroxyhexane-2-one (**B**) with wild type *Lactobacillus kefiri*,

- Whole cell immobilisation reduced cell activity but increased cell stability and reduced biocatalyst consumption.

- The best encapsulation matrix was sodium cellulose sulphate (technical grade).

- Reactions with immobilised cells were carried out in batch, repetitive batch and continuous mode with a plug flow reactor.

- Lowest biocatalyst consumption (0.5 g_{wcw} g_B^{-1}) was obtained in the repetitive batch setup.

- High selectivity (95 %) and space-time yield (87 g_B L^{-1} d^{-1}) were obtained in the plug flow reactor setup.

- Gram-scale separation of (5*R*)-hydroxyhexane-2-one (**B**) by column chromatography (1.2 g_B) with high *ee* and purity of more than 99 %.

In the whole cell biotransformation of methyl acetoacetate (**MAA**) to (*R*)-methyl-3-hydroxybutanoate (**MHB**) with genetically modified *Escherichia coli*,

- First known storage of active induced cells in phosphate buffer of up to 3 weeks.
- For complete yield of (*R*)-methyl-3-hydroxybutanoate (**MHB**), at least 1.2 times more formate to methyl acetoacetate (**MAA**) in molar concentrations must be given.
- Batch to repetitive batch and continuous reactors were operated.
- Lowest biocatalyst consumption (0.9 g_{wcw} $g_{\mathbf{MHB}}^{-1}$) of *ee* > 99 % was obtained in the continuous setup.
- Rapid drop in conversion of **MAA** in continuous setup, possibly due to formate toxicity and leaky cell membrane.

In this study,

- Isolated enzyme-coupled systems gave low biocatalyst consumption but were costly.
- Wild type microorganism yielded higher biocatalyst consumption but was inexpensive.
- Immobilised wild type microorganism drastically improved the space-time yield and reduced the biocatalyst consumption of a process.
- Genetically modified cells could be designed with high gene expression and hence activity to reduce the biocatalyst consumption and cost of a process.

8 References

Ager DJ (1999) Handbook of chiral chemicals. Dekker, Inc., New York, United States of America.

Audet P, Paquin C, Lacroix C (1988) Immobilized Growing Lactic Acid Bacteria with κ-Carrageenan — Locus Bean Gum Gel. Appl Microbiol Biotechnol 29: 11-18.

Arnaud JP, Lacroix C, Choplin L (1989) Effect of Lactic Fermentation on the Rheological Properties of κ-Carrageenan/Locust Bean Gum Mixed Gels Inoculated with *S. thermophilus*. Biotechnol Bioeng 34: 1403-1408.

Audet P, Paquin C, Lacroix C (1990) Batch Fermentations with a Mixed Culture of Lactic Acid Bacteria Immobilized Separately in κ-Carrageenan Locust Bean Gum Gel Beads. Appl Microbiol Biotechnol 32: 662-668.

Bailey JE and Ollis DF (1986) Biochemical Engineering Fundamentals. McGraw-Hill, Inc., Singapore.

Bickerstaff GF (1997) Immobilization of Enzymes and Cells: Some Practical Considerations. In: Bickerstaff GF (ed.) Methods in Biotechnology, Vol. 1, Humana Press, Inc., New Jersey, United States of America, 1-11.

Blacker AJ and Holt RA (1997) Development of a Multi-stage Chemical and Biological Process for an Optically Active Intermediate for an Anti-glaucoma Drug. In: Collins AN, Sheldrake GN and Crosby J (eds.) Chirality in Industry II. John Wiley.

Bradshaw CW, Hummel W, Wong C-H (1992) *Lactobacillus kefir* Alcohol Dehydrogenase: A Useful Catalyst for Synthesis. J Org Chem 57: 1532-1536.

Bringer-Meyer S (2005) Personal communications.

Brown KA, Moser CA, Speaker TJ, Khoury CA, Kim JE, Offit PA (1995) Enhancement by Microencapsulation of Rotavirus-specific Intestinal Immune Responses in Mice Assessed by Enzyme-linked Immunospot Assay and Intestinal Fragment Culture. J Infect Dis 171: 1334-1338.

Brunner H, Amberger K, Wischert T (1991) Asymmetric Catalysis. 69. Enantioselective Hydrogenation of Dicarbonyl Compounds with Nickel Catalysts Modified with Sodium Bromide/L-(+)-tartaric acid. Bull Soc Chim Belg 100: 585-595.

Bujnicki R (2004) Personal communications.

Burk MJ, Feaster JE, Harlow RL (1991) New Chiral Phospholanes; Synthesis, Characterization, and Use in Asymmetric Hydrogenation Reactions. Tetrahedron: Asymmetry 2: 569-592.

Burk MJ (1992) Chiral Tridentate Bis(phospholane) Ligands. WO 9219630.

Carnell AJ, Head R, Bassett D, Schneider M (2004) Efficient Large Scale Stereoinversion of (*R*)-Ethyl 3-hydroxybutyrate. Tetrahedron: Asymmetry 15: 821-825.

Chen K-C and Lin Y-F (1994) Immobilization of Microorganisms with Phosphorylated Polyvinyl Alcohol (PVA) Gel. Enzyme Microb Technol 16: 79-83.

Chenault HK, Simon ES, Whitesides GM (1988) Cofactor Regeneration for Enzyme-catalysed Synthesis. Biotechnol Genetic Engineering Rev 6: 221-270.

Chickering D, Jacob J, Mathiowitz E (1996) Poly(fumaric-co-sebacic) Microspheres as Oral Drug Delivery Systems. Biotechnol Bioeng 52(1): 96-101.

Chin-Joe I, Straathof AJJ, Pronk JT, Jongejan JA, Heijnen JJ (2002a) Effect of High Product Concentration in a Dual Fed-batch Asymmetric 3-Oxo Ester Reduction by Baker's Yeast. Biocatal Biotransform 20(5): 337-345.

Chin-Joe I, Haberland J, Straathof AJJ, Jongejan JA, Liese A, Heijnen JJ (2002b) Reduction of Ethyl 3-Oxobutanoate using Non-growing Baker's Yeast in a Continuously Operated Reactor with Cell Retention. Enzyme Microb Technol 31: 665-672.

Csuk R and Glaenzer BI (1991) Baker's Yeast Mediated Transformations in Organic Chemistry. Chem Rev 91: 49-97.

Csuk R and Glaenzer BI (2000) Yeast-mediated Stereoselective Biocatalysis. In: Patel RN (ed.) Stereoselective Biocatalysis. Dekker, Inc., New York, United States of America, 527-578.

D'Arrigo P, Pedrocchi-Fantoni G, Servi S (1997) Old and New Synthetic Capacities of Baker's Yeast. Adv Appl Microbiol 44: 81-123.

D'Arrigo P, Pedrocchi-Fantoni G, Servi S (2000) Stereoselective Synthesis of Chiral Compounds Using Whole-cell Biocatalysts. In: Patel RN (ed.) Stereoselective Biocatalysis. Dekker, Inc., New York, United States of America, 365-396.

Daussmann T (2005) Personal Communications.

Davis BR, Rewcastle GW, Stevenson RJ, Woodgate PD (1977) Clemmensen Reduction. Part 5. Chiral γ-Hydroxy-ketones. J Chem Soc, Perkin Trans 1 19: 2148-2154.

De Man JC, Rogosa M, Sharpe ME (1960) A Medium for the Cultivation of Lactobacilli. J Appl Bact 23(1): 130-135.

Doleyres Y, Fliss I, Lacroix C (2004) Continuous Production of Mixed Lactic Starters Containing Probiotics Using Immobilized Cell Technology. Biotechnol Prog 20: 145-150.

Durieux A, Nicolay X, Simon J-P (2000) Continuous Malolactic Fermentation by *Oenococcus oeni* Entrapped in LentiKats. Biotechnol Lett 22: 1679-1684.

Eckstein M, Daussmann T and Kragl U (2004) Recent Developments in NAD(P)H Regeneration for Enzymatic Reductions in One- and Two-phase Systems. Biocatal Biotransform 22(2): 89-96.

Embleton JK and Tighe BJ (1993) Polymers for Biodegradable Medical Devices. X. Microencapsulation Studies: Control of Poly-hydroxybutyrate-hydroxyvalerate Microcapsules Porosity via Polycaprolactone Blending. J Microencapsulation 10(3): 341-352.

Endo T and Koizumi S (2001) Microbial Conversion with Cofactor Regeneration Using Genetically Engineered Bacteria. Adv Synth Catal, 343(6-7): 521-526.

Ernst MB (2003) Enantioselektive Enzymatische Reduktion von Carbonylverbindungen mit Cofaktor-Regeneration in Rekombinanten *Escherichia coli*. Diplom Thesis, Fachhochschule Gelsenkirchen, Germany.

Ernst M, Kaup B, Mueller M, Bringer-Meyer S, Sahm H (2005) Enantioselective Reduction of Carbonyl Compounds by Whole-cell Biotransformation, Combining a Formate Dehydrogenase and a (*R*)-Specific Alcohol Dehydrogenase. Appl Microbiol Biotechnol 66: 629-634.

Foerster M, Mansfield J, Schellenberger A, Dautzenberg H (1994) Immobilization of Citrate-producing *Yarrowia lipolytica* Cells in Polyelectrolyte Complex Capsules. Enzyme Microb Technol 16: 777-784.

Fraeter G (1979) Ueber die Stereospezifitaet der α-Alkylierung von β-Hydroxycarbonsaeureestern. Helv Chim Acta 62(8): 2825-2828.

Frost & Sullivan (2003) Developments in Global Chiral Technology Markets. B105-39.

Gåserød O, Sannes A, Skjåk-Bræk (1999) Microcapsules of Alginate-chitosan. II. A Study of Capsule Stability and Permeability. Biomaterials 20: 773-783.

Gelpke AES, Kooijman H, Spek AL, Hiemstra H (1999) Synthesis of the Dibenzofuran-based Diphosphine Ligand BIFAP and Its Water-soluble Derivative BIFAPS and Their Use in Ruthenium-catalyzed Asymmetric Hydrogenation. Chem Eur J 5(9): 2472-2482.

Groboillot A, Boadi DK, Poncelet D, Neufeld RJ (1994) Immobilization of Cells for Application in the Food Industry. Crit Rev Biotechnol 14(2): 75-107.

Groeger H, Hummel W, Buchholz S, Drauz KH, Van Nguyen T, Rollmann C, Huesken H, Abokitse K (2003) Practical Asymmetric Enzymatic Reduction Through Discovery of a Dehydrogenase-compatible Biphasic Reaction Media. Org Lett 5: 173-176.

Grunwald J, Wirts B, Scollar MP, Klibanov AM (1986) Asymmetric Oxidoreductions Catalyzed by Alcohol Dehydrogenase in Organic Solvents, J Am Chem Soc 108: 6732-6734.

Gul-Karaguler N, Sessions RB, Clarke AR, Holbrook JJ (2001) A Single Mutation in the NAD-specific Formate Dehydrogenase from *Candida methylica* Allows the Enzyme to Use NADP. Biotechnol Lett 23: 283-287.

Haberland J, Kriegesmann A, Wolfram E, Hummel W, Liese A (2002a) Diastereoselective Synthesis of Optically Active (2*R*,5*R*)-Hexanediol. Appl Microbiol Biotechnol 58: 595-599.

Haberland J, Hummel W, Daussmann T, Liese A (2002b) New Continuous Production Process for Enantiopure (2*R*,5*R*)-Hexanediol. Org Process Res Dev 6: 458-462.

Haberland J (2003) Verfahrensentwicklung zur Darstellung von (2*R*,5*R*)-Hexandiol mit *Lactobacillus kefir* DSM20587. Ph.D. Dissertation, University of Bonn, Germany.

Hahn-Haegerdal B (1990) Physiological Aspects of Immobilized cells: A General Overview. In: de Bont JAM, Visser J, Mattiasson B, Tramper J (eds.) Physiology of Immobilized Cells. Elsevier Science Publishers B.V., Amsterdam, The Netherlands, 481-486.

Hollmann F and Schmid A (2004) Electrochemical Regeneration of Oxidoreductases for Cell-free Biocatalytic Redox Reactions. Biocatal Biotransform 22(2): 63-88.

http://www.accessexcellence.org. Recombinant microorganism.

http://www.geniaLab.de/download/tt-english.pdf. Operating Instructions of LentiKats®.

Huebner H and Buchholz R (1997) In: Maramorosch K and Mitsuhashi J (eds.) Invertebrate Cell Culture: Novel Directions and Biotechnology Applications. Science Publishers, New Hampshire, United States of America, 123-130.

Huebner H and Buchholz R (1999) Microencapsulation. In: Flicker MC, Drew SW (eds.) Encyclopedia of Bioprocess Technology: Fermentation, Biocatalysis and Bioseparation, Vol. 4. John Wiley & Sons, Inc., New York, United States of America, 1785-1798.

Hummel W and Kula M-R (1989a) Dehydrogenases for the Synthesis of Chiral Compounds. Eur J Biochem 184: 1-13.

Hummel W, Boermann F and Kula M-R (1989b) Purification and Characterization of an Acetoin Dehydrogenase from *Lactobacillus kefir* Suitable for the Production of (+)-Acetoin. Biocatalysis 2: 293-308.

Hummel W (1990) Reduction of Acetophenone to *R*(+)-Phenylethanol by a New Alcohol Dehydrogenase from *Lactobacillus kefir*. Appl Microbiol Biotechnol 34: 15-19.

Hummel W (1997) New Alcohol Dehydrogenases for the Synthesis of Chiral Compounds. Adv Biochem Engin Biotechnol 58: 145-184.

Hummel W (1999) Large-scale Applications of NAD(P)-dependent Oxidoreductases: Recent Developments. Trends Biotechnol 17: 487-492.

Hummel W, Liese A, Wandrey C (2002) Process for Reducing Keto-group Containing Compounds. EP 1067195.

Hummel W (2005) Personal Communications.

Ikeda H, Sako E, Sugai T, Ohta H (1996) Yeast-mediated Synthesis of Optically Active Diols with C2-Symmetry and (*R*)-4-Pentanolide. Tetrahedron 52: 8113-8122.

Jekel M, Buhr A, Willke T, Vorlop K-D (1998) Immobilization of Biocatalysts in LentiKats. Chem Eng Technol 21(3): 275-278.

Kandler O and Kunath P (1983) *Lactobacillus kefir* sp.nov., a Component of the Microflora of Kefir. System Appl Microbiol 4: 286-294.

Kaluzna IA, Feske BD, Wittayanan W, Ghiviriga I, Stewart JD (2005) Stereoselective, Biocatalytic Reductions of α-Chloro-β-keto Esters. J Org Chem 70: 342-345.

Karel SF, Libicki SB, Robertson CR (1985) The Immobilization of Whole Cells: Engineering Principles. Chem Eng Sci 40(8): 1321-1354.

Kataoka M, Rohani LPS, Yamamoto K, Wada M, Kawabata H, Kita K, Yanase H, Shimizu S (1997) Enzymatic Production of Ethyl (*R*)-4-Chloro-3-hydroxybutanoate: Asymmetric Reduction of Ethyl 4-Chloro-3-oxobutanoate by an *Escherichia coli* Transformant Expressing the Aldehyde Reductase Gene from Yeast. Appl Microbiol Biotechnol 48: 699-703.

Kataoka M, Yamamoto K, Kawabata H, Wada M, Kita K, Yanase H, Shimizu S (1999) Stereoselective Reduction of Ethyl 4-Chloro-3-oxobutanoate by *Escherichia coli* Transformant Cells Coexpressing the Aldehyde Reductase and Glucose Dehydrogenase Genes. Appl Microbiol Biotechnol 51: 486-490.

Kataoka M, Kita K, Wada M, Hasegawa J, Shimizu S (2003) Novel Bioreduction System for the Production of Chiral Alcohols. Appl Microbiol Biotechnol 62: 437-445.

Kaup B (2005) Personal communications.

Kitamura M, Tokunaga M, Ohkuma T, Noyori R (1993) Asymmetric Hydrogenation of 3-Oxo Carboxylates Using BINAP-Ruthenium Complexes: (*R*)-(-)-Methyl 3-Hydroxybutanoate. Org Synth 71: 1-13.

Kizaki N, Yasohara Y, Hasegawa J, Wada M, Kataoka M, Shimizu S (2001) Synthesis of Optically Pure Ethyl (S)-4-chloro-3-hydroxybutanoate by *Escherichia coli* Transformant Cells Coexpressing the Carbonyl Reductase and Glucose Dehydrogenase Genes. Appl Microbiol Biotechnol 55: 590-595.

Klinkenberg G, Lystad KQ, Levine DW, Dyrset N (2001) Cell Release from Alginate Immobilized *Lactococcus lactis* ssp. *lactis* in Chitosan and Alginate Coated Beads. J Dairy Sci 84: 1118-1127.

Koeller KM and Wong C-H (2001) Enzymes for Chemical Synthesis. Nature 409: 232-240.

Komentani T, Yoshii H, Kitatsuji E, Nishimura H, Matsuno R (1993) Large-scale Preparation of (*S*)-Ethyl 3-Hydroxybutanoate With a High Enantiomeric Excess Through Baker's Yeast-mediated Bioreduction. J Ferment Technol 76(1): 33-37.

Kondo K, Otono T, Matsumoto M (2004) Preparation of Microcapsules Containing Extractants and the Application of the Microcapsules to the Extractive Fermentation of Lactic Acid. J Chem Eng Japan 37(1): 1-6.

Kramer A and Pfanler H (1982) Synthese von (*R*)- und (*S*)-Lavandulol. Helv Chim Acta 65(1): 293-301.

Kriegesmann A (1999) Ganzzellbiotransformationen mit *Saccharomyces cerevisiae* und *Lactobacillus kefir* zur Darstellung Enantiomerenreiner 2,5-Hexandiole. Diplom Thesis, University of Bonn, Germany.

Kroutil W, Mang H, Edegger K, Faber K (2004) Recent Advances in the Biocatalytic Reduction of Ketones and Oxidation of *Sec*-Alcohols. Curr Opin Chem Biol 8:120-126.

Kukula P and Červený L (2002) Effects of Reaction Variables on Enantioselectivity of Modified Raney Nickel Catalyst. J Mol Catal A: Chem 185: 195-202.

Kula M-R and Kragl U (2000) Dehydrogenases in the Synthesis of Chiral Compounds. In: Patel RN (ed.) Stereoselective Biocatalysis. Dekker, Inc., New York, United States of America, 839-866.

Lacroix C, Paquin C, Arnaud J-P (1990) Batch Fermentation with Entrapped Growing Cells of *Lactobacillus casei*. Optimization of the Rheological Properties of the Entrapment Gel Matrix. Appl Microbiol Biotechnol 32: 403-408.

Leenen EJTM (2001) Description of the Support Material. In: Wijfels RH (ed.) Immobilized Cells. Springer-Verlag, Heidelberg, Germany, 6-14.

Le-Tien C, Millette M, Mateescu M-A, Lacroix C (2004) Modified Alginate and Chitosan for Lactic Acid Bacteria Immobilization. Biotechnol Appl Biochem 39: 347-354.

Liese A, Seelbach K, Buchholz A, Haberland J (2000a) Processes. In: Liese A, Seelbach K, Wandrey C (eds.) Industrial biotransformations. Wiley-VCH, Weinheim, Germany, 93-392.

Liese A, Seelbach K, Rao N (2000b) Basics of Bioreaction Engineering. In: Liese A, Seelbach K, Wandrey C (eds.) Industrial biotransformations. Wiley-VCH, Weinheim, Germany, 57-91.

Mansfeld J, Foerster M, Hoffmann T, Schellenberger A (1995) Coimmobilization of Yarrowia lipolytica Cells and Invertase in Polyelectrolyte Complex Microcapsules Enzyme Microb Technol 17: 11-17.

Mansfeld J and Dautzenberg H (1997) Immobilization of Cells in Polyelectrolyte Complexes. In: Bickerstaff GF (ed.) Methods in Biotechnology, Vol. 1, Humana Press, Inc., New Jersey, United States of America, 309-317.

Mikami M, Korenaga T, Ohkuma T, Noyori R (2000) Asymmetric Activation/Deactivation of Racemic Ru Catalysts for Highly Enantioselective Hydrogenation of Ketonic Substrates. Angew Chem Int Ed Engl 39: 3707–3710.

Mori K (2000) Chemoenzymatic Synthesis of Pheromones, Terpenes, and Other Bioregulators. In: Patel RN (ed.) Stereoselective Biocatalysis. Dekker, Inc., New York, United States of America, 59-85.

Mueller M, Wolberg M, Schubert T, Hummel W (2005) Enzyme-catalyzed Regio- and Enantioselective Ketone Reductions. Adv Biochem Engin/Biotechnol 92: 261-287.

Murano E (1998) Use of Natural Polysaccharides in the Microencapsulation Techniques. J Appl Ichthyol 14: 245-249.

Nakai T and Chiba T. (1986) Azetidinone Derivative and Processes for Production Thereof. EP 171064.

Nakamura K, Kawai Y, Nakajima N, Ohno A (1991) Stereochemical Control of Microbial Reduction. 17. A Method for Controlling the Enantioselectivity of Reduction with Baker's Yeast. J Org Chem 56: 4778-4783.

Nedović V and Wilaert R (2004) Fundamentals of Cell Immobilisation Biotechnology. In: Hofman M and Anné J (eds.) Focus on Biotechnology, Vol. 8A, Kluwer Academic Publishers, The Netherlands.

Niefind K, Mueller J, Riebel B, Hummel W, Schomburg D (2003) The Crystal Structure of *R*-Specific Alcohol Dehydrogenase from *Lactobacillus brevis* Suggests the Structural Basis of Its Metal Dependency. J Mol Biol 327: 317-328.

Noyori R and Ohkuma T (2001) Asymmetric Catalysis by Architectural and Functional Molecular Engineering: Practical Chemo- and Stereoselective Hydrogenation of Ketones. Angew Chem Int Ed Engl 40: 40–73.

Ogawa J and Shimizu S (2002) Industrial Microbial Enzymes: Their Discovery by Screening and Use in Large-scale Production of Useful Chemicals in Japan. Curr Opin Biotechnol 13: 367-375.

Patel RN, McNamee CG, Banerjee A, Howell JM, Robison RS, Szarka LJ (1992) Stereoselective Reduction of β-Keto Esters by *Geotrichum candidum*. Enzyme Microb Technol 14: 731-738.

Ribeiro JB, Ramos M, Neto FR, Leite SGF, Antunes OAC (2003) Microbiological Enantioselective Reduction of Ethyl Acetoacetate J Mol Catal B: Enzym 24-25: 121-124.

Rissom S (1995) Isolierung und Charakterisierung einer Diol-Dehydrogenase aus *Bacillus smithii* und ihre Anwendung in der Synthese chiraler Diole. Diplom thesis, University of Bonn, Germany.

Rissom S (1999) Membranverfahren fuer Redoxenzyme Gasversorgung-Reaktion-Produktextraktion. Ph.D. Dissertation, University of Bonn, Germany.

Santos VA, Tramper J, Wijffels RH (1993) Simultaneous Nitrification and Denitrification Using Immobilized Microorganisms. Biomat, Art Cells & Immob Biotech 21(3): 317-322.

Sato T and Tosa T (1993) Production of L-Aspartic Acid. In: Tanaka A, Tosa T and Kobayashi T (eds.) Industrial Application of Immobilized Biocatalysts. Marcel Dekker, Inc., New York, United States of America, 15-24.

Scannell AGM, Hill C, Ross RP, Marx S, Hartmeier W, Arendt EK (2000) Continuous Production of Lacticin 3147 and Nisin Using Cells Immobilized in Calcium Alginate. J Appl Microbiol, 89: 573-579.

Schmelzer AE, deZengotita VM, Miller WM (2000) Considerations for Osmolality Measurement Under Elevated pCO_2: Comparison of Vapor Pressure and Freezing Point Osmometry. Biotechnol Bioeng 67(2): 189-196.

Schmid A, Dordick JS, Hauer B, Kiener A, Wubbolts M, Witholt B (2001) Industrial Biocatalysis Today and Tomorrow. Nature 409: 258-268.

Schubert T, Hummel W, Kula M-R, Mueller M (2001) Enantioselective Synthesis of Both Enantiomers of Various Propargylic Alcohols by Use of Two Oxidoreductases. Eur J Org Chem 22: 4181-4187.

Schuler ML and Kargi F (1992) Enzymes. In: Bioprocess Engineering Basic Concepts. Prentice-Hall, Inc., New Jersey, United States of America, 58-97.

Seebach DZ and Zueger M (1982) Ueber die Depolymerisierung von Poly-(*R*)-3-hydroxy-buttersaeureester (PHB). Helv Chim Acta 65(2): 495-503.

Seebach DZ and Zueger MF (1985) On the Preparation of Methyl and Ethyl (*R*)-(-)-3-Hydroxy-Valerate by Depolymerization of a Mixed PHB/PHV Biopolymer. Tetrahedron Lett 25: 2747-2750.

Seebach D, Sutter MA, Weber RH, Zueger MF (1990) Yeast Reduction of Ethyl Acetoacetate: (*S*)-(+)-Ethyl 3-Hydroxybutanoate. Org Synth Coll Vol VII: 215-220.

Seebach DZ, Beck AK, Breitschuh R, Job K (1993) Direct Degradation of the Biopolymer Poly[(*R*)-3-hydroxybutyric Acid] to (*R*)-3-Hydroxybutanoic Acid and Its Methyl Ester. Org Synth 71: 39-47.

Seelbach K (1994) Verwendung von Umkehrosmosemembranen zur Cofaktorrueckhaltung in Enzym-Membranreaktoren am Beispiel neuer NADP(H)-abhaengiger Enzyme. Diplom Thesis, University of Bonn, Germany.

Seki M and Furusaki S (1996) An Immobilized Cell System for Taxol Production. Chemtech 26(3): 41-45.

Serov AE, Popova AS, Fedorchuk VV, Tishkov VI (2002) Engineering of Coenzyme Specificity of Formate Dehydrogenase from *Saccharomyces Cerevisiae*. Biochem J 367: 841-847.

Sharpe ME (1981) The Genus *Lactobacillus*. In: Starr MP, Stolp H, Trueper HG, Balaus A, Schlegel HG (eds.) The Prokaryotes II, Springer Verlag, Heidelberg, Germany.

Shieh W-R, Gopalan AS, Sih CJ (1985) Stereochemical Control of Yeast Reductions. 5. Characterization of the Oxidoreductases Involved in the Reduction of β-Keto Esters. J Am Chem Soc 107: 2993-2994.

Shimizu S, Kataoka M, Kita K (1998) Chiral Alcohol Synthesis with Yeast Carbonyl Reductases. J Mol Catal B: Enzym 5: 321-325.

Sigma-Aldrich catalogue (2004/2005)

Stewart JD (2000) Organic Transformations Catalyzed by Engineered Yeast Cells and Related Systems. Curr Opin Biotechnol 11: 363-368.

Stillger T, Boenitz M, Villela M, Liese A (2002) Ueberwindung von Thermodynamischen Limitierungen in Substratgekoppelten Cofaktorregenerierungsverfahren. Chem Ing Tech 74: 1035-1039.

Stillger T (2004) Enantioselektive C-C Knuepfung mit Enzymen. Ph.D. Dissertation, University of Bonn, Germany.

Straathof AJJ, Panke S, Schmid A (2002) The Production of Fine Chemicals by Transformations. Curr Opin Biotechnol 13: 548-556.

Sun ZM, Poncelet D, Conway J, Neufeld RJ (1995) Microencapsulation of Lobster Carotenoids Within Poly(vinyl alcohol) and Poly(D,L-lactic acid) membranes. J Microencapsulation 12(5): 495-504.

Tai IT and Sun AM (1993) Microencapsulation of Recombinant Cells: A New Delivery System for Gene Therapy. FASEB J 7: 1061-1069.

Tishkov VI, Galkin AG, Fedorchuk VV, Savitsky PA, Rojkova AM, Gieren H, Kula MR (1999) Pilot Scale Production and Isolation of Recombinant NAD^+- and $NADP^+$-specific Formate Dehydrogenases. Biotechnol Bioeng 64: 187-193.

Trueper HG and De' Clare L (1997) Taxonomic Note: Necessary Correction of Specific Epithets Formed as Substantives (Nouns) "in Apposition". Int J Syst Bacteriol 47(3): 908-909.

Villela M (2003) Enantioselective Reduction of Hydrophobic Keto Compounds in Multiphase Bioreactor. Ph.D. Dissertation, University of Bonn, Germany.

Vuorilehto K, Luetz S, Wandrey C (2004) Indirect Electrochemical Reduction of Nicotinamide Coenzymes. Bioelectrochem 65: 1-7.

Walton AZ and Stewart JD (2004) Understanding and Improving NADPH-dependent Reactions by Nongrowing *Escherichia coli* Cells. Biotechnol Prog 20: 403-411.

Wandrey C (2002) Kinetik Enzymatischer Reaktionen/Kontinuierliche Producktion von NADH im Enzym-Membran Reaktor. In: Technisches/Biotechnologisches Pratikum, University of Bonn, Germany.

Ward OP and Young CS (1990) Reductive Biotransformations of Organic Compounds by Cells or Enzymes of Yeast. Enzyme Microb Technol 12: 482-493.

Watanabe S, Mitsuhashi S, Kumobayashi H (1998) Process for Producing Optically Active Gamma-hydroxyketones. EP 592881.

Weast RC (1986) CRC Handbook of Chemistry and Physics. CRC Press, Inc., United States of America.

Wilaert RG and Baron GV (1996) Gel Entrapment and Micro-encapsulation: Methods, Applications and Engineering Principles. Rev Chem Engin, 12 (1-2): 1-205.

Wichmann R and Vasic-Racki D (2005) Cofactor Regeneration at the Lab Scale. Adv Biochem Engin/Biotechnol 92: 225-260.

Wittlich P and Vorlop K-D (1998) New Processing Methods for Bioconversions: Immobilized Biocatalysts. CTVO-Net Workshop: New Applications for Vegetable Oils, Copenhagen, Denmark.

Wolberg M, Hummel W, Wandrey C, Mueller M (2000) Highly Regio- and Enantioselective Reduction of 3,5-Dioxocarboxylates. Angew Chem Int Ed Engl 39: 4306-4308.

Wolberg M, Hummel W, Mueller M (2001) Biocatalytic Reduction of β,δ-Diketo Esters: A Highly Stereoselective Approach to All Four Stereoisomers of a Chlorinated β,δ-Dihydroxy Hexanoate. Chem Eur J 7:4562-4571.

Wolfson A, Vankelecom IFJ, Geresh S, Jacobs PA (2003) The Role of the Solvent in the Asymmetric Hydrogenation of β-Keto Esters with Ru-BINAP. J Mol Catal A: Chem 198: 39-45.

Wong CH, Drueckhammer DG, Sweers HM (1985) Enzymatic vs Fermentative Synthesis: Thermostable Glucose Dehydrogenase Catalyzed Regeneration of NAD(P)H for Use in Enzymatic Synthesis. J Am Chem Soc 107: 4028-4031.

Wong C-H and Bradshaw CW (1994) *Lactobacillus kefir* Alcohol Dehydrogenase. US 005342767.

Yamada H and Shimizu S (1988) Microbial and Enzymatic Processes for the Production of Biologically and Chemically Useful Compounds. Angew Chem Int Ed Engl 27: 622-642.

Yamamoto H, Matsuyama A, Kobayashi Y (2002) Synthesis of Ethyl (*R*)-4-Chloro-3-hydroxybutanoate with Recombinant *Escherichia coli* Cells Expressing (*S*)-Specific Secondary Alcohol Dehydrogenase. Biosci Biotechnol Biochem 66(2): 481-483.

Yang Y, Kayser MM, Rochon FD, Rodríguez S. Stewart JD (2005) Assessing Substrate Acceptance and Enantioselectivity of Yeast Reductases in Reactions with Substituted α-Keto-β-lactams. J Mol Catal B: Enzym 32: 167-174.

Zemlin C (2004) Untersuchung zur Enzymatischen Reduktion eines β-Ketoesters. Diplom Thesis, Fachhochschule Merseburg, Germany.

9 Materials and Methods

9.1 Materials

9.1.1 Laboratory equipment

Agilent Technologies GmbH, Waldbronn, Germany	ChemStation software A.09.01 GC system 6890
Beckmann-Coulter GmbH, Krefeld, Germany	Centrifuge Avanti™ J-20 XP Polypropylene centrifuge bottles
Becton-Dickinson, New Jersey, United States of America	Hypodermic needles Plastipak disposable syringe (50 mL)
BEST, Bornheim, Germany	Swagelok connectors
Biorad, Munich, Germany	HPLC column: Aminex HPX-87H
BIO-TEC Instruments GmbH, Bad Friedrichshall, Germany	PowerWave microplate reader
Brand GmbH + Co. KG, Wertheim, Germany	PMMA semi-micro cuvettes (1.5 mL)
Branson Ultrasonics Corporation, United States of America	Sonification Branson W-250
Buechi Labortechnik, Konstanz, Germany	Rotary evaporator R-111 Vacuum pump Vac V-513 Water bath B-191
Chrompack, EA Middelburg, the Netherlands	GC column: CP-Chirasil-Dex CB (25 m × 0.32 mm ID)
CTC Analytics AG, Zwingen, Switzerland	Cycle Composer software 1.5.2 GC Autosampler CombiPAL
Deutsche Metrohm GmbH + Co., Filderstadt, Germany	Dosimat 665 Impulsomat 614 pH meter 632
Eppendorf, Hamburg, Germany	Eppendorfs Centrifuge 5415D ThermoStat plus
Fedegari Auroclavi Spa, Italy	Autoclave 4507 E
Forschungszentrum Juelich GmbH, Juelich, Germany:	
Central Division of Analytical Chemistry (ZCH)	Varian Inova NMR (400 MHz)
Glass Workshop	Chromatography columns Jacketed glass reactors (30 – 500 mL)
Mechanical Workshop	Stacking racks Stainless steel enzyme membrane reactor (10 mL)
GeniaLab BioTechnologie – Produkte und Dienstleistungen GmbH, Braunschweig, Germany	LentiKats® Printer

GFL	Fermentation Shaker GFL 3033
Greiner Bio-One GmbH, Solingen, Germany	Polypropylene centrifuge tubes Petridishes
Haake, Karlsruhe, Germany	Water bath
Hellma, Muelheim, Germany	Quartz cuvettes
IKA Labortechnik, Staufen, Germany	Magnetic stirrers and heating plates
ISMATEC Laboratoriumstechnik GmbH, Wertheim-Mondfeld, Germany	Multichannel peristaltic REGLO Analog MS-4/6 pumps
JASCO, Gross-Umstadt, Germany	Borwin software 1.50 HPLC system: Autosampler AS 1550 Degasser DG 1580-53 Detector DAD MD 1510 Mixer LG 1580-62 Pump PU 1580
Macherey-Nagel GmbH + Co. KG, Dueren, Germany	ChromFil cellulose acetate acrodisc filter (0.2 µm) GC columns: Permabond Carbowax 20 M (50 m × 0.32 mm ID) Lipodex E (25 m × 0.25 mm ID)
Mettler Toledo, Giessen, Germany	pH electrodes: 405-DPAS-SC-K8S/150 InLab® 423
Millipore GmbH, Schwalbach, Germany	Ultrafiltration cell 8010 Ultrafiltration membrane YM10 (10 kD)
Pall GmbH, Dreieich, Germany	Bacterial air vent (0.2 µm) Stainless steel tangential-flow filter holder Ultrafiltration cassette (300 kD)
Pharmacia LKB, Freiburg, Germany	Double-cylinder dosing pump P500 Fraction collectors SuperFrac-100 and 2070 Ultrorac® II Peristaltic pump P100
Polymer Laboratories, Darmstadt, Germany	Evaporative light scattering detector PL-ELS 1000
Reichelt Chemie Technik, Heidelberg, Germany	Thomafluid heat-exchanger EPDM tubings Thomafluid precision microdosing pumps
Retsch	Retsch glass milling apparatus MM2000
Sartorius AG, Goettingen, Germany	Weighing balances
Scientific Industries, Inc., Bohemia, United States of America	Vortex Genie 2
Schott AG, Mainz, Germany	Fermentation shakeflasks
Shimadzu Europa GmbH, Duisburg, Germany	Spectrophotometer UV-1601
Sigma-Aldrich Chemie GmbH, Taufkirchen, Germany	Atmos®Bag™ Suba seal red rubber septa
SIM-Aminco Spectroscopic Instruments, Illinois, United States of America	French press

Watson-Marlow GmbH, Rommerskirchen, Germany	Peristaltic pumps 101U/R, 504U Pump tubings
University of Erlangen-Nuremberg, Institute of Bioprocess Engineering, Erlangen, Germany	Encapsulation equipment
VWR International GmbH, Langenfeld, Germany	Cryogenic vials Peristaltic pump tubings Tubing connectors

9.1.2 Chemicals and biological materials

Aldrich, Taufkirchen, Germany	Ammonium citrate dibasic Poly(diallyl-dimethylammonium chloride) of low molecular weight (100000 – 200000) Trifluoroacetic acid anhydride
Bitop AG, Witten, Germany	*Lactobacillus kefiri* DSM 20587
Calbiochem, Bad Soden, Germany	Bovine serum albumin
Carl Roth GmbH + Co., Karlsruhe, Germany	Carbenicillin (sodium salt) Isopropyl-β-D-thiogalactopyranoside (IPTG) Kanamycin sulphate
CP Kelco, Lille Skensved, Denmark	κ-carrageenan (GENU®)
EuroFerm GmbH, Berlin, Germany	Sodium cellulose sulphate (NaCS, technical grade)
Fluka, Steinheim, Germany	(2,5)-Hexanedione (2*R*,5*R*)-Hexanediol Methyl acetoacetate (*R*)-Methyl-3-hydroxybutanoate (*S*)-Methyl-3-hydroxybutanoate Potassium dihydrogen phosphate Di-Potassium hydrogen phosphate Sodium acetate anhydrous Sodium alginate (71238) Sodium borohydride Sodium dihydrogen phosphate Sodium formate Sodium hydroxide Trifluoroacetic acid
Forschungszentrum Juelich GmbH, Institute of Biotechnology 1, Juelich, Germany	*Escherichia coli* DH5α *Escherichia coli* BL21 Star (DE 3) Formate dehydrogenase (FDH) plasmid from *Mycobacterium vaccae* Alcohol dehydrogenase (*Lb*ADH) plasmid from *Lactobacillus brevis*
GeniaLab BioTechnologie GmbH, Braunschweig, Germany	LentiKat® liquid and stabiliser
Invitrogen, Germany	S.O.C. medium

Juelich Fine Chemicals GmbH, Juelich, Germany	Alcohol dehydrogenase (*Lb*ADH) from *Lactobacillus brevis* Formate dehydrogenase (FDH) from *Pseudomonas* sp. (5*S*)-Hydroxyhexane-2-one (2*S*,5*S*)-Hexanediol $NAD(P)^+$ NAD(P)H
Merck KGaA, Darmstadt, Germany	Acetic acid Agar-agar Calcium chloride Casein peptone Chloroform Ethyl acetate Glucose Isopropanol Magnesium sulphate heptahydrate Manganese sulphate monohydrate Meat extract Potassium chloride Silica gel 60 (0.040 – 0.063 mm) Sodium chloride di-Sodium hydrogen phosphate dihydrate Tween 80 Yeast extract granulate
NovaMatrix, Brakerøya, Norway	Chitosan chloride (Protasan UP CL113)
Qiagen GmbH, Hilden, Germany	QIAprep spin miniprep kit
Sigma-Aldrich Chemie GmbH, Taufkirchen, Germany	Bradford reagent
University of Erlangen-Nuremberg, Institute of Bioprocess Engineering, Erlangen, Germany	Sodium cellulose sulphate (NaCS, medical grade)

9.2 Analytical methods

9.2.1 Gas chromatography

9.2.1.1 System involving γ-hydroxyketone production

Identification of (2,5)-hexanedione (**A**), (5*R*)-hydroxyhexane-2-one (**B**), (2*R*,5*R*)-hexanediol **(C)** and ethanol was performed with Agilent HP-6890 gas chromatograph with a Permabond Carbowax 20 M column (50 m × 0.32 mm ID, Macherey-Nagel, Dueren, Germany). The oven was heated at 70 °C for 6 min, with an increase of 25 °C min^{-1} till 160 °C, and kept constant at 160 °C for another 19 min. Hydrogen gas (1 bar) was used as a carrier gas with a flame ionisation detector. 50 mM *n*-

butanol was used in equivolume with the samples as an internal standard. The retention times as shown in Figure 9.1 were 2.9 min (ethanol), 7.0 min (*n*-butanol), 12.0 min (**A**), 13.7 min (**B**) and 18.8 min (**C**).

The compounds were quantified using area integration of the chromatogram peaks with the following equations (Eqs. 9.1 – 9.4).

$$C_A\,(mM) = 47.545 \times \frac{Area_A}{Area_{n-Butanol}} \qquad \text{(eq. 9.1)}$$

$$C_B\,(mM) = 61.165 \times \frac{Area_B}{Area_{n-Butanol}} \qquad \text{(eq. 9.2)}$$

$$C_C\,(mM) = 41.024 \times \frac{Area_C}{Area_{n-Butanol}} \qquad \text{(eq. 9.3)}$$

$$C_{Ethanol}\,(mM) = 125.58 \times \frac{Area_{Ethanol}}{Area_{n-Butanol}} \qquad \text{(eq. 9.4)}$$

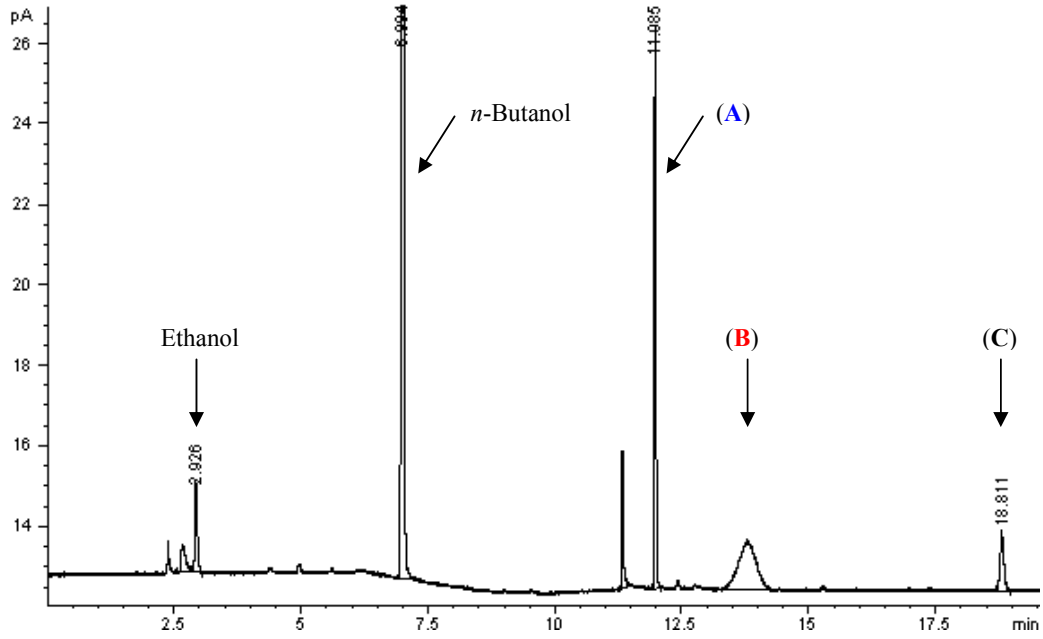

Figure 9.1. Gas chromatogram of ethanol (2.9 min), (2,5)-hexanedione (A) (12.0 min), (5*R*)-hydroxyhexane-2-one (B) (13.7 min) and (2*R*,5*R*)-hexanediol (C) (18.8 min) with *n*-butanol (7.0 min) as internal standard.

To determine the enantiopurity of (5*R*)-hydroxyhexane-2-one (**B**), derivatisation of the aqueous samples with trifluoroacetic acid anhydride (TFAA) was needed prior to analysis. 150 µL aqueous sample was extracted twice with equivolume of chloroform. The organic phase (300 µL) was separated and 300 µL of TFAA was added to it. It was incubated at 70 °C for 30 min, evaporated to dryness before dissolving with 300 µL chloroform.

The derivatised sample was injected into an Agilent HP-6890 gas chromatograph fitted with a CP-Chirasil-Dex CB column (25 m × 0.32 mm ID, Chrompack, EA Middelburg, the Netherlands). The oven was heated and kept constant at 55 °C for 15 min. Hydrogen gas (0.6 bar) was used as a carrier gas with a flame ionisation detector. The retention times of 5-hydroxyhexane-2-one were 9.9 min (*R*-isomer, **B**) and 10.3 min (*S*-isomer), (2,5)-hexanediol were 7.9 min (*S*,*S*-isomer) and 9.0 min (*R*,*R*-isomer, **C**) and (2,5)-hexanedione (**A**) was 11.6 min (Figure 9.2).

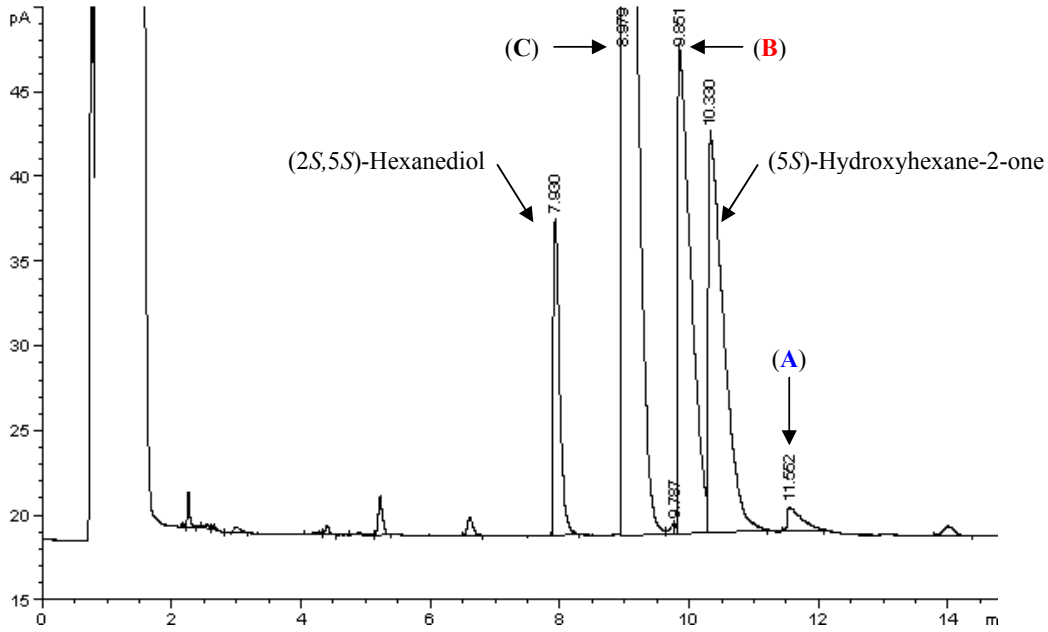

Figure 9.2. Gas chromatogram of (2,5)-hexanedione (A) (11.6 min), (5*R*)-hydroxyhexane-2-one (B) (9.9 min), (5*S*)-hydroxyhexane-2-one (10.3 min), (2*R*,5*R*)-hexanediol (C) (9.0 min) and (2*S*,5*S*)-hexanediol (7.9 min).

9.2.1.2 System involving 3-hydroxybutanoate production

Identification of methyl acetoacetate (**MAA**) and (*R*)-methyl-3-hydroxybutanoate (**MHB**) was performed with Agilent HP-6890 gas chromatograph with a Permabond Carbowax 20 M column (50 m × 0.32 mm ID, Macherey-Nagel, Dueren, Germany). The oven was heated at 70 °C for 6 min, with an increase of 25 °C min^{-1} till 160 °C, and kept constant at 160 °C for another 3 min. Hydrogen gas (1.0 bar) was used as a carrier gas with a flame ionisation detector. 50 mM *n*-butanol was used in equivolume with the samples as an internal standard. The retention times as shown in Figure 9.3 were 6.9 min (*n*-butanol), 10.6 min (**MAA**) and 11.5 min (**MHB**).

The compounds were quantified using area integration of the chromatogram peaks with the following equations (Eqs. 9.5 and 9.6).

$$C_{MAA}\,(mM) = 144.9 \times \frac{Area_{MAA}}{Area_{n-Butanol}} \qquad \text{(eq. 9.5)}$$

$$C_{MHB}\,(mM) = 57.14 \times \frac{Area_{MHB}}{Area_{n-Butanol}} \qquad \text{(eq. 9.6)}$$

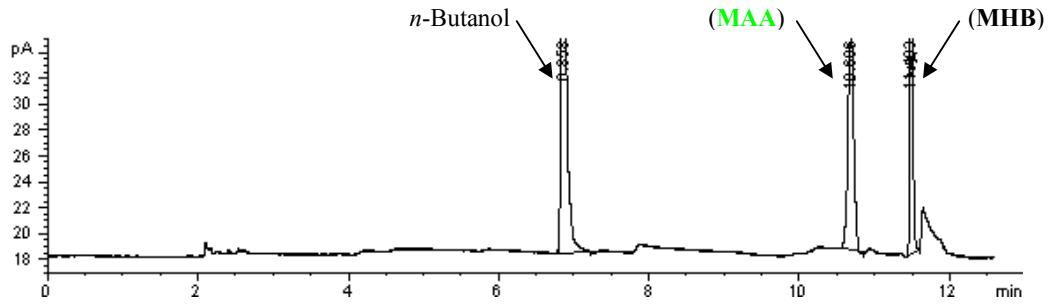

Figure 9.3. Gas chromatogram of methyl acetoacetate (MAA) (10.6 min) and (*R*)-methyl-3-hydroxybutanoate (MHB) (11.5 min) with *n*-butanol (6.9 min) as internal standard.

For the enzyme-coupled system, the samples (100 µL) were extracted with 200 µL ethyl acetate (containing 50 mM *n*-butanol) prior to GC analysis. The factors in Eqs. 9.5 and 9.6 were replaced by the values of 243.85 and 138.83 for methyl acetoacetate (**MAA**) and (*R*)-methyl-3-hydroxybutanoate (**MHB**) respectively.

The enantiopurity of (*R*)-methyl-3-hydroxybutanoate (**MHB**) was determined (without prior derivatisation) with an Agilent HP-6890 gas chromatograph fitted with a Lipodex E column (25 m × 0.25 mm ID, Macherey-Nagel, Dueren, Germany). The oven was heated and kept constant at 75 °C for 25 min. Hydrogen gas (0.6 bar) was used as a carrier gas with a flame ionisation detector. The retention times of methyl-3-hydroxybutanoate were 8.6 min (*S*-isomer) and 10.8 min (*R*- isomer, **MHB**) and methyl acetoacetate (**MAA**) was 17.5 min (Figure 9.4).

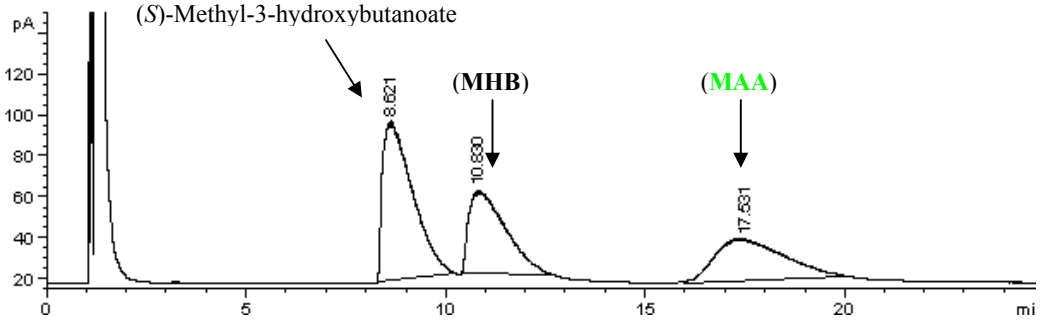

Figure 9.4. Gas chromatogram of methyl acetoacetate (MAA) (17.5 min), (*R*)-methyl-3-hydroxybutanoate (MHB) (10.8 min) and (*S*)-methyl-3-hydroxybutanoate (8.6 min).

9.2.2 High pressure liquid chromatography

Identification of cosubstrates (glucose and formate) and metabolites (lactate and acetate) was performed with JASCO high pressure liquid chromatograph (HPLC) fitted with an Aminex HPX-87H column (30 m × 7.5 mm ID, Biorad, Munich, Germany). The column was heated constantly at 65 °C for 30 min. Trifluoroacetic acid (0.5 % by volume) was used as solvent and the chemicals (formate, lactate and acetate) were detected with a diode array detector (λ = 220 nm). Glucose was detected with an evaporative light scattering detector PL-ELS 1000 (Polymer Laboratories, Darmstadt, Germany) connected to the HPLC. Nitrogen (0.7 L min^{-1}, 5 bar) was used as a carrier gas and the temperature of the nebuliser and evaporator were fixed at 90 and 120 °C respectively. 20 µL of sampling volume was used and the retention times were 10.8 min (glucose), 14.9 min (lactate), 16.1 min (formate) and 17.4 min (acetate) (Figures 9.5 - 9.7).

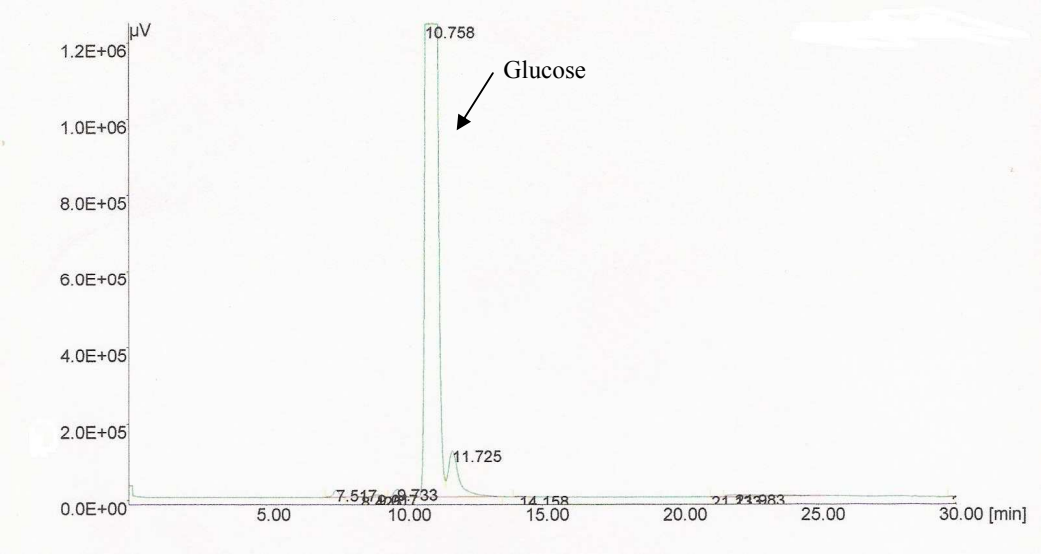

Figure 9.5. High pressure liquid chromatogram of glucose (10.8 min) detected with an evaporative light scattering detector.

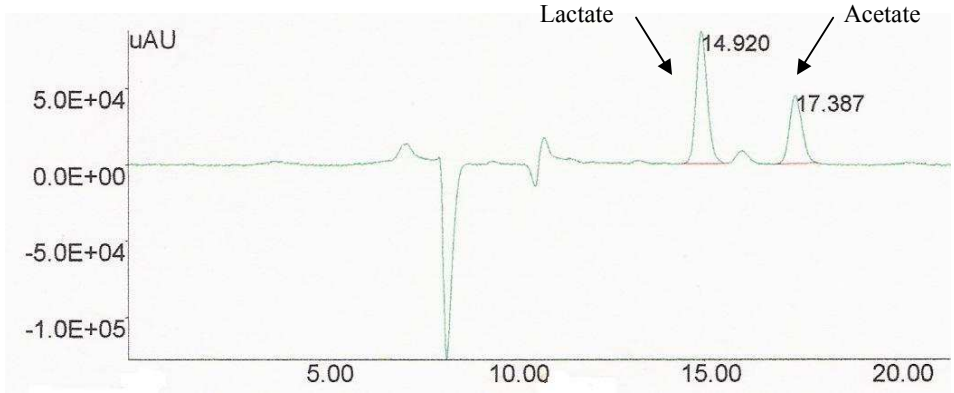

Figure 9.6. High pressure liquid chromatogram of lactate (14.9 min) and acetate (17.4 min) detected with a diode array detector.

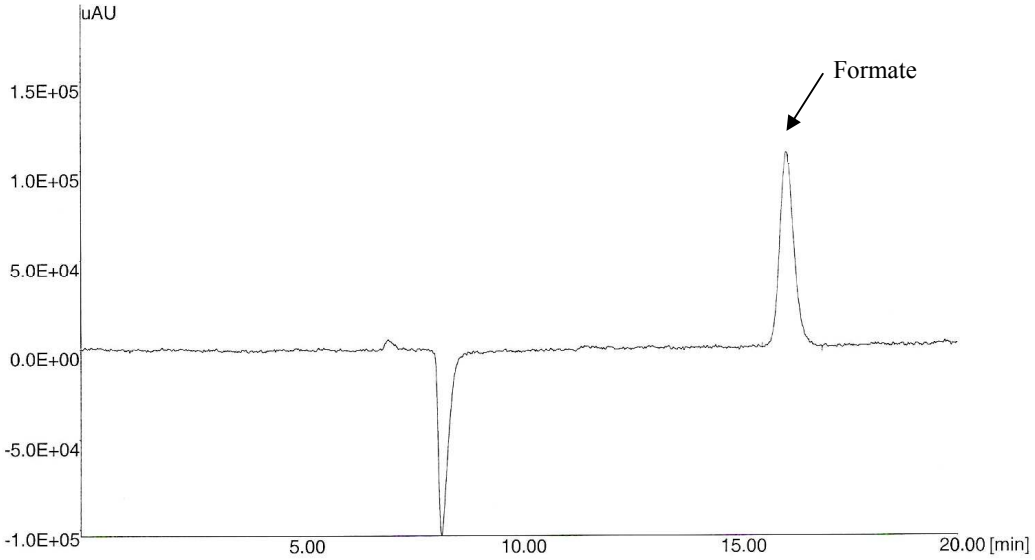

Figure 9.7. High pressure liquid chromatogram of formate (16.1 min) detected with a diode array detector.

The compounds were quantified using area integration with the following equations (Eqs. 9.7 – 9.10).

$$C_{Glucose}\,(mM) = \frac{Area_{Gluocse}}{369250} \qquad \text{(eq. 9.7)}$$

$$C_{Lactate}\,(mM) = \frac{Area_{Lactate}}{81341} \qquad \text{(eq. 9.8)}$$

$$C_{Acetate}\,(mM) = \frac{Area_{Acetate}}{35083} \qquad \text{(eq. 9.9)}$$

$$C_{Formate}\,(mM) = \frac{Area_{Formate}}{46588} \qquad \text{(eq. 9.10)}$$

9.2.3 Nuclear magnetic resonance

The purity of (5*R*)-hydroxyhexane-2-one (**B**) was investigated with nuclear magnetic resonance (NMR) at the Central Division of Analytical Chemistry (ZCH) at Forschungszentrum Juelich GmbH, Juelich, Germany. Using a Varian Inova NMR of 400 MHz and 2D measurement with $CDCl_3$ as solvent, the below spectra were obtained at 25 °C (Figures 9.8 and 9.9).

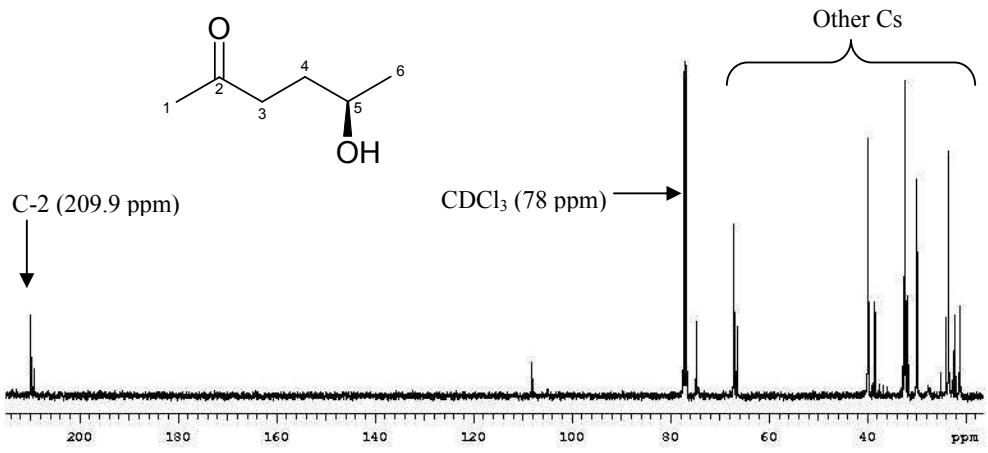

Figure 9.8. Full spectrum of nuclear magnetic resonance analysis of (5*R*)-hydroxyhexane-2-one (B).

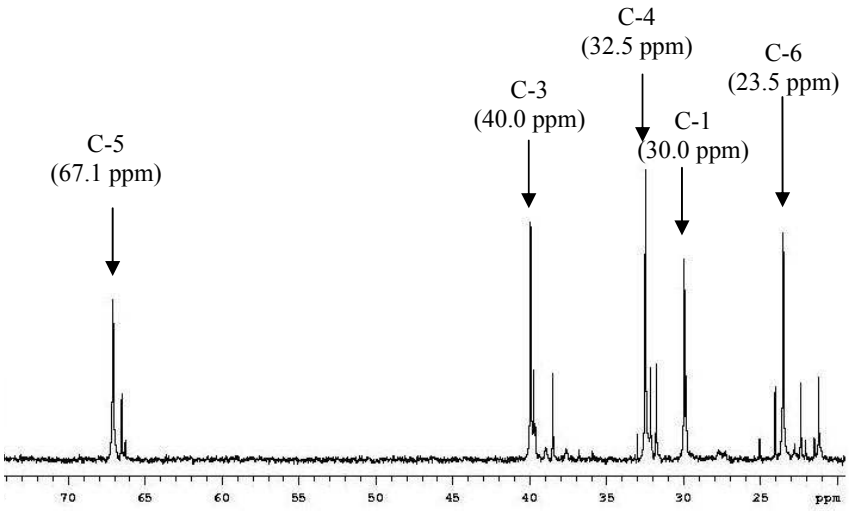

Figure 9.9. Zoomed spectrum (20 – 70 ppm) of nuclear magnetic resonance analysis of (5*R*)-hydroxyhexane-2-one (B).

9.2.4 Bradford assay

Protein content determination using Bradford assay was performed for isolated enzymes *Lactobacillus brevis* alcohol dehydrogenase (*L*bADH) and formate dehydrogenase from *Pseudomonas* sp. (FDH). A calibration curve with bovine serum albumin was used as a standard for protein content. The samples were analysed in a 96-well plate by a microplate reader (BIO-TEC Instruments GmbH, Bad Friedrichshall, Germany) at wavelength of 595 nm at room temperature for 1 min.

9.3 Biotransformations methods

9.3.1 Genetic work

Recombinant plasmids encoding *Lactobacillus brevis* alcohol dehydrogenase (*Lb*ADH) and formate dehydrogenase from *Mycobacterium vaccae* (FDH) were performed by the group of Dr. S. Bringer-Meyer (Institute of Biotechnology 1, Forschungszentrum Juelich GmbH, Juelich, Germany). The low copy plasmids, pBtacLB-ADH (800 bp, 26.7 kDa, carbenicillin resistance) and pBBR1MCS2*fdh* (1200 bp, 44 kDa, kanamycin resistance) were amplified separately in *Escherichia coli* DH5α (Ernst, 2003). Figure 9.10 summarises the genetic work performed.

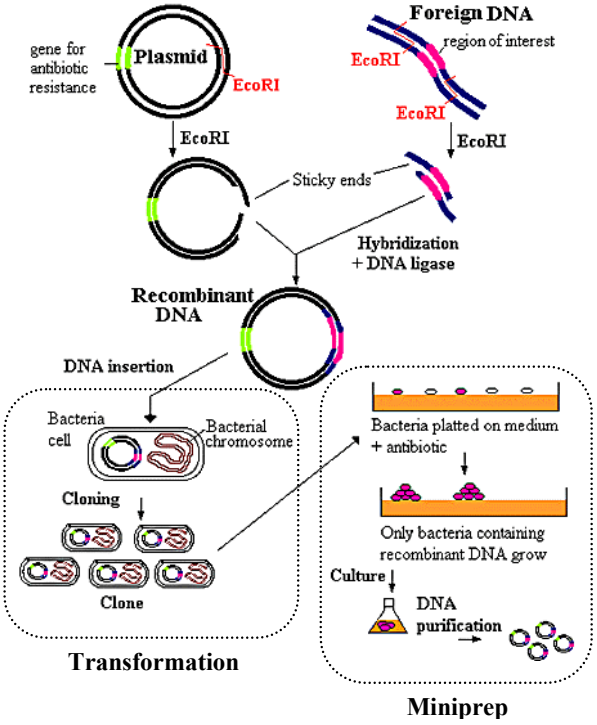

Figure 9.10. Summary of genetic work on *Escherichia coli* (www.accessexcellence.org).

9.3.1.1 Plasmids amplification

Plasmids (1 µL from stock) were individually introduced into a suspension of *E. coli* DH5α (50 µL) in a 1 mL Eppendorf under the following steps (Figure 9.11):

- Uptake of plasmids: Incubation at 4 °C for 20 min,
- Inactivation of nucleases: Heating at 42 °C for 90 s,
- Further uptake of plasmids: Incubation at 4 °C for 5 min,

- Repair of cell membrane: Addition of 400 µL S.O.C. medium with light shaking at 37 °C for 35 min,
- Transformed cells stock: Streak 25 µL of cell suspension on agar plate (with corresponding antibiotics) and incubate at 37 °C overnight.

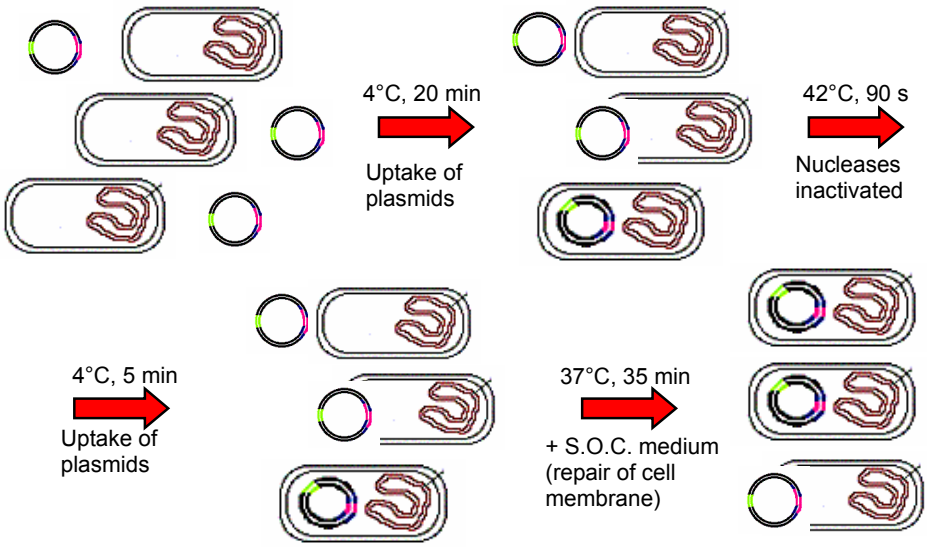

Figure 9.11. Amplification of plasmids.

9.3.1.2 Plasmids purification

Miniprep was done in accordance to the methods given in the QIAprep spin miniprep kit (Qiagen GmbH, Hilden, Germany). Thereby, *Lb*ADH and FDH plasmids of high purity were obtained. The plasmids were stored at -20 °C prior to use.

9.3.1.3 Transformation of two plasmids

*Lb*ADH plasmids (2 µL from stock) were introduced into a suspension of *E. coli* BL21 Star (DE3) (100 µL) in a 1 mL Eppendorf. A stock of transformed cells containing *Lb*ADH plasmids was made according to the protocol in Chapter 9.3.1.1.

In order to make competent cells containing *Lb*ADH plasmids, the following steps were performed:

- Selection of separate cell colonies from agar plate to shakeflasks (each containing 10 mL LB medium),
- Fermentation: Incubate shakeflasks at 30 °C overnight,
- Add 1 mL of cell suspension to 100 mL LB medium, 2 mL $MgSO_4$ solution (1 M), 1 mL $CaCl_2$ solution (1 M) and 1 mL KCl solution (1 M),

- Incubate shakeflasks at 30 °C for a further 3 h,
- At O.D. 0.3 – 0.5, centrifuge cell suspension at 4 °C for 10 min at 3000 rpm,
- Resuspend cell pellet with 15 mL TFB 1 solution, thereafter stand in ice for 20 min,
- Centrifuge cell suspension at 4 °C for 15 min at 3000 rpm,
- Resuspend cell pellet with 2 mL TFB 2 solution.

The introduction of FDH plasmids into *E. coli* BL21 Star (DE3) containing *Lb*ADH plasmids were performed similar to the procedure in Chapter 9.3.1.1. The transformed cells were stored at -80 °C prior to use.

9.3.2 Fermentation

Fermentation of *Lactobacillus kefiri* DSM 20587 was done on a 2800 L-scale by bitop AG (Witten, Germany), according to MRS medium (Table 9.1). The cells were stored at -20 °C.

Table 9.1. MRS medium composition for fermentation of *Lactobacillus kefiri* DSM 20587.

Medium composition	Concentration (g L^{-1})
Glucose·H_2O	22
Casein peptone	10
Meat extract	10
Yeast extract	5
Sodium acetate	5
K_2HPO_4	2
Ammonium citrate	2
Tween 80	1
$MgSO_4 \cdot 7H_2O$	0.2
$MnSO_4 \cdot H_2O$	0.05

Fermentation of *Escherichia coli* BL21 Star (DE3) was carried out with standard LB medium, with carbenicillin and kanamycin added to select cells containing the ADH and FDH plasmids respectively (Table 9.2). The fermentation and induction protocol is summarised in Figure 9.12.

Table 9.2. Luria-Bertani (LB) medium composition for fermentation of *Escherichia coli* BL21 Star (DE3).

Medium composition	Concentration (g L^{-1})
Glucose·H_2O	4
Casein peptone	10
Yeast extract	5
NaCl	10
Carbenicillin	0.05
Kanamycin	0.05

Cell colonies from an agar plate were selected and a large pool of feedstock containing cells with similar activities was stored in 50 % v/v glycerol at –80 °C. Fermentation was proceeded in a 1 L shakeflask (containing 200 mL LB medium) at 37 °C for 4 h, followed by a cooling step to 30 °C for another 2 h. The cells reached the early exponential phase of growth (around O.D. 1.2) and induction with isopropyl-β-D-thiogalactopyranoside (IPTG) to a final concentration of 0.7 mM was initiated for a period of 7 h at 27 °C. The cells were then harvested by centrifugation, washed twice with 50 mM potassium phosphate buffer (pH 6), and stored in 50 mM potassium phosphate buffer (pH 6) at 4 °C.

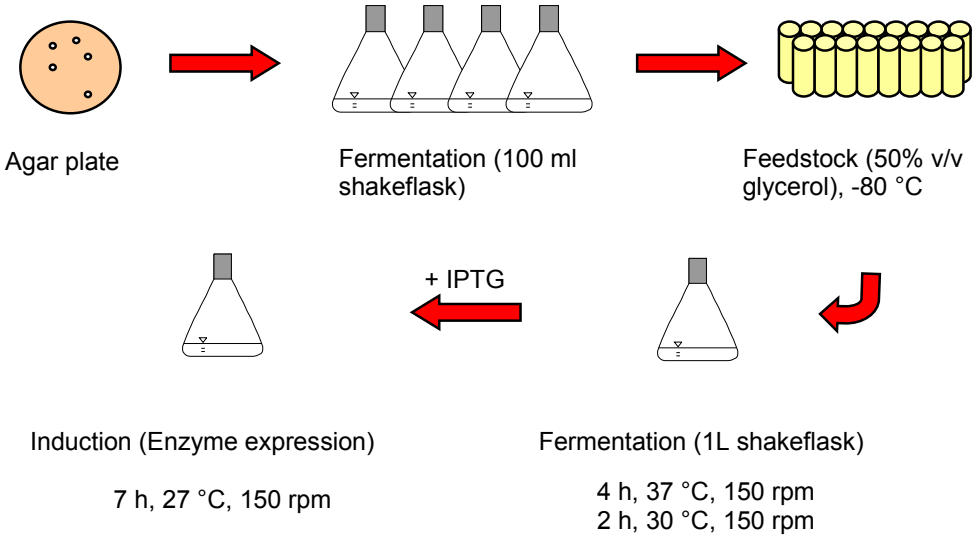

Figure 9.12. Summary of fermentation and induction protocol for rec. *E. coli*.

9.3.3 Whole cell immobilisation

9.3.3.1 Treatment of cells

Prior to immobilisation of *Lactobacillus kefiri*, cleaning of the cells was performed. The frozen cells were thawed, resuspended in 50 mM phosphate buffer (pH 6) and centrifuged at 5000 rpm for 15 min at 4 °C. The supernatant was discarded and the cell pellet was washed once more with 50 mM phosphate buffer and centrifuged. For cell immobilisation, the cell pellet was further suspended in 50 mM phosphate buffer (containing 2 mM Mg^{2+} and 0.7 mM Mn^{2+} salts) and added as a cell slurry (200 % w_{wcw}/v) into the immobilisation matrices. One exception is the cell immobilisation with κ-carrageenan which also involved the suspension of the cell pellet in 0.9 % w/v NaCl (0.15 M) solution instead of Mg^{2+}/Mn^{2+}-containing phosphate buffer. All cell immobilisation techniques were performed with 10 % wet biomass loading of *L. kefiri*.

9.3.3.2 Immobilisation equipment

Polyvinyl alcohol immobilisates (LentiKats®) were made with a LentiKats® Printer (GeniaLab BioTechnologie GmbH, Braunschweig, Germany) while the other immobilisates were made with an encapsulation apparatus loaned from the Institute of Bioprocess Engineering, University of Erlangen, Erlangen-Nuremberg, Germany.

9.3.3.3 Polyvinyl alcohol matrix

Polyvinyl alcohol polymer (10 % w/v) was heated up to 95 °C until a colourless gel was obtained. The melt was then cooled to 40 °C and the cell slurry was introduced to the matrix with stirring until well mixed. Polyvinyl alcohol immobilisates (LentiKats®) were made with a LentiKats® Printer, dried (up to 72 % w/w) in argon atmosphere and rehydrated in a stabiliser solution in accordance to the instructions from GeniaLab GmbH (www.geniaLab.de/download/tt-english.pdf). The LentiKats® were then washed with distilled water and 50 mM phosphate buffer, pH 6, before storing at 4 °C in 50 mM phosphate buffer, pH 6.

9.3.3.4 Alginate matrices

Sodium alginate powder was dissolved in distilled water to form an alginate concentration of 2 % w/v. It was then heated to 70 °C and stirred for 2 h until total dissolution of the alginate, giving a light brown clear liquid. The alginate liquid was cooled to 30 °C with stirring before the cell slurry was introduced. The alginate liquid (containing cells) were passed through the encapsulation apparatus and

extruded into a solution of NaCl (0.2 M) and $CaCl_2$ (0.05 M) with stirring. The alginate beads (2 – 3 mm diameter) remained in the stirred NaCl/$CaCl_2$ solution for 45 min to harden. The alginate beads were then stored in the NaCl/$CaCl_2$ solution at 4 °C.

To prepare alginate-chitosan immobilisates, additional steps were required. Chitosan chloride solution (0.3 g L^{-1}) was made by dissolving chitosan chloride in 0.02 M sodium acetate/acetic acid buffer (pH 5) containing 0.3 M $CaCl_2$. The alginate beads were first formed and hardened as described above before adding the beads to the chitosan chloride solution. The chitosan-coated alginate beads (2 – 3 mm diameter) remained stirred in the chitosan chloride solution for 2 h, then washed with 0.02 M sodium acetate/acetic acid buffer, pH 5, before storing in NaCl/$CaCl_2$ solution (as above) at 4 °C.

9.3.3.5 κ-Carrageenan matrices

κ-Carrageenan granules were partially dissolved in distilled water at 70 °C for 1 h to form a carrageenan concentration of 2 % w/v. It was then further heated to 90 °C and stirred for 15 min until total dissolution of the carrageenan, giving a light brown clear liquid. The carrageenan liquid was cooled to 45 °C with stirring before the cell slurry was introduced. Two types of cell slurries were used, one consisting of Mg^{2+}/Mn^{2+}-containing phosphate buffer (2 mM Mg^{2+}, 0.7 mM Mn^{2+}, 50 mM phosphate buffer, pH 6) and the other consisting of 0.9 % w/v NaCl (0.15 M). The carrageenan liquid (containing cells) were passed through the encapsulation apparatus and extruded into a solution of KCl (0.3 M) with stirring. The carrageenan strands (2 mm thickness) remained in the stirred KCl solution for 2 h to harden. The carrageenan strands were then washed with and stored in 50 mM phosphate buffer (pH 6) at 4 °C.

9.3.3.6 Sodium cellulose sulphate matrix (NaCS)

Sodium cellulose sulphate (NaCS) strands were dissolved in 0.9 % w/v NaCl solution (0.15 M) overnight with stirring, forming a clear colourless liquid of 2.5 % w/v NaCS concentration. Poly(diallyl-dimethylammonium chloride) solution (PDADMAC) containing 2.2 % v/v PDADMAC and 0.9 % w/v NaCl (0.15 M) was used as hardening bath. The cell slurry was introduced into the NaCS liquid, passed through the encapsulation apparatus and extruded into a stirred solution of PDADMAC (2.2 % v/v). The NaCS beads (2 – 3 mm diameter) remained in the stirred PDADMAC solution for 15 min to harden. They were then washed with 0.9 % w/v NaCl solution (0.15 M) thrice before storage in 50 mM phosphate buffer (pH 6) at 4 °C.

9.3.4 Reaction techniques for *Lactobacillus kefiri*

9.3.4.1 Batch runs

All batch reactions were performed at 30 °C with 10 % w/v biocatalyst (equivalent to 10 % w/v wet cells in non-immobilised and 1 % w/v wet cells in immobilised batches respectively). The biocatalyst was suspended with the stock solution and incubated in the reactor for 30 min. Flushing of the reactor with argon or helium was carried out to remove excess traces of oxygen. The batch reaction was started by the addition of 50 mM (2,5)-hexanedione (**A**), and the pH was controlled by an autotitrator (Dosimat 665, Metrohm, Herisau, Switzerland) dispensing 4 M NaOH. Samples (500 µL) were withdrawn and centrifuged at 13200 rpm, 1 min. The cell pellets (for non-immobilised cells) were discarded and the supernatants were analysed.

Stock solution:

50 mM Potassium phosphate buffer (pH 6)		50 mL
containing:	2 mM $MgSO_4$	
	0.7 mM $MnSO_4$	
	400 mM Glucose	

9.3.4.2 Repetitive batch runs

Repetitive batch runs were performed similar to batch runs, with centrifugation (non-immobilised cells) and filtration (immobilised cells) steps in between of batches to separate the biocatalyst from the reaction solution.

9.3.4.3 Plug flow reactor (PFR)

The plug flow reactor (PFR) was constructed from the barrel of a 50 mL Plastipak disposable syringe (Becton-Dickinson, New Jersey, United States of America). At the base of the barrel lined a cellulose acetate filter paper (0.45 µm) as packing tray. NaCS immobilisates (technical grade) were tightly packed into the barrel before placing a similar cellulose acetate filter paper (0.45 µm) on the top of the packed bed as liquid distributor. Attached to the Luer-lock tip of the syringe is an acrodisc filter (0.2 µm), while the mouth of the barrel with stoppered with a suba seal septum (Sigma-Aldrich Chemie GmbH, Taufkirchen, Germany). A hypodermic needle (0.9 mm) was pierced through the septum as vent, with its tip in the headspace of the syringe barrel and not in contact with the liquid distributor and NaCS immobilisates.

A PFR cascade was set up with pH control (4 M NaOH) in a small reservoir (1 mL) in between of the columns. Different flow rates of feed were applied in a one-pass operating mode (without recycle) through the PFR cascade at 31 °C. The pH values

of the output from the PFR were measured sporadically during long residence times (or low flow rates), thereby keeping a minimum pH value of 5 with a maximum allowable operating residence time of 3.3 h.

Feed:

50 mM Potassium phosphate buffer (pH 7)	1 L
containing: 2 mM $MgSO_4$	
0.7 mM $MnSO_4$	
50 mM (2,5)-Hexanedione (**A**)	
400 mM Glucose	

9.3.5 Reaction techniques for enzymes

9.3.5.1 Activity assay (pH)

Determination of activity of *Lb*ADH was performed in a 1.5 mL cuvette (Brand GmbH, Wertheim, Germany) and measured spectrophotometrically (λ = 340 nm) at 20 °C for 60 s. The reaction was started by the addition of *Lb*ADH to the reaction mixture.

50 mM Potassium phosphate buffer	970 µL
containing: 2 mM $MgSO_4$	
40 mM Methyl acetoacetate (**MAA**)	
10 mM NADPH	20 µL
*Lb*ADH	10 µL
(12.6 mg L^{-1} in cuvette)	

Determination of activity of FDH was performed at 20 °C in a similar manner as above. The reaction was started by the addition of FDH to the reaction mixture.

50 mM Potassium phosphate buffer	970 µL
containing: 240 mM Sodium formate	
10 mM $NADP^+$	20 µL
FDH	10 µL
(5.6 mg L^{-1} in cuvette)	

9.3.5.2 Activity assay (temperature)

Determination of activity of *Lb*ADH was performed in a 1.5 mL cuvette (Brand GmbH, Wertheim, Germany) and measured spectrophotometrically (λ = 340 nm) for 60 s. The reaction was started by the addition of *Lb*ADH to the reaction mixture.

50 mM Potassium phosphate buffer (pH 6)	970 µL
containing: 2 mM $MgSO_4$	
40 mM Methyl acetoacetate (**MAA**)	
10 mM NADPH	20 µL
*Lb*ADH	10 µL
(12.6 mg L^{-1} in cuvette)	

Determination of activity of FDH was performed in a similar manner as above. The reaction was started by the addition of FDH to the reaction mixture.

50 mM Potassium phosphate buffer (pH 6)	970 µL
containing: 240 mM Sodium formate	
10 mM $NADP^+$	20 µL
FDH	10 µL
(5.6 mg L^{-1} in cuvette)	

9.3.5.3 Stability of isolated enzymes

Determination of activity of *Lb*ADH over time was performed in a 1.5 mL cuvette (Brand GmbH, Wertheim, Germany) and measured spectrophotometrically (λ = 340 nm) for 60 s. The reaction was started by the addition of *Lb*ADH to the reaction mixture.

In the absence of Mg^{2+} salts, the reaction mixture was:

50 mM Potassium phosphate buffer (pH 6)	970 µL
containing: 11 mM Methyl acetoacetate (**MAA**)	
10 mM NADPH	20 µL
*Lb*ADH	10 µL
(6.7 mg L^{-1} in cuvette)	

In the presence of Mg^{2+} salts, the reaction mixture was:

50 mM Potassium phosphate buffer (pH 6)	970 µL
containing: 2 mM $MgSO_4$	
40 mM Methyl acetoacetate (**MAA**)	
10 mM NADPH	20 µL
*Lb*ADH	10 µL
(3.3 mg L^{-1} in cuvette)	

Determination of activity of FDH over time was performed in a similar manner as above. The reaction was started by the addition of FDH to the reaction mixture.

In the absence of Mg^{2+} salts, the reaction mixture was:

50 mM Potassium phosphate buffer (pH 6)	970 µL
containing: 240 mM Sodium formate	
10 mM $NADP^+$	20 µL
FDH	10 µL
(5.6 mg L^{-1} in cuvette)	

In the presence of Mg^{2+} salts, the reaction mixture was:

50 mM Potassium phosphate buffer (pH 6)	970 µL
containing: 2 mM $MgSO_4$	
200 mM Sodium formate	
10 mM $NADP^+$	20 µL
FDH	10 µL
(5.6 mg L^{-1} in cuvette)	

9.3.5.4 Stability of cofactors

Determination of stability of $NADP^+$ over time was performed in a 1.5 mL cuvette (Brand GmbH, Wertheim, Germany) and the extinction values were measured spectrophotometrically (λ = 340 nm). The initial extinction value was measured with the addition of FDH to the reaction mixture.

50 mM Potassium phosphate buffer (pH 6)	970 µL
containing: 240 mM Sodium formate	
10 mM $NADP^+$	20 µL
FDH	10 µL
(5.6 mg L^{-1} in cuvette)	

The final extinction value was obtained when there was no longer a change in the extinction value. The difference between the final and initial extinction values correlated to the concentration of active $NADP^+$ present in the reaction mixture.

Determination of stability of NADPH over time was performed in a similar manner as above. The initial extinction value was measured with the addition of ADH to the reaction mixture.

50 mM Potassium phosphate buffer (pH 6)	970 µL
containing: 11 mM Methyl acetoacetate (**MAA**)	
10 mM NADPH	20 µL
*Lb*ADH	10 µL
(6.7 mg L^{-1} in cuvette)	

The final extinction value was obtained when there was no longer a change in the extinction value. The difference between the initial and final extinction values correlated to the concentration of active NADPH present in the reaction mixture.

9.3.5.5 Batch kinetics of isolated enzymes

Determination of batch kinetics of *Lb*ADH was performed in a 1.5 mL cuvette (Brand GmbH, Wertheim, Germany) and measured spectrophotometrically (λ = 340 nm) at 20 °C for 60 s. The reaction was started by the addition of *Lb*ADH to the reaction mixture.

For the NADH-bounded *Lb*ADH, the reaction mixture was:

50 mM Potassium phosphate buffer (pH 6)		970 µL
containing:	2 mM $MgSO_4$	
	Methyl acetoacetate (**MAA**)	
	((*R*)-methyl-3-hydroxybutanoate (**MHB**))	
	(NAD^+)	
80 mM NADH		20 µL
*Lb*ADH		10 µL
(0.126 mg L^{-1} in cuvette)		

For the NADPH-bounded *Lb*ADH, the reaction mixture was:

50 mM Potassium phosphate buffer (pH 6)		970 µL
containing:	2 mM $MgSO_4$	
	Methyl acetoacetate (**MAA**)	
	((*R*)-methyl-3-hydroxybutanoate (**MHB**))	
	(NAD^+)	
10 mM NADPH		20 µL
*Lb*ADH		10 µL
(0.126 mg L^{-1} in cuvette)		

Determination of batch kinetics of FDH was performed in a similar manner as above. The reaction was started by the addition of FDH to the reaction mixture.

50 mM Potassium phosphate buffer (pH 6)		970 µL
containing:	Sodium formate	
	(NADPH)	
10 mM $NADP^+$		20 µL
FDH		10 µL
(8.7 mg L^{-1} in cuvette)		

9.3.5.6 Enzyme-coupled batch run

The batch was performed at 20 °C in a 2.0 mL Eppendorf (Eppendorf, Hamburg, Germany) and samples were analysed by gas chromatography. Prior to analysis, the samples (100 µL) were extracted with ethyl acetate (200 µL) containing 50 mM *n*-butanol. The batch was started by the addition of *Lb*ADH and FDH to the reaction mixture.

50 mM Potassium phosphate buffer (pH 6)	1462.5 µL
containing: 40 mM Methyl acetoacetate (**MAA**)	
100 mM Sodium formate	
2 mM $MgSO_4$	
0.2 mM $NADP^+$	
*Lb*ADH	3 µL
(0.025 g L^{-1} in Eppendorf)	
FDH	34.5 µL
(1.0 g L^{-1} in Eppendorf)	

9.3.5.7 Enzyme-coupled repetitive batch run

The repetitive batches were performed at 20 °C in a 10 mL ultrafiltration cell (Amicon Model 8010, Millipore GmbH, Schwalbach, Germany) fitted with an ultrafiltration YM-10 membrane (10 kD cut-off). The membrane was washed with 1 g L^{-1} bovine serum albumin solution before use. The enzymes *Lb*ADH (24 µL, 0.03 g L^{-1} in reactor) and FDH (274 µL, 1.2 g L^{-1} in reactor) were added in the first batch, and retained by the membrane for subsequent batches. A stock solution was used for the repetitive batches and fresh amount of $NADP^+$ was added to each repetitive batch. Filtration was done at 5 bar in between of batches, and each repetitive batch was started by the addition of stock solution and $NADP^+$ to the reaction mixture.

Stock solution:

50 mM Potassium phosphate buffer (pH 6)	10 mL
containing: 40 mM Methyl acetoacetate (**MAA**)	
100 mM Sodium formate	
2 mM $MgSO_4$	

Amount of fresh cofactor:

0.2 mM $NADP^+$	1.57 mg

Samples were taken throughout the batches for chemical and activity analyses. Prior to chemical analysis by gas chromatography, the samples (100 µL) were extracted with ethyl acetate (200 µL) containing 50 mM *n*-butanol. Activity measurements of *Lb*ADH and FDH were carried out in 1.5 mL cuvettes (Brand GmbH, Wertheim, Germany) and measured spectrophotometrically (λ = 340 nm) at 20 °C for 60 s. The activity measurement was started by the addition of 10 µL sample from the reactor to the cuvette.

For activity measurement of *Lb*ADH, the reaction mixture was:

50 mM Potassium phosphate buffer (pH 6)	930 µL
containing: 2 mM $MgSO_4$	
1 M Methyl acetoacetate (**MAA**)	40 µL
10 mM NADPH	20 µL
Batch sample	10 µL

For activity measurement of FDH, the reaction mixture was:

50 mM Potassium phosphate buffer (pH 6)	770 µL
containing: 2 mM $MgSO_4$	
1 M Sodium formate	200 µL
10 mM $NADP^+$	20 µL
Batch sample	10 µL

9.3.5.8 Enzyme-coupled continuous run

The continuous run was performed at 20 °C in a 10 mL stainless steel enzyme membrane reactor (Forschungszentrum Juelich GmbH, Juelich, Germany) fitted with a 10 kD cut-off ultrafiltration YM-10 membrane (Amicon GmbH, Witten, Germany) . The membrane was washed with 1 g L^{-1} bovine serum albumin solution before use. The enzymes *Lb*ADH (60 µL, 0.075 g L^{-1} in reactor) and FDH (680 µL, 3.0 g L^{-1} in reactor) were added in reactor, and retained by the membrane throughout the run. A stock solution was used for the feed and kept cool at 4 °C. Fresh amount of $NADP^+$ was added daily to the existing stock solution. Prior to entry in the reactor, the feed was heated to 20 °C and passed through a sterile filter (0.1 µm).

Stock solution:

50 mM Potassium phosphate buffer (pH 6)	1 L
containing: 40 mM Methyl acetoacetate (**MAA**)	
100 mM Sodium formate	
2 mM $MgSO_4$	

Amount of fresh cofactor:

0.2 mM $NADP^+$	15.7 mg/100 mL stock solution

Samples were taken from the continuous run for chemical (from outlet of reactor) and activity (from reactor) analyses. Gas chromatography was used for the chemical analysis while activity measurements of *Lb*ADH and FDH were carried out in 1.5 mL cuvettes (Brand GmbH, Wertheim, Germany) and measured spectrophotometrically (λ = 340 nm) at 20 °C for 60 s. The activity measurement was started by the addition of 10 µL sample from the reactor to the cuvette.

For activity measurement of *Lb*ADH, the reaction mixture was:

50 mM Potassium phosphate buffer (pH 6)	930 µL
containing: 2 mM $MgSO_4$	
1 M Methyl acetoacetate (**MAA**)	40 µL
10 mM NADPH	20 µL
Reactor sample	10 µL

For activity measurement of FDH, the reaction mixture was:

50 mM Potassium phosphate buffer (pH 6)	770 µL
containing: 2 mM $MgSO_4$	
1 M Sodium formate	200 µL
10 mM $NADP^+$	20 µL
Reactor sample	10 µL

9.3.6 Reaction techniques for recombinant *Escherichia coli*

9.3.6.1 Batch run

All batch reactions were performed at 30 °C with 2 % w/v biocatalyst. The biocatalyst was suspended with the stock solution given below. The batch reaction was started by the addition of 100 mM methyl acetoacetate (**MAA**) and the pH was controlled by an autotitrator (Dosimat 665, Metrohm, Herisau, Switzerland) dispensing 5 M HCl. Samples (500 µL) were withdrawn and centrifuged at 13200 rpm, 1 min. The cell pellets were discarded and the supernatants were analysed.

Stock solution:

50 mM Potassium phosphate buffer (pH 6)	36.5 mL
containing: 2 mM $MgSO_4$	
120 mM Sodium formate (ratio of **MAA**:formate = 1:1.2)	

9.3.6.2 Repetitive batch runs

Repetitive batch runs were performed similarly to batch runs, with 1 or 2 % w/v biocatalyst loading, but with the addition of 40 mM methyl acetoacetate (**MAA**). Centrifugation (5000 rpm, 4 °C, 5 min) was employed in between of batches to separate the biocatalyst from the reaction solution.

9.3.6.3 Continuous run (CSTR)

The continuous run was carried out in a 250 mL jacketed glass reactor (Forschungszentrum Juelich GmbH, Juelich, Germany) with 3 % w/v biomass loading. Cell recycle was made possible through a tangential flow ultrafiltration membrane of 300 kD cut-off (Pall GmbH, Dreieich, Germany). pH control was achieved with 5 M HCl and temperature was controlled with a water bath at 30 °C.

The continuous run was initiated by the start of a peristaltic pump directing the feed into the reactor. The operating residence time was set at 1 h.

Feed:

50 mM Potassium phosphate buffer (pH 6) 5 L
containing: 2 mM $MgSO_4$
30 mM Methyl acetoacetate (**MAA**)
62.5 mM Sodium formate

10 Appendix

The following model (MicroMath® Scientist® for Windows™, Version 2.0) was used for the enzyme-coupled batch reaction in Chapter 4. The kinetics constants of each system (NADH-dependent and NADPH-dependent *Lb*ADH and NADP-dependent FDH) were derived individually and compiled together. Kinetics constants for NAD^+-dependent FDH were obtained from Wandrey (2002).

```
//MicroMath Scientist ADH coupled batch kinetics (NADH vs NADPH) with enzymes/cofactors
deactivation
//xxxxP refers to reaction rate for NADPH-dependent ADH reduction
//xxx refers to reaction rate for NADH-dependent ADH reduction
IndVars: t
DepVars: MAA, MHB, MAAP,MHBP,NADH,NADPH
DepVars: ADHP,ADH,Vadh,Vadhp
DepVars: FORM,FORMP,NAD,NADP
DepVars: FDHP, FDH, Vfdh, Vfdhp
Params: VMmaa,VMmaap,KMmaa,KMmaap,KMnadh,KMnadph, KImaap
Params: VMform,VMformp,KMform,KMformp,KMnadp,KMnad,KInadph,KInadh
//
//Equations
RP=VMmaap*(MAAP/(KMmaap+MAAP+(MAAP*MAAP)/KImaap))*NADPH/(KMnadph+NADP
H)
R=VMmaa*(MAA/(KMmaa+MAA))*NADH/(KMnadh+NADH)
RFP=VMformp*(FORMP/(KMformp+FORMP))*NADP/(KMnadp*(1+NADPH/KInadph)+NADP)
RF=VMform*(FORM/(KMform+FORM))*NAD/(KMnad*(1+NADH/KInadh)+NAD)
Vadh=ADH*R
Vadhp=ADHP*RP
Vfdh=FDH*RF
Vfdhp=FDHP*RFP
MAA'=-Vadh
MHB'=Vadh
MAAP'=-Vadhp
MHBP'=Vadhp
FORM'=-Vfdh
FORMP'=-Vfdhp
NADH'=-Vadh+Vfdh-NADH*0.12/60
NADPH'=-Vadhp+Vfdhp-NADPH*0.12/60
NAD'=Vadh-Vfdh
NADP'=Vadhp-Vfdhp
ADH'=-ADH*0.03/60
ADHP'=-ADHP*0.03/60
//ADH deactivates at 3% per h
//ADHP deactivates at same rate as ADH (3% per h)
//NADPH deactivates at 12% per h
//Assume NADH deactivates at same rate as NADPH (12% per h)
//
//Initial conditions (t in min, conc in mM)
t=0
MAA=40
MAAP=40
MHB=0
MHBP=0
FORM=100
FORMP=100
NAD=0.2
```

```
NADP=0.2
NADH=0
NADPH=0
//
//Enzyme conc (g/L)
ADH=25E-03
ADHP=25E-03
FDH=100E-02
FDHP=100E-02
//
//Parameters (mM)
VMmaap=32.4659
KMmaap=0.30599
KImaap=163.98362
KMnadph=0.00384
VMmaa=30.41
KMmaa=84.27
KMnadh=1.6
VMformp=0.69961
KMformp=20.895
KMnadp=0.03874
KInadph=0.01367
VMform=0.62
KMform=4.99
KMnad=0.042
KInadh=0.022
//
***
```

Curriculum Vitae

Name: Ai Wei Ivy Tan
Date of birth: 1st August 1977
Place of birth: Singapore
Nationality: Singapore citizen

Work experiences

Finance clerk (National University Hospital, Singapore)	12/1995 – 05/1996
Industrial intern (Chemical engineer, Petrochemical Corporation of Singapore)	07/1999 – 12/1999
Graduate student demonstrator (UMIST, United Kingdom)	09/2000 – 06/2001
Administrative assistant (Project organisation/management, Singapore Management University)	01/2002 – 03/2002
Supervision of Diplom and practical students (Forschungszentrum Juelich, Germany)	since 04/2002

Academic training

Raffles Girls' Primary School, Singapore	01/1984 – 12/1989
Raffles Girls' Secondary School, Singapore	01/1990 – 12/1993
Raffles Junior College, Singapore	01/1994 – 12/1995
Bachelor studies in Chemical Engineering: The National University of Singapore, B.Eng.(Chemical), with 2nd class lower Honours	07/1996 – 08/2000
The National Undergraduate Research Opportunities Programme	09/1998 – 06/1999
Research Masters in Chemical Engineering (Biotransformations): UMIST, Manchester, United Kingdom, M.Phil.	09/2000 – 11/2001
Ph.D. Thesis Institute of Biotechnology, Forschungszentrum Juelich GmbH /University of Bonn, Germany	04/2002 – 10/2005

Academic award

Innovation Awards (Merit) for B.Eng.(Chemical) thesis — Faculty of Engineering, The National University of Singapore	07/2000